
**DYNAMIC IMPACT TESTING AND COMPUTER SIMULATION
OF
WHEELCHAIR TIEDOWN AND OCCUPANT RESTRAINT SYSTEMS
(WTORS)**

A thesis submitted to Middlesex University
in partial fulfilment of the requirements for the degree of
Doctor of Philosophy

Jun Gu *B.Sc. Eng. (Hons)*

ROAD SAFETY ENGINEERING LABORATORY
SCHOOL OF ENGINEERING SYSTEMS

MIDDLESEX UNIVERSITY

August 1999

ABSTRACT

Occupant Restraint Systems (ORS) have been widely used in Public Service Vehicles (PSVs). A Wheelchair Tiedown and Occupant Restraint System (WTORS) has been developed to provide effective occupant protection for disabled people who are seated in wheelchairs. An international laboratory study had been conducted to produce a compliance test protocol that included specification of the sled deceleration versus time history and the crash pulse corridor. Currently effort at the international level is being focused through the International Standards Organisation (ISO) to produce standards for WTORS and transportable wheelchairs.

Dynamic sled testing of WTORS was conducted in Middlesex University Road Safety Engineering Laboratory (MURSEL) to develop a test protocol in a WTORS system. This research has been concerned with the effects to which the occupant of a wheelchair secured by a WTORS is subjected in a frontal impact. Both occupant Forward Facing Frontal (FFF) and Rearward Facing Frontal (RFF) impact configurations have been considered. A surrogate wheelchair with a tiedown restraint system, a surrogate occupant restraint system, and an Anthropomorphic Test Dummy (ATD) were used to facilitate highly controlled tests. Production wheelchairs were also crash tested to validate the response of the surrogate system. A 48 km/h-20g crash pulse falling within the ISO standard crash pulse corridor was specified.

The Crash Victim Simulation (CVS), one of the computer modelling methods, and Finite Element Analysis (FEA) models were designed to study the dynamic response of a restrained wheelchair and its occupant in a crash environment. Two CVS computer packages: MADYMO^{®*}, DYNAMAN^{®**} and one of FEA programs: PAFEC were used in WTORS models to predict the occupant response during impacts and hence provide data to optimise future system design. A modelling protocol for WTORS was developed based on the results of ninety (90) sled tests of WTORS surrogate system and forty (40) dynamic tests of production wheelchairs. To illustrate the potential of these models the results of simulations were validated by sled tests. A

* MADYMO[®] is the trademark of TNO Road Vehicles Research Institute

** DYNAMAN[®] is the trademark of GESAC

random effects statistical method was used to quantify the results. The load-time histories were also traced to qualify the test and model results.

A literature review highlighted twenty years of wheelchair crash research. The correlation between computer model and experimental results was made more accurately. The modelling technique of interconnection of FEA models into CVS program was also introduced. The velocity profile and the natural frequency of WTORS analysis were used to explain why the wheelchair and dummy experienced acceleration amplifications relative to the sled. The shoulder belt load at floor-mounted configuration was found to be higher than that at B pillar configuration. Energy principles were also applied to show why more compliant wheelchair tiedown systems subjected restraints to a less severe crash environment. A decomposition of forces using the computer model showed why quasi-static analysis is insufficient in WTORS design. It is concluded that the B pillar anchorage of the occupant diagonal strap is superior to the floor-mounted configuration.

ACKNOWLEDGEMENTS

I would like to acknowledge the director of my studies, Mr. Peter Roy, for his guidance during my research at the Middlesex University Road Safety Engineering Laboratory (MURSEL). I would like to thank my supervisor, Professor Anthony White for his kind advice and corrections. I am indebted to the personnel at MURSEL for their assistance and co-operation throughout my research. I am also grateful for the help of Mr G. T. Savage and Mr C. T. Witherington for the performance of the dynamic tests.

This research project was performed at MURSEL, with funding provided by the Department of Transport (DOT). Some of the work described in this thesis forms part of a research programme directed by Mr Edward Stait of the DOT. The views expressed are not necessarily those of the Department.

Finally, I could not have completed this work without the encouragement and love of my parents, my wife and daughter.

AUTHOR'S DECLARATION

Some of the work documented within this thesis have been presented elsewhere by the author or co-written with the author. The work was conducted between January 1995 and December 1998 whilst the author studied at Middlesex University.

Three research projects included in this thesis (TRL, ISO, and Taxi) were conducted on behalf of the Department of Transport (DOT). They have been completed and documented in three contract reports, Gu J. & Roy P. (1994), (1995), and (1997) respectively. These also form the basis of three papers that were presented at the international conference [1][2][3]. Part of the finite element three-dimensional (3D) model was published by the Institution of Physics Conference [4].

Part of MADYMO3D Crash Victim Simulation (CVS) of Child Restraint System (CRS) in side impact was presented by the author at the 2nd International MADYMO User's Conference [5]. This work is not included in this thesis.

The research programme had to be postponed due to MURSEL closing down. The final stage of modelling research, the thesis writing and the paper 'Structural Modelling of Wheelchair Tyre Using MADYMO' were completed in the author's own time. The hybrid tyre model validation will be further studied.

The standards quoted in this thesis are draft ISO Wheelchair Tiedown and Occupant Restraint System (WTORS) standards: ISO/CD 10542-1 (1994, 1995, 1996), ISO/CD 10542-2 (1994, 1995, 1996) and ISO WD 7176/19. At present, these standards are open for discussion and the Draft International Standards (DIS) are being used in place of the ISO standards.

TABLE OF CONTENTS

ABSTRACT.....	2
ACKNOWLEDGEMENTS	4
AUTHOR'S DECLARATION	5
TABLE OF CONTENTS	6
LIST OF SYMBOLS	11
LIST OF ACRONYMS	14
LIST OF FIGURES	16
LIST OF TABLES	22
CHAPTER 1: INTRODUCTION AND BACKGROUND	
1.1 Road Safety and Dynamics	24
1.2 Wheelchair Occupant Safety and Requirements	25
1.3 Worldwide Regulations for WTORS	27
1.4 Interlab Testing of WTORS	32
1.5 MURSEL	33
1.6 Research Programme	35
CHAPTER 2: ELEMENTS OF WTORS	
2.1 Wheelchair Structure	39
2.2 Wheelchair Tiedown Systems	41
2.3 Occupant	44
2.4 Occupant Restraint System.....	45
2.5 Surrogate WTORS	48

CHAPTER 3:	WTORS CRASH ENVIRONMENT	
3.1	Modes of Simulation.....	50
3.2	Crash Simulator - Sled.....	53
3.3	Test Conditions	56
3.4	Visual Recording of Movements.....	62
3.5	Instrumentation	64
3.6	Signal Control System	66
CHAPTER 4:	RESTRAINT INJURY MECHANISMS IN WTORS	
4.1	Introduction	70
4.2	Restraint Injury Mechanisms	72
4.3	Restraint Injury Prevention	78
4.4	Injury Parameters	80
4.5	Summary	83
CHAPTER 5:	DYNAMIC SLED TESTING OF WTORS	
5.0	Introduction	85
6.3	Industry Tests (Group 1).....	87
6.4	TRL Tests (Group 2).....	88
5.3	ISO Tests (Group 3).....	91
5.4	Taxi Tests (Group 4)	98
5.5	Summary	104
CHAPTER 6:	THEORETICAL MODELLING OF WTORS	
6.1	Mathematical Modelling Procedure	106
6.2	A Simple Wheelchair Model	108
6.3	A Wheelchair-Sled Model	109
6.4	Improvement of WTORS Model	110
6.5	Further Studies of WTORS Model	113

CHAPTER 7:	FINITE ELEMENT ANALYSIS OF WHEELCHAIR	
7.1	Introduction	118
7.2	FEA Model Requirements	119
7.3	Loading Analysis of a Manual Wheelchair	123
7.4	Modal Analysis of TRL Surrogate Wheelchair	127
7.5	Correlation of Wheel Contact Characteristics	130
7.6	Summary	131
CHAPTER 8:	CRASH VICTIM SIMULATION (CVS) AND APPLICATIONS	
8.1	Introduction	133
8.2	Co-ordinate Systems	135
8.3	Multibody Systems	137
8.4	Multibody Belt Model	139
8.5	Hybrid Belt Model	143
8.6	Contact Interaction Models	148
8.7	Acceleration Field Model	152
8.8	Hybrid Tyre Model	152
8.9	Input and Output Parameters	157
CHAPTER 9:	CVS MODELLING OF WTORS	
9.1	TRL Frontal Impact Model	159
9.2	ISO Frontal Impact Model	165
9.3	Taxi Rearward Facing Frontal Impact Model	172
9.4	Modelling Discussions	175
9.5	Summary	177

CHAPTER 10:	CVS MODEL VALIDATION AND ANALYSIS	
10.1	Model Post-Process	179
10.2	TRL Frontal Impact Model Validation	180
10.3	ISO Frontal Impact Model Validation	193
10.4	Rearward Facing Frontal Impact Model Validation	195
10.5	Simulation Analysis	196
10.6	Summary	203
CHAPTER 11:	GENERAL DISCUSSIONS OF WTORS	
11.1	Investigation of the Amplification Effect	204
11.2	Beam Element Analysis of Shoulder Loads	205
11.3	Load Characteristics in WTORS	209
11.4	Energy Analysis of Tiedown Loads	212
11.5	Rebound Characteristics in a Sled Simulation	214
CHAPTER 12:	CONCLUSIONS AND FURTHER WORK	
12.1	Research Progresses	218
12.2	Experimental Conclusions	220
12.3	Mathematical Model Conclusions	224
12.4	Further Work	225
REFERENCES	228

Appendix 1A:	ISO Standards for WTORS	241
Appendix 1B:	Crash Victim Simulation (CVS) Programs.....	243
Appendix 2:	Modification of ISO Surrogate Wheelchair (SWC)	249
Appendix 3:	Load Cell Theory and Design.....	258
Appendix 4:	Running MADYMO and EASi-MAD.....	262
Appendix 5A:	Interpretation of Industry Test Results.....	268
Appendix 5B:	Interpretation of TRL Test Results	276
Appendix 5C:	Interpretation of ISO Test Results	280
Appendix 5D:	Interpretation of Taxi Test Results.....	284
Appendix 6:	Dynamic Vibration Theory and Applications	293
Appendix 7A:	Running PAFEC and FEA Model Input Data	297
Appendix 7B:	Contact Characteristics in CVS Models	303
Appendix 9A:	TRL Frontal Impact Model Data File.....	312
Appendix 9B:	ISO Frontal Impact Model Data File	325
LIST OF PUBLICATIONS	330

LIST OF SYMBOLS

$a(t)$	Sled deceleration time history or crash pulse
a_{rh}	Resultant acceleration of the dummy head
a_{rc}	Resultant acceleration of the dummy chest
a_x, a_y, a_z, \dots	x,y,z component acceleration of the dummy or wheelchair
a_m	Acceleration amplification
b	Beam thickness
c	Coefficient of viscous damping
C_d	Positive damping coefficient
C_f	Sum of vertical loads on occupant seat
E	Young's modulus
E_M	Total mechanical energy of the system, that is, K + J
E_o	Output voltage
E_i	Input voltage
f	Frequency or function
F	Friction force or element force
g	Acceleration of gravity
H_{exc}	Dummy head target maximum excursion
I	Mass Moment of Inertia (MOD)
I_x, \dots	Principal moment of inertia
I_{xy}, \dots	Product of inertia
J	Potential energy
k	Spring stiffness, such as, the stiffness of wheelchair rear tiedown
K	Kinetic energy
l	Length
L	Initial position of the sled before triggering
L_τ	Final position of the sled after triggering
m_F	Mass of wheelchair
m_D	Mass of dummy
M	Mass of a wheelchair-occupant system
M_o	Moment about original point
M_{max}	Maximum Moment
n	Number of samples
N	Normal component of reaction
O	Origin of co-ordinates
P_o	Wheelchair's reference point P at time zero
r	Sensitivity index
R	Common nominal resistance of all gauges, or resultant of element force
ΔR	Change in resistance
S	Sample standard deviation

$S_f(B)$	Occupant shoulder load function in B pillar configuration in the direction of torso centre line
$S_f(F)$	Occupant shoulder load function in floor configuration in the direction of torso centre line
t	Time of peak diagonal top strap tension (T_1)
t_0	Time zero
t_b	Period of the base excitation, the duration of the excitation, such as, crash pulse length
T_p	Period, that is, $2\pi/\omega$
T	Spring force
T_r	Rear tiedown force
T_f	Front tiedown force
T_1	Diagonal top strap tension
T_2	Diagonal bottom strap tension
T_3	Lap strap tension
T_4	Buckle strap tension
u	A distance from its equilibrium position, u_m is maximum displacement
$u(t)_w$	Absolute displacement of the wheelchair
$\ddot{u}(t)_w$	Absolute acceleration of the wheelchair
$u(t)_s$	Absolute displacement of the sled
$\ddot{u}(t)_s$	Absolute deceleration of the sled
v	Velocity
Δv	Sled velocity change or delta 'V'
v_o	Initial velocity of the sled or wheelchair
v_e	Final velocity of the sled
V_{max}	Maximum vertical load
W	Work of a conservative force
w	Beam width
x, y, z	Rectangular co-ordinates
x_i	Particular sample from a population
X_{wc}	The horizontal distance relative to the sled platform between the contrast target placed at or near point P_0 on the surrogate wheelchair at time t_0 , to the point P_0 target at the time of peak wheelchair excursion.
X_{knee}	The horizontal distance relative to the sled platform between the ATD's knee-joint target at time t_0 , to the knee-joint target at the time of peak knee excursion.
X_{head}	The horizontal distance relative to the sled platform between the ATD's head above the nose at time t_0 , to the Forward-Most-Point (FMP) on the ATD's head at the time of peak head excursion.
y	The distance from the neutral axis where stress or strain is measured
α	Diagonal top strap angle to the horizontal at the time of peak value of T_1
β	Occupant torso forward angle from vertical at the time of peak value of T_1
γ	Diagonal top strap angle with reference to a vertical plane parallel to the sled fore and aft centre line

θ_r	Angle between the sled platform and the wheelchair rear tiedown
θ_f	Angle between the sled platform and the wheelchair front tiedown
δ	Elongation of the tiedown system
δ_s	Elongation of the spring
ε	Relative elongation of belt, or element strain
μ	Coefficient of friction
ρ	Density
ϕ	Phase angle
ω_0	Undamped natural frequency of the wheelchair-occupant system
σ	Element stress, σ_{max} is the maximum allowable tensile stress
σ_y	Yield stress
τ	Natural period of the wheelchair-occupant system
Δ	Node deflection

LIST OF ACRONYMS

ACT.....	Aluminium Crumple Tubes
ADA.....	Americans with Disabilities Act
AIS	Accident Injury Scale or Abbreviated Injury Scale
ASTM.....	American Society for Testing and Materials
ATB.....	Articulated Total Body. This is the Air Force enhanced version of the Crash Victim Simulator (CVS) Program developed by Calspan Corporation for the Department of Transport, USA
ATD.....	Anthropomorphic Test Dummy
CG.....	Centre of Gravity
CRS	Child Restraint System
CSA.....	Canadian Standards Association
CSI	Chest Severity Index
CV.....	Coefficient of Variation
CVS	Crash Victim Simulation
DCIEM.....	Defence and Civil Institute of Engineering Medicine, Canada
DDAS.....	Dynamic Data Acquisition System
DOT.....	Department of Transport, UK
DYNAMAN.....	One of CVS programs, developed by GESAC, Inc.
EASi-MAD	Pre- and Post-process program for MADYMO, produced by EASi Engineering, USA
FDF.....	Force Deflection Functions
FEA.....	Finite Element Analysis
FFF	Forward Facing Frontal impact
FMP.....	Forward-Most Point
FMVSS	Federal Motor Vehicle Safety Standards, USA
HIC	Head Injury Criterion

ISO	International Standards Organisation
MADYMO.....	MAThematical DYnamic MOdel, one of the CVS programs, produced by TNO, The Netherlands
MOI	Moment Of Inertia
MURSEL	Middlesex University Road Safety Engineering Laboratory
NHTSA	National Highway Traffic Safety Administration, USA
PSVs.....	Public Service Vehicles
PTT	Polyurethane Tapered Tubes
RD.....	Residual Deformation
RFF	Rearward Facing Frontal impact
SAE.....	Society of Automotive Engineers
SDOF.....	Single Degree of Freedom
TRL	Transport Research Laboratory, formerly the Transport and Road Research Laboratory (TRRL), Department of Transport, UK
UMTRI.....	University of Michigan Transportation Research Institute, USA
UVA	University of Virginia, Transportation Rehabilitation Engineering Centre, USA
WSTC	Wayne State Tolerance Curve
WTORS.....	Wheelchair Tiedown and Occupant Restraint Systems

LIST OF FIGURES

Figure 1.6: Research flow diagram	37
Figure 2.0: Four elements of WTORS	39
Figure 2.1a: TRL surrogate wheelchair	40
Figure 2.1b: ISO surrogate wheelchair	41
Figure 2.2a: Clamping device	43
Figure 2.2b: Webbing restraint (4 point)	43
Figure 3.1: Breakdown of fatal and injury accidents (NHTSA), 1992	52
Figure 3.2a: MURSEL rig	54
Figure 3.2b: Sled test platform with upper anchorage frame	55
Figure 3.3a: Acceleration variation	58
Figure 3.3b: Section through olive/tube assembly	60
Figure 3.3c: Sled pulse from polyurethane tubes	60
Figure 3.3d: ECE R44 envelope for frontal impact	61
Figure 3.3e: ISO corridor	61
Figure 3.4a: High-speed video analysis	62
Figure 3.4b: Kodak EktaPro motion analyser	63
Figure 3.6: Data acquisition processing at MURSEL	67
Figure 4.2a: A response envelope of head resultant acceleration	74
Figure 4.2b: The dummy collar bone collapsed during FFF impact	76
Figure 4.4a: Comparison of Δa at two types of wheelchair	82
Figure 4.4b: Comparison of Δa at two configurations of a manual wheelchair	83
Figure 4.4c: Comparison of Δa at two types of a manual wheelchair	83
Figure 5.0: Four groups of dynamic sled tests	86
Figure 5.2: Three levels of sled deceleration pulses used in TRL tests	89
Figure 5.3a: Three levels of sled pulses used in ISO tests	92
Figure 5.3b: B pillar anchorage	94

Figure 5.3c: Floor anchorage	94
Figure 5.3d: Wheelchair misalignment after impact	95
Figure 5.3e: Comparison of peak shoulder load function in two configurations	95
Figure 5.3f: Seat sum loads for B pillar configuration	97
Figure 5.4a: Sled pulse for RFF impact	100
Figure 5.4b: A vertical rigid frame	102
Figure 5.4c: A back support structure	102
Figure 5.4d: Dummy head contacted with the headrest	103
Figure 6.1: The modelling flow diagram	106
Figure 6.2: Force distribution in a crate	108
Figure 6.3: A wheelchair-sled system.	110
Figure 6.4a: Two mass and spring model of WTORS	112
Figure 6.4b: Two mass and dashpot model of WTORS	113
Figure 6.5a: TNO-10 dummy	114
Figure 6.5b: Joints of dummy	114
Figure 7.2a: Element force characteristics	120
Figure 7.2b: The relationship of four physical parameters in a FEA model	121
Figure 7.2c: FEA modelling flow diagram	122
Figure 7.3a: Classic Universal wheelchair	124
Figure 7.3b: Element structure simulation of a manual wheelchair	127
Figure 7.4a: Beam structure elements in TRL wheelchair	128
Figure 7.4b: Five modes analysis of TRL wheelchair	129
Figure 7.5a: A wheelchair tyre model by FEA	131
Figure 7.5b: Tyre non-linear stiffness	131
Figure 8.2: General co-ordinate system convention	136
Figure 8.3a: Joints linked with three bodies	137
Figure 8.3b: Relative orientation of coordinate systems using Bryant angles	138
Figure 8.4a: Webbing belt segment contact	141
Figure 8.4b: Slip between two belt segments	141

Figure 8.4c: Kinematics of a LD belt model	142
Figure 8.5a: Finite element floor-mounted shoulder belt	145
Figure 8.5b: Pre-setting of finite element belt connected to multibody belt	146
Figure 8.6: The plane-segment contact	149
Figure 8.8a: A wheel tyre hybrid model	154
Figure 8.8b: Tyre mesh block	155
Figure 8.8c: Tyre mesh lay-out	156
Figure 9.1a: CVS modelling of WTORS	159
Figure 9.1b: Diagonal strap belt configurations	160
Figure 9.1c: The function of shoulder belt loads and the shoulder belt angles	162
Figure 9.1d: The function of lap belt loads and the shoulder belt angles	163
Figure 9.1e: The function of the buckle loads and the shoulder belt angles	163
Figure 9.1f: The function of wheel loads and the shoulder belt angles	164
Figure 9.2a: CVS modelling of ISO surrogate wheelchair	165
Figure 9.2b: ISO model by MADYMO	166
Figure 9.3a: Taxi model set-up	172
Figure 9.3b: A back support FE belt model and lap FE belt	174
Figure 9.4: Wheelchair submarining	176
Figure 10.1a: CVS model post-process	179
Figure 10.1b: Model tuning loop	180
Figure 10.2a: Comparison of the single rear wheel loads for TRL tests (T2779) ...	182
Figure 10.2b: Comparison of the single rear wheel loads for TRL tests (T2780)	182
Figure 10.2c: Comparison of the single rear wheel loads for TRL tests (T2781)	183
Figure 10.2d: Comparison of the single rear wheel loads for TRL tests (T2782) ...	183
Figure 10.2e: Comparison of the single rear wheel loads for TRL tests (T2793)	184
Figure 10.2f: Comparison of the single rear wheel loads for TRL tests (T2794)	184
Figure 10.2g: Comparison of the single rear wheel loads for TRL tests (T2795)	185
Figure 10.2h: Comparison of the single rear wheel loads for TRL tests (T2796)	185
Figure 10.2i: Comparison of the single rear wheel loads for TRL tests (T2783)	186

Figure 10.2j: Comparison of the single rear wheel loads for TRL tests (T2786)	186
Figure 10.2k: Comparison of the single rear wheel loads for TRL tests (T2787) ...	187
Figure 10.2l: Comparison of the single rear wheel loads for TRL tests (T2788)	187
Figure 10.2m: Comparison of the single rear wheel loads for TRL tests (T2789)	188
Figure 10.2n: Comparison of the single rear wheel loads for TRL tests (T2790)	188
Figure 10.2o: Comparison of the single rear wheel loads for TRL tests (T2791) ...	189
Figure 10.2p: Comparison of the single rear wheel loads for TRL tests (T2792) ...	189
Figure 10.2q: Comparison of the single rear wheel loads for TRL tests (T2818) ...	190
Figure 10.2r: Comparison of the single rear wheel loads for TRL tests (T2819)	190
Figure 10.2s: Schematic comparison of test and CVS model in WTORS	191
Figure 10.2t: Kinematics of TRL wheelchair with TNO-10 dummy	192
Figure 10.3a: Comparison of sled test and CVS models	193
Figure 10.3b: Kinematics of ISO wheelchair with Hybrid II dummy	194
Figure 10.4: Simulated kinematics of a RFF impact of WTORS	196
Figure 10.5a: Comparison of headrest effect on chest acceleration	198
Figure 10.5b: Comparison of headrest effect on head acceleration	198
Figure 10.5c: Comparison of headrest effect on wheelchair back load (portside)	198
Figure 10.5d: Comparison of headrest effect on wheelchair back load (starboard)	198
Figure 10.5e: Comparison of headrest effect on wheel load (portside)	198
Figure 10.5f: Comparison of headrest effect on wheel load (starboard)	198
Figure 10.5g: Comparison of headrest effect on rear tiedown load	199
Figure 10.5h: Comparison of wheelchair type effect on chest acceleration	199
Figure 10.5i: Comparison of wheelchair type effect on head acceleration	199
Figure 10.5j: Comparison of wheelchair type effect on wheelchair back load (pt)	200
Figure 10.5k: Comparison of wheelchair type effect on wheelchair back load	200
Figure 10.5l: Comparison of wheelchair type effect on wheel load (portside)	200
Figure 10.5m: Comparison of wheelchair type effect on wheel load (st)	200
Figure 10.5n: Comparison of wheelchair type effect on rear tiedown load	200
Figure 10.5o: Comparison of wheelchair handles effect on chest acceleration	201

Figure 10.5p: Comparison of wheelchair handles effect on head acceleration	201
Figure 10.5q: Comparison of wheelchair handles effect on wheelchair back load (Pt)	202
Figure 10.5r: Comparison of wheelchair handles effect on wheelchair back load (St)	202
Figure 10.5s: Comparison of wheelchair handles effect on wheel load (portside)	202
Figure 10.5t: Comparison of wheelchair handles effect on wheel load (starboard)	202
Figure 10.5u: Comparison of wheelchair handles effect on rear tiedown load	202
Figure 11.2a: Static analysis of shoulder belt loads	206
Figure 11.2b: Free body diagram for occupant torso	207
Figure 11.2c: Load distribution in B pillar configuration	208
Figure 11.2d: Load distribution in floor-mounted configuration	208
Figure 11.2e: Peak parameter variation (B pillar configuration)	209
Figure 11.2f: Peak parameter variation (floor-mounted configuration)	209
Figure 11.3a: Static analysis of wheel loads	210
Figure 11.3b: Further analysis of wheel loads	211
Figure 11.5a: A sled mass-spring model	215
Figure 11.5b: Loads from position 1 to 2	215
Figure 11.5c: Loads from position 2 to 3	216

Appendix

Figure 1A: Shoulder belt positions on dummy	241
Figure 1B.1: CVS modelling flow diagram	245
Figure 1B.2: Structure of CVS models input file: Overview	246
Figure 1B.3: Structure of DYNAMAN input file: Overview	247
Figure 1B.4: Structure of DYNAMAN input file: Segment	248
Figure 3A.1: Wheel load plate	258
Figure 3A.2: Load plate dimensions and strain gauge placement	259
Figure 3A.3: A 'dogbone' dimensions and gauge placement	261
Figure 4A.1: The path structure of MADYMO and EASi-MAD	264
Figure 4A.2: The process of running MADYMO	266
Figure 5B.1: Comparison of rear wheel loads in WTS/WTORS	278
Figure 5B.2: Dynamic testing of rear wheel loads in WTORS	278
Figure 5B.3: Comparison of frontal wheel loads in WTS/WTORS	279
Figure 5B.4: Wheel load variation in WTORS as a function of crash pulse	279
Figure 6A.1: The potential energy, J	294
Figure 6A.2: Sled and TRL wheelchair impact	296
Figure 7B.1: L/D seat belt characteristics	304
Figure 7B.2: Wheelchair tiedown characteristics	304
Figure 7B.3: L/D seat belt MADYMO input	305
Figure 7B.4: L/D seat belt DYNAMAN input	305
Figure 7B.5: Wheelchair tiedown MADYMO input	306
Figure 7B.6: Wheelchair tiedown DYNAMAN input	306
Figure 7B.7: Static testing of wheelchair tyres	308
Figure 7B.8: Wheel stiffness in ISO surrogate wheelchair	310
Figure 7B.9: Wheel stiffness in TRL surrogate wheelchair	310

LIST OF TABLES

Table 1.2a: Passengers injured in PSVs, UK.....	25
Table 1.2b: Summary of design conditions and requirements for WTORS	27
Table 1.3: A summary of the current worldwide standards of WTORS	31
Table 1.5: Performance specification of MURSEL facility	34
Table 3.3: Vehicle crash pulse types	61
Table 4.2: Chest deflection limit	76
Table 5.2: TRL test programme	88
Table 5.3a: ISO test programme	92
Table 5.3b: Load duration (B pillar) - Level I, II	96
Table 5.3c: Load duration (floor-mounted) - Level I, II	96
Table 5.3d: Shoulder load difference between two configurations	97
Table 5.4: Taxi test conditions	101
Table 6.5a: CG calculation of Hybrid II dummy	115
Table 6.5b: CG calculation of TNO-10 dummy	115
Table 6.5c: CG calculation of TNO-10 dummy (without leg).....	116
Table 8.3: Joint position DOF for 3D joint types.....	139
Table 8.5: Finite element belt stiffness characteristics	144
Table 8.8: Te wheel/tyre mesh ealculations.....	157
Table 9.1a: CVS model results for diagonal strap belt configurations	161
Table 9.1b: Optimised configuration of a diagonal strap	164
Table 9.1c: Comparison of sled test and CVS model results	164
Table 10.2a: Comparison of TRL test and CVS results	181
Table 10.2b: The difference between TRL tests and CVS model results	181
Table 10.3: Comparison of ISO tests and CVS model results	193
Table 10.4a: Comparison of taxi tests and CVS results (Series I & II)	195

Table 10.4b: Comparison of taxi tests and CVS results (Series III & IV)	195
Table 11.2a: Shoulder load calculation at B pillar configuration	207
Table 11.2b: Shoulder load calculation at floor-mounted configuration	208

Appendix

Table 1A: WTORS requirements (ISO/CD 10542-1)	242
Table 4A.1: Summary of SGI station	263
Table 4A.2: Transferring files via FTP or Kermit	267
Table 5A.1: A sample of test report for clients	268
Table 5A.2: Buddy wheelchair test results	269
Table 5A.3: Sunrise wheelchair test results	270
Table 5A.4: Sled tests for Cirrus wheelchairs	271
Table 5A.5: Sled tests for UNWIN restraint system	272
Table 5A.6: Sled tests for manual wheelchairs	273
Table 5A.7: Invarcare wheelchair test results	274
Table 5A.8: SCN wheelchair test results	275
Table 5B.1: Load differences between Level I and II	276
Table 5B.2: Load differences between WTS and WTORS	277
Table 5B.3: Load differences among Level I, II and III	277
Table 5C.1: ISO test results (Level I)	282
Table 5C.2: ISO test results (Level II)	283
Table 5C.3: ISO test results (Level III)	283
Table 5D.1: Taxi test results (peak) - Series I	287
Table 5D.2: Taxi test results (peak) - Series II	290
Table 5D.3: Taxi test results (peak) - Series III	290
Table 5D.4: Taxi test results (peak) - Series IV	291
Table 5D.5: Taxi test results (peak) - Series V	292
Table 7B: Wheelchair compressive test results	309

CHAPTER 1: INTRODUCTION AND BACKGROUND

1.1 Road Safety and Dynamics

More than 10,000 people die as a result of accidents of one form or another in the UK every year. Over one-third of these fatalities occur on the roads. The economic cost of road trauma in the UK in 1993 represented 1.7 per cent of Gross Domestic Product (GDP). It was about 1.6 per cent of GDP in Australia in 1994. This figure is typical of the economic significance of road accidents in other industrialised countries. United States of American (USA) estimates would suggest economic cost of between 1.0 and 1.5 per cent of GDP.

Society attempts to reduce this toll and enormous loss. Firstly, the immediate practical causes of different types of road accident have to be discovered. Secondly, Occupant Restraint Systems (ORS) have been designed for the safety of all users. One important aspect of road safety is the incidence of serious and fatal accidents following a collision. If there is an accident or collision, the velocity changes can be damaging to both humans and the ORS system. A proper appreciation of current methods and proposals requires an understanding of the basic scientific and engineering concepts of dynamics.

Although approximately one third of fatal car accidents are frontal collisions, serious injury and fatality are also seen in other types of car accidents such as side and rear impacts. Thus, in order to increase the integrity for crashworthiness, studies of various types of crash situations are required. The extension of crashworthiness calculations to various aspects of the crash would greatly enhance the structural integrity of the ORS. It is desirable to have a simulation tool for investigation of better crashworthiness performance, such as, sled tests and computer models, thereby decreasing the burden of full-scale tests of prototype vehicles. There are more stringent requirements to protect the disabled occupant sitting in a wheelchair travelling in a vehicle during impact. These requirements include restraint systems both for disabled occupants and wheelchairs.

Considerable advances have been made in the crash injury protection of wheelchair occupants over the past two decades, but motor vehicle accidents still waste enormous human potential. How to make new progress in crash injury protection of wheelchair occupants is still a challenge to the whole world.

1.2 Wheelchair Occupant Safety and Requirements

The accident data related to Public Service Vehicles (PSVs) passengers in the UK, excluding those injured while they were boarding or alighting, were obtained from the police STATS19 (1981) form, given in nation-wide coverage. The breakdown for the year 1981 is typical and is given in Table 1.2a.

Table 1.2a Passengers injured in PSVs, UK

Impact Types	Severity of Injury		% of Total
	Fatal	Serious	
Front	0	171	38%
Rear	1	6	1%
Offside	0	16	4%
Near side	2	7	2%
Rollover	2	60	13%
No impact	3	186	42%
Total	8	446	

Two most important types of accident were found in Table 1.2a. The first is an injury happened when no vehicle impact takes place, but emergency braking or sudden manoeuvres cause passengers to be thrown against the bus structure (42% of the total injuries). In such an event, unrestrained wheelchairs would be free to roll and represent a danger not only to the wheelchair occupants but also to other users of the PSVs. The second event from Table 1.2a is the direct frontal impact (38% of the total injury). Accident data have shown that the priority requirements for the wheelchair restraint are to hold the chair and occupant in place during normal driving. These requirements are summarised in 'Code of Practice: the safety of passengers in wheelchairs on buses' (VSE87/1). Roy (1995) drew attention to differences between types of occupant restraint system observed during ISO surrogate wheelchair tests.

The mechanical response of the wheelchair during impacts depends on the anchorage of the dummy's occupant restraint, attached either to the floor or to B pillar.

Manufacturers noted that wheel brakes were insufficient in securing a wheelchair during normal driving manoeuvres. The tiedown restraint systems have to be developed to limit wheelchair movement. Unfortunately, these restraint devices were designed to prevent excessive wheelchair and occupant movement in transport, giving little attention to basic crashworthy principles. In 1976, Orne suggested basic design criteria for Wheelchair Tiedowns and Occupant Restraint Systems (WTORS), and produced a WTORS prototype (Orne, et al, 1976). In 1978 and 1979, dynamic sled impact tests were conducted at the University of Michigan to evaluate the effectiveness of several commercially available WTORS (Schneider, et al, 1979). The results revealed that most tiedown and occupant restraint equipment were inadequate for protecting wheelchair passengers in a crash environment and suggested a need to develop WTORS performance standards.

These studies resulted in two draft ISO standards: the standard for WTORS (ISO/CD 10542-1) and the standard concerning the strength of the wheelchair itself (ISO WD 7176-19). These are only draft standards which are continually changing. The final standards have not yet been issued.

In the above ISO standards, the production wheelchair was anchored to the sled using either its own specified restraint systems or a defined surrogate system. The dummy of mass 75 kg was used. When subjected to impact WTORS should meet the following requirements:

- *Retain the test dummy and wheelchair on the sled. The test wheelchair should remain in the upright position.*
- *Not show any fragmentation or complete separation of any load carrying part.*
- *Not allow the horizontal excursions of the test dummy and test wheelchair to exceed the limits defined in Appendix 1A.*
- *Allow the dummy and wheelchair to be released from the sled without the use of tools.*
- *Prevent the wheelchair loading the occupant by exhibiting a ratio:*

(maximum knee excursion)/(maximum chair excursion) > 1.1

- *Secure electric batteries without any leakage.*
- *Not deformed to cause serious injury to the occupant.*

The accident investigations have been conducted through WTORS environment studies, dynamic testing of production wheelchair and its restraint system, wheelchair users and manufacturers. The design conditions and requirements for WTORS are summarised in Table 1.2b.

Table 1.2b Summary of design conditions and design requirements for WTORS

Design Conditions	Design Requirements
Accident Environment	<ul style="list-style-type: none"> • Frontal impact • Rear impact • Side impact • Emergency braking (a deceleration of 0.8g)
Wheelchairs	<ul style="list-style-type: none"> • Electric powered and manual wheelchairs • Battery securement: no breakaway and no acid spills in accident
Wheelchair Restraint System	<ul style="list-style-type: none"> • Secured to vehicle under accident environment • No entrapping of passenger in accident • Fit into most types of vehicles • Fit within space envelope of wheelchair • Easy to install and remove • Easy to mass produce (low unit costs)
Disabled Occupant	<ul style="list-style-type: none"> • Survive accident conditions with little or no injury • Lower human tolerance values (HIC or 3MS) than for able-bodied occupant • Passive rather than active restraint preferred • Simple operation of devices

1.3 Worldwide Regulations for WTORS

Numerous countries have adopted legislation and standards to ensure that people in wheelchairs travel safely in the PSVs. These call for experimental work and computer models under conditions of impacts with monitoring of the integrity of WTORS. Many authorities are actively concerned with increasing the safety of

wheelchair occupants, such as the International Standard Organisation (ISO), motoring associations, accident prevention societies, university impact engineering departments, car manufacturers and governments.

Work has continued both in the UK and internationally in the development of standards for wheelchairs carried in vehicles and for restraint systems used on them. ISO Committees have involved in drawing up international standards in these fields. They are also liaison closely with the manufacturers to ensure that standards are set on the basis of the best practice and research experience.

In 1982, the UK government introduced legislation, which for the first time in the UK provided a statutory framework requiring all forms of domestic land based public transport to be accessible by disabled people. The legislation covers buses, coaches, trains, trams and taxis. The Transport Research Laboratory (TRL) test site at Crowthorne in Berkshire has conducted numerous experiments on road surface, layout and car design in co-operation with both local government experts and car manufacturers. In 1981, the Department of Transport (DOT) issued a Code of Practice and Special Provisions for the Carriage of Passengers in Wheelchairs on Public Service Vehicles (VSE518). Currently advice on the safe carriage of wheelchair occupants in buses in the UK is provided by the Code of Practice VSE 87/1, which was substituted for VSE 518. This Code describes how wheelchair should be secured when travelling in a bus. A bus is defined as a vehicle for more than eight (8) seats, including those in wheelchairs. The Code of Practice defines the recommended space and headroom inside the vehicle to manoeuvre the wheelchair, and the width of the door and gangway. Middlesex University Road Safety Engineering Laboratory (MURSEL) has involved in some aspects of crash environments and maintenance, including advice to the government on road safety improvement and safety legislation, which have contributed to international standards (ISO/CD 10542-1 and ISO WD 7176-19).

In the Netherlands, the TNO-Road Vehicles Research Institute has involved in a long-term research programme on the transport of wheelchair occupants (Kooi J. and Janssen E.G., 1988). TNO has formulated requirements and recommendations regarding instructions for use, design and durability of the wheelchairs. A working

group of the Dutch Standardisation Office (Netherlands Normalisation Institute, NNI) has started preparation to transform this work into standards.

In France, the order of July 1982 on the collective transport of persons for vehicles with more than ten (10) seats was issued. This order stipulates that the wheelchair must be anchored to the floorboard of the vehicle and that the passenger must be secured in the wheelchair. Schneider (1979) examined the case of children in wheelchairs subject to 48 km/h frontal impact and concluded that the means of restraint existing at the time for forward facing impact was not the best solution.

In Germany, the standard DIN 75078 (1985) covers the transport in vehicles with less than 12 seats, which must be equipped with a complicated wheelchair and occupant restraint system. The wheelchair restraint system has been impacted in the University of Heidelberg Research Centre for Rehabilitation and Prevention, West Germany (Kallieris D., et al., 1981). Studies have been carried out by reconstructing frontal and rear impact accidents involving light vehicles and minibuses. The aim was to propose solutions for the wheelchair occupant restraint systems.

In Sweden, regulations published in 1989 and recommended two different restraint systems, one for the wheelchair and another for the occupant. These regulations outline objectives to be attained with regard to restraint of the wheelchair and lay down requirements concerning the position of anchoring points for the occupant's seat belts. They apply to vehicle seats less than twelve (12) persons. Petzall (1995) tested production wheelchairs restrained using systems adapted. During tests with heavy electric powered wheelchairs, breakage of the strap-type system was observed.

In Australia, the standard AS2942 (1987) served as the starting point for the work of the ISO group.

In North America, government regulations ensure that safety restraint systems can be used to protect passengers in all modes of transportation meet certain minimum performance criteria. The concern for the safety of wheelchair passengers in transit arose in the mid-1970's in USA. In 1990, the Americans with Disabilities Act (ADA) extended civil rights protection to people with disabilities. It was conducted by setting minimum performance standards to protect wheelchair passengers in public transit.

Unfortunately, the safety of wheelchair passengers in personally-licensed vehicles, such as vans, has not been addressed in legislation in the form of a WTORS standard. To consider this oversight, the Society of Automobile Engineering (SAE) Adaptive Devices Committee Wheelchair Restraints Task Group has recommended practices which led to a national standard for personally-licensed vehicles. The ultimate goal is to ensure that all passengers in all forms of transportation are guaranteed the same level of protection in the event of a crash. Adams (1994) highlighted the problem of the position of the shoulder belt anchorage either to the floorboard or to an upright. This problem made more difficult in the case of coaches with large surface areas of glass to the sides.

The current world-wide standards including the issues and the performance requirements are summarised in Table 1.3. An ISO Technical Committee was set up in 1970s to manage working groups of experts, whose task was to draft standards concerned with wheelchairs. With the increased mobility of wheelchair occupants in the early 1980s, particularly of those travelling in personally licensed vehicles, a new working group (WG6) was established in 1988. It was given the task of drafting an appropriate restraint standard. Membership of the group includes a wide assortment of professionals, researchers, government officials, users, rehabilitation engineers and manufacturers from nine (9) countries. In November 1995, technical experts in this group met at MURSEL to work on a standard for the crash protection of wheelchair occupants.

In an effort to provide consistency among all standards world-wide, the ISO Wheelchair Restraint Systems Working Group (ISO/TC-173/SC-1/WG6) is currently working on the development of standards for both WTORS (ISO/CD 10542-1) and Wheelchair Transportable System (WTS) (ISO WD 7176/19), applicable to both personally licensed vehicles and public transportation. The ISO 10542 standard places particular emphasis on design requirements, test procedures, and performance requirements with regard to the dynamic performance of WTORS in a frontal impact. It incorporates a severity of impact of 48 km/h with a maximum deceleration of 26g. In this standard, the occupant is restrained by a traditional 3-point seat belt attached to

the structure of the vehicle. The wheelchair is positioned facing to the front of the vehicle and is held by a tiedown system secured to the floorboard of the vehicle.

Table 1.3 A summary of the current worldwide standards of WTORS

Country/ Standards	Vehicle types	Occupant restraints	Evaluation criteria	Performance requirements
UK/ VSE 87/1	Motor vehicles for more than 8 seats	Lap & torso	Static tests: 4.4 kN for chair restraint; 8.8kN occupant restraint.	The restraint should withstand applied forces without failing or separating from the attachment; Movement of chair < 200 mm
Netherlands	Road transport vehicles	Lap & torso	Dynamic tests: 30 km/h, 10g maximum	Movement of chair < 200 mm
France/ Order 1982	Vehicles more than 10 seats	Lap & torso	Sled tests	Chair must be anchored on the floorboard
Germany/ DIN75078 (1985)	Road transport vehicles	Lap & torso	Sled test: frontal impact, 10g	No specifications for vehicles seating more than 12 seats
Sweden/ Regulations (1989)	Buses built after 1989, 12 seats maximum	Lap & torso with inertia reels	Static test: 5 kN for manual wheelchair	Wheelchair must remain steady
Australia/ AS 2942 (1987)	All motor vehicles	Lap & torso	Sled test: front, side, and rear impacts	Horizontal excursion of dummy hip point
Canada/ CSA-Z604 (1992)	Motor vehicles (other than passenger vehicles)	Lap belt required	Dynamic test: driving manoeuvres	Motion of wheelchair must be limited in any direction
USA/ ADA (1990)	All motor vehicles	Lap & torso	Sled test: 48 km/h, 20g - 30g within specified frontal impact corridor	Dummy head, hip and knee forward excursions; chair must not load occupant; entire system must remain intact, allow egress without the aid of tools

The objectives for the new standard should ensure the following requirements:

- *Occupant injuries are reduced to a minimum in an accident.*
- *The chair and occupant are held securely in place during the journey.*
- *Equipment is simple to fit, comfortable to wear, to provide the occupant with confidence and to incorporate an emergency quick release.*
- *Equipment is adaptable between different wheelchair designs and preferably uses common attachment points.*
- *Systems are affordable.*

1.4 Interlab Testing of WTORS

During the work on the standards, a number of key issues emerged so that further investigations are required. The main area of research centred on finding answers to the following questions:

- *What are the appropriate restraint systems?*
- *What are the appropriate crash conditions?*
- *What test protocol is required to ensure compliance of products?*
- *What is a satisfactory performance?*

A multi-lab comparison test was conducted to determine if the test protocol was sufficiently defined to produce reusable and reproducible results at different crash laboratories. This international laboratory study (interlab) also served to provide useful information regarding the relative effects of test parameters. Four laboratories participated in the interlab study: University of Virginia (UVA), University of Michigan Transportation Research Institute (UMTRI), Defence and Civil Institute of Engineering Medicine (DCIEM), and MURSEL. Four mechanisms have been applied to retard their sleds, each of which exhibited different shapes of deceleration-time characteristics. The interlab testing results are summarised in a paper (Roy et al, 1995).

The interlab study proved that wide crash pulse variations within the ISO corridor do not significantly affect response parameters such as loads, deceleration, and excursions. Although future investigation into the relative influences of peak sled

deceleration and velocity change (Δv) are necessary, the crash pulse specification (48 km/h) of the proposed ISO standard is sufficient.

The deceleration-time characteristics for each of the sleds achieved during the research programme was different. The UMTRI peaked early, followed by the MURSEL and the UVA later. The communication between the laboratories stated that these differences were due to a combination of different sled dynamics, wheelchair restraint systems. The most significant difference was the way in which the occupant restraints were anchored. The practice in the UK had been to use a shoulder belt attached over the shoulder to the floorboard whereas elsewhere was to mount the belt above the shoulder (B pillar), in a similar way to that in a car. The resulting downward force on the occupant from the floor-mounted configuration made the chair collapse. With the standard ISO 7176/19 to explore wheelchair performance, an industry test programme has been conducted to test a number of proprietary production wheelchairs to obtain a more accurate measurement of their crash performance and to contribute to the drafting of this standard.

1.5 MURSEL

MURSEL is the university centre for impact engineering in the research, teaching and commercial fields. In 1979, in collaboration with KL Automotive Products Ltd (now named Jeenay Plc who produced the world's first child safety seat for cars in 1962), a tracked moving sled indoor installation was built (Gregg, D.J. and Roy, P., 1983). The design is basically an improved version of the British Standards Institution (BSI) facility at its Hemel Hempstead site. The facility at MURSEL is hence ideally suited for conducting dynamic tests in accordance with the appropriate British and other European standards. The wheelchair crash tests in MURSEL started in 1982.

The impact test rig was constructed at the University's Hendon campus to test the performance of dummies and vehicle components during impacts representative of road accident crash situations without having to destroy complete vehicles each time. The test rig comprises a thirty-three (33) metre long track, one sled and the impact head, which is secured to an eighty (80) tonnes concrete impact block. The rail mount

sled propelled by bungees is decelerated using the appropriate European standard (ECE R44) polyurethane deceleration tubes and olives. The crash sequence is monitored using a high speed camera or video. Transducer outputs are recorded and displayed using PCs. Standard data processing techniques are employed during the analysis. The details of performance specification of the MURSEL facility are listed in Table 1.5.

Table 1.5 Performance specification of MURSEL facility

Parameters	Descriptions of ranges
Velocity change	A total sled mass of 1250 kg can be decelerated to 65 km/h. With a reduced mass of 520 kg, an initial velocity of 80 km/h is available.
Deceleration distance	Distances up to 1 metre are available.
Sled input pulse	The magnitude and the shape of the pulse is a function of the combinations of steel olives and polyurethane tubes or crumple tube dimensions. In particular the requirements of the dynamic tests to the standards can be met.
Test seats	Both adult and child seats are available, conforming to the appropriate standards.
Impact directions	Impacts can be carried out to simulate frontal, rearward, side and oblique crash conditions.
Instrumentation	
Dummies	Hybrid II and TNO-10 adult dummy, the range of TNO child dummies
Transducers	Appropriate transducers are available to measure the following parameters: Sled: stop Distance, velocity and deceleration (Endevco 7232C); Dummy: tri-axial chest and head acceleration (Endevco 7267A); Restraint: anchorage and strap loads (Denton gages and 'dogbone' load cells
Data recording	Signals received from the sled borne transducers via signal conditioning units are displayed on a computer. The signals are filtered using appropriate software. Twenty-four high speed A/D input channels are available.
Video camera	A Hadland Hyspeed S2 camera or a Kodak EktaPro high speed video motion analysis system are used to monitor dummy movement during impact.
Computer modelling	ATB/DYNAMAN, MADYMO, EASi-MAD, PAFEC
Static rig and the others	Static seat belt rig can apply static loads up to 35 kN to seat belt systems. Small impact rig consists of a sled mass which can be varied up to 25 kg. The mass can be accelerated to an impact velocity of 18 km/h. Wheelchair static rig is operated on behalf of TRL. Approval tests to the Code of Practice VSE 87/1 were carried out on this rig.

The Crash Victim Simulation (CVS) programs used at MURSEL are described in Appendix 1B. The research in WTORS is aimed at producing some significant advances in the production of a computer model in order to study the effect of the variation of appropriate parameters on the impact performance. This complements the test work that has been carried out in MURSEL and funded by the Department of Transport. The research programme has been part of the UK contributions in the areas of occupant restraint crash performance. The outputs of the research have generally been as research reports followed by papers submitted to national and international conferences (see Lists of Publications). The results of this research have also been used as the basis of proposals to write or amend the following standards: ISO/CD10542-1, ISO WD 7176-19.

On the commercial side, MURSEL is a centre that approves products to meet the requirements of national and international standards. It has carried out work for a number of organisations: Department of Transport (DOT), British Standards Institution, New Zealand Standards Institution and a number of companies: UNWIN, Sunrise, Britax, Irvin (GB), Klippan, MIRA, Peugeot, AB Volvo, etc. Some industry test results for WTORS and production wheelchairs are shown in Appendix 5A.

1.6 Research Programme

A literature review highlighted twenty years of wheelchair crash research, and showed that there were still many issues not fully understood. The original WTORS concept in ISO 10542 standard relies only on the shoulder belt being anchored to B pillar in frontal impact. The main parameters that are accepted as judgmental criteria for satisfactory crash performance were established for head and chest accelerations and their displacements.

1.6.1 Objectives

This research programme has been set to develop the expertise in three dimensional computer models to validate experimental results and accurately predict performance of occupant restraint systems. The computer models have been built up in order to

- analyse the dynamic performance of occupant restraint systems
- demonstrate and evaluate interactions between restraint systems and the wheelchair
- predict dynamic performance parameters of tiedown restraint systems
- evaluate the biofidelity of ATD dummies

1.6.2 Research flow diagram

The research has been conducted by the author through three tools as accident investigations, dynamic experimental testing and mathematical models (Figure 1.6). In this thesis, the initial four Chapters provide background information and most of practical work conducted in this programme. This includes a literature survey of related work and relevant worldwide regulations for WTORS. It continues with the presentation of work conducted to examine the various parameters, which affect WTORS performance and the injury potential of the occupant (Chapter 4).

Examination of the dynamic performance of WTORS was conducted both by impact tests and mathematical models. The experimental work was carried out at MURSEL. The mathematical model was conducted using computer software packages called ATB/DYNAMAN and MADYMO designed as Crash Victim Simulation (CVS) models, and a Finite Element Analysis (FEA) software called PAFEC used to model the wheelchair structure. Both techniques are described in general (Chapter 6 and 7) and then in more detail, specific to work conducted for this thesis in Chapter 8 and 9.

The CVS modelling includes the following sequences:

1. *Estimation of the initial kinematics and external forces reacting on the models, based on the analysis of real impact record from the video footage and accident investigations (Chapter 5, 6)*
2. *Preparation of elementary modelling of WTORS and its contacts (Chapter 7, 8)*
3. *Assembly of the elementary models into a proper simulation (Chapter 9)*
4. *Validation of dynamic impact tests (Chapter 10)*
5. *Assessment and analysis of crash performance of WTORS (Chapter 11).*

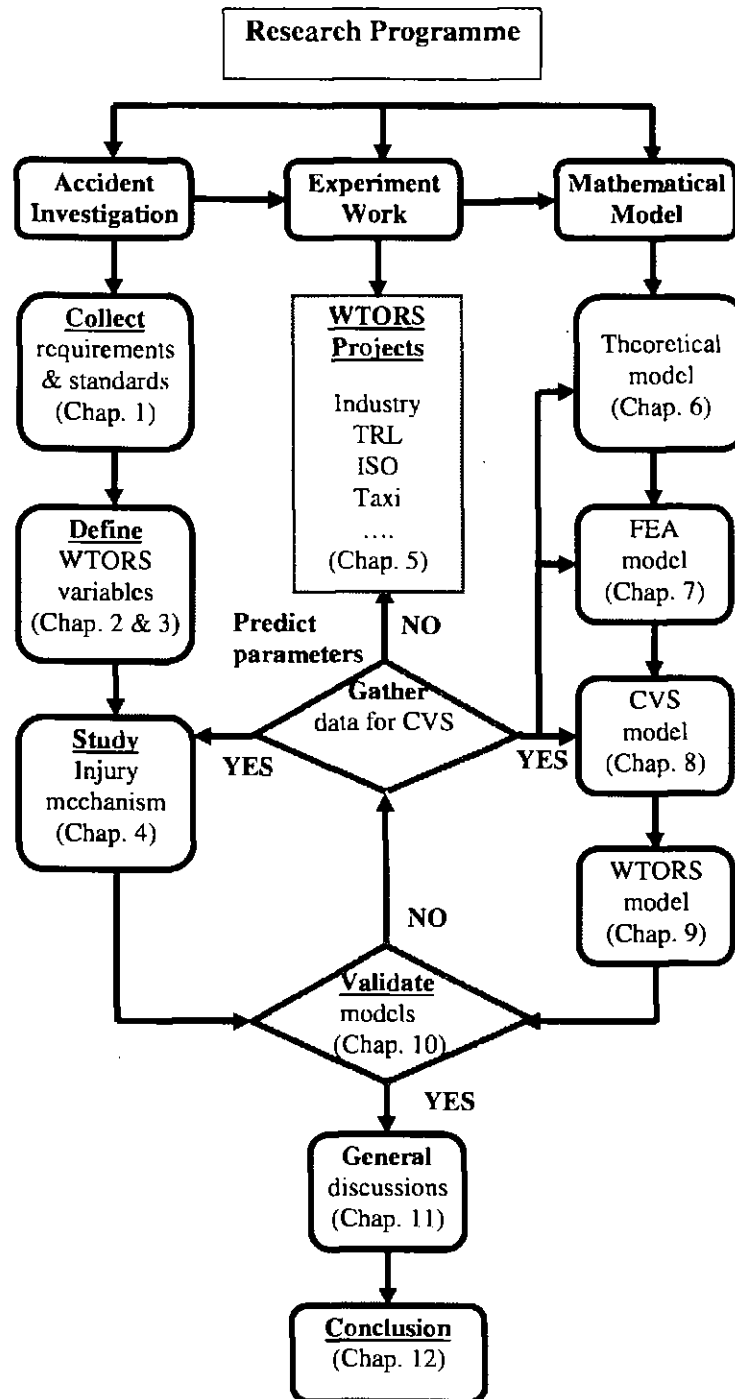


Figure 1.6 Research flow diagram

Results of the experimental investigation into the parameters which affect WTORS performance are interpreted in the relevant Appendix to Chapter 5

(Appendix 5A, 5B, 5C and 5D). The industry test (Group 1) was for production wheelchair crash performance survey. The TRL and ISO tests (Group 2 and 3) were conducted with surrogate wheelchairs design parameters to evaluate floor reaction forces and effect of diagonal strap anchorage configuration on occupant restraint system respectively. The taxi test (Group 4) involved production wheelchair and surrogate wheelchair to investigate the crash performance of a rearward facing wheelchair occupant system in frontal impact.

The results of CVS model validation of experimental work are presented in Chapter 10. The final two chapters (Chapter 11 & 12) draw together the results in a general discussion and conclusion of work. The discussion work was conducted using basic work-energy balance analysis methods.

CHAPTER 2: ELEMENTS OF WTORS

As currently defined in the draft ISO wheelchair standard (ISO/CD 10542-1, 1994), WTORS is a 'complete restraint system designed to provide effective occupant protection for motor vehicle drivers and/or passengers seated in a wheelchair'. It includes a system or device for wheelchair tiedown as well as a system for restraining the occupant.

In this Chapter the basic four elements of WTORS: wheelchair, wheelchair tiedown restraint system, occupant and its restraint systems are presented in Figure 2.0. The certain test configurations are compared. The crash environment for WTORS will be discussed in Chapter 3 and the misuse of WTORS effects on injuries will be discussed in Chapter 4.

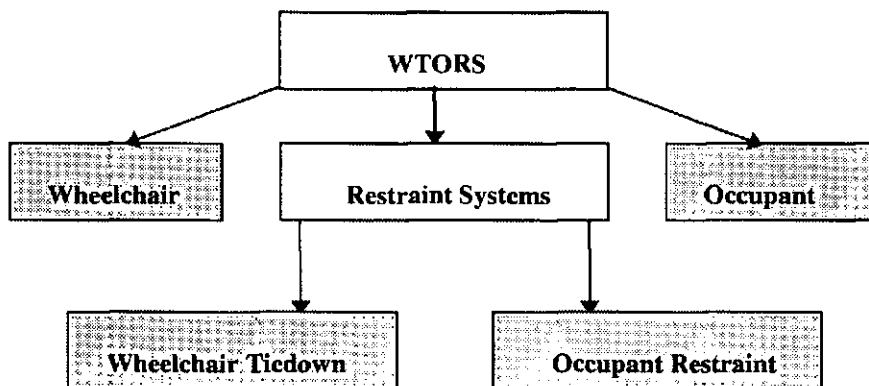


Figure 2.0 Four elements of WTORS

2.1 Wheelchair Structure

A wheelchair is a 'seating system comprising a frame, a seat, and wheels that is designed to provide support and mobility for persons with physical disabilities' (ISO/CD 10542-1, 1996). Many types of production wheelchairs have been used in WTORS testing in the past, such as standard manual wheelchairs, electrically powered wheelchairs, scooter-type wheelchairs, and special wheelchairs. As a result of these tests, the strong and weak points of standard wheelchairs have been determined, and

the performance of specific tiedown systems with certain chairs has been observed. Power wheelchairs are typically used in WTORS tests because the chair weight (approximately 85 kg) makes a representative loading case. Industry testing results (Appendix 5A) have revealed that for the some parts, the brazed frame of manual and powered wheelchairs could not withstand the forces generated in a 48 km/h (30 mph), 20g frontal impact.

For the purposes of WTORS acceptance and evaluation testing, the use of production chairs is not feasible. The extreme crash always results in a large amount of chair deformation and involves the high cost of replacing damaged parts. Another problem to use production wheelchairs involves deciding which models to use as there are many designs of unique weights and geometry. The use of various production chairs introduces too many variables.

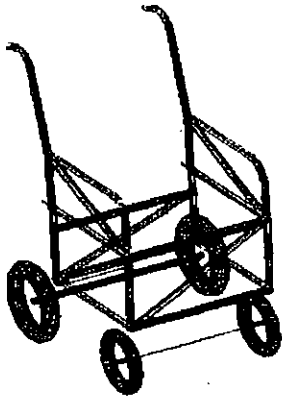


Figure 2.1a

TRL surrogate wheelchair

A solution to the problems associated with WTORS testing is the use of a reusable Surrogate Wheel Chair (SWC). SWC is a chair having the general dimensions, shape, and geometry of a typical standard production wheelchair, but suitably reinforced to ensure that the chair will not permanently deformed in a 48 km/h crash.

The reasons why a reusable SWC is needed are explained as follows:

- SWC is specified in the dynamic test for the Australian and Canadian WTORS standards (Standards Association of Australia, 1991, Canadian Standards Association, 1992), and has been adopted by ISO for their draft standards.
- SWC facilitates a standardised test, assuring that all WTORS can be tested repeatable within-lab consistency and reproducibly between-lab consistency. In essence, the surrogate wheelchair provides a level playing field for all WTORS.
- SWC presents a worst case loading severance for systems as it is rigid. Since the chair does not permanently deform, i.e., dissipate energy, the entire energy management of the crash could be sustained by the restraint systems.

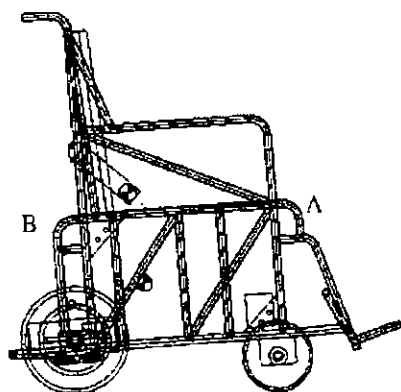


Figure 2.1b
ISO surrogate wheelchair

The Australian surrogate wheelchair has skids in place of wheels (no wheels). The Canadian chair's 51 mm tubular diameter frame appears grossly over designed but it is in compatible with docking system hardware. One of the SWC designed by the Transport Research Laboratory (TRL) in the UK was selected in this research programme (TRL-SWC in Figure 2.1a). The design for the chair was based on standard powered wheelchairs in the UK. The TRL design was adopted because it provides a more realistic simulation of power wheelchairs. It has an industry standard 22 mm diameter tubular frame. The extra masses were attached to the chair so that the total chair mass was 85 kg. It is the average mass of standard power wheelchairs as determined in a survey for the Canadian Standards Association (CSA).

Another surrogate wheelchair used in this research programme was the ISO wheelchair (ISO-SWC in Figure 2.1b). It was found 50 mm (2") higher than TRL surrogate wheelchair. A modified ISO surrogate wheelchair was designed and fabricated for the purpose of sled testing. The tiedown hardware attachment is an important modification. In the new design of ISO-SWC, two solid attachments or opening points (A and B in Figure 2.1b) were provided on the wheelchair front and rear.

2.2 Wheelchair Tiedown Systems

A wheelchair tiedown is 'a device or system designed to secure a wheelchair in place in a motor vehicle' (ISO/CD10542-1, 1996). The wheelchair rests on the floorboard of the vehicle and is secured either by a manual tiedown connection or by an automatic connection system. The tiedown anchorage was either locked into rails or bolted to the floorboard. Two configuration designs (type I and II) of wheelchair tiedown restraint system were tested dynamically in the UK (Roy et al. 1995). Type I restraint (floor mounted) used the various anchorage rails with a lap belt only. Type II

is a system using an adjustable A-type frame, which it is placed at the back of the wheelchair in sockets on the floorboard and roof of the vehicle. The wheelchair can then be held onto the A frame either by webbing or by clamps. Loads transmitted through the wheelchair can result in its frame collapse. As the frame failed, the loads of the wheelchair restraint increased with the possibility of sudden failure. Modifications to the wheelchair structure can delay the start of failure. The floorboard structure in the vehicle must be sufficiently strong not only to hold the restraint anchorage but also to withstand the reaction forces through the wheelchair wheels.

Five generic categories have been adopted in the wheelchair tiedown system:

- (1) *Rear locking system (Rearlok) and U-shaped bracket*
- (2) *Easy Locking device (Easilok)*
- (3) *clamping device*
- (4) *webbing belt*
- (5) *docking system*

The rear locking system (Rearlok), developed by UNWIN Safety System Ltd, is a restraint attached to the backrest of the wheelchair. It holds the wheelchair securely without the need for additional attachments on the front of the wheelchair. Rear locking system includes a horizontal member located directly below the cross members of the chair, which spans from the left side to the right in a wheelchair. The horizontal member supplies pressure at these two points on wheelchair when the vertical component of the T-bar is clamped to the vehicle floorboard.

U-shaped bracket systems consist of U-shaped brackets locked to two vertical bars of the wheelchair. The wheelchair is secured in this system by moving the chair backrest against the restraint members. Two bars are entered in the structural slot by placing a rod or pin through the U-bracket. This system has been tested initially in dynamic sled testing in production wheelchairs, and all types have performed poorly, due mainly to the fact that the attachment points (bars) are one of the chair's weakest structural members.

The easy locking device (Easilok) is the latest wheelchair and passenger restraint in the UK. However, many studies have documented their poor performance in the crash environment. Their deficient crash protection is most likely due to the fact

that a single vertical member is responsible for restraining the entire system. Also, since the restraint relies on downward pressure, the mechanism for restraint often forces the chair to start deforming.

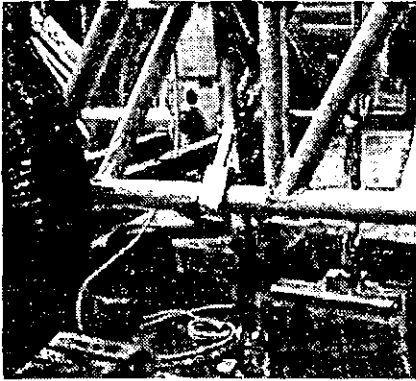
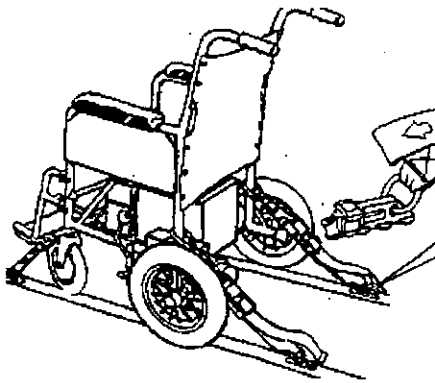


Figure 2.2a Clamping device

The performance of wheelchair was further investigated by the use of clamp. A wheelchair clamping device consists of a hook, which is connected to the vehicle floorboard by a pin jointed bracket. The wheelchair restraint is accomplished by fitting the hook around the tubular frames of the chair (Figure 2.2a). The attachment rods are sometimes added to the wheelchair to provide attachment points of sufficient rigidity. These systems, which require considerable operator assistance, are far more popular in UK than four strap tiedowns but have the disadvantage of concentrating the loads in the wheelchair structure.



**Figure 2.2b
Webbing restraint (4 point)**

Belt systems are generally considered as the most effective and crashworthy of the wheelchair tiedown systems (Schneider, 1979). These systems consist of adjustable straps, which either hook onto the wheelchair or loop around structural members for securement. The belt systems are typically configured in a four-point symmetrical arrangement, usually with two attachment points in the front and another two in the rear. The belt securement to the vehicle is usually accomplished by connection to track fittings mounted to the floorboard of the vehicle. Positive aspects of this system include good crash performance, excellent adaptability to a wide range of wheelchair models and it is easily adjusted. A drawback of these systems is their large space requirements.

The 4-point webbing belt (Figure 2.2b, Karabiner type) was developed by UNWIN Ltd. The wheelchair is positioned over the rail and brakes applied. Two front straps are attached to wheelchair and clipped to the rail. Two rear straps are hooked to the wheelchair as high up the centre of gravity in a wheelchair as possible.

Docking systems involve hardware mounted to the underside of the wheelchair that latches into hardware on the vehicle floorboard. This restraint system is relatively new, and as a result, has not been crash tested as extensively as the other systems. An advantage of docking systems is that they take up no more room than the wheelchair itself. Another advantage is their ease of use, the user just needs to roll the wheelchair into position and lock it into place. A disadvantage of this system is that it is not easily adjusted and expensive.

The webbing belt tiedown system is the most common in use in the world. Acknowledging this, WTORS standard was based on this tiedown system in an effort to encourage manufacturers to use these designs. In the following Chapters, the webbing belt tiedown system will be further investigated.

2.3 Occupant

The primary reason for the occupant investigation in WTORS study is to provide the loading paths and interactions with the wheelchair so that the potential for occupant injury could be investigated (Chapter 4). Cadavers have been used extensively in automotive crash testing and in WTORS research as well (Kallieris, et al, 1981). It was believed that cadavers pose a higher level of biofidelity compared to Anthropomorphic Test Dummies (ATD), and consequently, offer a more accurate assessment of injury severity. Unfortunately, it is nearly impossible to accomplish repeatedly with human surrogates since no two cadavers are alike.

Unlike cadavers, ATD can be precisely calibrated and set-up for a given test, thus assuring excellent control of an important test variable. Another major advantage of ATD is that they could generate the loads and loading paths of the human occupant and mass distributions of the human body so that occupant kinematics can be approximated. They provide a tool for assessing the likelihood and severity of injuries resulting from a crash. To accomplish this accurately, ATD must provide a human-

like response to the crash environment and contain integral instrumentation to quantify the responses of different body regions.

Since WTORS evaluation testing should provide a typical case loading environment, the adult-sized 50th-percentile male dummy (75 kg) is specified in ISO standard. In this program, two types of adult ATD were used in WTORS crash research, TNO-10 and the Hybrid II. TNO-10 dummy was developed by TNO (addendum 15, ECE R16, 1990) and was used to test the wheelchair and its restraint systems. Since the primary purpose of testing is to provide the loads and loading paths generated during a wheelchair crash, standard dummy instrumentation used for injury assessment was not required.

Hybrid II was developed by General Motors in 1972 (Foster, et al, 1977). The new version of Hybrid II, called Hybrid III, was developed in 1977. It more closely resembles human response in the head, neck, and chest, and provides measurements of chest deflection and femur loads. Hybrid III can be used to provide a much better assessment of injury due to secondary impacts compared to the Hybrid II.

2.4 Occupant Restraint System

The fourth element of WTORS, the occupant restraint, is defined as 'a system or device designed to restrain a motor-vehicle occupant to prevent ejection and prevent or minimise contact with the vehicle interior components during a crash' (ISO/CD 10524-1, 1994).

The question is why safety belts should be used. The consequences of the impact on the occupant depend upon the deformation characteristics of the object struck. The object of all interior safety devices is to reduce the force applied to the body as much as possible by absorbing the maximum proportion of the original kinetic energy of the occupant. Clearly we want to spread the absorption of this energy over the greatest possible distance and greatest interval of time. The safety belts can be used to improve this to some extent. Further analysis has shown that maximum protection can be achieved when the belts stretch uniformly at constant load.

In the UK, automotive seat belts came onto the optional equipment market in the early sixties, conforming to a British Standard (BS3254, 1960). In 1965, the car

manufacturers were obliged to provide anchorage points for front seat belts. The front belts became compulsory items in cars and minivans purchased from 1967 onwards. The compulsory wearing of front belts was imposed on January 1983. The seat belt has achieved a sustained high level of public awareness and compliance. The concept of the passive restraint emerged, in which the occupant is automatically protected, for example, by a belt arrangement which moves into effect when the door is closed, or by an inflatable cushioning device to be triggered in an impact, i.e. the airbag concept. The lap and diagonal (L/D) self adjusting impact sensitive configuration is now the accepted form.

A typical wheelchair occupant restraint consists of both an upper torso restraint and a lower torso restraint. The upper torso restraint may be in the form of a traditional shoulder belt or a shoulder harness. The shoulder harness is a double inertia reel and stalk system with independent lap and diagonal shoulder straps for maximum security and comfort. Straps are provided with lockable clips that may be set to alleviate strap pressure on the occupant. The reel assembly is fitted with a shield to protect the plastic covers of the spring chambers from damage. Both components are mounted on the unique lockable rail fittings for ease of installation and removal, and can be securely clamped to the track to avoid rattles. The system has been fully tested and certified in accordance with Section 3.3 of Practice VSE 87/1 for lap and diagonal safety harness.

The upper anchor points of the upper torso restraint are located on the wall of the vehicle (B or C pillar), and the lower anchor points may be attached on the rear tiedown belt securing the wheelchair (integral securement), or direct to the vehicle floorboard (independent securement). The lower torso restraint is the traditional lap belt, whose function is to provide pelvic restraint for the occupant.

Independent securement refers to the case when the occupant is secured independent of the wheelchair. Integral securement refers to the case when the occupant restraint is anchored to either the wheelchair tiedown or the wheelchair itself. The independent securement requires the wheelchair tiedown to restrain less load. A drawback of independent securement is the possibility of the wheelchair loading the occupant during the event (Schneider, 1979; Kallieris, et al, 1981). This

occurs when the wheelchair tiedown is more compliant than the occupant restraint and the wheelchair is allowed to move more than the occupant. Consequently, wheelchair restraint is accomplished through the occupant restraint, which could increase the likelihood of severe occupant injury and require the occupant restraint to withstand a greater load than it was designed for. This fit is difficult to achieve with independent securement because of wheel interference.

In the integral securement configuration, the lap belt portion of the occupant restraint is anchored to the wheelchair tiedown or the wheelchair itself. This arrangement would eliminate the possibility of the wheelchair loading the occupant during the crash (Kooi and Janssen, 1988). It also allows a better fit of the lap belt over the pelvic bones of the occupant's lower torso. This is important because when the lap belt does not traverse the bony pelvis correctly, occupant submarining may occur, allowing the lap belt to ride up over the occupant's abdomen, leading to severe internal injuries. A study in 1981 at the University of Heidelberg using cadavers noted that a poor lap belt fit resulted in a liver injury (Kallieris, et al, 1981). A drawback of this configuration is that the load path is redirected from the occupant restraint through the wheelchair tiedown, requiring the wheelchair tiedown to withstand the inertial load of the occupant as well as the chair.

Many researchers concluded that independent securement is the optimal method, since the wheelchair restraint is responsible for securing only the wheelchair (Schneider, 1979). Although occupant restraint loads are not a main performance requirement of the compliance test, manufacturers may want the occupant restraint loads to be monitored. Load histories give manufacturers an idea of the magnitude of the loads experienced by their systems, and can aid in the improvement or redesign of their systems. In the following Chapters, the independent restraint configuration will be considered.

2.5 Surrogate WTORS

The use of a surrogate WTORS was a logical solution, both from an economical and a practical view.

2.5.1 Surrogate WTORS for FFF impact

The surrogate system was designed to ensure that the wheelchair and its occupant would be effectively restrained in a 48 km/h Forward Facing Frontal (FFF) impact. The design of the surrogate tiedown system enabled easy measurement of wheelchair tiedown loads, something that is very difficult to do when using commercial tiedown systems. Also, the design of the surrogate tiedown enabled pre-tension to be performed easily and precisely. Finally, the surrogate WTORS minimised test costs and allowed the control of a key test parameter, as the webbing belt could be replaced easily after each test. This allowed an easier analysis of cause and effect relationships.

In this research programme, a surrogate WTORS was designed and fabricated for the purpose of initial testing and test protocol development. The surrogate system consisted of a 4-point belt wheelchair tiedown and a 3-point occupant restraint system. The wheelchair rear tiedown was designed with two segments of 1320 mm-long, 50 mm-wide polyester seat belt webbing (11% elongation) maximum rated for 14.5 kN on each side of a shoulder belt (portside or starboard) in the crash severity of 48 km/h FFF impact. The shoulder webbing belt was constructed using a continuous length of 50 mm-wide webbing (11% elongation) and a 75 x 75 x 75 mm³ block for slack adjustment. The webbing belts have viscous-elastic characteristics that produce a velocity sensitive response. In addition to the section of webbing, each wheelchair rear tiedown leg consisted of a buckle for slack adjustment and a tension load cell (Denton) for tiedown load measurement. Since the primary purpose of the tiedown load is to provide the loads generated during impact, the front tiedown instrumentation used for load measurement during rebound was not required.

2.5.2 Surrogate WTORS for RFF impact

The design of the Surrogate framed Taxi Restraint System (STRS) to evaluate WTORS in Rearward Facing Frontal (RFF) impact was based on a London taxi (see Chapter 5). Computer modelling of the STRS was used in conjunction with this frame.

The belt types chosen for use with this taxi were:

- A surrogate belt, one standard webbing belt was attached to both anchorages with two standard reel-mounting brackets. This allowed greater movement of the wheelchair and belt route.
- A static lap belt with 25 mm (1") slack was used to restrict the movement of the wheelchair.

The methods of parameter variation for the various phases are itemised below:

- (1) The variations in a wheelchair centre of gravity were achieved with two different types of wheelchair, ISO-SWC and a manual wheelchair.
- (2) With or without handles in a manual wheelchair.
- (3) A modified headrest was bolted on the taxi bulkhead, allowing the head to be contacted onto required position.
- (4) Belt route could be changed by various holes placed in the side plates.

The details of the STRS will be discussed in Chapter 5.

CHAPTER 3: WTORS CRASH ENVIRONMENT

This Chapter outlines the research methodologies in the field of wheelchair and occupant crash environment, including model of simulation, crash simulator, test conditions, visual recording of movements, instrumentation and signal control system.

3.1 Modes of Simulation

The problem with some simulations is to find a correlation of a static load to the actual dynamic load paths in a given crash severity and to consider how the simulations represent the real crash.

3.1.1 Static and dynamic testing

Static testing involves applying a constant force to a structural member at a relatively low rate over a long period of time. Dynamic testing involves a force application of short duration (approximately 100 ms in WTORS sled tests) at a high rate.

Initial wheelchair tiedown evaluation testing involved static tests (Orne, et al, 1976). Historically, manufacturers designed their wheelchair restraints based on simple static calculations: restraint force = mass of chair times peak vehicle deceleration, and then tested their systems based on these force levels. Unfortunately, a static analysis invariably underestimates the loads generated for given crash conditions. This is due to the fact that a static test oversimplifies the crash, and can not account for phenomena unique to the dynamic environment, such as the acceleration amplification effect (see Chapter 11). A tiedown restraining a 85 kg wheelchair undergoing a 20g vehicle deceleration generated a horizontal force greater than 17 kN. The shortcomings of static testing also involve the force point of application. Ideally, the force point of application should be at the weakest point in WTORS system, however this location is never obvious due to the complexity of the entire system. Another problem of static testing involves how to determine the

direction of force application (load paths). During the actual crash, load paths in three directions are created. It is impossible to predict all of the load paths analytically using the inherent over-simplifications of static testing.

Since the early 1980's, dynamic testing has become the acceptable mode of testing WTORS in the United States (Schneider, 1979; Red, et al, 1982), and around the world (Kallieris, et al, 1981; Kooi and Janssen, 1988). Dynamic testing exposes systems to real-world crash environments. It also reveals modes of hardware failure, such as webbing belt rupture at the area of high stress concentration, which static tests could never reveal. In a supporting for the use of dynamic evaluation testing in the Dutch standard, Kooi and Janssen (1988) refer to the instance where a system passed a 16 kN quasi-static test but failed a 48 km/h dynamic test because stress concentrations were created due to inertial loading of the chair and its resulting deformation. There are a lot of important performance parameters, such as wheelchair and dummy excursions, chair and dummy interactions which could be evaluated only in dynamic testing. It is widely recognised that the secondary collision, the impact between the occupant and the interior structures of the vehicle resulting from occupant excursions, is the primary cause of injury and death in an accident. This could only be evaluated by dynamic crash.

For the reasons outlined above, a dynamic test has been specified for the evaluate WTORS in the ISO standards. However, dynamic testing is costly and time consuming. In an attempt to eliminate the need of dynamic testing of WTORS, attempts have been made to find a correlation between static and dynamic testing experimentally. A simple relation coefficient could be determined using computer simulation.

3.1.2 Front, rear and side impact

Evaluations in the direction of impact are performed for front, rear, and side impacts. The Australian standard, Wheelchair Occupant Restraint Assemblies in Motor Vehicles, specifies a forward, rearward, and side impact test (Standards Association of Australia, 1987). Statistical data suggested that frontal impacts comprised the majority of accidents, and should be the primary focus of WTORS

research and development. According to the National Highway Traffic Safety Administration (NHTSA) Traffic Safety Facts 1992, frontal accidents comprised 63% of all fatal accidents and 52% of all injurious accidents (NHTSA, 1992). A complete breakdown is found in Figure 3.1.

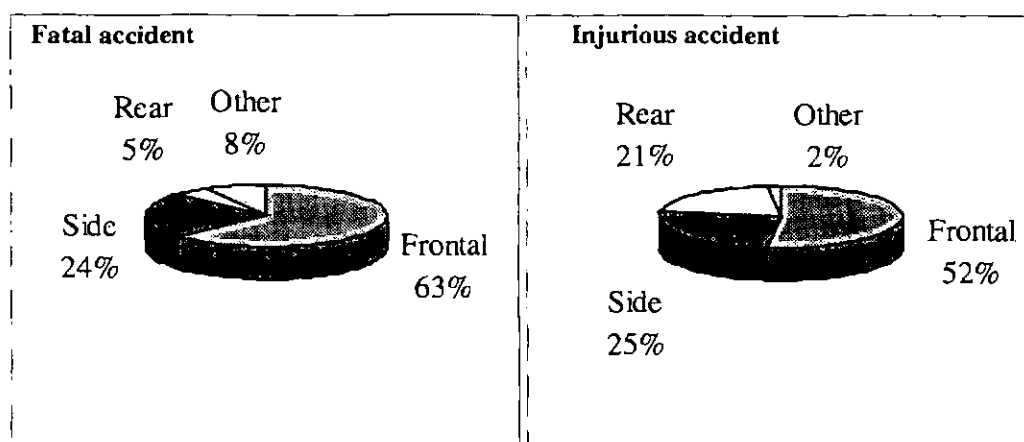


Figure 3.1 Breakdown of fatal and injury accidents (NHTSA), 1992

Extensive research has determined that the wheelchair and occupant should always be oriented parallel to the direction travel, either facing forward or rearward (Kooi and Janssen, 1988). Researchers also emphasised that when using rearward facing orientation, it is imperative that a headrest be provided to limit the flexure of the head in the case of a crash. Side-facing wheelchair orientations perform poorly in crash tests due to the inherent lateral instability of the chair and the tendency of the frame to fold up and tip over (Schneider, 1979).

Based on the current requirements for occupant protection in the automotive industry, wheelchair occupant sitting positions both in Forward Facing Frontal Impact (FFF) and Rearward Facing Frontal Impact (RFF) are the exclusive mode of testing in this research programme.

3.1.3 Vehicle and sled testing

Dynamic tests can be either using vehicle, when an actual vehicle is crashed into a barrier, or using a sled, when WTORS system is mounted on a test rig and crashed using a non destructive deceleration technique.

In vehicle tests, hardware costs are high as a new test vehicle is required for every crash. Sled testing provides a mechanism for conducting tests without destroying the test platform. Also the set-up time for sled tests is shorter than for vehicle tests. While vehicle tests are real life, there is a level of uncertainty associated with each test that makes it a difficult tool to use in a research and evaluation environment. There are structural differences in vehicles even of the same make and model. The poor ability to control key test parameters like crash pulse and test set-up makes it very difficult to produce repeatable and reproducible results in vehicle tests. Sled tests offer a much more controlled environment. The most important input parameter of the dynamic test is the deceleration time history or crash pulse, which can be reproduced more easily in a sled test compared with a vehicle test.

Because of these drawbacks associated with vehicle testing, using a sled is the acceptable mode of dynamic testing. However, the accuracy of sled testing has been questioned. Is sled testing adequate for providing a real life crash environment? What requirements should the sled crash pulse meet in order to achieve a representative simulation? How does the crash pulse affect the results? These will be discussed in the next few Chapters.

3.2 Crash Simulator - Sled

To evaluate the crash performance of WTORS system, a dynamic sled test has been evolved. The system is anchored to the sled which is impacted with a velocity change of 48 (+2,-0) km/h. To exhibit a satisfactory performance the system must demonstrate structural integrity, reasonable operation and excursions within a defined envelope. This section outlines one part of the apparatus used to simulate the dynamic crash environment: the sled.

The sled deceleration could be achieved by different systems. UVA's sled deceleration is accomplished by a probe contacting metal bands that lie across the track. UMTRI uses a rebound sled that impacts a pneumatic spring. The velocity after rebound is approximately equal to the velocity at impact. DCIEM and Millbrook use HYGE sled, which accelerates a stationary system rearward with a pneumatic cylinder

(Gilkey, 1983). MURSEL's deceleration is accomplished via conical probes extending from the sled carriage that insert into tubes mounted at the end of the track.

3.2.1 MURSEL rig

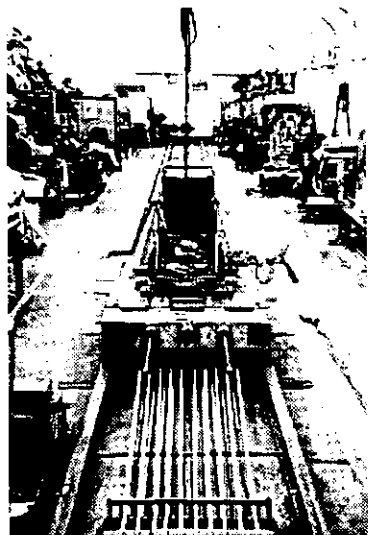


Figure 3.2a MURSEL rig

The impact rig facility at MURSEL consists of a rail mounted flat bed trolley (sled) restricted to only one degree of freedom (linear). The test sled has a run-up distance of 20 metre (33 metre track) and is capable of accelerating payloads of 682 kg to 80 km/h (50 mph). The platform is pulled backwards by a cable and electric winch and stretched by ten rubber cords (bungees), which enable the trolley to be accelerated towards the retardation device at a predetermined rate (Figure 3.2a). When the platform is released, the rubber cords accelerate the sled to the required velocity. At the point of impact, the sled has attained a constant velocity and is no longer subject to acceleration imposed by the bungees. The sled was pulled back a certain position (start length) by bungees and released by a bomb release. The start length is the distance from a reference position to the polypropylene tubes. This length has been predetermined from experience. The larger this distance is the greater the sled velocity can be achieved.

3.2.2 Sled test platform

The simulation of a selected occupant restraint condition is achieved by bolting the experimental assembly on the flat frame of the moving sled. The added assembly would generally comprise a seat structure, an anchorage frame appropriate to the particular restraint, the restraint system itself, e.g. lap and diagonal adult belt, and an instrumented dummy. A flat plate represents coach or minibus floorboard. A 105 kg mild steel plate has 1200 mm (48") long, 1200 mm wide, and 25 mm (1") thick. The underside of the plate is reinforced with 76 x 102 mm² steel tubing. An upper anchorage frame (52 kg), which is constructed with 50 x 102 mm² steel tubing,

was bolted to the platform to provide the upper anchorage point for the shoulder belt (Figure 3.2b).

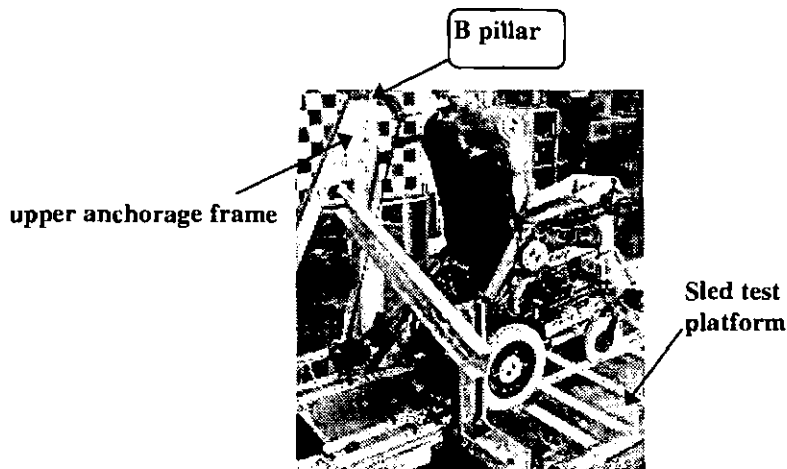


Figure 3.2b Sled test platform with upper anchorage frame

A highly rigid platform was chosen so that it would not deflect during the crash event, ensuring that the crash pulse of the sled was transferred to the wheelchair-occupant system without attenuation. This presented a worst case load scenario since it required the restraint system to absorb most of the energy associated with the crash. A disadvantage of rigid floorboard in WTORS compliance testing is that they may not always reveal a particular tiedown propensity for disengagement since there is no deflection at anchorage locations.

Preliminary tests conducted on the platform alone verified that the platform effectively transmitted the crash pulse to the system. The sled pulse (measured on the sled carriage) and the platform pulse (measured on the plate) were nearly identical. The small z-acceleration on the platform (up and down motion) indicated that the plate did not introduce significant vertical accelerations to the system. The platform chosen for this research did not contain interior vehicle components because the proposed ISO standard does not require the simulation of dummy contacts with the vehicle interior. The issue of occupant protection is addressed in the proposed ISO standard in terms of maximum allowable excursion limits (Appendix 1A).

3.3 Test Conditions

The severity of the crash environment determines the velocity change and deceleration, which a system would have to withstand. In automotive and wheelchair crash testing, the crash pulse determines the crash environment and provides a direct, visual statement regarding the severity of the crash event. A quantifying measurement of vehicle crash pulses was introduced and derived from the vehicles stroke time history by Matsui in 1976. The vehicle's stroke is the integral of the velocity time history, and gives a measure of the crush or displacement of the vehicle.

3.3.1 Crash pulse

The crash pulse, termed as the vehicle deceleration time history, is a direct relation to the severity of the crash event. A more difficult question to deal with the impact simulation is what the actual deceleration pulse is. Simply specifying the impact velocity is not enough. The amount of sled stopping distance (vehicle crush) for a given pulse shape should also be known before the peak acceleration is achieved. As the amount of information regarding actual vehicle deceleration pulses is very limited, the mean deceleration (in g's) could be estimated for a half-sine pulse shape in the following formula:

$$D_m = \frac{(\Delta v)^2}{2gS} \quad (3.0)$$

where Δv is the velocity change in m/s, S is the sled stopping distance in metres. Linear acceleration is often more conveniently in units of g's. One g is the acceleration caused by gravity. 0.8 g is heavy braking for a car. When the undeformed part of the car goes from 48 km/h to zero crashed into a rigid barrier in a distance of 0.61 metre (2 feet) produces a mean deceleration of 14g.

In vehicle impact, there are two components of the crash pulse. The first is the velocity change, or Δv . The second is acceleration or deceleration. In the previous study (Gu J., Roy P. 1994, 1995 and 1997), peak sled deceleration levels and Δv were varied to study the effects of both velocity and deceleration on typical outputs such as

floor reaction forces or wheel loads, wheelchair seat loads and head excursions. The previous study concluded that the magnitude of the constant velocity of the sled at impact had a greater influence on wheelchair damage and dummy injury than the peak level of deceleration.

(i) Velocity change (Δv)

The Δv is defined as the difference in vehicle velocity immediately before and after the main impact or crash event, and is given by the following relation:

$$\Delta v = |v_e - v_0| \quad (3.1)$$

where: v_e is the sled velocity immediately following impact, v_0 is the initial sled velocity. An extreme case is when a very heavy truck and a small relatively lightweight car collide head-on, with both vehicles initially travelling at 48 km/h. The truck will continue to go forward at a slower speed, while the car will reverse direction. The result is that the truck Δv will be less than 48 km/h and the car Δv will be greater than 48 km/h. For most sled testing, as there is rebound in the crash event to varying degrees, the Δv are always greater than the initial velocity of the sled. Also as it is very difficult to determine the rebound velocity of the sled accurately, direct interpretation of the sled crash pulse is the preferred technique of calculation Δv :

$$\Delta v = \int_t a(t) dt \quad (3.2)$$

where: $a(t)$ is the acceleration time history or crash pulse. Δv is not directly related to the force levels experienced in a crash and is related to the total energy of the crash. The kinetic energy, K , is the amount of energy represented by a moving mass and given by:

$$K = \frac{1}{2} m(v_e^2 - v_0^2) \quad (3.3)$$

This is an important consideration in WTORS design and testing, because the kinetic energy of the event should be managed effectively by the restraint system, and consequently, could have a significant affect on the failure of mechanical components. This consideration will be made to analysis the impact phenomena in Chapter 11.

(ii) Acceleration or deceleration

The second component of the crash pulse is the rate of velocity change, that is, acceleration or deceleration.

Acceleration is the rate of velocity change and is normally given the symbol 'a'. Negative acceleration are often referred to as deceleration, i.e. where the magnitude of the velocity decreases. Vehicle manufacturers would like to keep the deceleration pulses as low as possible and ideally a square pulse if they could. Crumple zones in vehicle have the effect of absorbing energy and lowering the pulse.

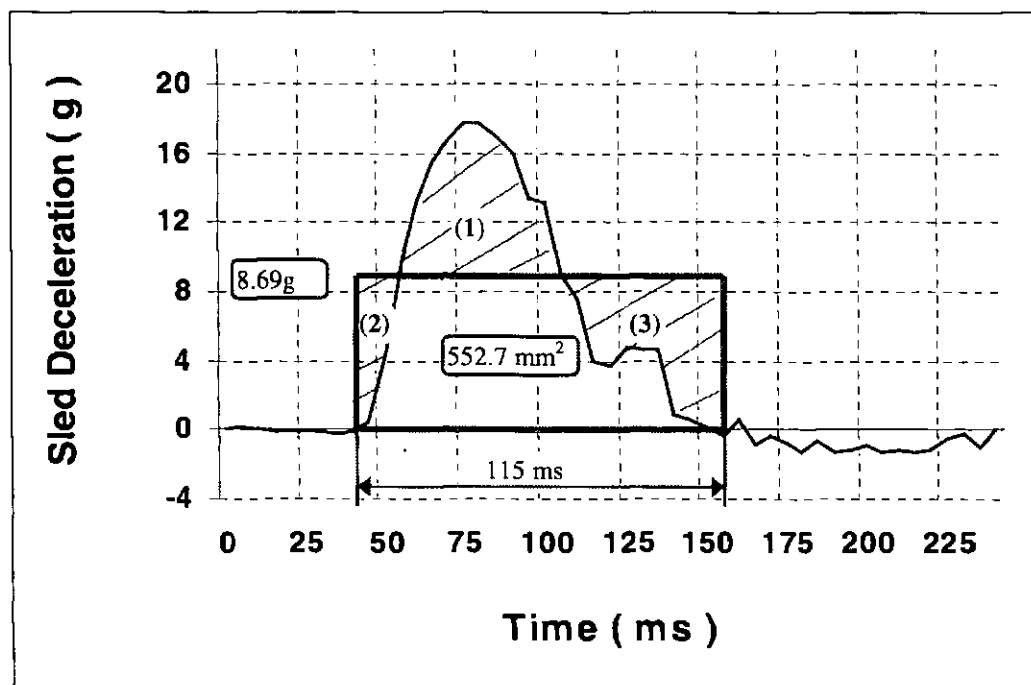


Figure 3.3a Acceleration variation

A constant acceleration was assumed to simplify our calculations. However dynamic experimental results indicated that acceleration varies appreciably. Figure 3.3a shows a typical variation in which the rectangle frame line indicates the constant

deceleration required bringing the sled to rest in the same time. It was measured by a fixed arm planimetre (series no. 35015). The maximum deceleration (18g) is much greater than in the constant deceleration case (approximately 8.69g) and the risk of serious injury is therefore greater. The area (1) equals total area (2) and area (3). The total area of the rectangle is 552.7 square millimetres.

3.3.2 Two deceleration regimes: ACT and PTT

The level of the peak vehicle deceleration is due in large part to the crush characteristics of the vehicle. A vehicle with a short crush zone will have relatively less time to undergo the Δv compared to a vehicle with a large crush zone. A larger crush has the effect of reducing the crash event and lowering the peak deceleration experienced by the vehicle. According to Newton's Second Law, acceleration is directly proportional to force. Thus the deceleration level of the crash event (measured in g's) is a direct statement on the forces required to restrain the occupant. The 'g' level provides a rough estimate of what the restraint forces would be for a given wheelchair-dummy system, due to the acceleration amplification effects.

The nature of the deceleration pulse experienced by the sled is commonly referred to as the sled pulse. It reflects the deceleration pulse experienced by the safety vehicle during an accident. Two deceleration regimes were employed at MURSEL, Aluminium Crumple Tubes (ACT) and Polyurethane Tapered Tubes (PTT).

In order to approximate the impact of a vehicle, ACT are employed to reproduce the effect created by the crumple zone of the vehicle. ACT are aluminium cylinders with 1 metre long, 75 mm (3") diameter and 1.87 mm (0.075") wall thickness, which buckle axially when struck by the sled. The buckling force generated is approximately constant, yielding a roughly constant deceleration of the sled. A sled pulse of this type is clearly the most desirable for secured victims of an accident to an optimum level of deceleration and associated loading as it has the minimum peak value.

For practical reasons of cost and repeatability, the internally tapered polyurethane tubes are widely used, in particular for approval purposes. The PTT is held within steel sleeves that are rigidly fixed to the impact block. A probe (one metre

long), which is attached to the front of the platform, has a tapered steel ball (olive) on the end (Figure 3.3b). The olive has a larger diameter than the tapered hole in the tube and is guided into the tube as the sled approaches.

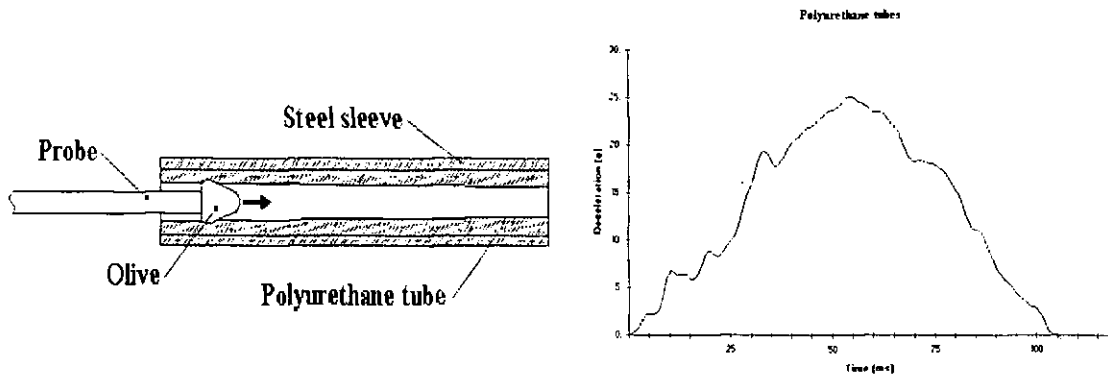


Figure 3.3b Section through olive/tube assembly Figure 3.3c Sled pulse from polyurethane tubes

The PTT absorbs the sled energy by quasi-plastic deformation as the olive is forced down the tube length. The tube will recover to its original shape in twenty-four (24) hours. It provides a repeatable method of sled deceleration pulse, which is roughly sinusoidal in shape. The number of tubes depends upon the mass to be retarded. Corrections have to be made for changes in ambient temperature, sled mass, velocity and tube wear in order to achieve the consistent deceleration.

The sled pulse, which is achieved by the PTT, approximates to a half sine wave in form to represent an actual vehicle deceleration pulse. Figure 3.3c details a typical sled pulse achieved by use of polyurethane tubes. The PTT testing is the defined method of sled deceleration in the European seat belt standard (ECE R16, 1994).

3.3.3 ISO corridor

Choice of a suitable crash pulse is a function of the vehicle in which WTORS system is being carried. Initially four generalised crash pulses were considered which are displayed in Table 3.3. These are usually quantified by the velocity change (ΔV) of the vehicle and its peak deceleration, although vehicle mean deceleration may be a better predictor of impact severity in many cases. As a result of discussion in interlab testing of

WTORS, the car pulse was rejected as too severe, and a pulse close to type 2 was adopted.

Table 3.3 Vehicle crash pulse types

Vehicle Type	Pulse Type	Velocity Change (ΔV) km/h	Peak Deceleration g
Car	1	50	32
US minivan	2	50	26
European Mini Bus	3	32	20
Large Transit Bus	4	32	10

The European Child Restraint System (CRS) approval standard ECE R44 calls for dynamic testing in frontal impacts to be conducted using a sled pulse whose parameters fall within a pre-defined envelope. Figure 3.3d details the approval envelope for ECE R44 test pulses. The deceleration limits are defined in terms of corridors, which specify overall pulse duration (120 ms), maximum deceleration level (28g), rate of onset, and a minimum time for which the deceleration should be at a certain level.

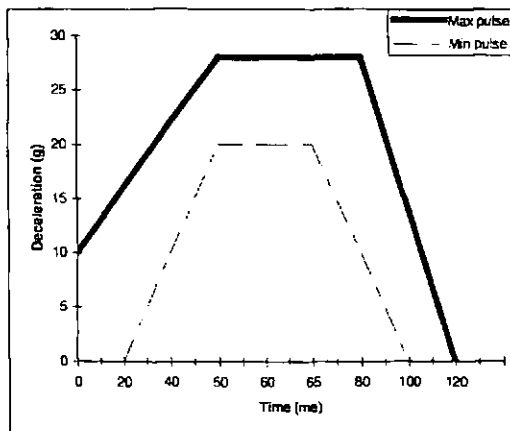


Figure 3.3d ECE R44 envelope for frontal impact

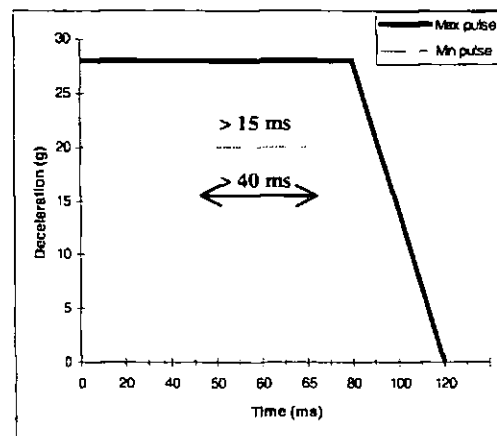


Figure 3.3e ISO corridor

Currently for WTORS, the accepted deceleration corridor (Fig 3.3e) is the one adopted by ISO. The ISO corridor is based on the deceleration time histories resulting from frontal barrier crashes of minivans travelling at 48 km/h and the ECE R44 envelope. This corridor is consistent with the Australian and Canadian standards in

which it specifies a peak deceleration larger than 20g for a minimum of 15 ms, and larger than 15g for 40 ms (ISO/CD 10542-1, 1996).

3.4 Visual Recording of Movements

Relative movements are defined as the total forward displacement of a point relative to the starting position. How does the occupant's head and body move? How does the wheelchair flex? How did the seat belt, buckle and tiedown restraint perform? These questions can be answered by high speed camera or high speed video, which is linked to a computer and can be instantly assessed frame by frame.

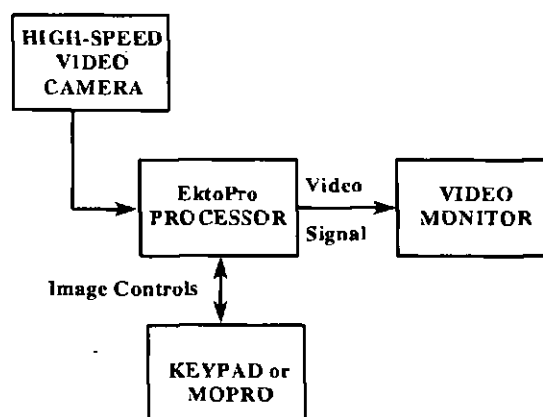


Figure 3.4a High speed video analysis

The high speed cine camera (Hadland Hyspedc S2) was used at a rate of 500 frame per second (fps) with 16 mm colour negative cine film (Eastman 7292). Scaled measurements were taken using a calibrated graticule on each frame of the film. High speed video analysis was conducted and the side view of the crash event was recorded by using Kodak EktoPro 1000 analyser, operating nominally up to 1000 fps. The 500 fps speed was used in this research programme to allow chair and dummy positions to be determined at least every two milliseconds. This system comprises one video camera linked to the main recording and processing unit (Figure 3.4a). The digitised images from the camera are recorded in real-time on a specially designed video tape cassette, which is loaded in the main unit. The video image (black and white) is composed of a 240 x 192 pixel array with 256 gray scale levels for clear

differentiation. Once it is recorded in high density tapes, a playback of the event is available for immediate analysis.

Measurements of the recording can either be directly made in pixels using a menu-driven keypad or scaled measurements using a PC based motion program called MOPRO. When the impact frames are recorded, the object movement during impact can be analysed by using the vertical and horizontal cursors and the time between each frame (Figure 3.4b). Accuracy of the measurements is limited by the number of pixels, which create the image, and definition of two objects with similar scales. Typically the best accuracy of this system is ± 8 mm although it depends upon how close you zoom into the measured object.

Comparing of high speed video analysis methods, the cine film yields high quality colour images which allow greater accuracy of measurement. However the cine film could not be viewed during a test series, and also does not allow for simpler transfer of measurement data to other PC software packages. In this research programme, high speed video analysis was used. A lateral recording of the crash was also recorded by normal VHS camcorder being placed at a sufficient distance from the track to minimise the effects of lens distortion and parallax. Unfortunately, an overhead view was not recorded for the assessment of gross dummy and chair movements because of the limitations of MURSEL facility.

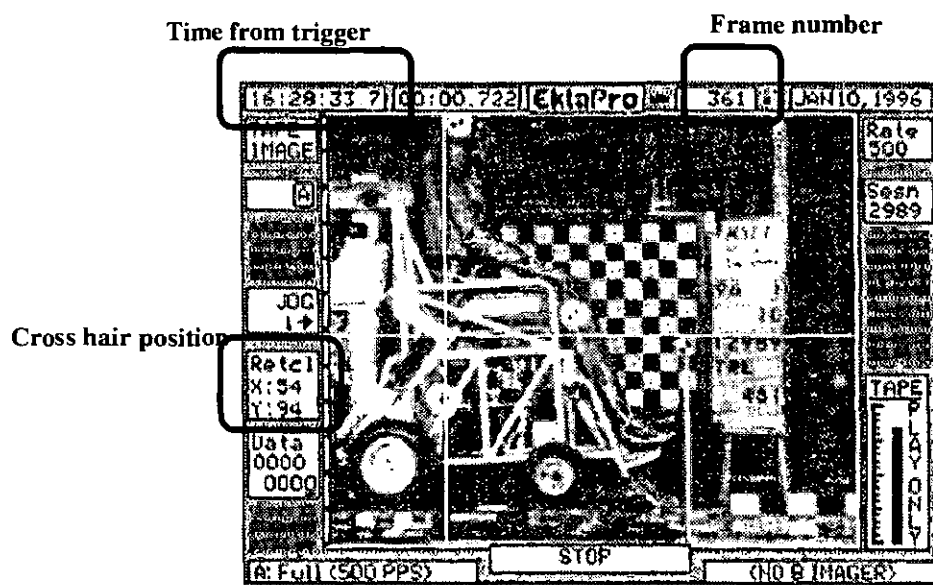


Figure 3.4b Kodak EktaPro motion analyser

3.5 Instrumentation

All components in the dynamic test system, such as the sled, wheelchair, occupant, and restraint systems should be suitably instrumented to record and evaluate the dynamics of the crash event. This section outlines the instrumentation for each component of the test system and the methods used to acquire and process the deceleration, loads, and excursions in order to characterise the event.

3.5.1 Sled

The sled platform was instrumented with one uni-axial accelerometer (Endevco Piezo-resistive Shock Accelerometers, 7232C). This accelerometer was placed at the rear of the platform and approximately at the centreline to record the deceleration time history, that is, crash pulse of the event.

A photo-optic speed trap was used to record the sled velocity just prior to impact. One-metre bar on the side of the sled passed through the trap and blocked the light sensor located on one side of the trap. It triggered a digital counter to record the total time of the blocked light. Once the bar has fully passed through the trap, the counter stopped. The final readout indicated the time when it took the sled to travel one metre (second per metre). From this, the sled velocity change could be converted:

3.5.2 Wheelchair

A tri-axial accelerometer (Endevco Type 7267A) was placed on the centre of gravity of the wheelchair to record the acceleration time history of the chair during the event. As the direction of sled travel (x-direction) is the principal direction of interest, the wheelchair acceleration is always measured in this direction. The lateral acceleration is y-direction and vertical accelerations is z-direction. The acceleration gives a indication of the wheelchair tiedown ability to secure the chair without excessive movement during normal travel.

The floor vertical loads under the wheels of the chair were recorded using cantilever wheel load plates. Because there is a movement of the chair during the crash event, a transducer is required having a relatively large surface area over which

wheel loads can be measured accurately. Details of the design of this load cell are described in the Appendix 3.

On the chair, the reference point 'P' and the centre of gravity (CG) were tracked by high contrast photo targets. The point 'P' is defined as the centre of a 100 mm-diameter circle that sits tangent to the intersection of the chair's backrest and seating plane. The P-point was adopted by ISO from the Australian standard to serve as a convenient point for tracking the movement of the chair. A piece of white tape was stuck transversely across the floor plate used to limit parallax errors in the measure of the horizontal displacement of the wheelchair.

3.5.3 Test Dummy

Two tri-axial accelerometers (Endevco, Type 7267A) were placed in the dummy chest and head respectively for measuring of dummy chest and head accelerations. The local x, y, and z accelerations were recorded. The resultant acceleration was determined, given by

$$a = (a_x^2 + a_y^2 + a_z^2)^{1/2} \quad (3.4)$$

The resultant acceleration is standard practice since the orthogonal directions by themselves are of limited value. Their co-ordinate frame of reference is changing with time due to the forward rotation of the head and chest during the crash.

In order to measure the movement of the dummy during the crash, the photo targets were placed on the dummy head and knee. Whenever possible, a photo target was placed at the hip. Unfortunately, this point was usually obscured during the crash by the wheelchair frame or the dummy's lap belt. On the dummy, the head CG, the Forward-Most Point of the head (head FMP), and the knee were tracked. The FMP of the dummy is defined as the point above the nose that is most-forward at any given time. All movements were referenced to their positions in the platform frame of reference.

3.5.4 Restraints

A very important output parameter in WTORS test is the time history. This measurement could be made relatively easily for belt type wheelchair tiedown. In this research programme, precision 'dogbone' type load cells (Appendix 3) were placed in series with the MURSEL surrogate webbing tiedown. This allowed an accurate measurement of the load time history for the rear tiedown. The extreme loads on each side of rear tiedown in Level III crash severity for TRL tests were found in excess of 14 kN. On the right side (starboard) between the hip and the floor anchor point of the L/D restraint system, a 'dogbone' was installed for FFF impact.

To measure occupant restraint loads, 'Denton' type belt load transducers were also used. The shoulder belt Denton was placed between the upper anchor point (B pillar) and the point where the belt goes over the left shoulder. On the left side (portside) between the hip and the floor anchor point, a lap belt 'Denton' was also placed for FFF impact.

3.5.5 Calibration

All accelerometers were calibrated on a regular basis by the traceable laboratories. The 'dogbone' load cells and cantilever wheel load plates were calibrated on-site using a calibrated universal testing machine. Calibration factors were verified on a regular basis prior to testing. Each instrument was calibrated prior to using and monitored during the test to ensure the validity of the signal.

3.6 Signal Control System

The instrumentation used at MURSEL conforms to SAE recommended practice J 211 for instrumentation of impact tests (SAE J211, 1987) and the data acquisition processing is shown in Figure 3.6.

3.6.1 Data Acquisition Processing

During impact, data is read from transducers, such as accelerometers, 'dogbone' and 'Denton' load cells, etc. These transducers are supplied with an input voltage (transducer excitation, usually 10 VDC) to match the input sensitivity of the

data acquisition device by the EMI-SE1054 signal conditioning unit. This unit is linked with transducers by twelve umbilical cords (channels) extending from the platform to the control room. It also provides amplification of the analogue output signal.

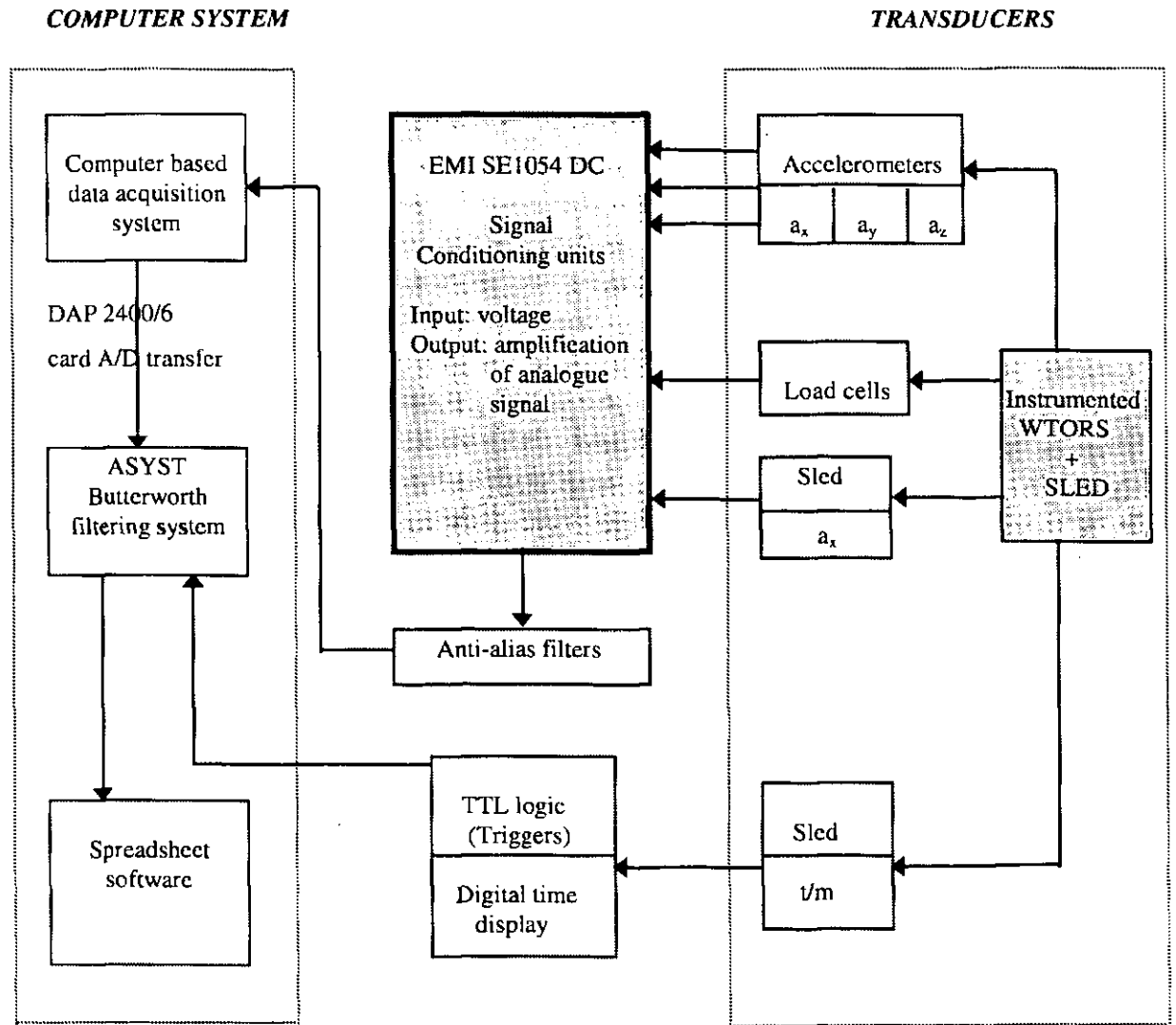


Figure 3.6 Data acquisition processing at MURSEL

The signal is then passed from the signal conditioning units to Kemo anti-alias filters (low-pass 4 kHz, pre-set required dependent upon sample rate) and then into the data acquisition system. The low-pass filters are used exclusively for anti-alias, at a cut-off frequency (filter) of 100 Hz for the sled (CFC60). Once amplified, the signals

are converted into a 12-bit digital word by the digitiser. The digitised data (in millivolts) could then be downloaded to the PC.

The data acquisition system comprises a Microstar acquisition card (DAP 2400/6) which is mounted in a PC computer. The data acquisition card converts the analogue signal to digital form. A software package called ASYST (version 4.01, DOS based) is used to control the cards and analyse the data. All test signals are recorded by real-time digitisation at the sampling rate of 10 kHz per channel (set to ± 2.5 volts). The sampling time is 400 ms to give 4000 data points per channel, so it can be imported to a spreadsheet (Quattro Pro or Excel program).

3.6.2 Filters

Analogue signals measured during experiments usually need to be low-pass filtering before being digitised and recorded. There are some forces of resonant vibration caused by WTORS, which is excited and usually needs to be filtered out before an underlying shape can be seen. The higher frequencies should also be filtered out to give an approximate acceleration pulse. When determining the peak acceleration of WTORS, filtering gets rid of any spikes caused by spurious noise. There are three reasons for filtering as follows:

- (1) to prevent alias errors during subsequent sampling
- (2) to reduce high frequency environment noise
- (3) to remove high frequencies that are considered not important for the phenomena being studied.

Sampling is initiated by a trigger generated by the velocity gate circuit. Of this total sampling time, approximately 45 ms is pre-trigger at the crash severity of 32 km/h. Digital filtering of the data is conducted by ASYST program using a Butterworth filtering system and the data is also converted by multiplication with a calibration factor. The acquisition times and duration data are stored in ASYST and plotted a graphic for a single test.

In the CVS models, it is important to conform to an accepted standard in order to enable comparison of data from different sources. The low-pass filters available in MADYMO are defined of Channel Filter Class (CFC) (SAE J211, 1987). Among the

specifications by the SAE J211 Draft, there are four filters, denoted as CFC60, CFC180, CFC600, and CFC1000. The lower the CFC number, the lower the cut-off frequency of the filter. In MADYMO model the cut-off frequency divided by the CFC number is somewhere between 1.67 and 1.98. For simplicity, all transducer output was filtered to CFC180 (300 Hz).

CHAPTER 4: RESTRAINT INJURY MECHANISMS IN WTORS

4.1 Introduction

The field of injury biomechanics deals with the effect on the human body by mechanical loads, in particular impact loads. Also the biomechanical response would experience due to the mechanical and physiological changes and injury would take place if the response is beyond a recoverable limit. Injury criteria are normally defined as a biomechanical index of exposure severity, which indicate the potential for impact. Many injury criteria are based on accelerations, forces, displacements and velocities. Some injury criteria need a mathematical evaluation of a time history signal.

Quantitative studies have been made for injury description, injury mechanism, the severity index and tolerance limit. Many schemes have been proposed for ranking and quantifying injuries. Anatomical scales describe the injury in terms of its anatomical location, the type of injury and its relative severity. The most well known worldwide-accepted anatomical scale is the Abbreviated Injury Scale or Accident Injury Scale (AIS). This scale is used by engineers to code the severity of injuries. The AIS distinguishes the following levels of injury:

- 0 *no injury*
- 1 *minor*
- 2 *moderate*
- 3 *severe (not life threatening)*
- 4 *serious (life threatening but survival probable)*
- 5 *critical (survival uncertain)*
- 6 *maximum injury (cannot be survived)*
- 9 *unknown*

Unfortunately AIS is difficult to evaluate the injuries associated with forces used in impact engineering analysis. An engineering approach to injury analysis of WTORS includes many physical and biomechanical factors influencing the restraint system. It is difficult to assess the importance of these factors in the absence of in-depth investigation of the following five crash factors in WTORS:

-
- *Vehicle crash severity*
 - *Wheelchair design*
 - *Restraint system performance*

The restraint system performance includes restraint design features such as anchorage geometry, webbing areas, webbing material elongation, force limiting energy absorbing devices, retractor behaviour and pretensions, etc.

- *Occupant factors*

Occupant factors that contribute to injury tolerance include stature, weight, age, gender, obesity and pre-existing health conditions. In this research programme, these factors were considered and based on the ATD dummy database.

- *Usage variables*

The usage variables could be pivotal to successful belt performance, such as anatomical positioning, pre-impact position and belt slack, etc.

Currently little in-depth data exists concerned with injuries to wheelchair occupants in vehicle accidents. The restraint injury mechanisms in WTORS has not yet been addressed by current engineering requirements although several suggested mechanisms for the healthy occupants have been made by different researchers (Mertz et al 1967, Simpson and Foret-Bruno et al 1991, Bandstra, Lawson and Lundell et al 1998). In order to be able to know what engineering facts to investigate in WTORS, the simulation results and the results of the injury mechanism research in WTORS need to be evaluated. A new comparative injury parameter, Δa , is proposed in this programme and defined as the deviation between the peak resultant acceleration force applied to the chest and head in the ATD. It has been used to estimate the potential for a particular injury mechanism and then to evaluate the designs for a wheelchair and its restraint system.

The computer modelling program, MADYMO3D (Appendix 4) has been used to perform injury parameter calculations, such as, Head Injury Criterion (HIC) for head injury, 3 ms Criterion (3MS) for thorax injury, the resultant belt loads and seat loads for shoulder injury or spinal injury. These were carried out on the linear acceleration signal of a selected ATD body. The HIC and 3MS indices for assessing possible head and chest injury were computed from the resultant linear accelerations.

4.2 Restraint Injury Mechanisms

The most important vehicle crash safety innovation, which should contribute to injury reduction in wheelchair occupants, is the proper use of WTORS restraint systems, such as, wheelchair tiedown system, lap and diagonal seat belts, head restraint and wheelchair backrest.

Four important sites of possible injury related to WTORS restraint systems are the head, neck, thorax and lumbar region. This research also considered that disabled people in WTORS could be difficult to sit in their seating positions due to wheelchair backrest inclination. Questions are:

- How misuse of restraint systems can lead to restraint injury?
- How the loads imposed on the neck are transferred to loads and deformations of individual tissues of the neck?

These questions have been answered by injury mechanism analysis. The computer model and dynamic sled tests contributed to a better understanding of the following injury mechanisms.

4.2.1 Head injury

Head injury could be caused by translation, rotation, flexion or extension and direct impact. The direct impact has been researched at Wayne State University (WSU) (Lawson et al, 1998). The Wayne State Tolerance Curve (WSTC) is a head injury tolerance curve, which is based upon the assumption that linear skull fracture is linked to brain damage. The basic question is what happens when a head hits a flat plate, i.e. unrestrained occupants.

At present the head injury is predicted by the HIC:

$$\text{HIC} = \left[\frac{1}{t_2 - t_1} \int_{t_1}^{t_2} a(t) \cdot dt \right]^{2.5} (t_2 - t_1) \quad (4.1)$$

$n=2.5$ is weighting factor, based on a straight line approximation to the WSTC plotted on a log-log base between 2.5 ms and 50 ms, t_1 and t_2 are initial and final time during which HIC attains a maximum value, $\mathbf{a} = \mathbf{a}(t)$ is the resultant head acceleration

measured at the head CG. It can be calculated from the linear acceleration signal of the centre of mass of the head (LINACC).

This equation attempts to use mathematical functions to approximate the WSTC. It is estimated that the HIC of 1000 represents 8.5% risk of death from head injury. HIC has been effective in reducing of the risk of head injuries by the resulting levels of translation accelerations experienced by the head. Unfortunately this criterion neglected the effect of rotational acceleration on the severity of brain injury.

Recent pathological studies have found that brain damage is not necessarily linked to skull fracture (Simpson, et al 1991). Studies have also demonstrated that HIC deviates from the WSTC at pulse duration above 15 ms. To reduce the risk even further there is a need for even more sophisticated safety systems and products. This requires a better understanding of the biomechanics of head injury and the use of improved HIC. In this programme, the headrest effect on the physical head injury has been investigated by a response envelope for Hybrid II dummy head resultant accelerations in the following example.

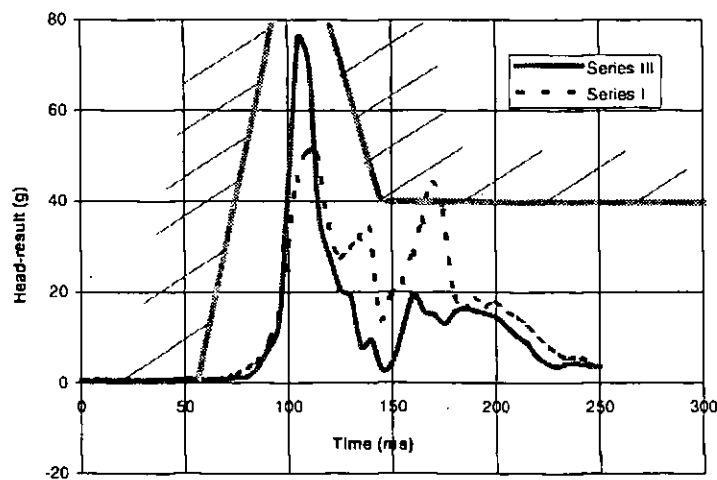


Figure 4.2a A response envelope of head resultant accelerations in RFF impact of WTORS

Figure 4.2a compares two traces of head resultant acceleration in a manual wheelchair without headrest (Series I) and with headrest (Series III) in a Rearward Facing Frontal (RFF) impact. Here the calculation was focused on the first peak. The

second peak response was at a relatively low level and was due to the secondary contacts, in particular in test Series I (without headrest). The bold straight line enclosed a response envelope. This type of response was used to determine a strategy for achieving low HIC values. For example, the wheelchair backrest restraint structure could be designed to give a square pulse with a maximum of 80g to control the initial peak. The low-density material in headrest should be used to avoid the inertial spike. In this case, the post peak response must be maintained below 40g.

4.2.2 Neck Injury

The neck consists of seven (7) cervical vertebrae. There are adjacent vertebrae separated by discs of tissue and stabilised by fibrous tissue (ligaments). The neck injury mechanisms are defined by forward flexion, rearward bending and extension. Neck injury biomechanical analysis suggests that shear forces on the neck are important in flexion prior to the chin contacting the chest. If the chin contacts the chest, it would cause a lower level of force to be developed in the posterior neck muscles. In addition the chin is parallel to the shear forces and hence aids the acceleration of the head.

Rear impact accounts for most diagnosed neck injuries. There are three parts of the head-neck motion during a rear-end collision: retraction, rearward angular velocity of the head and hyperextension. The neck injuries result in localised neck pain. Hyperextension injuries to adults have not been reported in accident studies as a high frequency event. Children in the CRS in which a crotch strap has not been used, submarining and fracture have occurred (Lowne et al, 1987).

AIS 1 minor neck injuries have been reported in all crash configurations. However the risk of sustaining a neck injury is higher in rear impacts as compared to other crash types. The prime injurious event is the forward flexion of the neck caused in FFF impact by the sudden deceleration of the torso held by the seat belt, in particular if no slack given in the shoulder belt.

The stiffer chair backrest of ISO surrogate wheelchair could cause rearward bending of neck during RFF impact. This could result in the force exerted on the torso by the chair backrest and hence the acceleration of the torso relative to the head being higher in the early stages of motion. The use of headrest with higher force/deflection

characteristics than that of the chair backrest could make neck forward flexion worse as they gave the head more rebound acceleration from the torso during RFF impact. This could be resolved by the use of energy absorbing foam both in the headrest and backrest.

Another alternative mechanism for neck injury indicates that the most harmful event occurs early in the motion sequence when the occupant head is moving backward relative to the shoulders. This produces shear forces, especially in the uppermost vertebrae, as the neck distorts into S shape, and this could also happen in frontal impacts (Walz et al, 1995; Minton 1998). The transition from the S shape to the extension mode involves a sudden change in the volume of the spinal canal. The pressure gradients induced by the sudden and rapid flow of blood and spinal fluid along the canal and through the associated transverse vessels could result in damage to the spinal ganglia.

4.2.3 Thorax Injury

Two types of injury happened in the thoracic area, ribs and internal organs. Rib fractures are not dangerous in themselves, but they cause more serious injuries if they puncture internal organs. The most serious case is a rupture of the thoracic aorta, which it is considered to be caused by compression between the sternum and the shoulder belt.

Thoracic criteria could be measured by 3MS, chest deflection, chest acceleration and shoulder belt load. Chest deflection limits are based on AIS 3 and a median clarifying age of 45 years (Table 4.2). 3MS is the highest acceleration level that is exceeded during at least 3 ms. It was achieved from the linear acceleration signal at the location of the thorax accelerometer (LINACC).

Table 4.2 Chest deflection limit

Occupant size	Sternum deflection limit (mm)
5th percentile female	60
50th percentile male	75
95th percentile male	90

The difficulty of measuring chest deflection has led to the adoption of chest acceleration as a criterion. Mertz (1967) reported that an instrumented man dropping onto a thick mattress from 17.4 m height experienced 46g chest accelerations. Federal Motor Vehicle Safety Standards (FMVSS 208) specifies 60g for dummies in seat belts, ECE R44 (child restraint systems) specifies a resultant of 55g and a 'z' component of 30g. From Foret-Bruno (1991) report, for occupants less than 30 years, no injury was found at belt loads less than 7.3 kN, for occupants above 50 years of age, fractures began at 4.2 kN. It should be noted that the results in the current research are for the people who are healthy, not disabled and lower values would be expected for older wheelchair occupants.

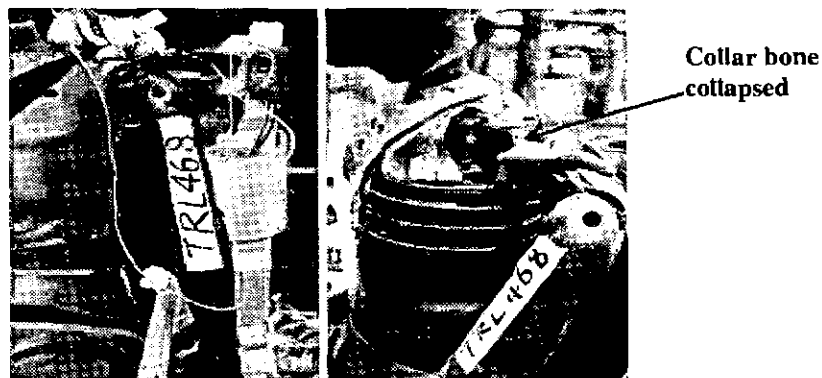


Figure 4.2b The dummy collar bone collapsed during FFF impact

In the FFF impact of WTORS, some yaw rotation of the torso was found due to lack of symmetry of the belt system on the torso. This could be inferred from the different amount of extension of the arms. The shoulder load calculations (Chapter 11) indicate that the dummy's shoulder loads in the floor-mounted configuration is 6.14 kN, which is about double values of the B pillar case. Figure 4.2b shows that the shoulder belt collapses the dummy's collar bone during FFF impact (B pillar configuration in ISO test). It suggests that at a crash severity 34 km/h, 20g, the occupant shoulder injury could be reduced if the shoulder load was limited to 5 kN.

4.2.4 Lumbar Injury

Various types of injury are frequently associated with a particular type of restraint system. The lumbar spinal and abdominal injuries often identified with lap

belt forces applied above the bony pelvis. As seat belt system usage has increased, seat belt injuries have been complained to be the result of acceleration forces being directed through the webbing belt to the underlying anatomical structures of the occupant (Bandstra, et al 1998).

The lumbar injury was found to be correlated with wheelchair backrest inclination in FFF impact. The excessively laid back seating posture was not accepted. However some disabled occupants have to incline their seats to keep their positions properly. This result gives rise to the question: what would have happened if the wheelchair backrest was inclined? If the backrest was gently inclined, the gap between the shoulders and the wheelchair backrest would be greater than that between the lumbar area and the backrest. The lumbar area would experience localised acceleration forces before the upper back. Another mechanism could be that the stretching of the spine axial caused the pelvis accelerate much more rapidly than the thorax in the horizontal direction due to the torso being inclined from the vertical.

In the FFF impact, TRL and ISO test results suggested that lumbar spine injuries have been shown to be associated with use of L/D 3-point belt due to flexion of the torso, while the pelvis was held relatively static. The rebound from the belt would result in the occupant impacting the chair backrest in the same way as it does. If the chair backrest was inclined, or no front tiedown used on wheelchair or front tiedown angle over 45-degree, it would experience the same localised loading of the lumbar region. This rebound contact with the chair backrest from a FFF impact would be much milder than the case in a RFF impact of equivalent severity. However, in practice, FFF impacts generally tend to be more severe than RFF impacts, so the risk of lumbar strain injury to an individual may be poorly correlated with impact direction. The tests and computer models also suggested that an occupant wearing a 3-point belt would acquire some rotational motion relative to the pelvis and thighs in the early stages of the impact, as the unrestrained shoulder moves further forward than to the restrained point like B pillar. As the occupant rebounds from the belt, this rotation would continue until it was damped out by contact with the chair backrest. An occupant with a highly inclined chair backrest is therefore likely to achieve a much greater angular displacement of the shoulders relative to the pelvis/thighs before their rotational motion is reduced. It is therefore bad for the lumbar spine.

4.3 Restraint Injury Prevention

The restraint injury is most relevant to the positions in the occupant, such as thorax and head. It was verified by measuring the dummy's acceleration in sled tests using standard chest and head accelerometers. The dummy-chair interaction was investigated by pancake type load cells. The neck accelerometer will be used for further investigation of restraint effect on dummy neck injury. The pelvis accelerometer will help to investigate dummy lumbar injury.

The acceleration forces applied to the head and torso were found to be quite larger in the surrogate wheelchair. In order to prevent wheelchair rebound at the end of the impact sequence, the corresponding deformation of the chair backrest must occur plastically (not elastically). The soft cushion on the headrest would not be compatible with this requirement unless the head is allowed to sink through it before significant acceleration force is applied to the torso. The headrest must also not be built on the chair as the wheelchair itself is movable during impact. A well adjusted headrest, which could be built on a fixed seat, would result in less severe injury than a badly adjusted one. An effort to research in restraint injury mechanisms resulted in the following injury protection guidelines and engineering requirements.

- ***Restraint systems***

Several general injury reduction principles could be identified with the restraint system design. Webbing belt systems with proper restraint design features are expected to limit to the extent practicable movement and reduce neck injury. Usage variables are expected for optimising belt performance. Headrest design should be improved to reduce occupant head acceleration. Head movement should be limited relative to the torso to an even greater extent than that required to prevent gross hyperextension. The chair backrest and headrest should geometrically support the curvature of the back and neck of occupant as precisely as possible. It will be not only achieved by positioning the occupant as close as possible to the wheelchair backrest and headrest, but also by designing a smart restraint system, such as a well adjustable headrest, and a tiedown restraint system with dynamic loading characteristics.

- ***Dummy model***

The biofidelity of the present dummy is such that none of injury parameters could accurately be considered to represent a true occupant response. The shape adopted by a seated occupant's back would be different from the specification of preferred shape for the hard frame structure in the surrogate wheelchair. The situation occurred where localised sections of the spine were in contact with much harder structures than adjacent areas of the back. If the chair follows the shape of the occupant well, this characteristic will tend to restrain the body evenly and thus allow minimum relative movement between the head and spine.

Few dummies exist today that would give an appropriate response of spinal injury in a crash test. A direct impact of the sub-system test should be conducted to determine the local distribution of force/deflection characteristics throughout the wheelchair backrest and headrest in order to simulate a human spine interaction with chair backrest. A mathematical model written in MADYMO3D with a segmented spine, as well as engineering judgement should be developed to minimise relative movements between adjacent vertebrae and the relative joint, i.e. the curvature of the spine should change as little as possible during the impact.

- ***Wheelchair design***

Wheelchair backrest material and structure should be improved to minimise the head and neck injury. This could be satisfied by using better energy absorption in the chair backrest. At present, no wheelchair design satisfies this requirement. Only a higher hysteresis chair backrest model was conducted by computer models. A quasi-static sub-system test of the wheelchair backrest was added during the initial engineering phase.

4.4 Injury Parameters

The philosophy for improving the occupant restraint performance in this work was to reduce Injury Parameters, such as 3MS, head excursions and the Δa , based on the following arguments:

- *What should we consider a reliable dummy response?*

-
- *What should we measure during the crash test?*
 - *What should we estimate the potential for a particular injury mechanism to be?*

The ATD used in this programme was instrumented with two tri-axial accelerometers, one in the upper torso and the other in the head. Three orthogonal traces from these accelerometers were studied individually and the resultant accelerations were also measured. The chest resultant 3 ms acceleration was used to assess the occupant restraint performance during experimental testing. The dynamic response rate was higher as the dummy was much more rigid than a human body. Acceleration traces exhibited many high spikes, due to this higher response rate. The higher peaks of these traces that were seen in the dummy response were generally neglected and only the three millisecond (3 ms) value was taken. The 3 ms value was calculated by neglecting acceleration peaks of total summed width 3 ms, moving a horizontal line down the acceleration curve until all the peaks crossed, occurred in a total time of 3 ms. A commonly stated human tolerance level for severe chest injury (AIS \geq 4) was a maximum linear acceleration in the centre of gravity of the upper thorax of 60g, sustained for 3 ms or longer. The 3 ms injury criterion was computed in MADYMO3D by tracing the resultant linear acceleration signal using a time window with a width of 3 ms.

The second measured parameter of dummy response was concerned with reducing the possibility of head contact with some part of the vehicle. In order to reduce this probability, the movement or excursion of the head was defined as the horizontal movement of the target on the side of the dummy head, relative to the head initial position.. The head movement was measured from high speed film or video recording. Both film and video analysis had the ability to provide output scaled position co-ordinates for any point in the picture. For the measurement of head excursion, the output was scaled in millimetres with a position origin at the fixed point, as both wheelchair and dummy were movable. In this programme, variations in head initial position occurred as different occupant restraint configurations were investigated. ISO/CD 10542-1 imposed a 650 mm limit on this value, but there was some concern that this is too high. The head excursion was stored from the file REDIS recording in MADYMO3D to output scaled position co-ordinates. The head

peak excursion was the maximum horizontal position of any point on the dummy head during the test and was measured from the target origin point, stored in the file PEAK.

The use of the MADYMO3D crash victim simulation allowed the consideration of other injury parameters, which were difficult to be measured during the sled test. The most important of these factors was the neck load and the head angular acceleration. These parameters were considered not as absolute values for injury assessment, due to the lack of biofidelity in the dummy. But it was considered appropriate to accept a reduction in these parameters as reduction in the potential for injury.

The RFF impact tests for WTORS suggested that collapse of the chair backrest and seat cushion generally had a beneficial effect on reducing spine injury. However, wheelchair backrest breakage design is undesirable in terms of preventing serious injuries in severe RFF impact. The backrest should be designed to undergo plastic deformation in RFF impact. Another possible solution is to design a chair backrest structure to allow the torso to move backwards relatively, going into the chair backrest, so that the head could maintain the same orientation relative to the torso, until the head was in contact with the headrest. From this point of view, the peak acceleration imparted by the headrest to the head (a_{th}) should be the same as that imparted by the chair backrest to the torso (a_{rc}) within 30 ms time period for a given input severity. Therefore, a new comparative injury parameter, Δa has been defined as the absolute values of the deviation between two accelerations, $\Delta a = |a_{rc} - a_{th}|$.

In taxi test results (see Appendix 5D), the peak value of Δa (delta 'a') in the manual wheelchair test was much less than that in surrogate wheelchair. It was approximately 15g difference at Level II and 40g difference at Level IV. As the input pulse increases for a given wheelchair this Δa seems to increase shown on the bar charts (Figure 4.4a). The peak value of chest acceleration in the surrogate wheelchair case is greater than that of head acceleration, due to a higher stiffness material characteristics of backrest in the surrogate wheelchair. After a headrest was removed in the given manual wheelchair, the peak value of Δa was greater than that in the same wheelchair with a headrest (approximately 22g difference for a given Level V input

severity). The peak value of head acceleration is greater than that of chest acceleration, due to higher stiffness material characteristics used in the headrest (Figure 4.4b). Figure 4.4b exhibits evidence of the need to match the head restraint stiffness to that of the chair backrest. The comparison of Δa at two configurations of a manual wheelchair (with and without handles) is shown in Figure 4.4c.

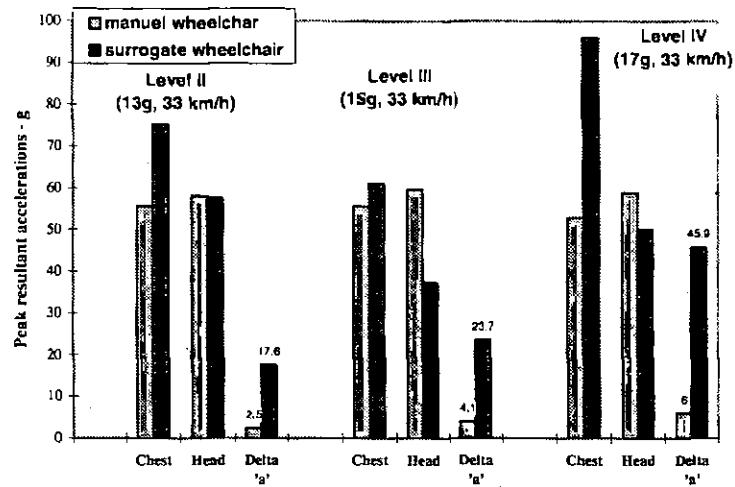


Figure 4.4a Comparisons of Δa at two types of wheelchair

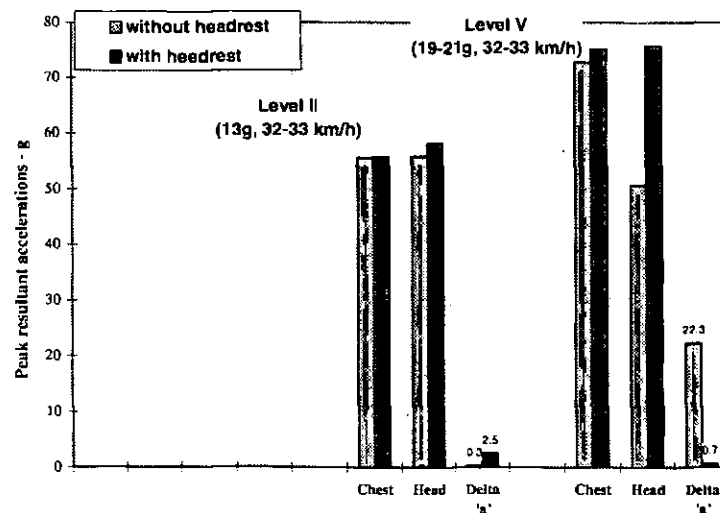


Figure 4.4b Comparisons of Δa at two configurations of a manual wheelchair (with and without headrest)

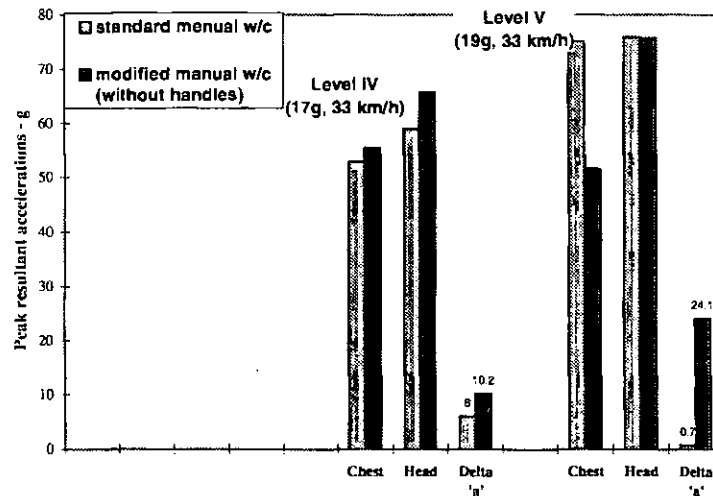


Figure 4.4c Comparisons of Δa at two types of a manual wheelchair (with and without handles)

The modified manual wheelchair without handles increased the peak value of Δa (approximately 23g at a given Level V). It indicates that it is not better design to cut the handles of the wheelchair off although it could be used to avoid the second contacts between the wheelchair and vehicle internal structure.

This comparative injury parameter is practicable in impact engineering analysis. It can be used to estimate the potential for a particular injury mechanism, and then to evaluate the design of wheelchair and its restraint systems. The smaller value the Δa is, the better the wheelchair design and the crash performances are.

4.5 Summary

Various types of injury are frequently associated with a particular type of restraint system.

- Restraint system performance needs to be improved. Webbing belt systems with proper restraint design features are expected to limit the head excursions and wheelchair movement, and then to reduce neck injury.
- Usage variables are expected for optimising belt performance, such as a well adjustable headrest, and a tiedown restraint system with dynamic loading characteristics. To improve the restraint performance and reduce injury, the chair

backrest and a well adjustable headrest in the vehicle structure should geometrically support the curvature of the back and neck of occupant as precisely as possible.

- Wheelchair backrest material and structure should be improved to minimise the forward rebound into the seat belt and then to reduce head and neck injury.
- There is an urgent need for the development of much more biofidelity dummy spine model than that currently available. The wheelchair occupant injury mechanisms will be further investigated to improve the current injury mechanism study.
- A response envelope for head resultant acceleration can be practicably used to determine a strategy for achieving head acceleration between 40g and 80g.
- A comparative injury parameter, the absolute values of the deviation between the peak resultant acceleration forces applied to the chest and head within 30 ms time period for a given input severity, Δa is a practical criterion in impact engineering analysis. It can be used to estimate the potential for a particular injury mechanism, and then to evaluate the design of wheelchair and its restraint systems.

CHAPTER 5: DYNAMIC SLED TESTING OF WTORS

5.0 Introduction

Over the years a considerable amount of research and testing have been carried out world-wide to determine the crashworthiness of Wheelchair Tiedown and Occupant Restraint Systems (WTORS). Most of this work has concentrated on the systems where the occupant faces forward, and the results have contributed to the development of draft international standards. These standards cover WTORS (ISO/CD 10542-1, 1996) and Transportable Wheelchairs (ISO WD 7176/19, 1995) for forward facing occupants. Within these proposed standards, a sled crash test was defined by a sled deceleration envelope using an adult dummy of mass 75 kg.

The ultimate purpose of this research was to develop testing and modelling protocols for WTORS evaluation. The experimental phase of this research provided the experience and knowledge necessary to develop complete modelling protocols. The computer modelling phase of this research will be validated in Chapter 10.

The dynamic tests were conducted using the sled at MURSEL. As described in Chapter 1 and 3, one sled platform, two types of surrogate wheelchairs (herein called the TRL-SWC and ISO-SWC), different types of production wheelchairs and one surrogate tiedown system were specially designed for this research programme. TNO-10 adult dummy and 50th-percentile male Hybrid II dummy were used for occupant simulation.

Four groups of dynamic testing were addressed concerning WTORS (Figure 5.0):

(1) In industry tests, different types of production wheelchairs, such as powered and manual wheelchairs were reviewed. TNO-10, Hybrid II and child dummies with commercial restraint systems without any instrumentation were used in this group of tests. Testing of actual wheelchairs under the identical crash conditions was conducted to produce a reference level against which the surrogate results can be compared.

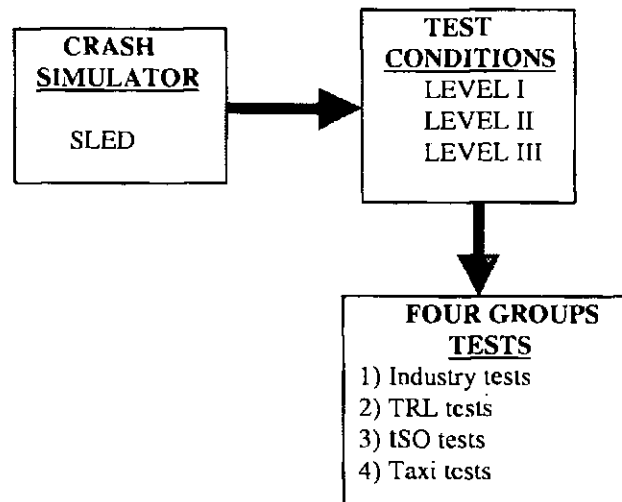


Figure 5.0 Four groups of dynamic sled tests

(2) In TRL tests, TRL-SWC, TNO-10 dummy and surrogate restraint systems were used. It was varied for rear tiedown angles to investigate the effects on wheelchair (wheel loads) and dummy (L/D loads) during Forward Facing Frontal (FFF) impact.

(3) In ISO tests, the pre-designed ISO-SWC, manual wheelchair (M-W/C), TNO-10 dummy, Hybrid II dummy and surrogate restraint systems were used. It was varied of upper diagonal strap belt angles to investigate the effects on the occupant injury (shoulder loads) during FFF impact.

(4) In taxi tests, in order to develop regulations for the carriage of rearward facing wheelchair occupants by taxi, research has been carried out to determine the crashworthiness of wheelchair systems in the Rearward Facing configuration in Frontal impact (RFF). The modified ISO-SWC was used. The effect of different wheelchair tyres and headrests on the dummy response was also investigated.

The above four groups of test results are summarised in tables following each section in this Chapter, separated by Appendix 5A, 5B, 5C and 5D. The experience and knowledge gained from these tests were used to draft a dynamic testing protocol for WTORS evaluation and validate the computer models.

5.1 Industry Test (Group 1)

A wheelchair, which is said to have passed the crash test, has met the test conditions required by the draft ISO standards (ISO/CD 10542-1, ISO WD 7176/19). For example the maximum forward movement of the wheelchair should not be greater than a defined amount (200 mm), batteries should not come off a powered wheelchair, etc. WTORS was secured on a sled, which is then propelled at 48 km/h into concrete block, the sled deceleration being around 20g. The wheelchair is occupied by a 75 kg test dummy representing the dimensions and weight of an average adult man.

Conventional wheelchairs are primarily constructed as a motion device for handicapped persons and not be able to withstand higher loads resulting from traffic accidents. The purpose of industry tests is to examine the behaviour of conventional wheelchairs during a crash.

Most of the damage to the powered wheelchair was caused by a failure of the wheelchair tiedown restraint. The wheelchair was then indirectly restrained by the occupant restraint system in B pillar configuration. Larger deformations were found at the wheelchair backrest, together with a slight deformation at the seat frame. During impact testing of a powered wheelchair (chair mass 57 kg, test number T3028), all loads on dummy and chair were taken by the lap and diagonal occupant belt (double inertial 3-point). Hence the dummy was forced backward into the chair resulting in chair backrest failure.

The wheelchair itself may become a dangerous projectile, especially the heavier battery (18 kg) operated power wheelchair, if it is not properly tied down or just attached to the wheelchair during an accident. The problem is further complicated by the danger of acid spilling from the battery. Unfortunately the battery attachments in the conventional wheelchair are not strong enough to resist high acceleration loading (Orme 1976).

Visual examination of conventional wheelchairs helped to understand that the tiedown restraint system provides complete occupant protection at 40 km/h and is probably good for 48 km/h in a manual wheelchair. If the manual wheelchair was properly used, the disabled occupant would be able to survive forward and rearward facing impacts up to about 40 km/h with an extremely high chance of receiving little

or no injury. At 48 km/h crash severity, the rear tiedown restraint structure deformed excessively but this would depend on the amount of sled stopping distance or peak sled deceleration specified.

The industry tests provided valuable information regarding the dynamics of actual powered wheelchairs in a crash severity of 48 km/h, 20g FFF impact and suggested as follows.

- The experiments revealed that the dummy significantly loaded the frontal wheels, footrests and seat. The vertical loading of the dummy on the seat caused the wheelchair collapse and resulted in dummy injury.
- Fragility of the battery cases and the potential for acid spills were found. Hanging battery boxes could be a potential hazard because they were easily dislodged in a crash.
- The deformation of the wheelchair backrest on dummy rebound allowed excessive rearward excursions. Although rebound is not addressed in the current standards, it appears that it could be a common mechanism for occupant injury and therefore should be addressed in the future. The rebound will be further discussed in Chapter 11.

5.2 TRL Tests (Group 2)

Table 5.2 TRL test programme

Set Up		WTRS (TRL-SWC only)				WTORS (TRL-SWC + dummy)				WTRS		WTORS	
Three Phases		Phase I				Phase II				Phase III			
Pulse Levels		Level I		Level II		Level I		Level II		Level III			
Stage No.		1	2	3	4	5	6	7	8	9		10	
Rear tiedown angle (°)		30	45	45	30	30	45	45	30	30	45	30	45
Sled pulse	g	8	8	13	13	7	7	11	11	20	20	18	18
ΔV	km/h	28	28	28	28	26	26	26	26	33	33	32	32

This group of tests involved three phases. Phase I testing used TRL surrogate wheelchair (TRL-SWC) only. The main purpose of this phase was to gain experience with wheelchair testing and computer modelling to assess the rigidity and durability of

the surrogate wheelchairs. Phase II involved testing of a full wheelchair-dummy system. The object of this phase was to gain experience testing of a full system and develop test procedures to validate the computer models. In order to preserve the structural integrity of the test wheelchair, testing was carried out at three levels of the sled deceleration pulses for WTORS (Figure 5.2). In keeping with the ISO standards, a nominal 32 km/h, 20g crash pulse (Level III) falling within the ISO corridor was finally selected in Phase III. TRL test programme is listed in Table 5.2.

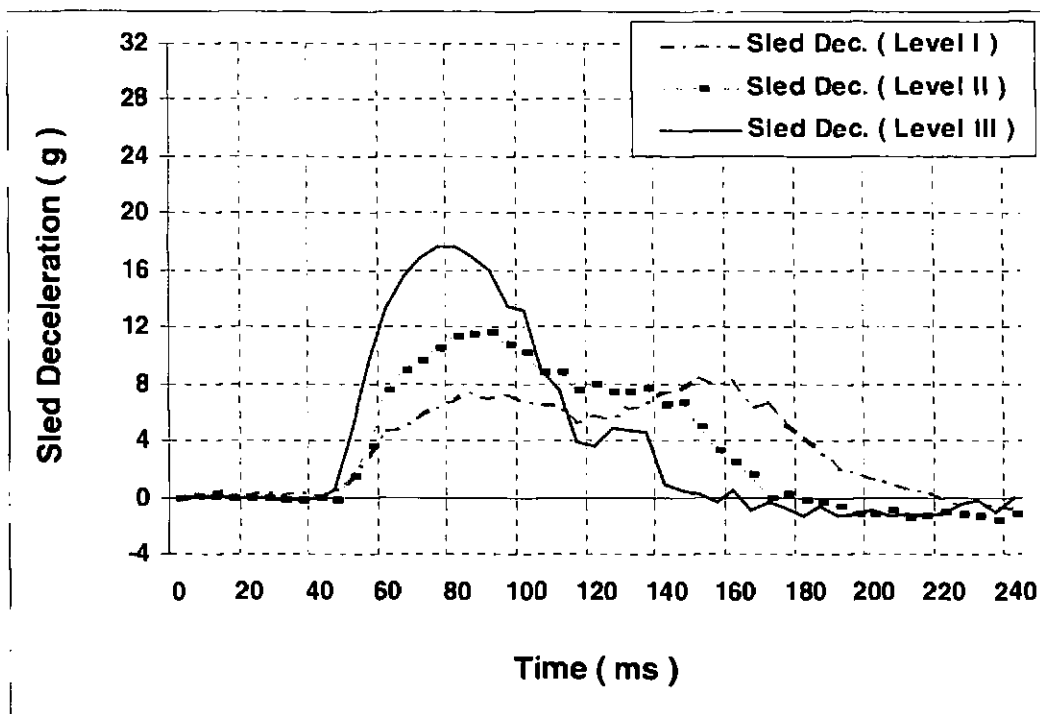


Figure 5.2 Three levels of sled deceleration pulses used in TRL tests

Phase I: TRL-SWC only (WTS)

First phase of the TRL test programme assessed the rigidity and durability of TRL surrogate wheelchair and provided valuable experience in wheelchair testing and computer simulations. Test procedures were developed in an effort to produce repeatable results from one test to another. Phase I consisted of two levels of crash pulse: Level I (28 km/h, 8g) and Level II (28 km/h, 13g).

The TRL wheelchair was restrained by a 4-point webbing surrogate tiedown strap, two straps in front and two in the rear. The rear tiedown angles were varied to

30 and 45 degrees. The chair was positioned by centring the wheels on the four load plates and aligning the chair with the longitudinal centreline of the sled platform. The tiedown straps were pre-tensioned by hand until they were tight. No particular pre-tension convention was used.

Wheelchair deformation was only found in the rear wheel axle. Deformation of the rear wheels continued in the subsequent tests. The chair was reinforced after Level II. The original rear axle was replaced by a stronger tool steel bar.

Phase I proved to be very instructive. Wheelchair testing and data analysis experience was gained, and procedures were developed for using in the replicate tests.

Phase II: TRL-SWC with dummy (WTORS)

Once it was proven that a high degree of repeatability could be achieved with Phase I, the next step involved adding the dummy to the system. Phase II involved four tests (Stages 5 - 8 in Table 5.2). This was the first opportunity to observe and study the dynamics of a complete wheelchair-dummy-tiedown system.

Procedures, which were incorporated into the overall test protocol from Phase I, were developed for dummy positioning and occupant restraint pre-tension. The ultimate goal was to develop a test protocol that would produce repeatable results in loads, acceleration, and excursions, for the wheelchair and the dummy.

The test set-up involved ensuring that the dummy's pelvis was located as rearward as possible and that the dummy was seated symmetrically in respect to the centreline of the chair. An occupant restraint pre-tension procedure was also added to this phase. A 75 mm³ wood block was placed perpendicular to the shoulder belt across the dummy's sternum as the 3-point system was tightened. The block was removed to give approximately 63 mm slack in the shoulder belt. The lap belt was arbitrarily tightened on both left and right sides of the chair.

Phase III: mid-severity pulse

Phase I and II of the test programme involved gaining test experience and developing a test protocol for producing highly repeatable results. With these goals

accomplished, phase III of the research was initiated using a mid-severity pulse (32 km/h, 20g).

The effect of the following three factors on the wheel loads was evaluated by experimental results.

- ***The geometry of restraint systems***

The rear wheel loads generated in the 45-degree case were higher than those in 30 degree case, the maximum difference being 56 % of the 30-degree values.

- ***The occupant***

In general without an occupant (WTS) the rear wheel loads were greater than the front. When the dummy was present (WTORS) the effect of mass transfer from the rear to the front partially reduced the rear wheel loads.

- ***The sled crash pulses***

For Level I and Level II the front wheel loads were less than those at the rear. However, when sled deceleration increased to Level III, the test results suggested that mass transfer to the front wheel, relatively increased the front wheel loads.

5.3 ISO Tests (Group 3)

This impact programme used a ISO defined surrogate wheelchair (ISO-SWC) to represent a mid-range powered wheelchair. It is more robust and stiffer than a production chair (M-W/C). In addition the Hybrid II dummy was seated on an aluminium plate above pancake load cells. Thus the centre of gravity (CG) of ISO-SWC was higher and the seat absorbed little energy when compared with a soft cushion and the more flexible structure of the conventional wheelchair. Therefore the peak loads would be expected to be higher than in the real world. The results of industry tests (Group 1) also supported this view.

WTORS restraint system consisted of two parts:

- (1) The wheelchair was secured by two rear tiedown straps and two front straps.
- (2) The dummy was restrained by a L/D occupant restraint.

Both of the restraint systems were independent of each other and anchored separately to the sled. The dummy sat on an aluminium alloy plate, which was placed

on the four pancake type load cells. The load cells were bolted to the wheelchair seat frame. The test programme is listed in Table 5.3a.

In order to avoid the onset of structural damage to the ISO-SWC, the impacts in the floor mounted occupant shoulder belt configuration ceased at a sled velocity change of 34 km/h. For the B pillar configuration it was increased to 51 km/h (2% above the ISO 10542 defined maximum value).

Table 5.3a ISO test programme

Set Up	M-W/C + TNO-10				ISO-SWC + TNO-10				ISO-SWC + Hybrid II				
Three Phases	Phase I				Phase II				Phase III				
Pulse Levels	Level I		Level II		Level I		Level II		Level I		Level II		
Upper shoulder anchorage	B p'ar	B p'ar	B p'ar	B p'ar	B p'ar	Floor	B p'ar	Floor	B p'ar	Floor	B p'ar	Floor	
Sled pulse	g	8	8	13	13	7	7	11	11	7	7	11	11
ΔV	km/h	28	28	28	28	26	26	26	26	26	26	26	26

Phase I: M-W/C + TNO-10 dummy

In order to preserve the structural integrity of the test wheelchair and the measurement devices using a proper crash severity, sled testing was initially carried out in three phases at three levels combined with appropriate velocity change to examine the effect on the wheel loads and shoulder load function (Figure 5.3a). The wheel loads were measured in the case of Level I and Level II tests only.

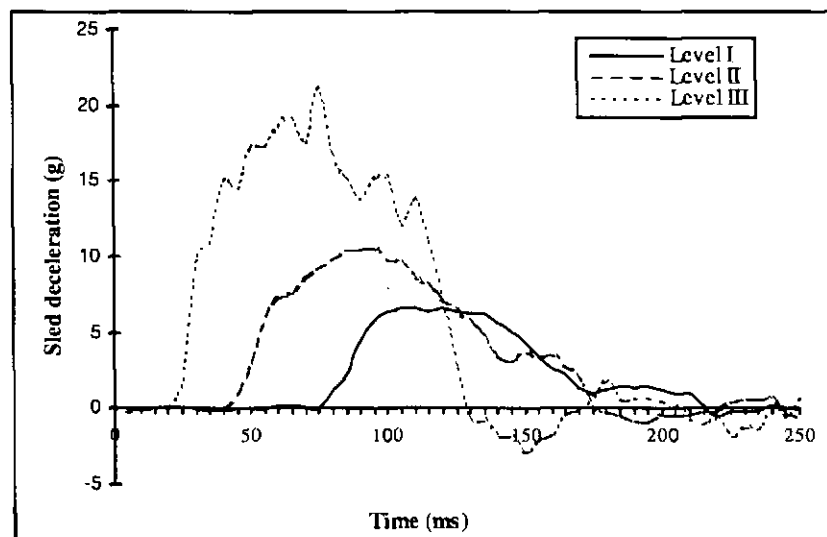


Figure 5.3a Three levels of sled pulses used in ISO tests

Level I:	6 - 10 g,	$\Delta V = 15 - 25$ km/h
Level II:	11 g,	$\Delta V = 27$ km/h
Level III:	13 - 21 g,	$\Delta V = 35 - 51$ km/h

Phase II: ISO-SWC + TNO-10 dummy

This phase of tests repeated the above using ISO-SWC instead of M-W/C. Initial work using a TNO-10 dummy has shown that the manual wheelchair (M-W/C) exhibits less severe damage when the diagonal strap of the occupant restraint was anchored to the 'B pillar' at shoulder height rather than anchored to the floor, for impacts of similar severity.

Analysis of video footage taken from a Kodak EktaPro 1000 Motion analysis system suggested that the crash dynamics of dummy were sensitive to the variations in the diagonal top strap anchorage positions.

Phase III: ISO-SWC + Hybrid II dummy

This phase presents the results of an investigation into the variation of wheelchair and occupant loads as a function of diagonal top strap anchorage configurations, these being anchored to the B pillar (Figure 5.3b) and the floor (Figure 5.3c). The pancake type load cells were inserted below the seat plat in order to measure the seat loads between dummy and wheelchair. The cantilever wheel load cells were placed under the four wheels to measure the vertical loads between wheels and sled floorboard.

The test series continued once the chair was reinforced. In an effort to improve test repeatability, the test set-up procedures were refined and straps were adjusted in order to accurately align the centreline of the wheelchair with the centreline of the platform.

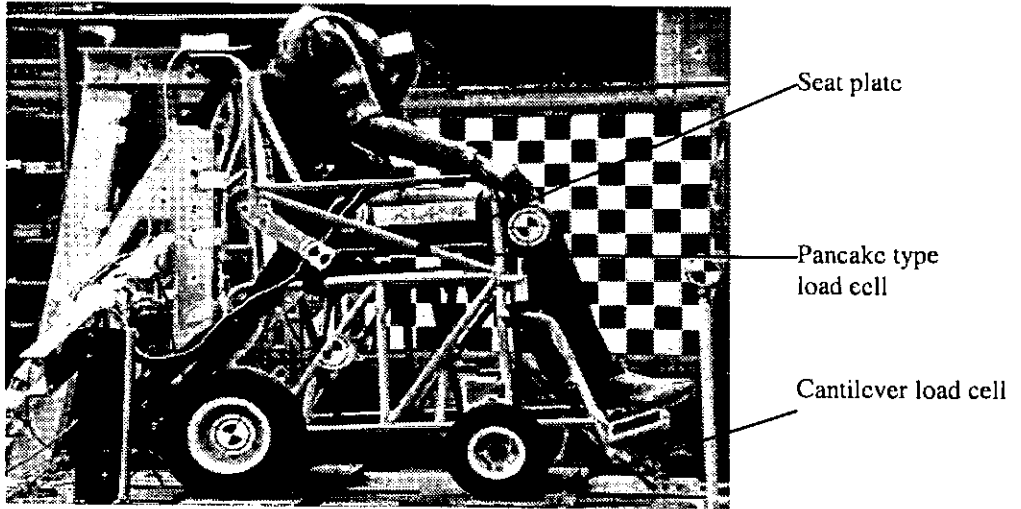


Figure 5.3b B pillar anchorage



Figure 5.3c Floor anchorage

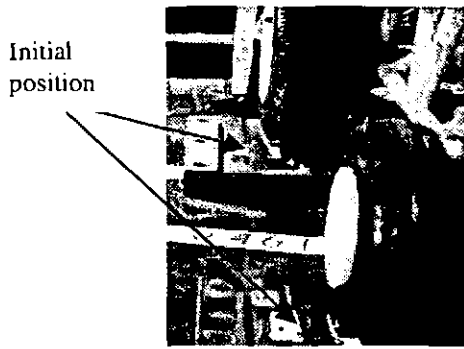


Figure 5.3d

Wheelchair misalignment after impact

Chair alignment was verified prior to and after pre-tension. Tiedown straps were tightened in small increments from left to right and from front to back to limit chair misalignment during impact (Figure 5.3d).

This investigation was also carried out by computer simulation using DYNAMAN and MADYMO packages (Chapter 9).

5.3.1 Discussion

The effect of the following three factors on dynamic responses was observed from ISO test results.

- *Comparison of the effect of diagonal top strap anchorage configuration*

ISO test results show that the front wheel loads were more sensitive to the anchorage configurations than the other parameters. In general the shoulder load (S_r) increased as the velocity change (ΔV) increased (Figure 5.3e). The floor mounted configuration always produced higher values of front wheel loads and diagonal top strap tensions at a given ΔV . The details of occupant shoulder load functions in B pillar [$S_r(B)$] and floor configurations [$S_r(F)$] are discussed in Chapter 11.

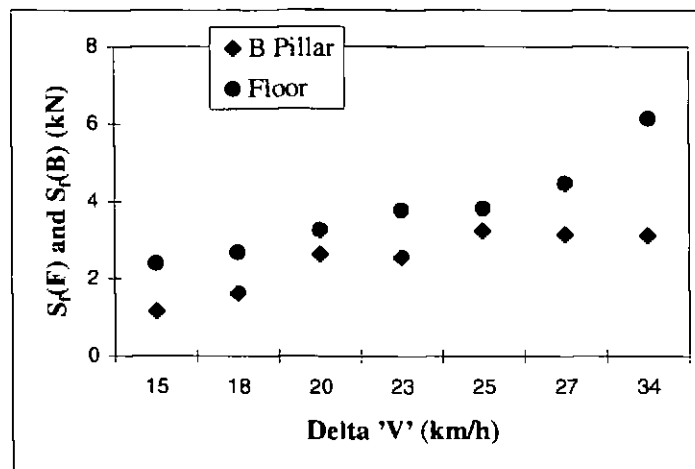


Figure 5.3e Comparison of peak shoulder load function in two configurations

The load comparisons between Tables 5.3b and Table 5.3c show that for the floor mounted configuration the peak time of diagonal top belt load (T_1) lagged the B pillar by 35 - 45 ms.

Table 5.3b Load duration (B pillar)- Level I, II

Parameters	Units	Load duration		
		Range (ms)	Period (ms)	Load range (kN)
Chest Res.	g	175 - 100	75	12.2 - 39.6
Diag. top (T_1)	kN	165 - 110	55	2.5 - 5.5
Lap (T_3)	kN	165 - 110	55	1.9 - 5.4
Buckle (T_4)	kN	165 - 105	60	3.5 - 7.8
Seat Sum (C_T)	kN	175 - 115	60	6.5 - 12
Wheel sum	kN	145 - 135	10	42.2 - 43.3

Table 5.3c Load duration (floor-mounted) - Level I, II

Parameters	Units	Load duration		
		Range (ms)	Period (ms)	Load range (kN)
Chest Res.	g	165 - 100	65	11.4 - 29.5
Diag. top (T_1)	kN	210 - 145	35	3 - 5.9
Lap (T_3)	kN	175 - 110	55	1.4 - 5.2
Buckle (T_4)	kN	170 - 110	60	2.7 - 6.9
Seat Sum (C_T)	kN	190 - 115	75	6.6 - 11.2
Wheel sum	kN	190 - 135	55	27.5 - 45.5

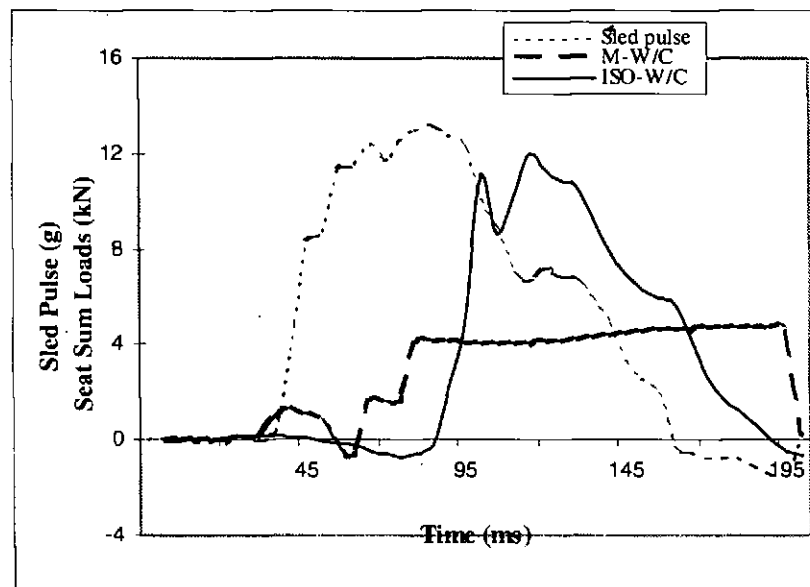
The shoulder load function difference of two configurations is summarised in Table 5.3d. It indicates that the minimum increase of shoulder load in the floor mounted configuration is 17% at ΔV 25 km/h.

Table 5.3d Shoulder load difference between two configurations

ΔV	$S_r(B)$	$S_r(F)$	diff.
km/h	kN	kN	%
15	1.17	2.41	106
18	1.61	2.68	66
20	2.63	3.24	23
23	2.54	3.78	49
25	3.25	3.81	17
27	3.17	5.46	41
34	3.13	6.14	96

- **Comparison of the effect of wheelchair structure**

The peak values of seat loads in the ISO-SWC were considerably higher than those in the M-W/C (Fig 5.3f). This suggested that the seat cushion in the M-W/C absorbed some of the energy from impact and reduced the peak seat loads.

Figure 5.3f Seat sum loads for B pillar configuration - $\Delta V = 31$ km/h

- **Comparison of the effect of sled crash pulses**

The front wheel loads varied considerably as a function of crash pulse. The test results suggested that weight transfer to the front wheels relatively increased the front wheel loads under the considerations of higher crash pulse.

5.3.2 Summary

The diagonal top strap anchorage configurations had a considerable effect on the dynamics of the system, such as, the values of the diagonal strap tensions and front wheel loads.

- At all values of sled velocity change, the floor mounted configuration exhibited a peak shoulder load greater than that for the B pillar configured system. At a velocity change of 34 km/h the value (6.14 kN) was higher by 96 %. The value at 51 km/h for the B pillar configuration was lower (5.74 kN).
- At all values of sled velocity change, the floor mounted configuration exhibited a maximum dummy head target excursion greater than that for the B pillar configured system. At a velocity change of 34 km/h the value of head excursion (450 mm) was higher by 52%. This value was not reached by the latter system: 384 mm at 51 km/h.
- The front wheel loads exhibited similar variations. They indicated that the weight transferred to the front of the wheelchair as the maximum head target forward excursion was reached.
- In general the peak seat sum load in Level I and II was slightly greater for the B pillar than the floor mounted configuration. However the loading phase for the former acted over a shorter period.

Taking into account the implications of the above conclusions on the occupant and the wheelchair it is considered that the B pillar anchorage of the occupant diagonal strap is superior to the floor mounting configuration.

5.4 Taxi Tests (Group 4)

Extensive research has determined that the wheelchair and occupant should always be orientated parallel to the direction of travel, either facing forward or rearward (Kooi and Janssen, 1988). There has been very little work on rearward facing travel safely for WTORS. The recommendation of a rearward facing restraint for wheelchair and occupants is recent regulatory practice in France and Germany (Maupas et al, 1996). Researchers emphasised that when using rearward-facing

orientation, a headrest must be addressed to limit the extension of the neck in the case of a crash.

In the United Kingdom wheelchair occupants are regularly carried in the rearward facing configuration in London taxis (known as 'black cab') operating under the regulations of the carriage office in London. In order to further develop the regulations for the carriage of rearward facing wheelchair occupants by taxi, it is necessary to obtain data on the dynamics of this configuration in frontal impact.

The following procedures have been carried out for a rearward facing wheelchair-occupant systems in frontal impact.

- 1) *Preliminary measurements of the geometry of a taxi installation to build a representative structure on the crash sled*
Components of London taxi, such as the window structure, the rear tiedown reel and occupant restraint anchorage, were incorporated into both the sled simulated structure and the computer model by scaling their positions.
- 2) *The back support structure was designed and constructed to simulate a taxi seat back.*
- 3) *The contact loads were recorded at the wheelchair backrest and wheel level.*
The forces acting on the taxi bulkhead were resolved by monitoring the horizontal wheel loads and the back support loads.
- 4) *The dynamic response of the dummy was recorded by monitoring the dummy's head and chest acceleration, head and knee displacement, and the wheelchair movement.*
- 5) *The restraint loads of rear tiedown and lap belt were also measured.*

This simulation provided data to contribute to the taxi design regulations in the UK, applying to the carriage of occupied wheelchairs. In this test group references have been made to the ISO surrogate wheelchair and the manual wheelchair.

5.4.1 Tests set-up

The sled was accelerated to a velocity up to 33 km/h and brought to a halt to give a deceleration of up to 22g. The tests were recorded on both high speed video (500 fps) from side shot and normal VHS video recorder for instant play back for analysis of the movements of dummy and wheelchair during the impact. Five series of sled tests were carried out as follows.

- Series I was programmed in standard manual wheelchair (M-W/C) tests.
- Series II was programmed in ISO surrogate wheelchair tests (ISO-SWC).
- Series III was carried out in the standard M-W/C tests with a headrest.
- In the test series IV, a modified M-W/C (without handles) was employed to further investigate the impact loads on the bulkhead, as a comparison with the results of series III.
- Series V test was to investigate the effect of velocity change on the crash performance.

A summary of test conditions is given in Table 5.4. A typical deceleration pulse is shown in Fig 5.4a.

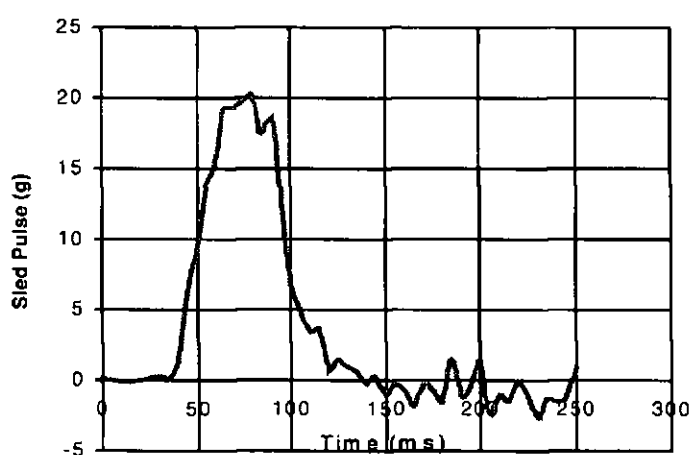


Figure 5.4a Sled pulse for RFF impact (Series I)

The ΔV corresponds to sled velocity change and sled 'g' corresponds to sled maximum deceleration. The accuracy of the transducers used is as follows: (i) sled velocity change: +/- 1.0 km/h; (ii) sled peak deceleration: +/- 2.5g.

The wheelchair used in the test series I and III was a standard folding wheelchair (mass 15 kg) made in the UK. A modified ISO surrogate wheelchair (mass 83 kg, without battery) was used in Series II tests. A modified manual wheelchair (without handles) was used in Series IV and V, comparing with the results from Series I and III.

Table 5.4 Taxi test conditions

	ΔV (km/h)	Sled 'g'	results
Series I	M-W/C (with handles)	without headrest	
Level I	25	11	OK
Level II	30	13	OK
Level V	32	21	OK
Series II	Modified ISO-SWC	with headrest	
Level I	32	11	OK
Level II	32	13	OK
Level III	32	15	OK
Level IV	32	17	failed
Series III	M-W/C (with handles)	with headrest	
Level II	33	13	OK
Level III	33	15	OK
Level IV	33	17	OK
Level V	33	19	OK
Series IV	M-W/C (without handles)	with headrest	
Level II	33	13	OK
Level III	33	15	OK
Level IV	33	17	OK
Level V	33	19	OK
Series V	M-W/C (without handles)	with headrest	
	21	13	OK
	25	16	OK
	29	19	OK
	33	22	OK

5.4.2 Test facility designed for taxi work

The simulated taxi installation was bolted to the sled floor plate. A simulated taxi system was designed by the author in four parts: a vertical rigid frame to represent

the taxi bulkhead, a back support structure to simulate a taxi seat backrest, an adjustable headrest fixed on the bulkhead 1200 mm above the floorboard. Two wheel load plates, which were bolted on a sheet of steel plate (916 x 916 x 10 mm) of the vertical bulkhead, to record the horizontal contact loads from the rear wheels of the wheelchair (Figure 5.4b). A transverse belt structure was positioned at 850 mm from the sled floorboard and fixed on the vertical frame. This was composed of two cantilevered channel sections, which supported a rolling reel at their free ends. A length of webbing (55 mm x 1150 mm) was passed around the reels and secured at each end via a 'dogbone' load cell to the vertical bulkhead (Figure 5.4c). An adjustment buckle was incorporated in order to pre-tension the webbing belt. The back support structure was attached to the rigid frame to resemble the units on a taxi.

It was subsequently found that the distance between the handle of wheelchair and bulkhead must be more than 265 mm (Series IV) to avoid the second collision during impact (Figure 5.4d).

The wheelchair was placed on the sled in the rearward facing configuration and secured with a typical black cab style 'Y' shape tiedown. The tiedown was instrumented using a 'Denton' load cell to measure loads generated on rebound from the impact. Inflation pressure of the wheelchair's tyre was 345 kN/m² (50 psi) according to the manufacturer's recommendation. The rearward facing wheelchair was placed on the platform surface and centred with respect to the back support structure. Both brakes were applied. The front castors were positioned backwards and wedged by a wood block to prevent any movement before the acceleration phase of the sled.

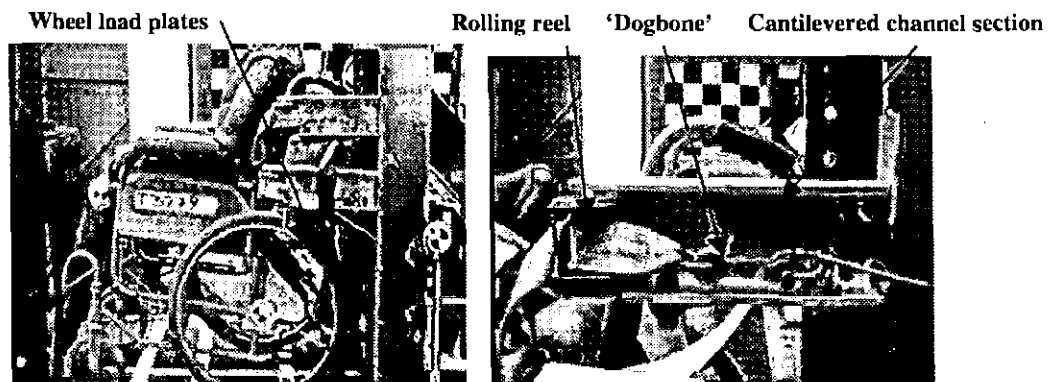


Figure 5.4b A vertical rigid frame

Figure 5.4c A back support structure

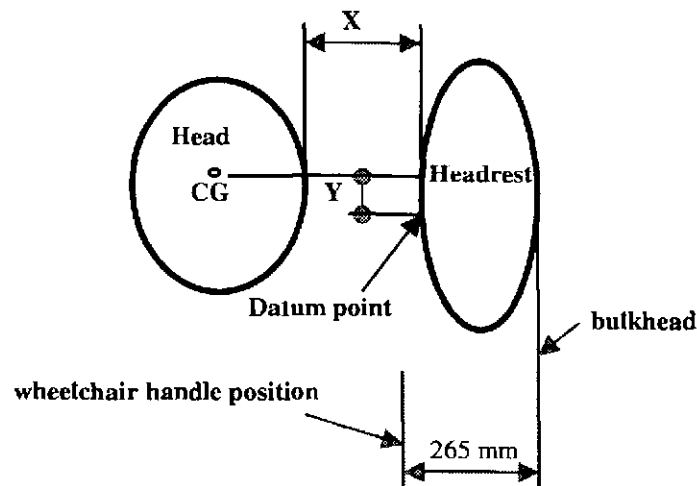


Figure 5.4d Dummy head contacted with the headrest

The occupant was simulated using a Hybrid II 50th percentile male dummy. The seated dummy shoulder rested against the wheelchair backrest. The arms were placed on the armrests of the wheelchair, the hands resting on the front of the armrest. It was equipped with tri-axial accelerometers to measure both chest and head accelerations. The dummy was lightly taped at the shoulder to the bulkhead to prevent it falling over during the pre-impact sled acceleration phase. It was restrained by a static lap belt, which was of similar geometry and design to that currently used in the black cabs.

5.4.3 Discussion

The RFF impact of the wheelchair-occupant system demonstrated more effective capacities for protecting the occupant than the FFF impact (Gu and Roy, 1995). Analysis of the dynamics of this group test helped to draw the following discussions:

- *The chest resultant acceleration at a certain time (100 ms) is higher than the head's*

This phenomenon could be explained by the fact that when the wheels contact the load plates, the wheelchair and dummy seem to pivot at the onset of the impact.

The wheelchair backrest therefore makes contact with the transverse webbing later than rear wheels contact with the load plates, causing the peak values of the chest acceleration to be reached slightly earlier than the head.

- *The secondary collision*

The secondary collision is the impact between the wheelchair and the interior structure of the vehicle. It was observed during impact resulting from wheelchair deformation and occupant excursions. This is because of the small space between the wheelchair backrest and the bulkhead.

It is important to ensure there is adequate support for the wheelchair occupant's head and back. This means in practice that the headrest needs to be fixed on the bulkhead reaching at least a height of 1200 mm from the taxi floorboard. The distance between the wheelchair handle and the bulkhead must be more than 265 mm to avoid the second collision during impact.

- *The rearward facing back support structure system*

During impact this system is effective in spreading the loading over segments of the occupant's body and wheelchair, resulting in reduced acceleration and movement of the dummy's head, chest and wheelchair. Moreover, it eliminates deficiencies in the deformation and strength properties of the wheelchair. It offers adequate protection under conditions of RFF impact to a severity of 21g, 33 km/h deceleration in manual wheelchairs, provided some strengthening of chair backrest and seat cushion were incorporated. A rearward facing webbing restraint device has potential to be used in the taxi as it is simple, rapid to install and very few risks of incorrect use. The enormous advantage of a webbing device is that it does not occupy too much space.

5.5 Summary

- The dynamic test results were assessed both by quantitatively and qualitatively.

A quantitative assessment of the test results was performed using a standard statistical analysis of maximum outputs for a given test series. Maximum values were of particular interest because they revealed the severity of the crash conditions, which a WTORS system was exposed to. The maximum values were independent and identically distributed variables following a normal distribution. Observing and reporting maximum values alone oversimplifies test results, and consequently, does not offer a full description a particular output parameter.

A more comprehensive way of examining and evaluation test results is to study their time histories qualitatively. A time history plots an output at discrete intervals over the course of the entire event. This qualitative assessment provides a better evaluation of repeatability because output parameter responses could agree in different levels and time.

- The surrogate wheelchair testing based on the TRL design indicated that the rear axle and front castors were insufficiently reinforced. Once TRL-SWC was strengthened, it proved durable and reliable in subsequent testing. A surrogate WTORS system allowed many tests to be conducted repeatedly and facilitated observation and analysis of the crash environment.
- Production wheelchairs were crash tested and validated the surrogate system's ability to simulate the real crash dynamics. The production wheelchair tests provided insight into possible mechanisms for occupant injury and displayed areas on the chair that were structurally weak.
- Tight control of chair and dummy positioning improved the repeatability of test results.
- The preliminary test programme proved conclusively so that the replicated test results can be obtained when using a full chair-dummy system.
- All test results helped to gather contact functions and force characteristics for construction Crash Victim Simulation (CVS) models.

CHAPTER 6: THEORETICAL MODELLING OF WTORS

In order to gain a full understanding of the crash performance of the Wheelchair Tiedown and Occupant Restraint Systems (WTORS) impact test and dynamic system modelling, it is necessary to have an understanding of the dynamic theory that is involved.

6.1 Mathematical Modelling Procedure

The mathematical modelling depends not only on learning how to formulate the model equations but also on being able to prime the model with some data. The procedure with data flow incorporated is shown in Figure 6.1.

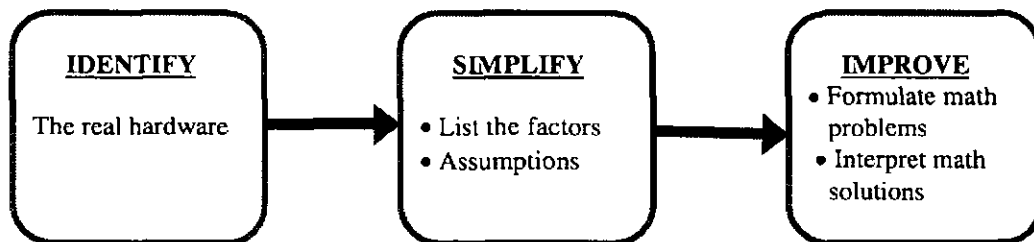


Figure 6.1 The modelling flow diagram

6.1.1 Identify of the real hardware

WTORS system was fixed to a vehicle or a sled and subjected to the forces caused by the action of the vehicle deceleration on it. The relationship between the forces due to the vehicle deceleration and the reaction of WTORS was identified. It largely determined the relevant properties of the system as follows:

- The masses of all the moving parts, such as, the vehicle (sled), the wheelchair and the occupant (dummy).
- The stiffness function (the force required to cause unit distortion) of each component, such as, the restraint systems both occupant restraint and

wheelchair tiedown restraint. It is determined by the shape of each component and the material of which it is made.

- The stiffness of the floorboard on which WTORS stands and the way where the system is attached to this floorboard.
- Friction forces between vehicle floorboard and wheelchair, also between the dummy and wheelchair.
- The set-up condition of WTORS, such as the dummy sat on the wheelchair, the tightness of the tiedown and webbing belts.
- The performance of the polyurethane tube was used to decelerate the sled. High precision test results are often kept at the same ambient temperature to prevent differential expansion of the tube giving incompatible sled pulses.
- Wear was another consideration here, closely connected with the pre-tension of webbing belts.

6.1.2 Simplify of the real situation

Simplicity is the mark of a good solution to a problem. An important part of the process of design is to identify the essentials and to eliminate unnecessary frills. The same principle has been involved in computer modelling.

To begin with simplicity we take notice only of the most important and most obvious of the relevant properties and neglect the rest. A very simple mass-spring model was set up in WTORS model based on the following assumptions:

- Neglect the mass of the sled and treat it as one rigid body. This is the first approximation as only sled pulse is used.
- Neglect the mass of the webbing belts and wheelchair tiedown, because it is smaller compared with that of the wheelchair and dummy. The tiedown is likely to be much more extensible, so it could be treated as a perfect spring.
- Assume the surrogate wheelchair to be built in the form of planes, as no deformation of this wheelchair was considered.
- Neglect the friction in comparison with the other forces.
- Assume that all parts fit perfectly together.
- Neglect the ambient temperature effect.

- Neglect the rebound effect.

6.2 A Simple Wheelchair Model

The force distribution was considered in a simplified WTORS. The surrogate wheelchair without the tiedown restraint system could be simplified as a crate (a wheelchair without wheels) resting on a vehicle floorboard (Figure 6.2). The crate could be assumed to be made of a homogeneous material, so that the CG is located at the centroid of the volume.

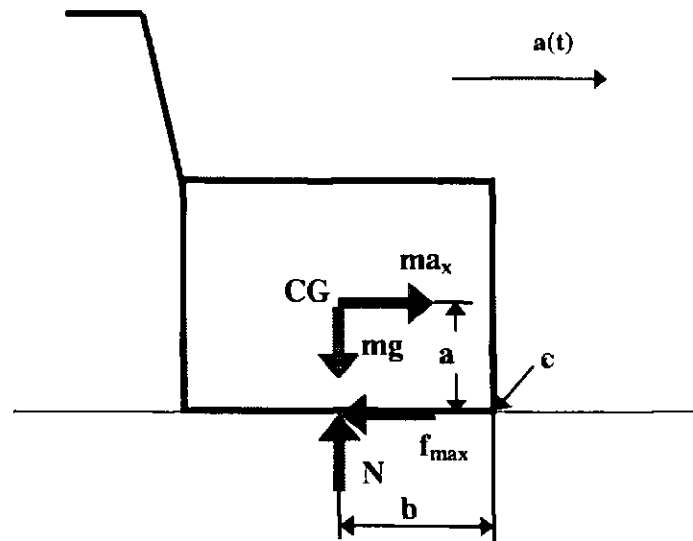


Figure 6.2 Force distribution in a crate

As an example, when the driver applied the brakes or the sled decelerated with tubes, the crate may slide relative to the floorboard or tip over. When the crate is at rest or moving with constant velocity, the weight force mg is equal to the normal force N on the crate. When the driver brakes, the vehicle is decelerating, $a(t)$, and the maximum permissible deceleration a_x is positive. The actual sense of the inertia force, interpreted as an external force applied to the crate, is to the right. Since this force tends to rotate the crate clockwise, the line of the reaction force of the bed of the vehicle on the crate moves to the right of its original position. The force f is the friction force exerted by the vehicle floorboard on the crate. The magnitude of the deceleration is now imagined to increase. The crate will tip rather than slide when the friction force attains its maximum value of

$$f_{\max} = \mu \cdot N \quad (6.2-1)$$

where μ is the coefficient of friction. The equations of motion for this case are

$$\sum F_y = 0 \quad N = m \cdot g \quad (6.2-2)$$

$$\sum F_x = 0 \quad a_x = \mu \cdot g \quad (6.2-3)$$

As the magnitude of the deceleration of the vehicle increases, the line of the reaction force of the crate continues to move rightwards. A limited condition is reached when this force acts on the forward edge of the crate. If the friction force at this condition is less than the maximum possible value μN , the crate will be in a condition of impending tipping motion about the forward edge 'c' point. The equilibrium requirements are

$$\sum M_c = 0 \quad a_x = (b/a) \cdot g \quad (6.2-4)$$

It can be observed that b/a defines the shape of the crate.

If $a_x > \mu g$ or $\mu < b/a$, the crate will slide without tipping; If $a_x > (b/a)g$ or $\mu > b/a$, the crate will tip without sliding. A special case occurs if $\mu = b/a$. In this case, sliding and tipping effects would occur simultaneously.

6.3 A Wheelchair-Sled Model

The Single Degree of freedom (SDF) model depicted in Figure 6.3 is analogous to the wheelchair-sled system. The mass m represents the mass of the wheelchair. The mass of the occupant was neglected from this analysis because the wheelchair and occupant are typically restrained independently of one another.

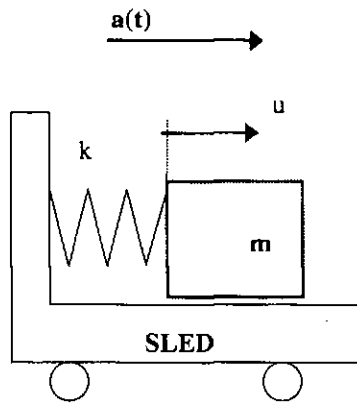


Figure 6.3 A wheelchair-sled system

In this highly simplified approach model, $a(t)$ is the sled deceleration force in the direction of the sled movement, other force components are neglected here; k is the stiffness of the rear wheelchair tiedown; u is the displacement of the wheelchair due to the deformation of the wheelchair and u_m is maximum displacement. We assume k to be a constant, which implies that force and extension are related by a straight

line like that of the perfectly elastic spring. Displacements to the right are taken as positive so that velocities, accelerations and forces will be subject to the same sign convention. The entire system is connected to a moving reference frame that represents the vehicle, to which the wheelchair is anchored.

The acceleration amplification is a function of the type of excitation ($a_m = u_m \cdot \omega_0^2$), i.e. crash pulse shape, the duration of the excitation (t_b), crash pulse length, and natural frequency of the system (ω_0). Since the natural frequency of the system is a function of k and m ($\omega_0^2 = k/m$), the tiedown stiffness and the system mass will affect the degree of acceleration amplification.

6.4 Improvement of WTORS Model

The following effects have been taken into account in order to improve the above WTORS model.

6.4.1 Effect of wheelchair stiffness and mass

In the previous model (Figure 6.3), we assumed that the frame of the wheelchair is rigid. This section demonstrates a way of accounting for the stiffness of the wheelchair frame to improve the model, although it inevitably adds complications.

The wheelchair frame is a relatively large mass of material, which is subject to deformation when acceleration force is applied to it, particularly for manual wheelchairs. If these forces change with time then the deformation changes too. Any

attempt to formulate models must take into account not only stiffness but also the mass of the frame. It is, in principle, possible to treat the frame as a continuous mass, which embodies a resistance to the deformation of any part relative to another. This kind of continuous system, however, is not very easy to analyse especially when the shape is as complicated as that of most wheelchair frames.

We therefore concentrate on the first stage of the model which we have used so far and only change some properties of a wheelchair, such as stiffness. The mass of the wheelchair was assumed to be entirely concentrated in some parts of the system. This is called a lumped parameter system. The word 'parameter' means any characteristic property of the system such as mass or stiffness. In this WTORS model, the simplicity obtained from lumping parameters was used to overcome the inherent lack of accuracy.

6.4.2 Effect of dummy

In order to take into account the effect of dummy, the continuous mass of the frame was dealt with by approximating it to a lumped parameter system (Figure 6.4a), and attaching this to the previous version of our model as shown in Figure 6.3.

The fixed surface shown at the left hand end of the model in Figure 6.4a represents the foundation of the vehicle. The spring shown with stiffness k_F represents the wheelchair effective stiffness of its frame and m_F is its effective mass. m_D is dummy mass and k_D is dummy stiffness contacted with wheelchair. More information is required to specify the instantaneous state of this model, because there are now two masses, which could be moved relative to another. The displacement of this system at any instant is now specified by the values of u_1 and u_2 . δ_s is the elongation of the spring.

The present version of the model is now a system with two degrees of freedom, whereas the previous version had only one.

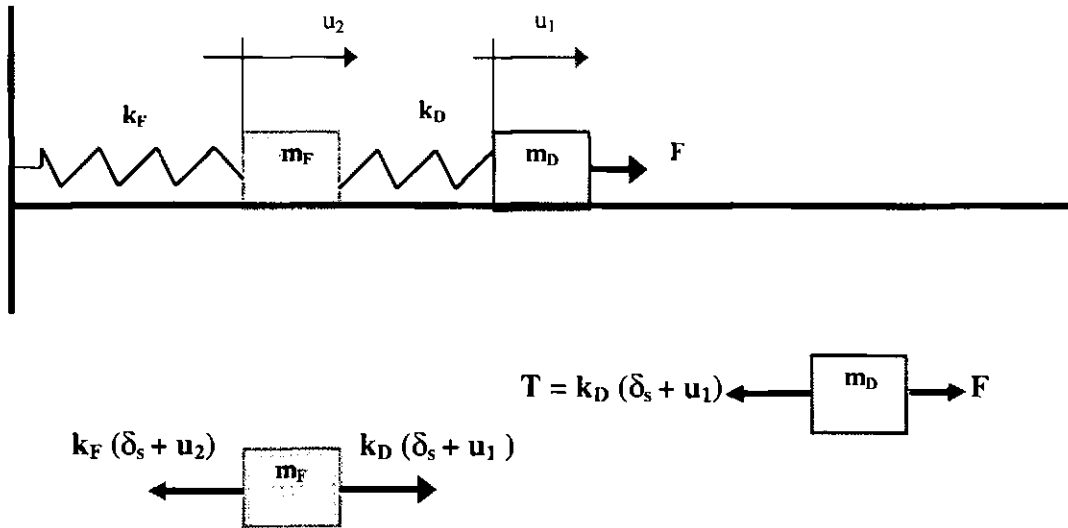


Figure 6.4a Two mass and spring model of WTORS

6.4.3 Effect of Coulomb friction

The effect of friction was considered because a small value of it can have an important effect on the behaviour of a dynamic system. We assumed that the frictional force was constant in magnitude but always opposed in direction to the motion. Friction that exhibits this ideal behaviour is known as Coulomb friction.

Now we want to apply our discussion of friction to our model of WTORS. The easiest way was to assume that all the friction acted in one place (preferably acting on the mass) and to choose a value of which would account for all the friction in the system. It is difficult to represent all the features in one simple model. One way to proceed was to neglect the static friction to represent the friction by an idealised element, which provides a resisting force (f) proportional to the sliding velocity. This element is called a dashpot shown in Figure 6.4b. It consists of a piston in a cylinder, the piston diameter being slightly smaller than that of the cylinder so that there is a small circular gap between them. This produces a resisting force proportional to the relative velocity between piston (v_p) and cylinder (v_c), so that $f = c(v_p - v_c)$, c is coefficient of viscous damping. It is a satisfactory qualitative guide to the effects of friction.

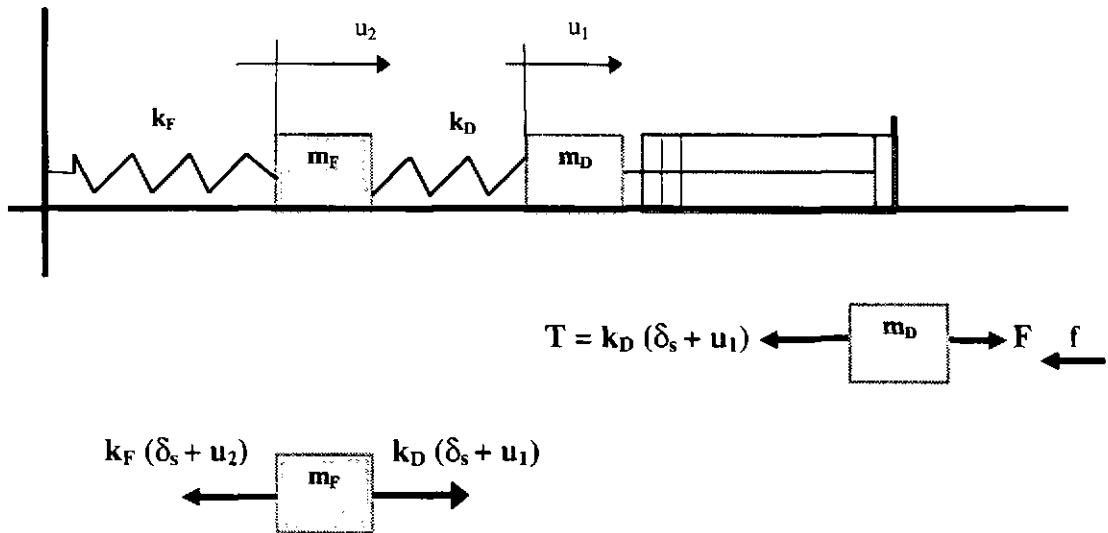


Figure 6.4b Two mass and dashpot model of WTORS

6.5 Further Studies of WTORS Model

WTORS mathematical models have been formulated using the MADYMO3D package for the special purpose of evaluating WTORS crash performance.

6.5.1 Dummy model

The centre of gravity of TNO-10 dummy elements (Figure 6.5a) was determined by free hanging of the element in two positions by a cord and correlated by the calculations in Table 6.5a and 6.5b. The moment of inertia of the dummy parts about an axis through the CG and perpendicular to the x-z plane had been measured with a torsion pendulum. The moment of inertia of the torso foam and skin could not be measured by this method and was estimated. The element masses, location of the centre of gravity and moments of inertia were determined by extrapolation and estimations from P3 dummy mass distribution data (Wismans et al, 1979).



Figure 6.5a TNO-10 dummy

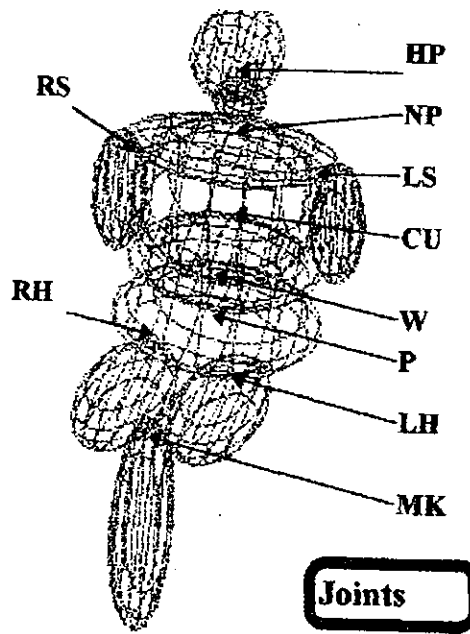


Figure 6.5b Joints of dummy

The resultant characteristics of the static resistance (stiffness) to rotation (including range of motions and joint stops) of the dummy joints were approximated by linear functions. A velocity dependent resistive torque (viscous damping) was defined for all of the joints. These were based on observations that the shoulder, elbow and knee were almost critically damped, while the damping in the neck, spine and hip joints were estimated to be lower than critical values. The initial position of the dummy, just prior to impact, obtained from high-speed video analysis and direct measurements. The centre of gravity of Hybrid II dummy was calculated and is listed in Table 6.5a. The centre of gravity of TNO-10 dummy was calculated and listed in Table 6.5b.

TNO-10 dummy was modelled and the joints of the dummy are indicated in Figure 6.5b. The inertial components were defined with respect to the wheelchair rear axle centreline, the positive direction being x-axis to forward, y-axis to the portside of a wheelchair and z-axis downward.

Table 6.5a CG calculation of Hybrid II dummy

Initial Positions (inertial reference)					
Seg	W	X	Z	M_x	M_z
Units	kg	m	m	kg*m	kg*m
LT	16.28	0.85	-0.65	13.83	-10.57
MT	2.20	0.78	-0.74	1.72	-1.64
UT1	18.82	0.76	-0.95	14.33	-17.93
UT2	4.15	0.76	-0.96	3.15	-3.98
NK	1.16	0.72	-1.15	0.83	-1.33
HD	5.08	0.72	-1.30	3.65	-6.58
RUL	6.17	1.11	-0.65	6.82	-4.00
RLL	3.26	1.34	-0.51	4.37	-1.68
RF	1.24	1.49	-0.26	1.84	-0.32
LUL	6.17	1.11	-0.65	6.82	-4.00
LLL	3.26	1.34	-0.51	4.37	-1.68
LF	1.24	1.49	-0.26	1.84	-0.32
RUA	2.03	0.79	-0.89	1.60	-1.80
RLA	1.72	0.89	-0.77	1.54	-1.32
LUA	2.03	0.79	-0.89	1.60	-1.80
LLA	1.72	0.89	-0.77	1.54	-1.32
RHD	0.58	1.10	-0.78	0.64	-0.45
LHD	0.58	1.10	-0.78	0.64	-0.45
total	77.67			71.13	-61.17
			CG_x	0.92	
			CG_z	-0.79	

Table 6.5b CG calculation of TNO-10 dummy

Initial Positions (inertial reference)					
Seg	W	X	Z	M_x	M_z
Units	kg	m	m	kg*m	kg*m
LT	16.28	0.85	-0.65	13.85	-10.57
MT	2.20	0.78	-0.74	1.72	-1.64
UT1	18.82	0.76	-0.95	14.35	-17.94
UT2	4.15	0.76	-0.96	3.16	-3.98
NK	1.15	0.72	-1.15	0.83	-1.32
HD	5.08	0.72	-1.30	3.66	-6.58
RUL	6.17	1.10	-0.65	6.82	-4.00
LUL	6.17	1.10	-0.65	6.82	-4.00
MLL	9.05	1.31	-0.50	11.83	-4.56
RUA	2.07	0.78	-0.89	1.60	-1.85
LUA	2.07	0.78	-0.89	1.60	-1.85
Total	73.20			66.24	-58.29
			CG_x	0.90	
			CG_z	-0.80	

The centre of gravity (CG) of components can be calculated by the following formula: $M_x = W \cdot X$, $M_z = W \cdot Z$, $CG_x = M_x/W$, $CG_z = M_z/W$. W is weight of components; X and Z are initial positions relative to inertial reference. M is moment of components. The centre of gravity of TNO-10 dummy without legs is calculated in Table 6.5c.

Table 6.5c CG calculation of TNO-10 dummy (without leg)

Initial Positions (inertial reference)					
Seg	W	X	Z	M_x	M_z
Units	kg	m	m	kg*m	kg*m
LT	16.28	0.82	-0.65	13.34	-10.57
MT	2.20	0.75	-0.74	1.65	-1.64
UT1	18.82	0.73	-0.95	13.75	-17.94
UT2	4.15	0.73	-0.96	3.03	-3.98
NK	1.15	0.69	-1.15	0.79	-1.32
HD	5.08	0.69	-1.30	3.50	-6.58
RUL	6.17	1.08	-0.65	6.64	-4.00
LUL	6.17	1.08	-0.65	6.64	-4.00
RUA	2.07	0.76	-0.90	1.57	-1.85
LUA	2.07	0.74	-0.89	1.54	-1.85
Total	64.15			52.44	-53.73
			CG_x	0.82	
			CG_z	-0.84	

6.5.2 Contact force model

Static force deflection characteristics of the contact situations were approximated by linear functions and correlated by dynamical tests and CVS models. Coulomb friction to resist the sliding of upper leg relative to the chair and the wheelchair relative to the vehicle floorboard were estimated.

More details of modelling of WTORS using CVS dynamic programs will be discussed in Chapter 7 and 8. Here we just indicate some possibilities as follows:

- A fairly obvious step should be involved to treat the foundation of WTORS in a similar manner to which was used for the dummy. This would result in a three degree of freedom system.
- Another parameter that should be taken into account is that of hysteresis in the material of the webbing belts. This would absorb some of the energy in WTORS. It

could be treated as a kind of friction. One might allow for this by putting a suitable dashpot in parallel with the spring k_F .

- One effect that has so far been neglected is the belt slippage because of anchorage deformation and wheelchair axle bending during impact. This effect is a non-linear effect that could not be avoided. It is rather awkward to handle mathematically and it will be further simulated using explicit finite element models.

CHAPTER 7: FINITE ELEMENT ANALYSIS OF WHEELCHAIR

Finite Element Analysis (FEA) is the result of applying of the discretisation principle. It was derived from structure matrix analysis, which was firstly named by Professor R. W. Clough in 1960 (Hoffmann et al, 1990). The FEA method has been widely used in both force analysis and equation calculation.

This Chapter presents a static and dynamic force analysis of the structures of both the surrogate wheelchair and the production wheelchair. A combination of FEA techniques with dynamic sled tests was employed to allow a more detailed description of the crash performance of the wheelchairs. The loading analysis of the production wheelchair was based on dynamic sled test results. The correlation between the computer models and experimental results was also presented. The dynamic analysis method was involved to investigate the crash performance of the surrogate wheelchair. The correlation of a static load to the actual dynamic load in a given crash severity was developed.

7.1 Introduction

The sled impact testing of WTORS has been presented in Chapter 5. It was shown that the wheelchair frame itself was the limiting factor in the frontal impact. Under impact condition, the loads transferred to the wheelchair are of sufficient magnitude to cause its deformation, and even collapse of the joints in the wheelchair frame and hence injury to the disabled occupant. In order to strengthen the joints of the wheelchair's tubular structure, it is necessary to determine the values and directions of the forces and moments acting on the individual joints and tubes of the wheelchair.

The FEA method applied to the solutions of force analysis of WTORS mechanism has facilitated the designers to gather data, such as the wheelchair Centre of Gravity (CG), the mass moment of inertia of the wheelchair in the three principal direction, I_x , I_y , and I_z , for the construction of CVS model (Chapter 9). All

components placed in the wheelchair, such as the tubular structure of the wheelchair, the battery and other parts, were incorporated into the model by scaling their masses and distributing them about the places where they are attached to the sled.

The solid modelling program, PIG and FEA modelling program, PAFEC (V7.4, 1992) were used running on the VAX cluster (Appendix 7A). The CVS programs, DYNAMAN and MADYMO were also used to consider the data supplied from the FEA model.

7.2 FEA Model Requirements

Finite Element Analysis is a numerical approximation method. Two errors could be occurring. One is called the discretisation error, which occurs when the calculation model is used to simulate the engineering cases. Another is called calculation error, which depends on the FEA program implementation. The fine mesh would reduce the discretisation error, but it also would increase calculation error. In general, the former error is much larger than the latter. The accuracy of structural FEA mainly depends on the discretisation, that is, the model set-up.

FEA model set-up should meet the following requirements:

- *Accuracy* - to co-ordinate between the component shape and structure;
to co-ordinate between the supporting systems and boundary conditions;
to co-ordinate between loading conditions and actual working conditions.
- *Economy* - to reduce pre-process and CPU time.

7.2.1 Boundary conditions

A wheelchair is a brazed pre-shaped tubular structure. There are two supporting systems to be co-ordinated with boundary conditions in a WTORS, rigid support and flexible support. The rigid support consists of wheelchair rigid frame supported by wheels. The flexible support considers wheels supported by ground floorboard as the wheels have large elastic deformation under external loading.

7.2.2 Loading conditions

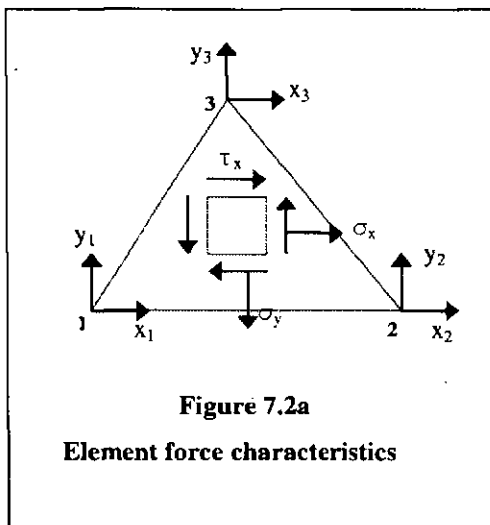
The loading conditions had been defined before FEA was used to analyse the component structure. The loading location depends on different working conditions.

Two loading cases were considered in a WTORS analysis: concentrated and distributed loading. Loading was also considered in the dynamic mode to take into account any variations as a function of time. For example, the structure of a wheelchair would sustain a complicated loading pattern when it was suddenly accelerated.

The following formula was reasonably used to estimate the loading conditions in a WTORS system design:

$$\begin{aligned} \text{the maximum tiedown force} &= \text{total mass of WTORS times} \\ &\quad \text{the peak resultant acceleration of dummy's chest} \end{aligned}$$

7.2.3 The FEA process



An infinite elastic continuum component can be simplified into finite degrees of freedom by a discretisation principle and solved by structural matrix analysis method. The FEA process could be summarised as follows:

1) *Discretisation of an infinite elastic continuum component*

Finite elements are defined and meshes are divided, including selection of the co-

ordinate systems, element type, mesh size, boundary conditions and loading conditions.

2) *Selection of element deflection functions to simulate the distribution rule within element deflection.*

3) *Analysis of element force characteristics*

As an example, membrane element was used to calculate the element stiffness matrix and equivalent node loading matrix. The details of membrane element will be described in Chapter 8. The loading of the membrane element is characterised by the

Cauchy stresses, which are constant within each membrane element. Three non-zero components of the stress are determined with respect to the element co-ordinate system. The positive direction of the x -axis can be determined as it corresponds with the direction of the right handed screw if rotation from node 1 past node 2 towards node 3 (Figure 7.2a).

The relationship of four physical parameters: node deflection $\{\Delta\}$, element strain $\{\epsilon\}$, element stress $\{\sigma\}$ and node force $\{F\}$ is illustrated in Figure 7.2b. The strain matrix $[S]$ and elastic matrix $[E]$ are constant matrices. $[k]$ is the element stiffness matrix. The element volume (V) is the element thickness times the element area.

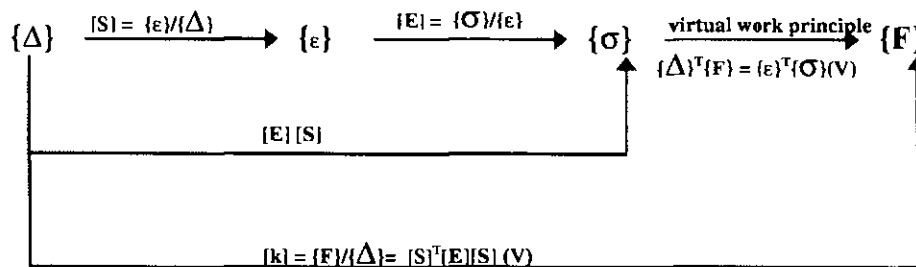


Figure 7.2b The relationship of four physical parameters in a FEA model

4) Integral calculation of total stiffness matrix

This calculation is based on the following principles:

- All elements have the same deflection on the combined nodes
- The node force is equal conditions to nodal loading.

The total structure stiffness matrix $[K] = \{R\}/\{\Delta\}$. $\{R\}$ is the resultant of element force $\{F\}$.

5) Modification of calculation model and design

The node deflection $\{\Delta\}$ was achieved by boundary conditions and $[K]$ modification.

6) Stress equivalent graphs

The stresses on the element and node were achieved and results were summarised in stress equivalent graphs. The flow chart of FEA process is listed in Figure 7.2c.

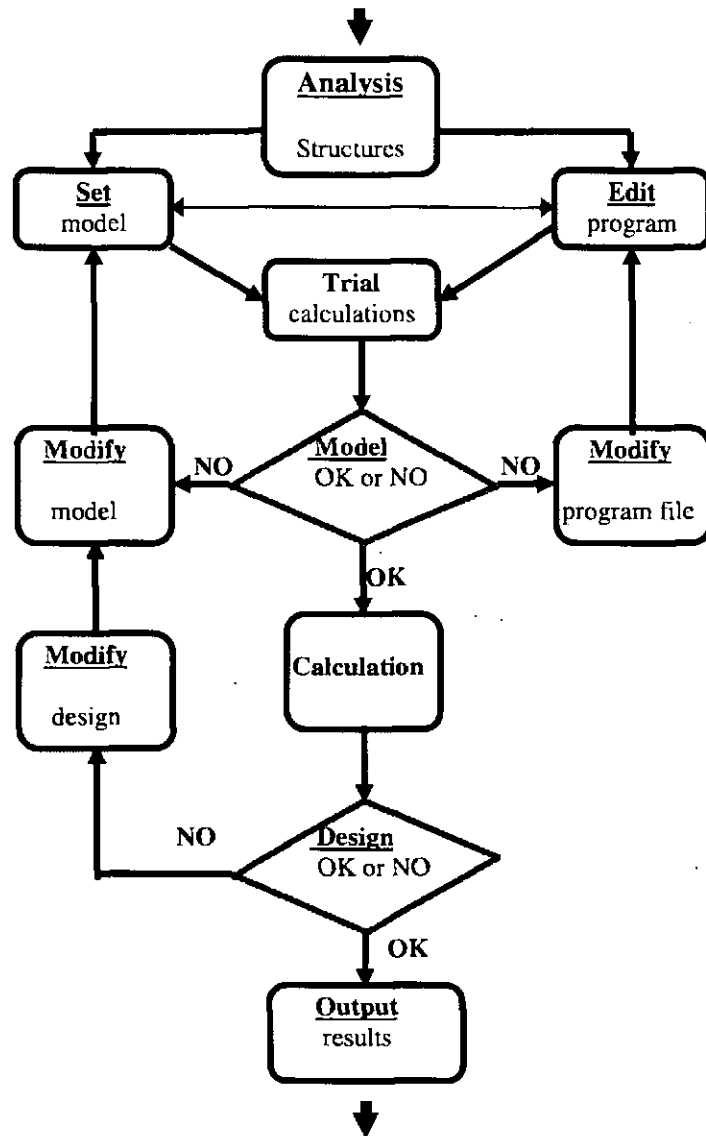


Figure 7.2c FEA modelling flow diagram

In the dynamic structure, the strain and stress vary not only with the space position but also with time. In this programme, one of dynamic FEA methods, modal frequency and shape analysis was employed. The natural frequencies and mode shapes of a structure are independent of any loading. The mode shapes were

calculated using a limited number of dynamic freedoms called masters, or eigenvalue (ω^2) and eigenvector ($\{\Delta\}$).

Rigid body modes were identified by very low frequencies from the shapes plotted out. The sizes of these rigid body frequencies provided a powerful check on the numerical accuracy of the calculation. PAFEC suggests that the true value probably lies in the following bounds (PAFEC 7.4, 1992):

$$f_i \cdot [1 \pm (f_r/f_i)^2]^{1/2} \quad (7.1)$$

This expression shows that if the highest rigid body frequency (f_r) is more than a third of the lowest non-rigid body frequency (f_i) then the errors in the latter exceed 6%. The following changes were involved for unacceptable inaccuracy:

- Re-mesh any areas where the elements are small since this gives rise to numerical calculation error
- Reduce the number of masters especially when manually chosen masters are used to increase the numerical precision.

7.3 Loading Analysis of a Manual Wheelchair

Many types of production wheelchair have been used in WTORS crash testing in the previous researches (Gu et al. 1995), such as standard manual wheelchairs, powered wheelchairs, scooter-type wheelchairs, and special wheelchairs. As a result of these tests, the strong and weak points of standard wheelchairs have been determined. The performance of specific tiedown systems with certain chairs has been observed.

The extreme crash severity results in a large amount of chair deformation and involves the high cost of replacing damaged parts. The surrogate wheelchair facilitates a standardised test, ensuring that all WTORS could be tested repeatable within-lab consistency and reproducibly between-lab consistency (Shaw et al. 1994). In essence, the surrogate wheelchair provides a base design field for all WTORS and presents a worst case loading severity for systems. In this Chapter reference has been made to TRL surrogate wheelchair and one of the manual wheelchairs (HNE, Classic Universal in Figure 7.3a).

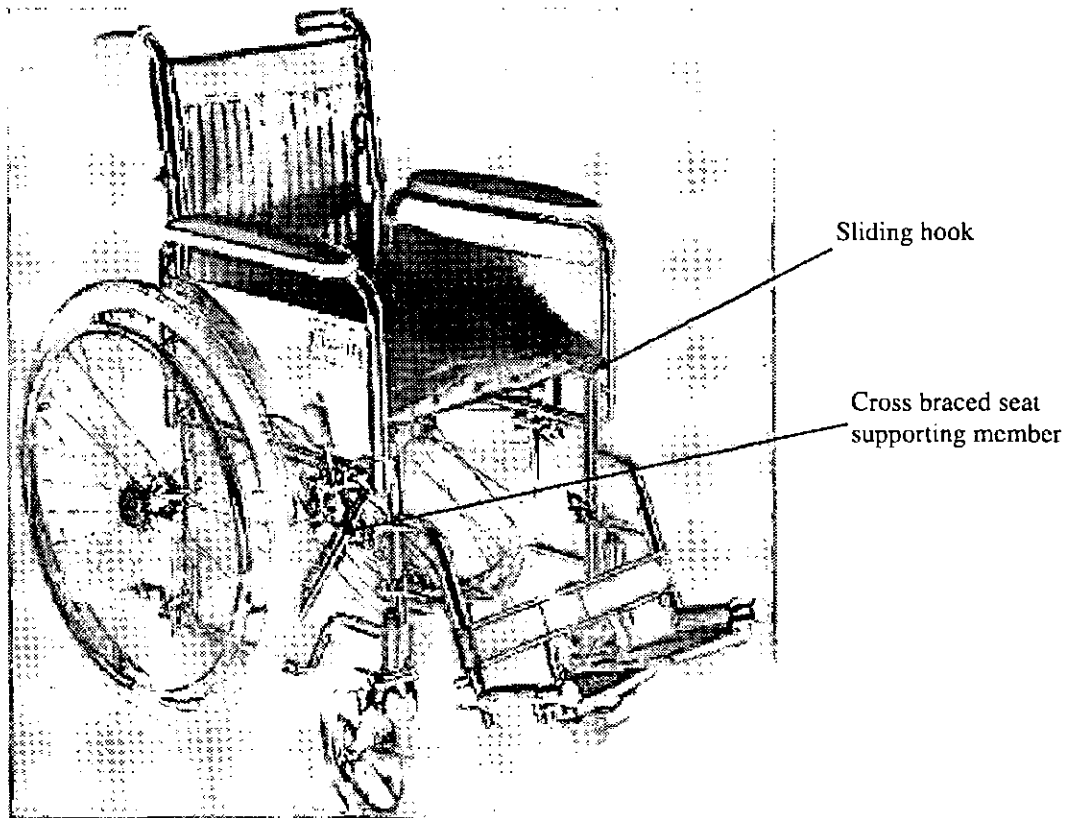


Figure 7.3a Classic Universal wheelchair

7.3.1 Load analysis from sled tests

Sled tests implied that the production wheelchair frame becomes severely distorted and that the tubes at certain load-bearing joints were pulled apart, such as, the castor tube. The forces causing the deformation are not pure tension or compression. It is the combined effect of tension and compression with large bending moments.

Dynamic sled tests also revealed that it is difficult to decide the magnitude and directions of loads acting on the wheelchair frame from the deceleration force of sled during impact. This is because the combination movements of dummy sitting on the wheelchair and wheelchair floating on the sled. After examination of the high speed video footage of testing, it was found that the wheelchair was progressively loaded by the sled deceleration and the loads transferred to the wheelchair moved forward to the front castor wheels. The impact tested wheelchairs were then examined to determine the areas of maximum deformation and gain an overall picture of the impact forces

effect on the wheelchair. All load cases are the result of initial assumptions of the force distribution in the frame of the wheelchair. The two halves of the wheelchair frame are initially assumed as equal force allocation due to the symmetry structure. The front edge of the seat is the worst possible position. If the seat belts restraining the movements of the dummy are loose the dummy body could slide forward until its CG lies directly over the front edge of the seat. The load can be increased on the front castor wheels causing them to fail.

The wheelchair (15 kg) was progressively loaded by dummy resultant acceleration (about 40g) at the sled severity of 48 km/h, 20g. The force acting through the CG of the dummy (mass 75 kg) was about 30 kN. Only about one quarter of this value (7.2 kN) was considered in a manual wheelchair seat load condition as the seat loads of 14.7 kN was found in ISO surrogate wheelchair (90 kg) tests in the same crash severity. This load transferred to the chair seat would be assumed in the order of about two-thirds in the front (4.4 kN) and one third in the rear (2.8 kN). Furthermore, the loads transferred to the chair backrest would be assumed in the order of about one-third to upper backrest (2.4 kN) and two-thirds to the lower backrest (4.6 kN).

7.3.2 Structural modelling of a manual wheelchair

The detailed real deformed parts were modelled as follows:

- *The sliding hook*

The sliding hook does not restrain the movements of the seat member in the z-plane and y-plane in the impact situation. The locating hook was modelled as the seat member is free to slide in the joint in the x-plane but is fixed and unable to rise in the y-plane.

- *Cross-braced seat supporting member*

The positioning of the cross-braced members was set behind the centre of the chair, which the occupant's centre of gravity lies directly overhead in normal operation, thus causing maximum bending moment at the cross braced joint.

- *Wheel assembly*

The rear wheel axles were modelled using the rear axle joint and the front castor wheel axles passing through front axle joint. The axle could not move in the y-axis and z-axis but is free to move in the x-axis. The same boundary conditions were

applied to the front castor wheels. All removable parts, such as armrests and footrests were removed. It was assumed that all these parts had no constructive part to play in the structural strength of the standard wheelchair.

7.3.3 Element types used in the model

A combination of the following four element types were used in FEA manual wheelchair model:

Type 1: *Simple beam element (34000)*

This is a straight uniform beam element with two nodes.

Type 2: *Shear deformation and rotary inertia beam element (34100)*

A straight uniform beam element with shear deformation is included. There are six degrees of freedom (u_x , u_y , u_z , ϕ_x , ϕ_y , ϕ_z) at each of the two nodes. This element was applied in seat hook structure and cross-braced seat supporting members.

Type 3: *Curved beam element (34300)*

This element is part of a circle. Two node numbers are given in the topology and these are positioned at the centres of area of the cross-section at the two ends of the element. Shear deformation and rotary inertia are included. This element was applied to all round corners in the manual wheelchair.

Type 4: *Tension Bar Element (34400)*

This is a straight uniform element that carried end load and applied in wheel axis.

7.3.4 Model results

A post-processing program, PIG was run to post process the simulation. As the larger deformation was found in this model, the static loading analysis was used to investigate the positions of higher loading. The higher load positions in the HNE wheelchair (marked as 1,2,3 in Fig 7.3b) were found from the model. The highlighted element 1 posses higher shear force (z) (range from 820 N to 1000 N) and higher bending moment (y) (range from 211 Nm to 251 Nm); The highlighted element 2 possesses higher shear force (y) (range from 580 N to 880 N) and higher bending moment (x) (range from 880 Nm to 990 Nm); The highlighted element 3 possesses

higher shear force (x) (range from 500 N to 880 N). The complete FEA modelling code is listed in Appendix 7A.

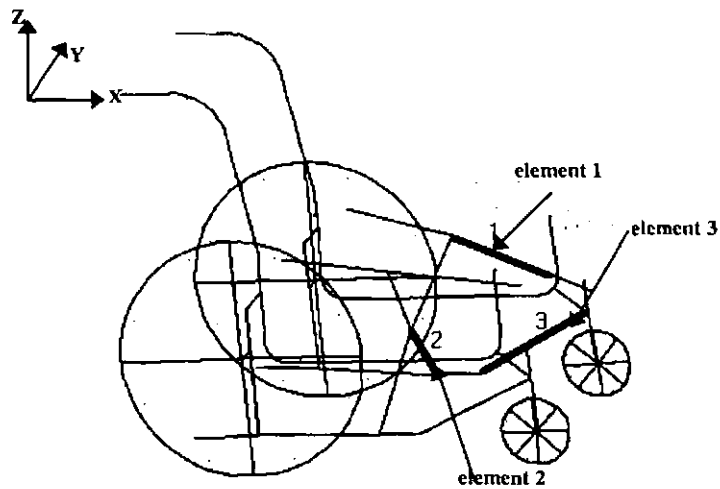


Figure 7.3b Element structure simulation of a manual wheelchair

7.4 Modal Analysis of TRL Surrogate Wheelchair

The most straightforward type of dynamic analysis is the determination of natural frequencies and mode shapes. This type of calculation gives considerable insight into the dynamic behaviour of a structure. All the separate elements of the surrogate wheelchair, such as tubes were built with a simple beam element (34000) (Figure 7.4a). The surrogate wheelchair was simplified as beam elements without wheels as the wheels were assumed no constructive part to play in the structural strength of the wheelchair.

Interest was drawn in low frequency property of the wheelchair as rigid body modes were identified by very low frequencies. Five modes were used to figure out the complete mode shape.

Figure 7.4b demonstrates the determination of natural frequencies in a restrained three dimensional surrogate wheelchair structures. The dotted line is the deformed mode. Mode 1 is the 1st twisting vibration along x axis. Mode 2 is the 1st bending vibration around y axis. The wheelchair rear part vibrated to a maximum around the rear wheel axis. Mode 3 is 2nd bending vibration around y axis. The wheelchair rear part vibrated to a maximum around the frontal wheel axis. Mode 4 is 3rd bend vibration around y axis. The wheelchair lower part did not vibrate. Mode 5

is 2nd twisting vibration in the rear part of the wheelchair. It was concluded that 1st, 2nd bending vibration and 2nd twisting vibration resulted in larger deformation of the rear part of wheelchair than the other parts. This was validated by dynamic tests where the dummy vibrated from the rear to front and to rear of wheelchair (rocking effects) during FFF impact. The investigation has also shown that a twisting of the wheelchair about the x-axis occurred causing uneven forces in the two halves of the wheelchair frame.

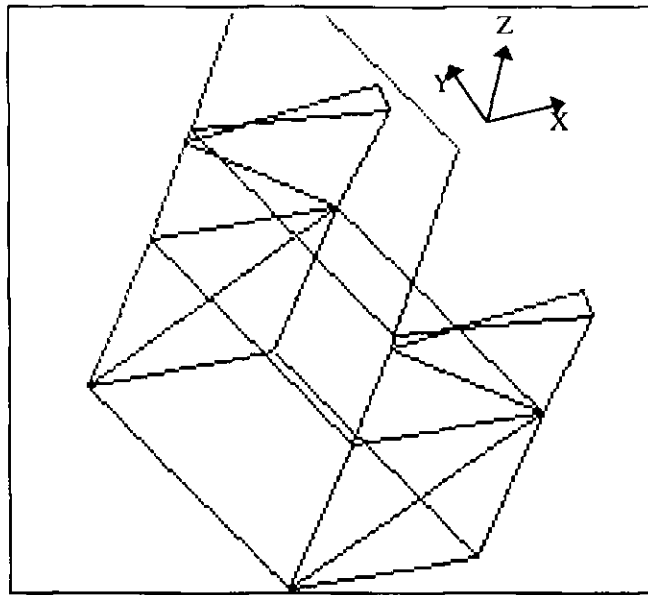


Figure 7.4a Beam structure elements in TRL wheelchair

Since parameter investigations using sled tests are costly and time consuming to perform, computer simulation has been popular to simulate the crash environment. It has been used as a tool for examining the effects of crash pulse variations. How to find the correlation between the static model and dynamic model is another subject in this research programme.

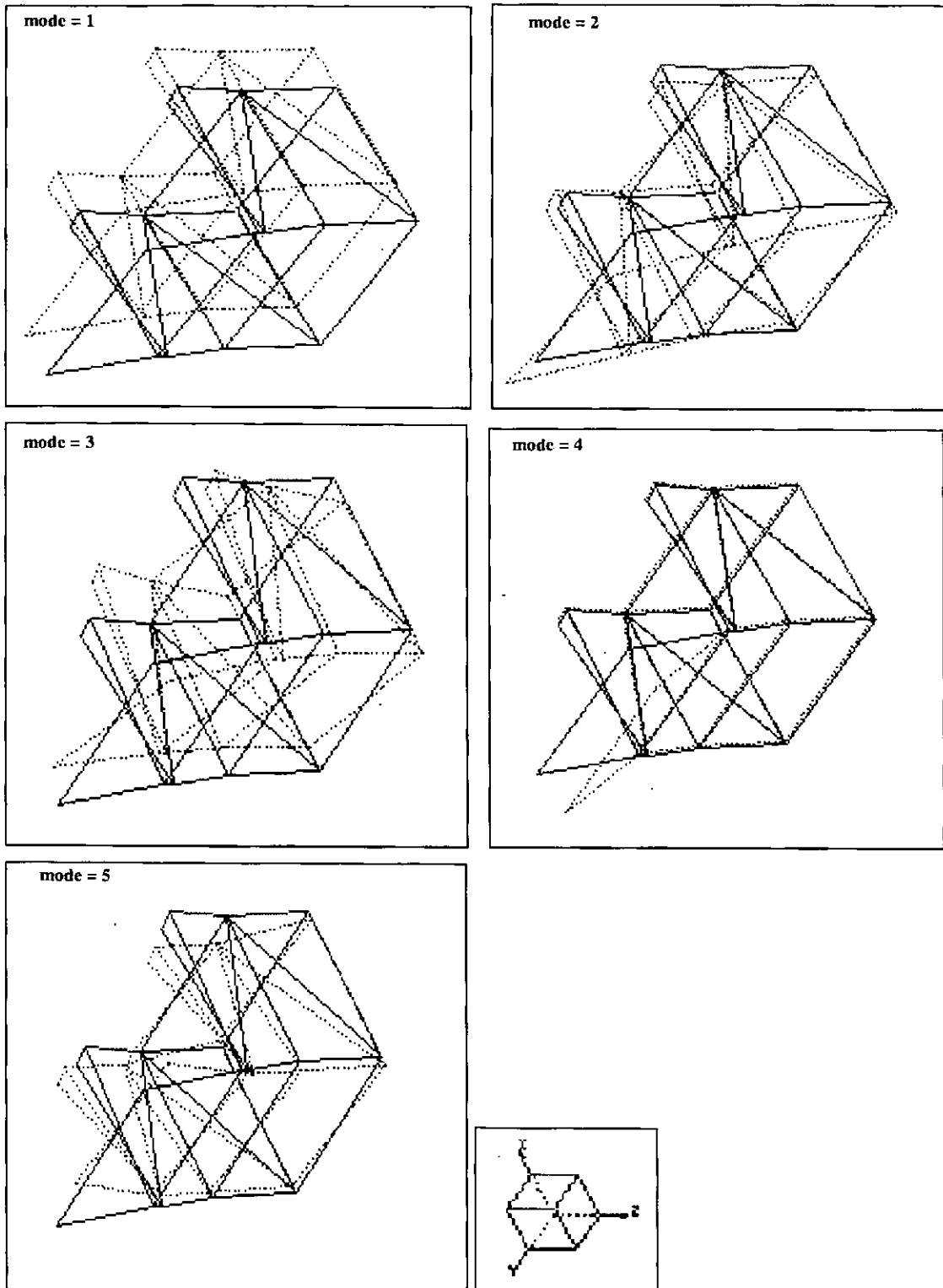


Figure 7.4b Five modes analysis of TRL wheelchair

7.5 Correlation of Wheel Contact Characteristics

The correlation between static model and dynamic experimental results was made more accurate by adjusting the various stiffness functions, friction penetration factors, and correction factors. More details of CVS modelling of WTORS using dynamic CVS program will be discussed in Chapter 9. Here we just indicate some possibilities to use FEA model results to support CVS model. Considering the data supplied from the above FEA model, a CVS model of TRL surrogate wheelchair was initially written within DYNAMAN program. The surrogate WTORS system was modelled as linear segments whose stiffness properties were initially determined experimentally from static testing. Finally, they were validated and adjusted by dynamic sled test results.

Observed from the high speed video footage (Appendix 5C and 5D), the rear wheels of the wheelchair were compressed downwards during the initial phase of impact and the front wheels were lifted off. The wheelchair was then shifted from its initial position to forward due to the dummy movement.

The wheelchair tyre contacted on the floorboard was considered as a non-linear elastic flexible support. The properties of the tyre were devised into two phases: a linear static phase before impact followed by a non-linear dynamic phase during impact. These phases were modelled by a main linear spring and an additional non-linear spring. When the main spring is deformed to a certain point, the additional spring is engaged to simulate the dynamic non-linear property of the tyre.

Two beam elements (\mathbf{b}_1 and \mathbf{b}_2) and one gap element (\mathbf{b}_3) were selected at spring forcing point 'C' (Figure 7.5a). A_1 is the section area of the beam element \mathbf{b}_1 , $A_1 = k_1 L_1 / E$, $k_1 = \tan \alpha_1$, k_1 is equivalent stiffness of first straight line. A_2 is the section area to the second beam element \mathbf{b}_2 , $A_2 = k_2 L_2 / E$, $k_2 = \Delta P / \Delta \delta$, k_2 is equivalent stiffness of second straight line (Figure 7.5b). The gap element is non-linear compressing element as the gap could not be predicted during loading period. If $\delta_1 = 0$, the beam element \mathbf{b}_2 is involved. The tyre deflection point 'C' was assumed as upward deformation. If point 'C' up deflection is larger than δ_1 , both beam elements are loaded, equivalent two springs parallel connected. If point 'C' up deflection is smaller than δ_1 , only beam element \mathbf{b}_1 is

loaded. The deflection is a function of the loading conditions. The values of k_1 and k_2 can be automatically varied by gap element.

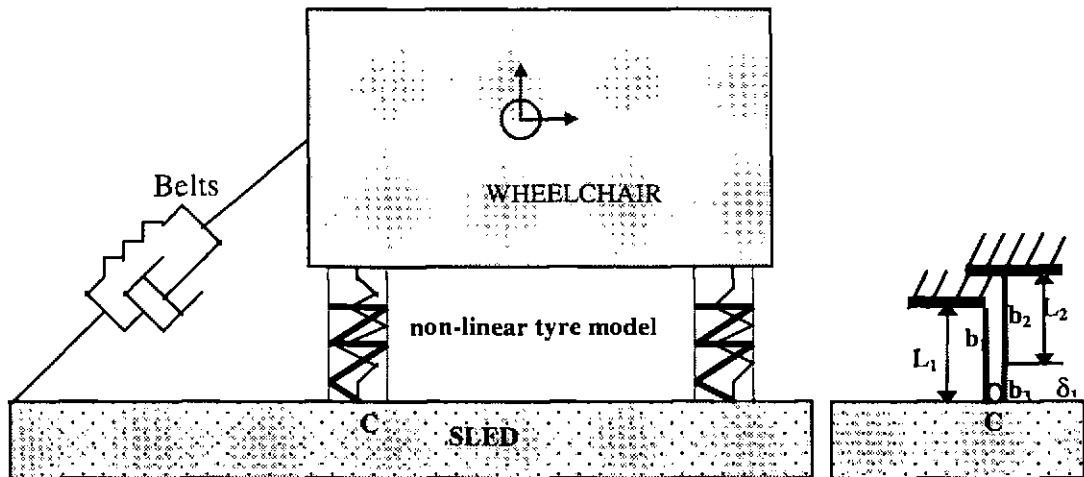


Figure 7.5a A wheelchair tyre model by FEA

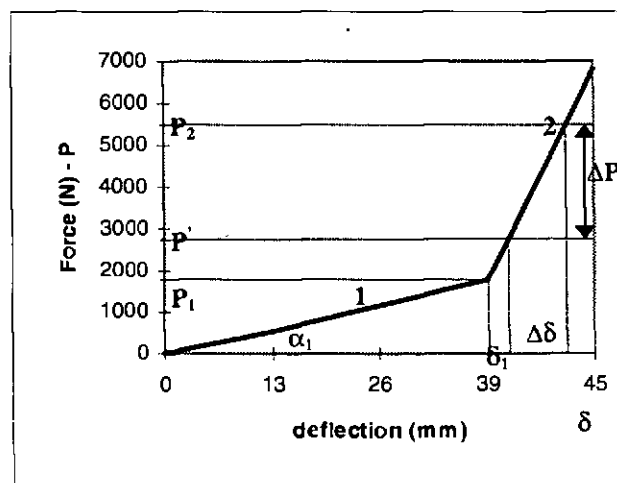


Figure 7.5b Tyre non-linear stiffness (correlation)

7.6 Summary

- The loading analysis can be achieved using FEA models to investigate different parameters effect on WTORS system.

- The correlation of a static load to the actual dynamic load in a given crash severity was investigated using an additional spring model. It is very important stage for modelling accurately of dynamic response of WTORS.
- Further study of impact properties is needed to get a better correlation between the models and experiments. One of the areas in which an improvement is required, is a means of modelling of the contact and friction forces exerted between the ground and the pneumatic tyre. Another area for improvement is the modelling of different restraint systems. The interconnect the FEA model into CVS model will be discussed in Chapter 8.

CHAPTER 8: CRASH VICTIM SIMULATION (CVS) AND APPLICATIONS

In this Chapter, the past and current computer modelling technique for vehicle industry are firstly reviewed. The Crash Victim Simulation (CVS) modelling method and its applications are introduced. This is followed by a description of the approach and theory used in MADYMO3D code. To illustrate the potential of this code the results of WTORS front impact simulations and experimental test results are compared. The techniques, which have been used to interconnect the finite element belt model and finite element tyre model into their relative CVS models, are also discussed in this Chapter.

8.1 Introduction

In the early design, lumped parameter models for predicting vehicle response using static crush data have been in use for several years (Grew, 1985 and Deng, 1988). Another method of modelling is by considering the structure as an assembly of a number of individual beams connected at nodal points. Structural properties are incorporated in the beam stiffness matrix. Collapse properties of the beams and joints are measured using quasi-static tests. Combination of the lumped mass approach and space frame modelling can be realised using a MULTIBODY approach, where the structure as well as the occupant are represented by rigid bodies interconnected by arbitrary kinematic joints. A comprehensive approach of modelling large deformations is by Finite Element Analysis (FEA) method. In this case, detailed information about the structural components must be available. A complete and accurate description of both component stiffness and mass distribution is essential for the analysis. Areas directly involved in the deformation have to be meshed in fine detail.

Back in 1963, McHenry proposed a 2D numerical model to describe the motion of a vehicle occupant in a collision event (McHenry, 1963). A 2-D computer model was developed by Automotive Safety Centre of Volvo Corporation in 1974.

Variations were introduced to standard half-sine crash pulse. The resulting affect on outputs such as occupant accelerations, Head Injury Criterion (HIC), Chest Severity Index (CSI), excursions and belt forces were examined. In conclusion, the author introduced a velocity tolerance band to characterise the sled crash pulse, as opposed to the traditional acceleration tolerance corridors. In 1977, Nissan Motor Corporation conducted a study using computer simulation in an effort to determine the influence of the vehicle deceleration curve on dummy injury criteria. MVMA-2D crash victim simulation package was used. It was found that for the same velocity change (ΔV), the dummy injury criteria could be drastically different. They concluded that the vehicle deceleration curves exhibited the higher residual deformations (RD), and coincidentally, the lower peak sled deceleration produced the smaller dummy injury criteria.

In 1970, a 3D occupant model was published by Robbins (Robbins, 1970). This initial development was followed by a number of more general occupant simulation tools. Parameter studies have been conducted by several researchers and engineers to assess the relative effects of varying input parameters on output parameters (Lundell, 1984). Elaborate computer simulations have been developed to study occupant kinematics and vehicle deformation patterns (Matsumoto, et al, 1990).

A single degree-of-freedom game theory, or a constrained optimisation method was used to find crash pulses falling within the bounds of the ISO crash pulse corridor at University of Virginia (Scavnicky, 1994). The occupant simulation package DYNAMAN was used to investigate the sensitivity of the ISO crash pulse corridor using the best and worst pulses derived from the optimisation technique.

In the last few years, computer simulation has been increasingly used as a method for optimising wheelchair structure and improving occupant protection (Grew, 1985, Adams, et al, 1994). A wheelchair-occupant model was built at the University of Virginia (Scavnicky, 1994) using ATB, a simple version of DYNAMAN. The same package was also conducted at University of Pittsburgh (Digges, K, 1994). In this research programme, computer simulation of WTORS in frontal impact has firstly been conducted using a sophisticated computer CVS program, MADYMO3D and finite element analysis techniques.

8.2 Co-ordinate Systems

There are four co-ordinate systems used in CVS modelling of WTORS:

- *Inertial (ground) Co-ordinate System (ICS)*
- *Vehicle Co-ordinate System (VCS)*
- *Body segment reference Co-ordinate System (BCS)*
- *Joint Co-ordinate System (JCS)*

Inertial co-ordinate system is defined in INERTIAL SPACE in the MADYMO program. The plane is defined by the direction of a right-handed screw rule (outside normal) by three points. A sled plane is required for frontal impact models to define the contact movement of the sled and wheelchair. In a WTORS frontal impact model, the origin of the inertial reference co-ordinate system was assumed to be zero (0,0,0) at the middle of the furthest left edge of the sled. The frame of reference was arbitrary and specified by defining the gravity vector to be pointing downward in the input. This was done by defining the three components of the gravity vector (0,0,9.81) to be represented by $g = 9.81 \text{ m/s}^2$. The x-axis is chosen in the initial direction of travel of the sled, the y-axis is then to the right (starboard). The inertial co-ordinate system is marked in Figure 8.2 by thick lines. The shortest axis is z-axis and the longest axis is x-axis.

The origin and frame of reference of the vehicle co-ordinate system was arbitrary and assumed to be (0,0,0). It was selected at the same position to the inertial system used to define the location of contact panels and tabular time histories of sled pulses in a fixed sled model.

The body local co-ordinate system is defined by GEOMETRY in a system. The co-ordinate of the joint on the corresponding parent body (distance from the last body) and co-ordinate of the centre of gravity of the child body are defined. The origin of BCS was selected at the location of the joint with the corresponding parent body. This restricts the allowed location of these origins on the bodies to points on the corresponding rotation axis. The origin of the wheelchair was defined in position at the centre of the wheelchair directly between the two rear wheel contact points to the sled (CHR shown in Figure 8.2).

Joint co-ordinate system is chosen at the centre of mass of each body to simplify the input of JCS. The x-axes are perpendicular to this plane, positive to the

right. The y - and z -axis of all body local co-ordinate system are chosen in the plane of symmetry. Thanks to this choice there is no need to specify the orientation of the inertial co-ordinate system.

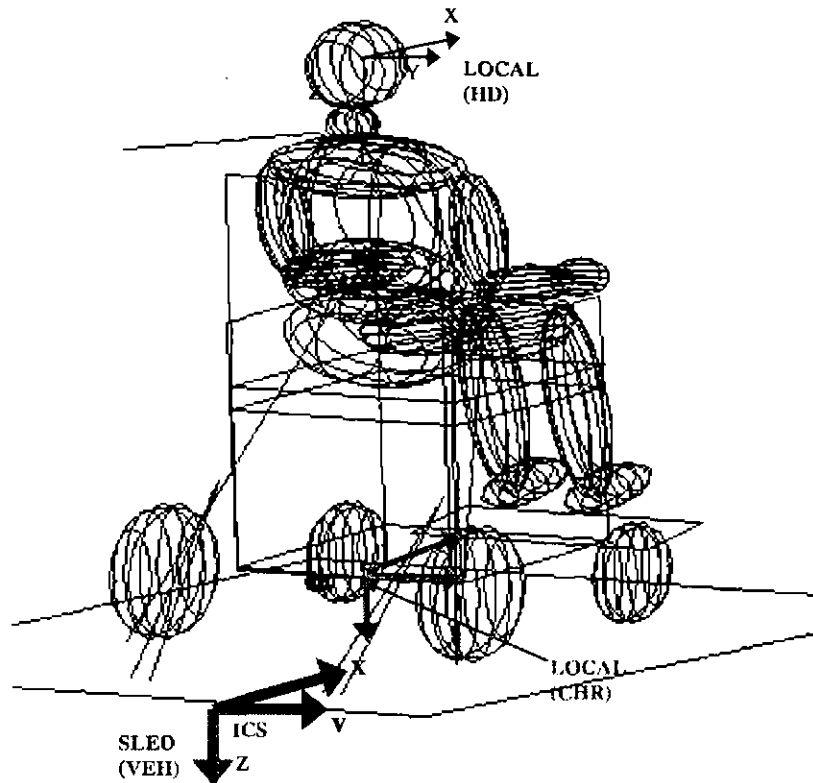


Figure 8.2 General co-ordinate system convention

If the JCS is not chosen at the centre of mass of each body, it has to be defined by ORIENTATIONS in the joints. Orientation can be specified using three methods: by up to three successive rotation angles in radians, by vector method and by screw axis method. In the vector method, the direction of two axes are defined by two vectors \mathbf{u} and \mathbf{v} . The vector, \mathbf{u} , must be parallel to the x -axis and the vector \mathbf{v} must be parallel to the x - y plane (not parallel to the x -axis). The components of these vectors are with respect to the (x_i, y_i, z_i) co-ordinate system. In screw axis method, the final orientation of the rotating co-ordinate system is the result of a single rotation about a screw axis.

8.3 Multibody Systems

Multibody systems include kinematic joint, 3D CARDAN restraint models, joint degrees of freedom and initial conditions for equilibrium analysis, etc.

8.3.1 Kinematic joints

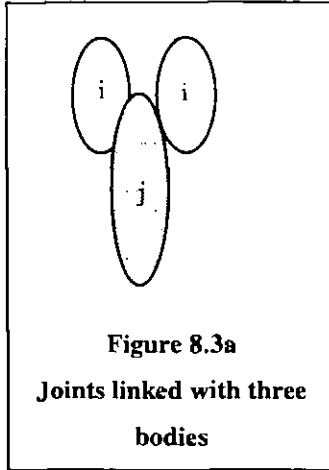


Figure 8.3a
Joints linked with three
bodies

The joints are defined in two groups in account of joint connection methods. Group 1 is Euler joint, which is a combination of pins connected together, such as universal joint and revolute joint. Group 2 is non-Euler joint, such as spherical joint, bracket joint, translational joint, cylindrical joint and free joint. Five Parameters were used in the joint specification, that is, joint stop angle, the energy dissipation function, and the linear, square, cubic torque coefficients. In addition, friction and damping can

be specified.

A kinematic joint constrains the relative motion of the pair of bodies. The parent body is denoted by *i* and the child body by *j*. As an example of TNO-10 dummy model, the lower leg connected two upper legs (Figure 8.3a). It was modelled using two joints, one joint connected between upper leg and lower leg, another joint connected between lower leg and the other upper leg. Both joints had the same location on lower leg.

8.3.2 CARDAN restraint models

The joint stiffness (force model) specified elastic, damping and friction loads for kinematic joints corresponding the joint degrees of freedom. Torque in spherical joints and free joints were specified using CARDAN RESTRAINTS and opposite torque was applied on the connected objects. A restraint co-ordinate system was defined on each body of the pair of bodies that were connected by a restraint. In the CARDAN restraint model the relative orientation of the restraint co-ordinate systems was described by means of three successive rotations, known as Bryant or CARDAN angles. The CARDAN angles define the orientation of restraint system *j* relative to restraint system *i*. The rotation angles phi (φ) fixed to body *i*, theta (θ) about a floating

axis and psi (Ψ) about an axis fixed to body j , carried out about x_j , y_j and z_j respectively (Figure 8.3b).

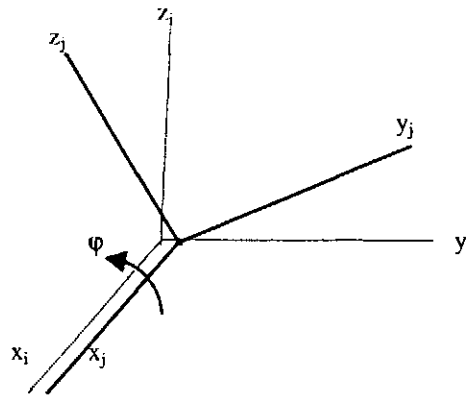


Figure 8.3b Relative orientation of co-ordinate systems using Bryant angles

8.3.3 Joint degrees of freedom

The relative motion of a pair of joint co-ordinate systems is described by three joint degrees of freedom (DOF): the joint position, velocity and acceleration. Joint position degree of freedom is as a function of time under the keyword MOTION. A spline interpolation was used to obtain the prescribed value at an arbitrary point of time. The corresponding joint velocity and acceleration degrees of freedom were determined from this spline approximation. The details of joint position DOF are listed in Table 8.3. The number of joint position DOF of a spherical joint equals four Euler parameters: q_0, q_1, q_2, q_3 , which define the relative orientation of the joint co-ordinate systems. In spherical and free joints, angles of rotation are introduced so that the relative orientations of the joint co-ordinate systems are defined. The non-linear elastic load Q_e is a function of the joint degree of freedom q :

$$Q_e = Q_e(q) \quad (8.1)$$

Table 8.3 Joint position DOF for 3D joint types

Joint type	Characteristics	Applications	Joint DOF						
			Q ₁	Q ₂	Q ₃	Q ₄	Q ₅	Q ₆	Q ₇
free	NO constrain of : the relative motion of interconnected bodies	LT	q ₀ 1	q ₁ roll right	q ₂ pitch down	q ₃ yaw left	s ₁ for- ward	s ₂ left- ward	s ₃ up- ward
spherical (ball and socket)	to constrain using: a rotation around origin of JCS	hip	q ₀ 1	q ₁ pitch down	q ₂ yaw left	q ₃ roll right			
		spine/thorax/ neck	1	roll right	pitch down	yaw left			
planer	to constrain using: $\eta\zeta$ -plane to coincident ξ -axcs \perp motion plane	'Impactor'	ϕ	s _{η}	s _{ζ}				
universal	to constrain using: rotation around ξ (ϕ_2) rotation around η (ϕ_1)	shoulder	ϕ_1 roll right	ϕ_2 pitch down					
revolute	to constrain using: rotation on ξ -axes of JCS. The origins of JCS remain coincident.	tyre knee/head elbow	ϕ (ξ)						

8.3.4 Initial equilibrium analysis

A WTORS system is initially kept in equilibrium, i.e. the wheelchair is upright and the vertical tyre forces are in equilibrium with the weight of the wheelchair and dummy. This position was modelled from a pre-simulation in which vertical damping was specified for the tyre (critically damped tyres) so that the wheelchair converged to its equilibrium position. In the initial equilibrium analysis, velocity and angular velocity were set to zero by JOINT DOF in the INITIAL CONDITIONS. The initial value of joint position DOF and joint velocity DOF were defined according to relative joint types.

8.4 Multibody Belt Model

The belt system is represented by a stretched string that contacts a series of reference points on the surface of one or more body segments (ellipsoids) (Figure 8.4a).

In a belt routine, the points move across the surface as determined by anchorage location, belt tension, belt physical properties, the longitudinal and transverse friction coefficients. The belt may penetrate the body surface, based on the

physical properties of the ellipsoid. Simple belt systems can be described by means of Kelvin elements. This force model calculates the forces produced by a spring parallel with a damper. The spring and damper forces act on the bodies at the attachment points of the Kelvin element. The accuracy of calculation depends on the position and numbers of the attached points as the belt force can only be obtained from the attached points.

The multibody model accounted for initial belt slack (initial strain) or pre-tension. The slack or pre-tension is specified by initial strain or initial length. The initial strain **dL** or pre-tension **PRET**:

$$\mathbf{dL} = [\mathbf{L}(t_0) - L_0] / L_0 \quad (8.2)$$

where $\mathbf{L}(t_0)$ is the actual distance between the attachment points at the starting time of the simulation, L_0 is the original spring length.

The belt stiffness characteristics were defined as a force-relative elongation function. Hysteresis, i.e. energy dissipation and permanent elongation, as well as rupture were specified for the belt material. The belt force was corrected by means of a correction factor **COR** to account for local body or anchorage deformation (MADYMO 5.3, 1998):

$$\mathbf{F}_{\text{belt}} = \mathbf{COR} * \mathbf{F}(\epsilon) \quad (8.3)$$

where $\mathbf{F}(\epsilon)$ is the pre-corrected belt force and ϵ is the relative elongation of the belt segment.

The multibody belt model allows slip between two adjacent belt segments. The slip depends on a friction coefficient. In Figure 8.4b, a slip ring was defined between two adjacent belt segments 2 and 3. The initial attachment point b_3 of the segment 3 was connected to the same body as the final attachment point e_2 of the adjacent segment 2 belt. A belt length correction parameter **COR** was specified to account for the belt length between e_2 and b_3 .

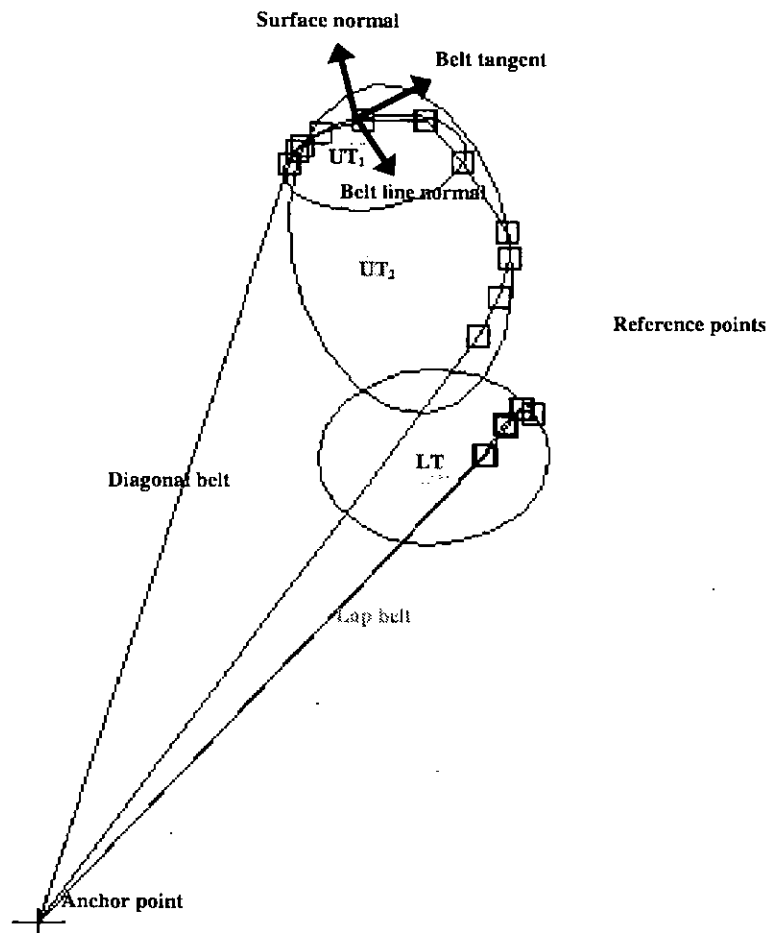


Figure 8.4a Webbing belt segment contact (L/D belt mounted to floor)

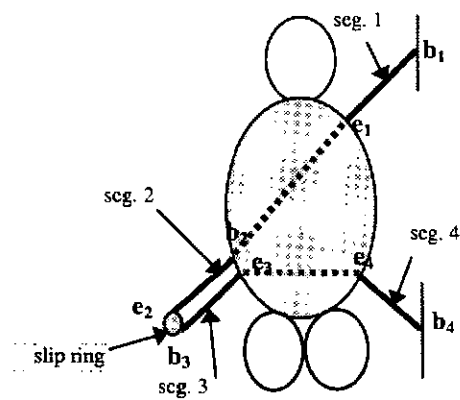


Figure 8.4b Slip between two belt segments

In a WTORS model, a restraint system was described as two types, L/D belts and webbing tiedowns. The L/D belts were joined together at tie-points. The diagonal belt was in contact with two segments at nine (9) points in the B pillar configuration and at eleven (11) points at floor mounted configuration. The kinematics of multibody L/D belt model is demonstrated in Figure 8.4c. Observed from this belt kinematics, it was found that the dummy movements twisted the lap belt very much. The attachment points of the lap belt was dropped from seven (7) points to three (3) during impact from 40 ms to 200 ms.

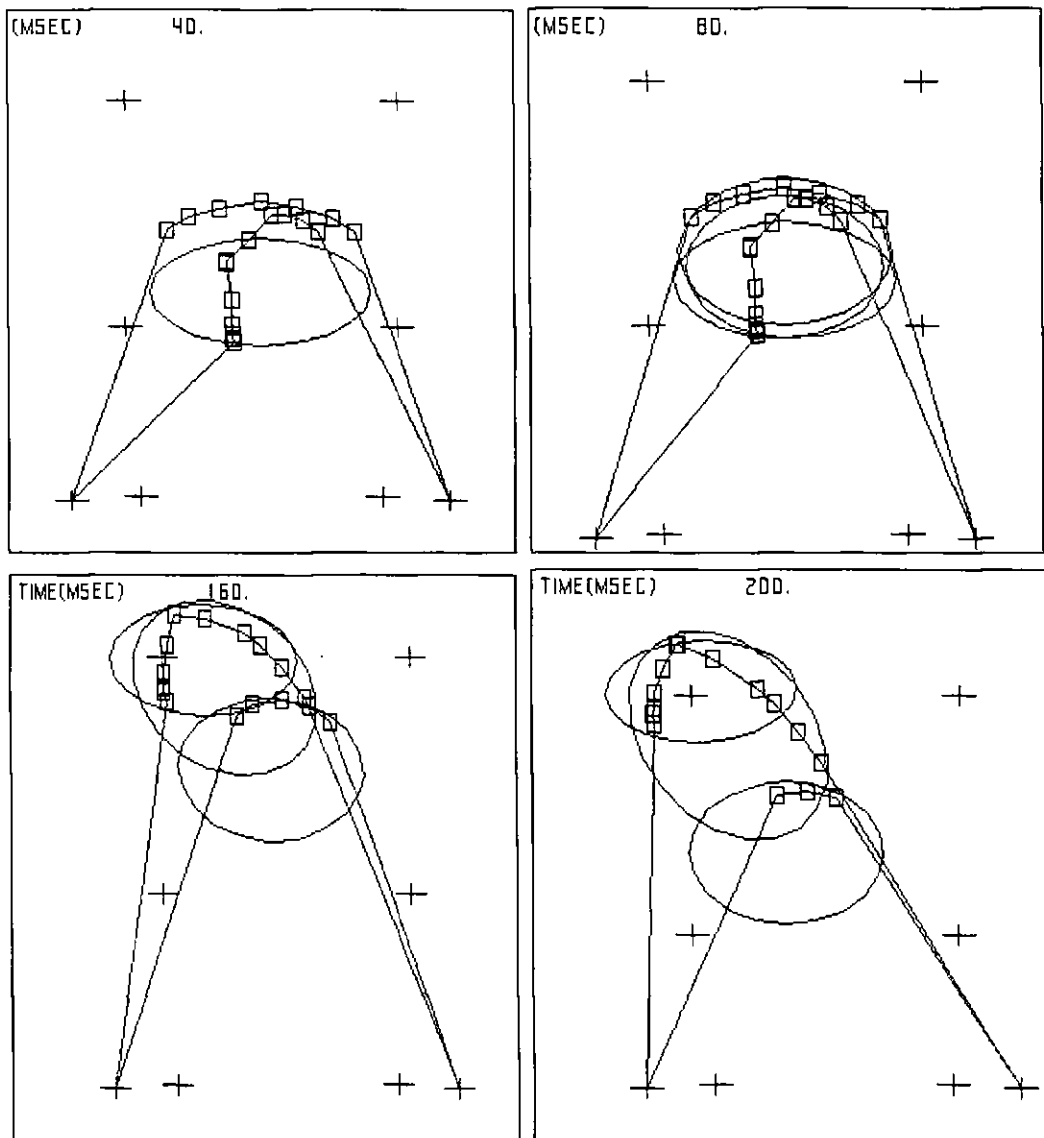


Figure 8.4c Kinematics of a L/D belt model

In the conventional multibody belt model the belt segments are connected to the bodies by attachment points, which are fixed to the body and thus only allow sliding of the belt in the direction of the belt segment. If a Coulomb friction model is used, the nodes could slide over the dummy surface arbitrarily. Unfortunately, the phenomena such as submarining and belt roll out of the body could not be demonstrated in the multibody belt model. These problems were solved by finite element belt which benefit from its simulation biofidelity and accurate force locations.

8.5 Hybrid Belt Model

A hybrid model is a combination of multibody model and a dynamic finite element model. The interaction of support and contact generates forces between the finite element model and the multibody system.

8.5.1 Dynamic finite element belt model

Using finite element method, a continuum component can be discreted into relatively simple finite elements representing its shape. The elements are interconnected at a discrete number of points, that is, the nodes. In the dynamic FEA belt model, the Lagrange description was used to define the nodes and elements fixed to the material. The time discretisation was also used, besides the spatial discretisation. A finite element time step was based on the Courant criterion calculated for the initial geometry. In MADYMO Version 5.3, it is still tiresome work for node/element numbering and the error-prone process of manually creating lists for material/property application.

- Elements

Two types of elements, truss and membranes, can be used for the FEA belt model. These are based on linear displacement interpolation and integrated at a single point at the centroid of the element. These elements are also based on a co-ordinate velocity strain (rate of deformation) formulation leading to linear and frame invariant kinematic relations. As truss element is one-dimensional two nodes connected

element, which can only carry axial tension and compression, the membrane element is more suitable for the webbing belt model.

MEM3NL elements (constant strain) are flat two-dimensional three nodes connected triangular membrane elements, which can carry in-plane loads. Due to the absence of bending, the deformations are fully determined by three transitional degrees of freedom of these nodes. MEM3NL uses a non-linear strain description to account for large deformations. The mass of the membrane is lumped and distributed over the three nodes by using element distribution factors. These factors are proportional to the angle enclosed by the two element edges joining in the vertex.

- Materials

The material of webbing belts was assumed homogeneous and isotropic. The material behaviour HYSISO was specified under the keyword MATERIALS. The Hysteresis model 1 or slope has a general non-linear material characteristics. The unloading is along hysteresis slope and unloading curve. It was used to model plastic deformation for contacts, such as tyres in the wheelchairs or webbing belts.

Table 8.5 Finite element belt stiffness characteristics

Characteristics	Element types	
	TRUSS2 (N)	MEM3NL (N)
Relative elongation		
0.025	0	0
0.05	500	2E7
0.075	7325	9.4E7
0.1	9575	1.6E9
0.125	12275	2E9
Unloading curve:		
0		0
0.1		2E7
Hysteresis model	1	1
Hysteresis slope (N/m)	5E5	6E9
Density (kg/m ³)	1	900

A strain-stress relationship of a webbing belt is listed in Table 8.5 (MADYMO V5.2.1, 1997). An unloading curve and a hysteresis slope were also specified in account of belt stiffness characteristics (Appendix 7B). A moderately steep hysteresis slope was chosen to determine the stable integration time step and save CPU time.

- Finite element modelling of seat belt

The triangular element MEM3NL (material HYSISO) was used to model the lap and diagonal (L/D) belt, total 80 elements and 63 nodes for B pillar shoulder belt, 148 elements and 113 nodes for floor mounted shoulder belt (Figure 8.5a). 96 elements were used to model the wheelchair backrest support structure in RFF impact model within MADYMO3D environment.

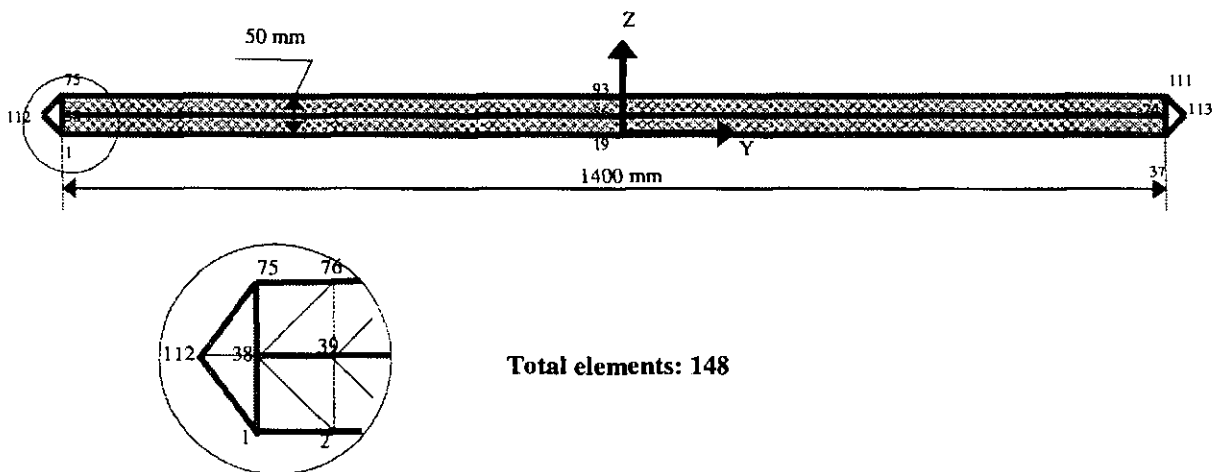


Figure 8.5a Finite element floor mounted shoulder belt

8.5.2 FE belt connected into the multibody belt

Sliding of a belt over one dummy surface can be analysed by modelling that part of the belt system with membrane elements. The FE belts were tied the outer nodes to the multibody belt system. The following bridge was used to link between pre-set FE belt and the multibody belts:

- Dragging FE belt using null systems

Three null systems, which were closed to the outer nodes of the finite element belt, were added in the pre-input file. One for B pillar (point 1 in Figure 8.5b), one for the buckle side of the belts (point 2) and one for the portside of lap belt (point 3). The null systems were given a displacement towards a point in inertial space so that after this displacement the end points of the belt segment were located at their original position, thus the finite element belt was dragged towards the dummy. The door side attachment points of the belt were located far behind the buckle attachment point. The position of null system originated as a function of time. The null system point 1 dragged the belt towards to the dummy starboard and keep belt along the dummy left shoulder. The part of pre-input file is listed as follows:

```

NULL SYSTEM
shoulder up B pillar
MOTION
POSITION
0 0.6 0 0.2
0.2 .0 -0.2 0
0.3 .0 -0.2 0
0.4 .0 0 0
1.1 0 0 0
-999
middle - buckle
MOTION
POSITION
0 0.3 0 0.2
0.1 .0 0 0
1.1 0 0 0
-999
lap belt - portside
MOTION
POSITION
0 0.6 0 0.2
0.1 .0 0 0
1.1 0 0 0
-999
END NULL SYSTEM

```

The finish points of the belt segments were tied to these null systems. The null systems were moved toward the origin of the inertial system (dummy).

- Belt body contact

At the start of the simulation initial penetrations of nodes in ellipsoids, planes or finite elements may lead to violent reaction forces. In order to stabilise the analysis, the damping of $\alpha = 100$ was added to the FE belt. The mass of the belt, such as the thickness of the belts, was increased to diminish the accelerations and the stiffness of

the belt. The element deformation was prevented by change the constant factor, PERM, for permeability of the materials, from 0.005 m to 1 m. The contact interactions between dummy ellipsoid and FE belt nodes were defined and the friction coefficient for nodal contacts was selected 0.4 to avoid the belt coming out of the dummy. The input file for contact interactions is listed as follows:

```
CONTACT INTERACTIONS
ELLIPSOID-NODE
* sternum to shoulder belt
1 2 1 0.4 1:63
* left shoulder to shoulder belt
2 1 4 0.4 1:63
* neck to shoulder belt
3 1 22 0.4 1:63
* abdomen to shoulder belt
4 1 25 0.4 1:63
* spine to shoulder belt
5 1 2 0.4 1:63
-999
END CONTACT INTERACTIONS
```

Sub-cycling of the finite element time integration with respect to the multibody time integration was implemented to reduce CPU times. The multibody time step was chosen as a multiple of the finite element time step. The kinematic model file (KN3 file) and finite element mesh file (FMS file) were included in the output options.

8.6 Contact Interaction Models

Besides the belt body contacts, several forms of other contacts: plane-segment, segment-segment, contacts between bodies and the point restraint contact have been involved in this programme.

8.6.1 The plane-segment contacts

Plane-segment contact functions depend on the deflection. If plane-segment contact functions are defined to be rate dependent, the total force deflection function is computed using the following equation:

$$F(\mathbf{u}, \dot{\mathbf{u}}) = F_1(\mathbf{u}) + F_2(\mathbf{u}) \bullet F_3(\dot{\mathbf{u}}) + F_4(\dot{\mathbf{u}}) \quad (8.4)$$

Where \mathbf{u} and $\dot{\mathbf{u}}$ are the deflection and deflection rate. F_1 , F_2 , F_3 and F_4 represent the force-deflection function (FDF), the inertial spike function (I), the energy absorption factor (R), and the permanent deformation factors (G) respectively.

The method for determining the magnitude, direction and location of segment to plane contact forces is illustrated in Figure 8.6. A perpendicular from the plane (three points P_1 , P_2 , and P_3 make one plane) to the point of maximum penetration of the ellipsoid (point A) defines the penetration function. This function was used to calculate the normal and frictional forces, based on force and displacement relationships cover in the input data set. Hysteresis was specified by I, R, and G. Friction forces were applied at the same point as the contact force, but parallel to the contact surface.

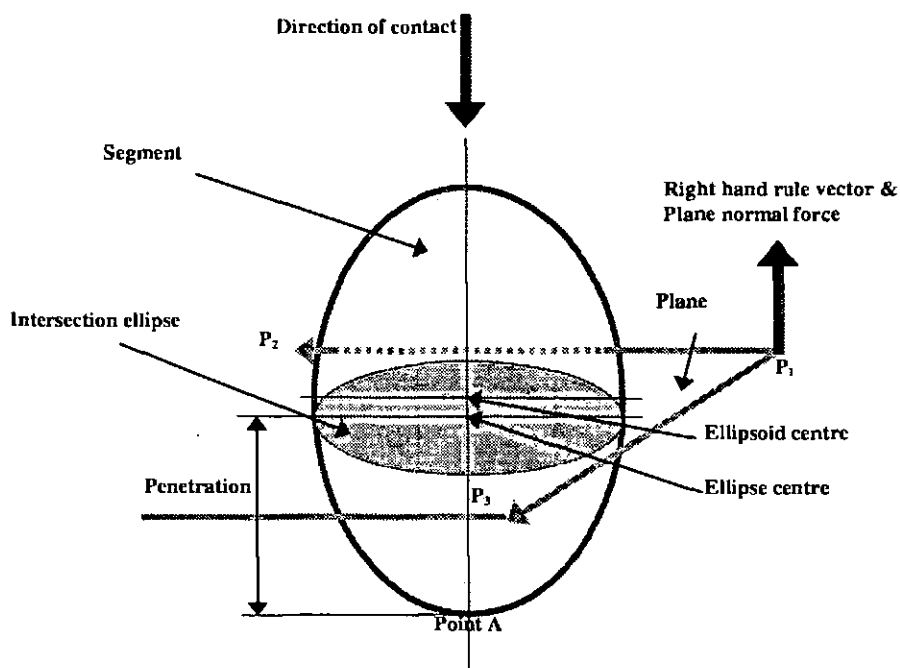


Figure 8.6 The plane-segment contact

The 'edge effect' option was used to ensure that the contact of a plane with an ellipsoid would not be ignored when the centre of the cross-sectional ellipse containing the area cut by the plane did not lie within the boundary of the plane. A Newton-Raphson scheme was employed to distribute this penetration between the two

surfaces so that the forces acting to the two surfaces at the contact point were equal.

The size of a plane for contact analysis was also determined by the parameter FIN within MADYMO3D program. The factor FIN is half of the width of the boundary contact area. The size of the plane could effect on the penetration in plane-segment contacts. Caution should be taken the error could occur if too stiffer function defined or poor configuration made. The following five factors were applied in WTORS model. All data were selected based on a trial-error method and the author's observation experience from sled tests and pre-simulation models.

- *Force Deflection Function (FDF)*

Surface contact forces were replaced by a single force applied at a specific point in a specific direction. The magnitude of normal force was a function of the maximum penetration. Friction force was proportional to the normal force and was in a direction so as to oppose the tangential velocity. In WTORS model, the chair seat (5 mm thickness of steel plate) and the ISO wheelchair backrest (10 mm thickness of rubber) were assumed to be rigid according to the previous testing experiences.

- *Inertial Spike Function (I)*

This function was used to model the effects of inertial loading condition that might take place when contact between a plane and a segment was initiated, e.g. breaking window glass in RFF impact model of taxi. In WTORS frontal impact model, the inertial spike was neglected as the contact spike was not found in the dynamic tests.

- *Energy Absorption Factor Function (R)*

This function was used to approximate the effects of hysteresis. With the permanent deflection factor it was used to calculate the path that the unloading and reloading curves would follow. The following factors in ISO wheelchair model were optimised to get the better results respectively: chair seat (0.1), backrest (0.1), floorboard (0.1), tyre (0.5), dummy chest (0.7). The R value of 0.5 for wheelchair tyres signifies that all energy spent in tyre deformation is recovered 50 per cent. This value will be verified using finite element tyre model.

- *Permanent Deformation Factor Function (G)*

This function was used to model the permanent deformation when contact force between plane and a segment started decreasing from a positive value. In ISO wheelchair model, the following factors were chosen: chair seat (0.5), backrest (0.5), floorboard (0.7), tyre (0.3), dummy chest (0.5).

- *Coefficient of Friction Function (FRIC)*

A complete definition of the friction contained two factors, FAC1 and FAC2 that can be used to exercise the impulse, globalgraphic and roll-slide options. The following factors in WTORS model were adjusted: chair seat (0.3), tyre roll (0.5).

8.6.2 Contacts between bodies (evaluations)

In a vehicle door model, the B pillar of a car is connected to a series of finite planes, which are attached to a vehicle representing the front and rear doors. If the stiffness of doors was assigned to each of the interactions separately, the pillar would penetrate several of the door planes at the same time and the effective total door stiffness in the model would be too high. Due to the sudden change of the contact point from one plane to another in multiple contact interactions between an ellipsoid and several other planes or ellipsoids, instabilities could arise. The option EVALUATIONS was used to specify that the forces resulting from just maximum values of these interactions were applied to the system bodies in the contact models.

8.6.3 The point restraint model

The point restraint model calculates elastic and damping forces on a fixed point P. This model could be considered as a combination of three orthogonal Kelvin elements with constant damping coefficients parallel to the co-ordinate axes x, y and z respectively. At one end the Kelvin elements are connected to point P and at the other end to slider joints in three orthogonal planes parallel to the point-restraint co-ordinate system. The point restraint was used to restrain the distance between two points of different bodies.

For example, the pin joint stiffness of the rear door in the vehicle was modified using point restraint model to adjust the accuracy of the door opening in the side impact. The bodies connected to the doors were fixed by P point restraint.

8.7 Acceleration Field Model

In WTORS models, an acceleration field model was used to simulate the effect of the deceleration forces of sled on the occupant during an impact. The sled was modelled as a body with a prescribed deceleration in impact. A deceleration measured at the sled was prescribed as a fictitious acceleration field on the occupant as the relative motion of the occupant to the sled is most relevant. This was assumed that the sled rotation can be neglected and the sled was fixed to the inertial space. A fictitious acceleration field based on the fact that the vehicle deceleration pulse is prescribed in the one-body system.

8.8 Hybrid Tyre Model

The wheels and tyres of an occupied wheelchair, restrained in a vehicle by a WTORS have a significant effect on the dynamic behaviour during impact. Major disturbance and control loads on WTORS arise from the contact of the tyres of the wheelchair with the vehicle. The vertical loads generated as a function of the mass of the wheelchair and occupant are applied to the vehicle. The vertical behaviour of tyres is the dominant factor for wheelchair stability as lateral tyre force is not required for controlling the direction of travel of the wheelchair during frontal impact. The tyre-floorboard contact loads depend on the characteristics of the tyre, the floor condition, and the motion of the tyre relative to the floorboard. The latter two characteristics of the tyre could be neglected if the wheelchair was restrained by four tiedown systems. A proper description of the dynamic behaviour of the wheelchair requires a good model of the tyre-floorboard contact loads and a detailed model of the tyre behaviour.

8.8.1 Model objectives

The objectives of this tyre model are:

- *Application of complex FEM modelling techniques within MADYMO3D environment*

- *Optimal design of wheelchair structures*
- *Determination of the potential injury reduction benefits to wheelchair occupant during impact.*

8.8.2 Initial conditions

The rear wheel tyre in a surrogate wheelchair has a radius of 0.64 m and a width of 0.1 m. The nominal vertical tyre load equals 2 kN. The vertical stiffness equals 52 kN/m (see Appendix 7B).

At the start of the dynamic test the wheelchair equilibrium position is upright and the vertical tyre forces react the total of the wheelchair and dummy weights. This position is obtained from a pre-simulation in which vertical damping is specified for the tyre so that the wheelchair reverted to its equilibrium position.

8.8.3 Modelling techniques

The wheelchair tyres could not be modelled using only the finite element module in MADYMO3D as no finite element contact is defined in the SYSTEMS module within MADYMO code, although finite element contacts are available in the CONTACT INTERACTIONS module. Mooney-Rivlin material of tyre (rubber-like materials) are incompressible and may undergo extremely large elastic deformations.

FACET surface can define a more detailed or a more general description of surfaces. In the tyre model, FACET surface was used to model the inner surface of the tyre. The triangular FACET surface was attached to a wheel body and defined by the co-ordinate of the vertices. The surface was designed to contact finite element models. One of the two contacting FACET surfaces was assumed to be compliant, the other to be rigid. The compliance was modelled by allowing the vertices of the compliant surface penetrate into the FACET of the rigid surface. The contact load was equal to the load that was needed to deform the compliant surface. This load was specified by the contact stress as a function of the vertex penetration of the resultant contact force.

The hybrid model was used to get more details of tyre interior characteristics. This model is a combination of FACET, FEM and MULTIBODY models as follows (Figure 8.8a).

- *Tyre core modelled by MULTIBODY system generated using MADYMO3D pre-processor*
- *Tyre inner structure modelled by FACET surface*
- *Tyre outer structure (tread) modelled by FEM mesh created using Microsoft Excel and the FEM module within MADYMO3D environment.*

The core of the tyre was modelled using ellipsoid and the rubber part (tread) was meshed using finite element model within MADYMO3D environment. The keyword SUPPORTS was used to connect finite element nodes and tyre bodies in the system. All directions were supported with respect to the specified body in the system. The contact between nodes and planes was specified under the keyword CONTACT INTERACTIONS. The initial orientation of the finite element reference co-ordinate system was by default parallel to the inertial co-ordinate system.

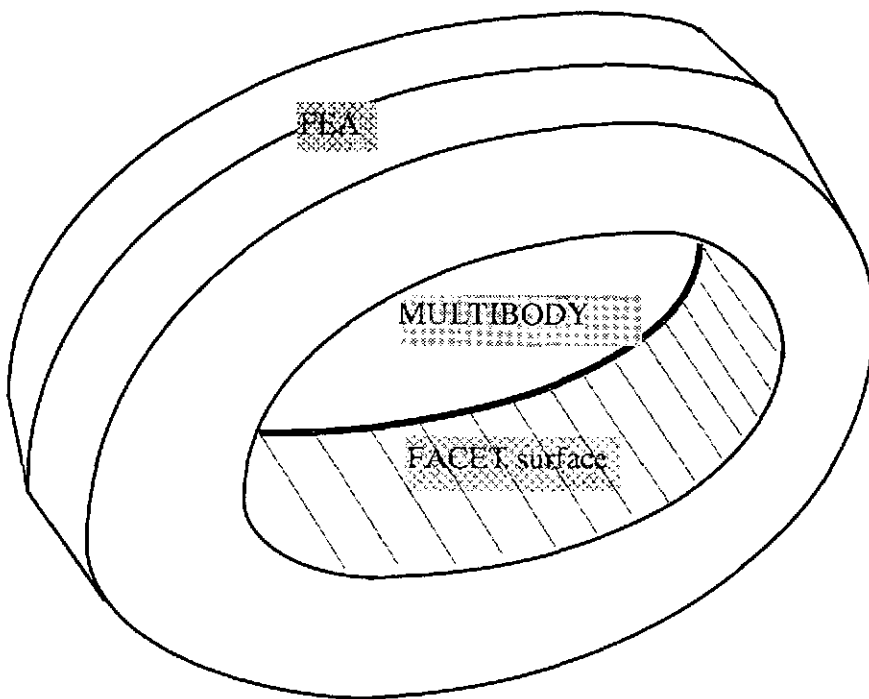


Figure 8.8a A wheel tyre hybrid model

As the symmetry of the tyre, only quarter of it was considered in order to reduce computing time. The initial co-ordinate of nodes (total nodes 536) were calculated in Excel format (Table 8.8). In this Table, the inner, outer and rim of the tyre are defined in three radius, r , R and M respectively. The mesh is layered in three levels, bottom (B), middle (M) and top (T). The mesh block is designed in Figure 8.8b and the meshes of tyres are laid out in Figure 8.8c. The element FACET6 (material ISOLIN) was used to model the contact surface between the core and rubber of the wheel (total 160 elements). The element SOLID1 (material LINVIS) was used to model the tread of the wheel (total 80 elements).

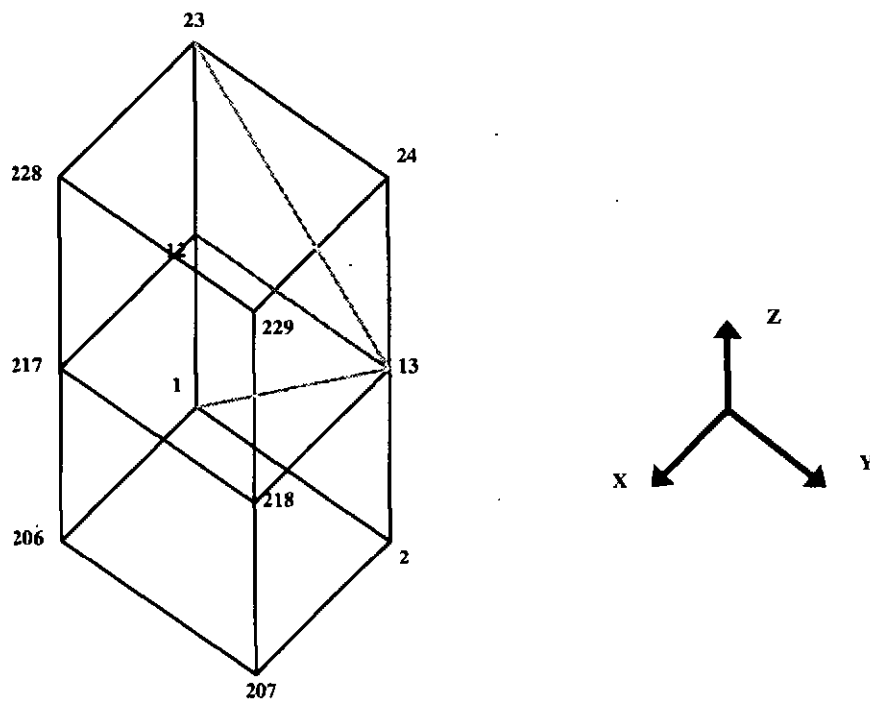


Figure 8.8b Tyre mesh block

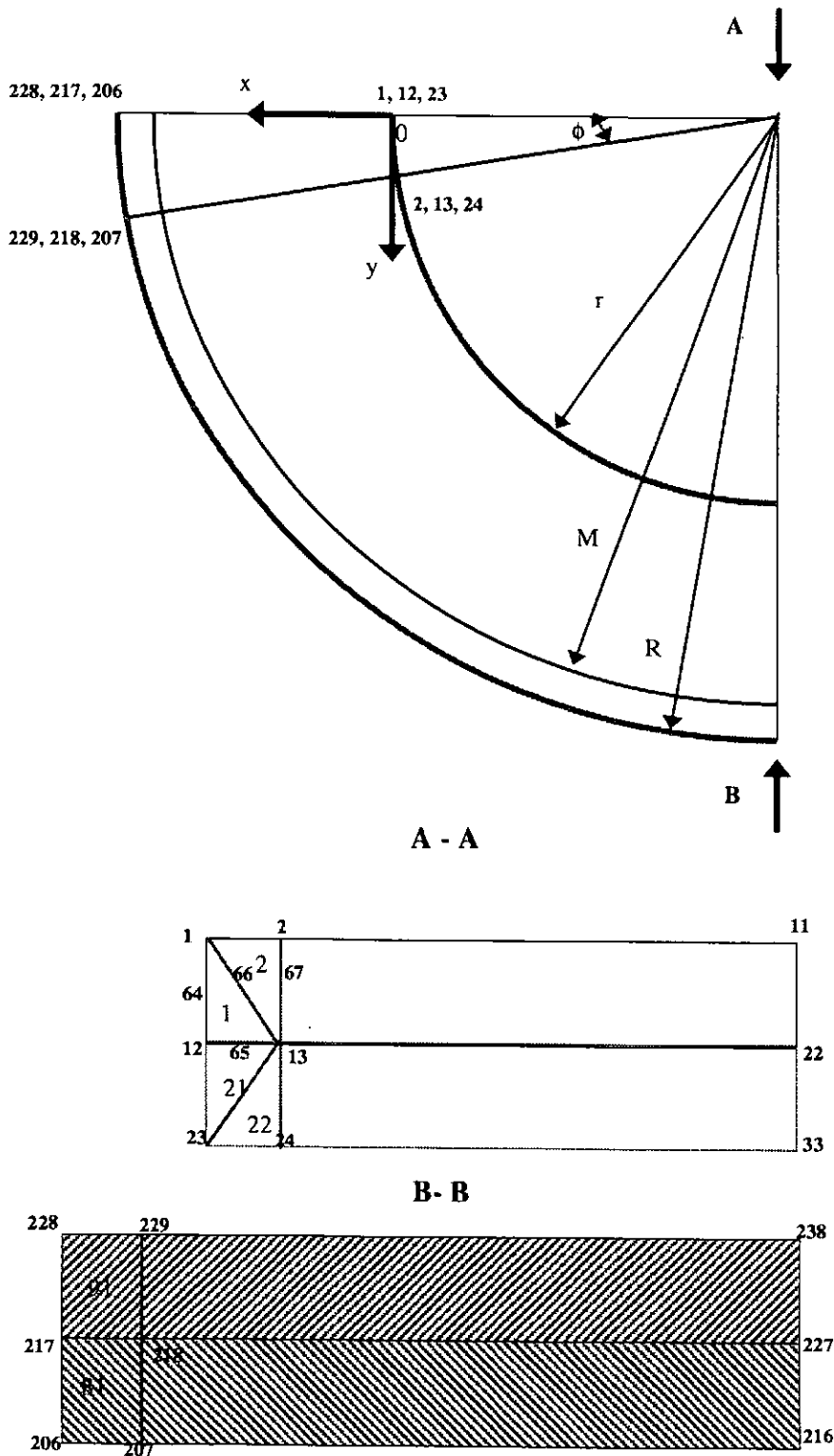


Figure 8.8c Tyre mesh lay-out

Table 8.8 The wheel/tyre mesh calculations

ϕ (°)	INNER (r)			OUTER (R)			RIM (M)	
	Node No.	x	y	Node No.	x	y	x	y
	B, M, T	mm	mm	B, M, T	mm	mm	mm	mm
0	1,12,23	0	0	206,217,228	61	0	51	0
9	2,13,24	-1	16	207,218,229	59	25	49	24
18	3,14,25	-5	31	208,219,230	53	50	44	47
27	4,15,26	-11	45	209,220,231	43	73	35	69
36	5,16,27	-19	59	210,221,232	30	95	22	89
45	6,17,28	-29	71	211,222,233	14	114	7	107
54	7,18,29	-41	81	212,223,234	-5	130	-11	122
63	8,19,30	-55	89	213,224,235	-27	143	-31	135
72	9,20,31	-69	95	214,225,236	-50	153	-53	144
81	10,21,32	-84	99	215,226,237	-75	159	-76	149
90	11,22,33	-100	100	216,227,238	-100	161	-100	151

MADYMO3D proved to be very effective tool for modelling and simulating of different interaction between complex MULTIBODY and FACET, FACET and FEM modelling sets. However it should be noted that the third objective of this tyre model, which it is used to assembly it into one proper simulation to determine the potential injury reduction benefits to WTORS will be achieved in future research.

8.9 Input and Output Parameters

The explicit numerical integration method was employed in this programme. The maximum time step that leads to a stable solution depends on the largest eigenvalue (non-linear differential equation of the solution) in the model. As the 1st order modified Euler method is more efficient than the Runge-kutta method (four function evaluations) it was used as initial model. A fourth order Runge-Kutta method with fixed time step was then conducted to get dynamic accurate response by step integration.

The RAMP was used to indicate the relation between jointed elements. The RAMP1, RAMP 2 indicated dry friction (Coulomb friction) torque C_p in the joints of dummy to avoid vibrations induced by dry friction torque. The RAC01, RAC02 are damping functions, which act in the direction opposite to the relative velocity of the components.

* RAMP1(rad/s) RAMP2 RAC01 RAC02(m/s)
0.0000 0.5000 0.0100 0.1000

The kinematic data was generated every 50 ms in the KIN3 file. Simulation results included the linear acceleration at the centre of gravity of the dummy's head and chest, the tyre contact loads, the L/D restraint loads and tiedown loads, etc.

CHAPTER 9: CVS MODELLING OF WTORS

In this Chapter, Crash Victim Simulation (CVS) of Wheelchair Tiedown and Occupant Restraint System (WTORS) has been summarised. The Child Restraint System (CRS) side impact model [5] is not included in this thesis.

9.1 TRL Frontal Impact Model

This model was initially written within ATB program and then modified using DYNAMAN package. The system 2, TNO-10 dummy data was developed and added in TRL wheelchair model. After simulation, the complete wheelchair-dummy model was created shown in Figure 9.1a.

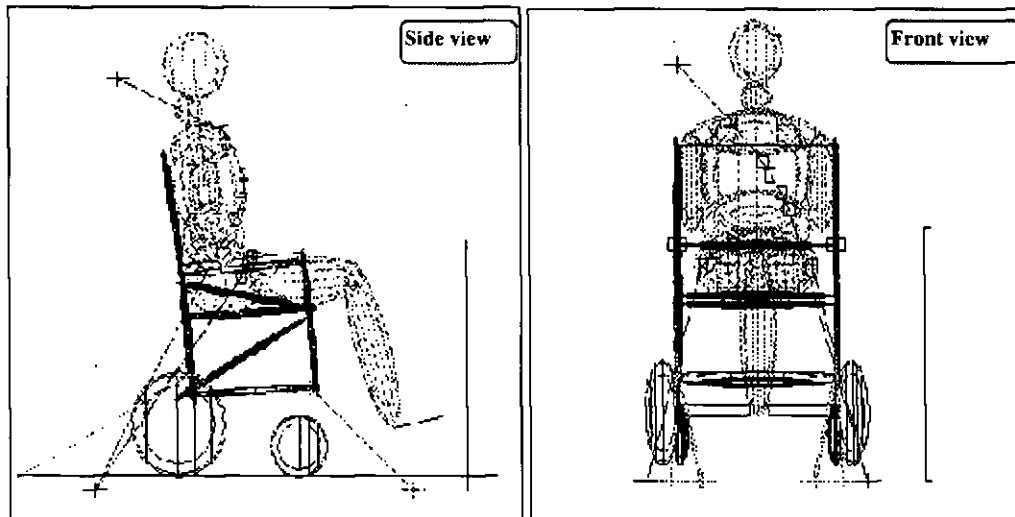


Figure 9.1a CVS modelling of WTORS (TRL model)

The surrogate WTORS system was modelled as linear segments. The stiffness properties of the segments were initially determined experimentally from static tests. Finally, they were validated and adjusted by dynamic sled tests and CVS models. Damping and permanent deformation properties of the system were also accounted for. Contacts between the wheels and vehicle floorboard, chair seat and dummy, seat belts and dummy torso were simulated using FDF, I, R, G, and frictional properties of

the various contacts. The crash was simulated by specifying the crash pulse and determining system responses at pre-determined time intervals. The crash pulse was discerned in a sled test pulse. The initial model was proved reliable by peak value, kinematic check and load trace validations. It was then used to investigate the effect on the location of diagonal trap belt anchorage (Figure 9.1b).

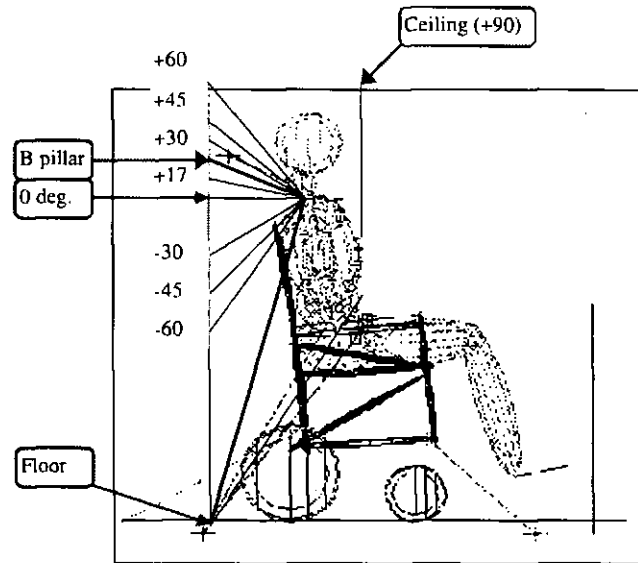


Figure 9.1b Diagonal strap belt configurations

Incorrect occupant restraint positioning relative to the occupant has been shown to cause severe internal injuries. Occupant restraint anchorage points were selected in accordance with the zones specified by ISO/CD 10542-1. The ISO recommended zones ensure that the geometry of the lap and shoulder belts is not injurious to the occupant in a crash. These zones were adapted from the Australian and Canadian WTORS standards (AS2942, 1987; CSA-Z604, 1992). The location of the upper shoulder belt anchorage locations was studied with the computer modelling of L/D belt. The result of this study was contributed to validate the ISO recommended zones and served as a tool for adjusting the zones more appropriately.

The height of the diagonal top strap belt anchorage point was varied in four basic positions: floor mounted, 2-metre above the floor simulating fixing to the ceiling of a minibus (+90 degree), 1.25-metre above the floor representing the B-pillar fixing point, and zero level to the occupant shoulder. Between the positions of floor and zero

degree, the shoulder belt was varied in three different angles to the level: negative 60-degree, 45-degree and 30-degree. Between the positions of zero and 90-degree, the shoulder belt was varied in four different angles to the level: positive 17-degree, 30-degree, 45-degree and 60-degree.

Table 9.1a CVS model results for diagonal strap belt configurations

Set up	Units	Floor	(-)60	(-)45	(-)30	0 deg	(+)17	B p'ar	(+)30	(+)45	(+)60	(+)90
Upper anchor	mm	0	449	720	878	1092	1168	1256	1306	1464	1735	*
RP tiedown	kN	14.04	14.14	14.48	14.62	14.66	14.54	14.52	14.42	14.28	12.64	13.98
peak time	ms	120	105	110	110	110	110	110	110	110	115	110
RP wheel	kN	14.85	15.73	15.47	15.49	15.53	14.62	14.44	14.35	14.12	13.91	13.68
peak time	ms	120	120	120	120	120	120	120	120	120	120	120
FP wheel	kN	9.98	9.96	10.45	9.78	9.86	9.51	9.17	7.99	7.62	7.38	7.19
peak time	ms	120	120	115	115	120	115	115	115	115	115	115
Shld Port	kN	11.12	11.12	7.24	6.39	7.79	7.71	9.79	9.39	9.89	9.72	10.64
peak time	ms	140	135	115	100	95	105	105	105	110	120	115
Lap Port	kN	5.07	4.49	4.04	3.67	3.51	3.91	4.84	4.61	5.02	5.61	5.45
peak time	ms	100	95	95	95	90	95	95	95	100	105	100
L/D Buckle	kN	12.41	9.78	10	10.02	11.22	9.67	11.05	10.52	11.37	12.43	15.11

Notes: peak time is the moment after the onset of impact at which maximum acceleration occurs

The model results are shown in Table 9.1a. The load investigation was conducted, for example, the shoulder belt portside (diagonal top strap) and starboard (diagonal bottom strap) loads are shown as 'Shld Port' and 'Shld ST' respectively, lap belt loads are 'Lap Port' and 'Lap ST', buckle loads are 'L/D Buckle', and portside rear and front wheel loads are 'RP wheel' and 'FP wheel' respectively.

From this model, it has been observed that the dummy movements are very sensitive to the belt attachment points on the dummy. These attachment points are functions of the anchorage locations. It should also be noted that the belt attachment points on the dummy are fixed in the multibody belt simulation. This multibody belt model has been replaced by finite element belt model in ISO frontal impact model.

- The difference between portside and starboard side shoulder belt load is reduced with the increasing angles of shoulder belt from 0 to 45-degree. This indicated that the dummy did not show too much twisting within this angle ranges (Figure 9.1c). The relative lower value of should belt load was found around angle ranges of negative 30 and 45-degree. This is explained as the wheelchair rocking effect resulted in the highest wheel loads at the same positions (Figure 9.1f).
- The difference between portside and starboard side lap belt load increases with the increased angle from (-60) degree to 0 degree. This indicated that the dummy did show twisting from starboard to portside within this angle ranges (Figure 9.1d, Figure 9.1e).

From this model, the optimum position (+17 degree) was determined by the best (minimum loads) and worst (maximum loads) method (Table 9.1b). This position was also comprehensively determined by minimum load difference between portside and starboard, as it would cause less injury to the occupant and less damage to the wheelchair. The difference between the sled test and computer model at B pillar configuration is compared in Table 9.1c.

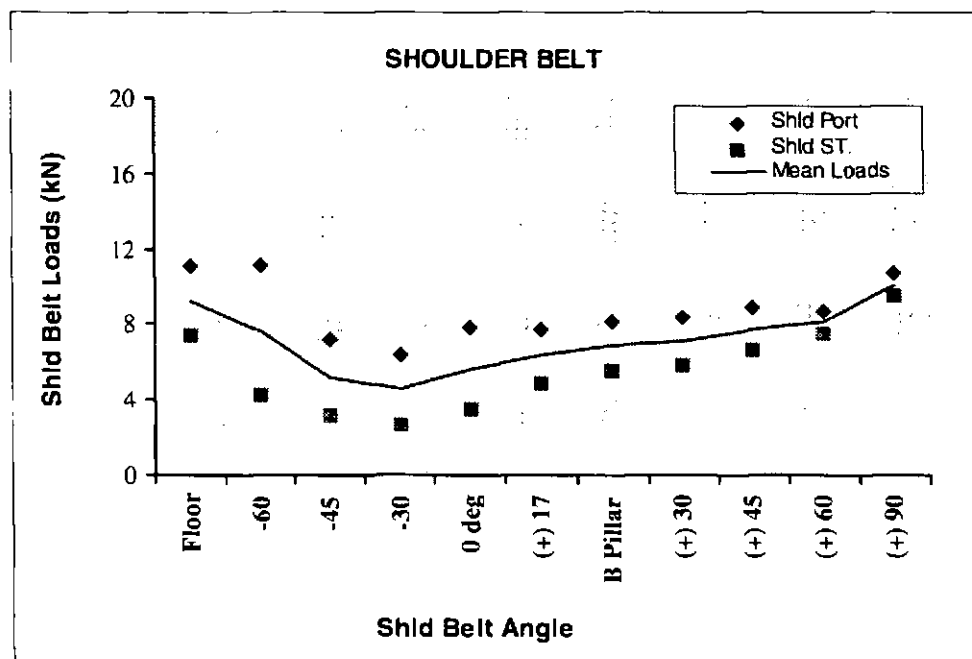


Figure 9.1c The function of shoulder belt loads and the shoulder belt angles

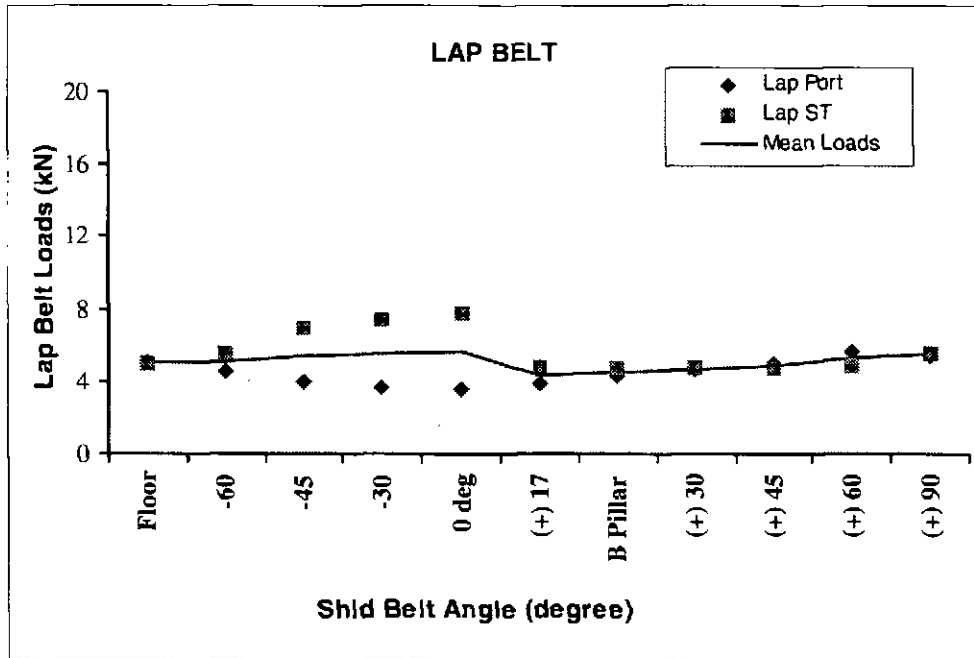


Figure 9.1d The function of lap belt loads and the shoulder belt angles

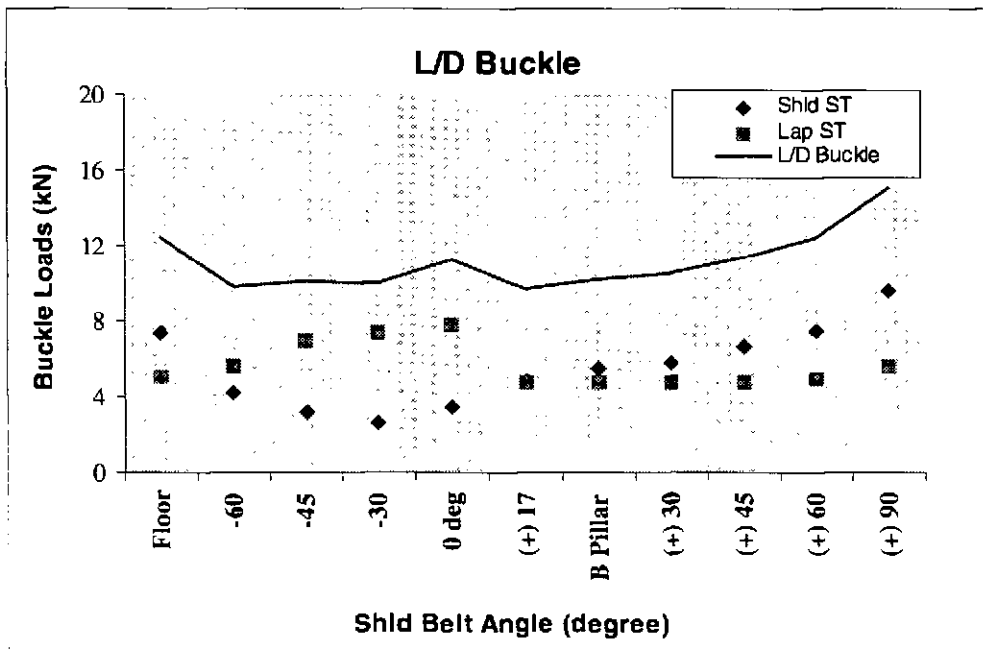


Figure 9.1e The function of the buckle loads and the shoulder belt angles

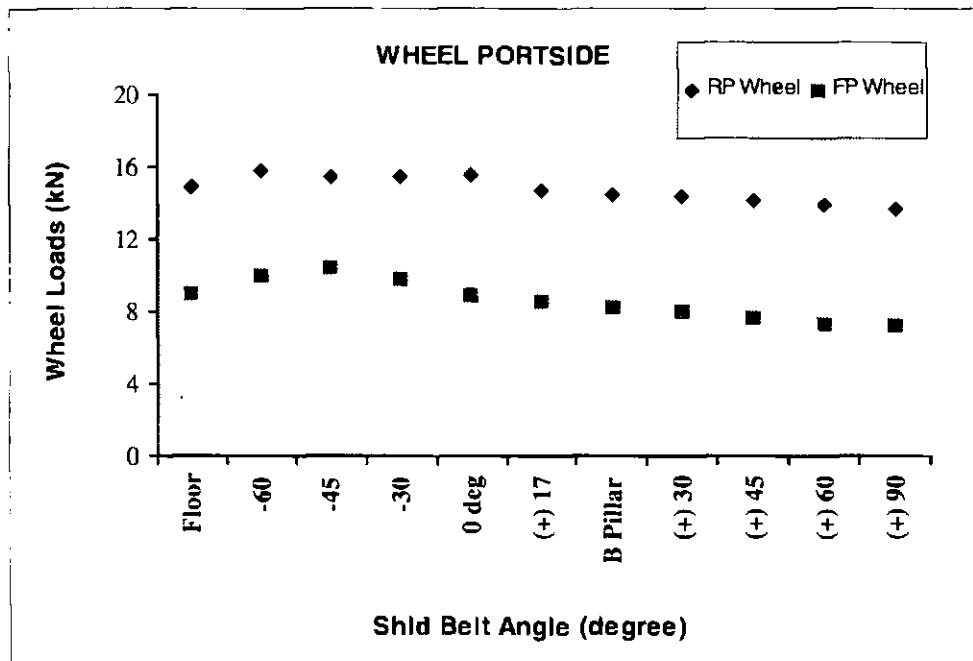


Figure 9.1f The function of wheel loads and the shoulder belt angles

Table 9.1b Optimised configuration of a diagonal strap

Loads	Min. (Best)	Max. (Worst)	Min. load difference between portside and starboard
Lap Port	0 deg	(+)60	(+)17 , (+)30, B pillar
Shld Port	(-)30	Floor, (+)90	(+)90, (+)60
Buckle	(+)17	(+)90	(+)17

Table 9.1c Comparison of sled test and CVS model results (peak value of B pillar diagonal strap configuration)

Parameters	Units	WTORS (45-degree rear tiedown angle) - 32 km/h, 18g					
Set up conditions		FP wheel	RP wheel	RP tiedown	L/D Buckle	Lap: PT	Shld: PT
Test	kN	10.9	10.8	14.8	12.1	6.9	9.1
CVS	kN	9.2	14.4	14.5	11.1	4.8	9.8
difference %		15.6	33.3	2	8.3	30.4	7.7

9.2 ISO Frontal Impact Model

ISO frontal impact model consisted of ISO surrogate wheelchair (ISO-SWC, 90 kg) with an Anthropomorphic Test Dummy (ATD). The webbing 4-point surrogate tiedown systems were simulated using beam segments. The final simulation set-up was identical to the actual test set-up (Chapter 5) to facilitate sled test results and to debug the computer model.

9.2.1 CVS modelling of ISO-SWC using DYNAMAN

This model was initially written within the DYNAMAN package. All segments placed in the wheelchair were incorporated in the model by sealing their mass. The following three systems were built in this model.

Inertial system: A sled was modelled by one plane.

System 1: The wheelchair was modelled using 27 segments and 6 planes (Figure 9.2a). The securement points were simulated by four segments.

System 2: Hybrid II dummy data was developed and added in ISO-SWC model.

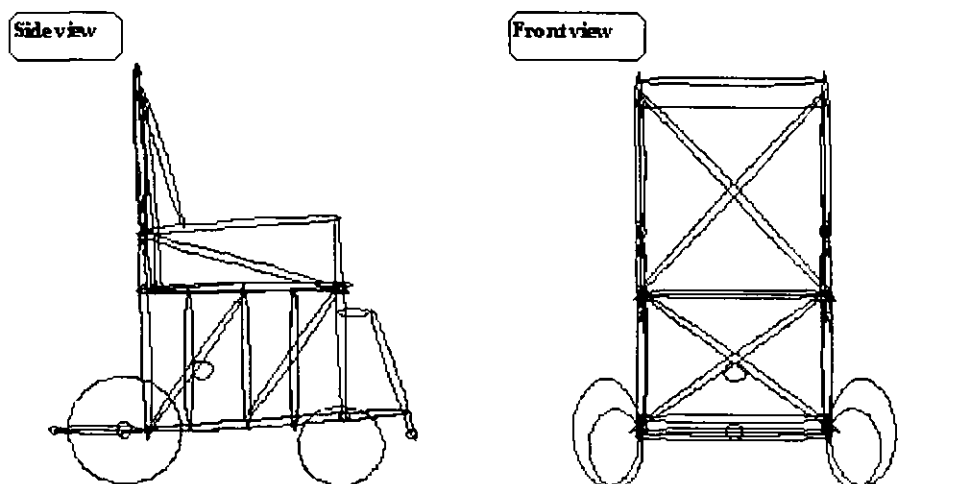


Figure 9.2a CVS modelling of ISO surrogate wheelchair

Beyond of the capability of DYNAMAN package to simulate the complete wheelchair-dummy model (over 43 segments), some of segments of the wheelchair had to be removed before simulation.

9.2.2 Interpretation of ISO model using MADYMO

The ISO model was also conducted using MADYMO3D program. The data file was written and interpreted as follows (Figure 9.2b):



Figure 9.2b ISO model by MADYMO

- System 1: wheelchair model

The origin of the wheelchair was defined in position at the centre of the wheelchair directly between the two rear wheel contact points to the sled. A moment of inertia (kgm^2) was obtained from the calculation in Appendix 2.

```
INERTIA
MOMENTS OF INERTIA (KGM2) WAS OBTAINED FROM THE CALCULATIONS
MASS IXX IYY IZZ
90 9.24 11.66 9.47
-999
```

The centre of gravity (CG) of the wheels was assumed to be at the origin of their semi-axes since the wheel geometry is symmetrical about the principal axle. No hysteresis was included in front solid wheel, as it was virtually rigid requiring no loading functions. The rear wheel stiffness (90 kN/m) was initially used to produce the function block for the rear wheel model, and then tuned by dynamic tests by adding the deflection/force data: 55 mm/50 kN to take into account of the wheel rim contacted to the floorboard.

```

ELLIPSOIDS
semi-axes (m)  centre of gravity
BODY A  B  C  MX MY  MZ  DEG LO UNLO HYS ID
1 0.161 0.05 0.161 0 -0.295 0.161 2 1 0 0 REAR.LH.WHEEL
1 0.161 0.05 0.161 0 0.295 0.161 2 1 0 0 REAR.RH.WHEEL
1 0.12 0.035 0.12 0.38 -0.275 0.12 2 0 0 0 FRONT.LH.WHEEL
1 0.12 0.035 0.12 0.38 0.275 0.12 2 0 0 0 FRONT.RH.WHEEL
.999
FUNCTIONS
8
0 0 0.008 400 0.015 800 0.022 1200 0.039 2000 +
0.045 2400 0.05 2600 0.055 50000
.999

```

No initial velocity was imposed on WTORS as the wheelchair was connected to the sled.

```

INITIAL CONDITIONS
X Y Z VX VY VZ CHO
0 0 -0.008 0 0 0 0

```

- System 2: Hybrid II dummy model

The Hybrid II (or called PART 572) dummy database was appended using MADYMO dummy databases. The dummy model was defined as system 2. The peripheral element of a branch was defined and element 1 (lower torso) was attached to inertial space in the module CONFIGURATION.

```

CONFIGURATION
5 4 3 2 1
7 6 3 2 1
9 8 3 2 1
11 10 1
13 12 1

```

The flexion-torsion joint model was applied in torso, spine, neck and head and the Carden joint model (ball and sockets) was applied in the rest parts of dummy.

```

GEOMETRY
RJX  Y      Z      CGX  Y      Z  ID
0.000 0.000 0.000  0.026 0.000 -0.079 LOWER TORSO
0.000 0.000 0.000  0.033 0.000 0.072 SPINE
0.000 0.000 0.132  0.029 0.000 0.162 UPPER TORSO
0.065 0.000 0.318  0.000 0.000 0.063 NECK
0.000 0.000 0.124  0.006 0.000 0.028 HEAD
0.030 0.189 0.260  0.000 0.000 -0.122 UPPER ARM LEFT
0.000 0.000 -0.261  0.000 0.000 -0.167 LOWER ARM LEFT
0.030 -0.189 0.260  0.000 0.000 -0.122 UPPER ARM RIGHT
0.000 0.000 -0.261  0.000 0.000 -0.167 LOWER ARM RIGHT
0.042 0.087 -0.072  0.000 0.006 -0.207 UPPER LEG LEFT
0.000 0.008 -0.405  0.016 0.000 -0.272 LOWER LEG LEFT
0.042 -0.087 -0.072  0.000 -0.006 -0.207 UPPER LEG RIGHT
0.000 -0.008 -0.405  0.016 0.000 -0.272 LOWER LEG RIGHT
-999

```

The orientation in the y-axis direction has been amended to the head inertial co-ordinate system (42-degree). This rotated the inertial of head in the rearward direction compensating for the main mass of the head brain. The joint head was relative to the preceding body in the branch (ICH = 0). The successive rotations (IOR = 1) was about y-axis of 0.733 rad.

```

ORIENTATIONS
BODY ICH IOR PAR1 PAR2
5 0 1 2. -0.733
-999

```

The Cardan joint characteristics were defined by three standard joint forces: non-linear elastic torque M_e , viscous damping M_d and Coulomb friction torque M_f in three principal directions (Bryant angles - PHI, THETA and PSI).

```

CARDAN JOINTS
ELASTIC          DAMPING          FRICTION
EL LO UNL HYS XEL L U H X  L U H X  PHI THETA PSI  PHI THETA PSI
10 1 0 0.0. 2 0 0.0. 3 0 0.0. 6.00 6.00 5.00 39. 39. 12.
12 1 0 0.0. 4 0 0.0. 3 0 0.0. 6.00 6.00 5.00 39. 39. 12.
11 5 0 0.0. 6 0 0.0. 6 0 0.0. 5.00 7.50 4.00 12.
13 5 0 0.0. 6 0 0.0. 6 0 0.0. 5.00 7.50 4.00 12.
6 7 0 0.0. 6 0 0.0. 8 0 0.0. 2.00 4.00 4.00 12. 0. 12.
8 7 0 0.0. 6 0 0.0. 9 0 0.0. 2.00 4.00 4.00 12. 0. 12.
7 10 0 0.0. 6 0 0.0. 11 0 0.0. 2.00 4.00 2.00 4. 0. 4.
9 10 0 0.0. 6 0 0.0. 11 0 0.0. 2.00 4.00 2.00 4. 0. 4.
-999

```

The reference segment of dummy, such as lower torso (LT), was positioned in relative to the local co-ordinate system of the sled (inertial) (ICH = -1).


```

INITIAL CONDITIONS
X Y Z VX VY VZ CHO
0.24 0.0 0.71
ORIENTATIONS
BODY ICH IOR PAR
1 -1 1 2. -0.5236
2 -1 1 2. -0.3236
3 -1 1 2. -0.2236
4 -1 1 2. 0.35
5 -1 1 2. 0.35
6 -1 1 2. -0.3926
7 -1 1 2. -1.57
8 -1 1 2. -0.3926
9 -1 1 2. -1.57
10 -1 1 2. -1.6708
11 -1 1 2. 0.0873
12 -1 1 2. -1.6708
13 -1 1 2. 0.0873
-999

```

- Force model

Acceleration field model

The acceleration field was applied to all bodies of all systems (SYS = 0). Linear interpolation function was used (function code > 0). The last time point (250 ms) was set larger than the total of simulation end time (TE) and time step (TS).

```

FORCE MODELS
ACCELERATION FIELDS
SYS BODY FUNCX Y Z
0 0 1 0 2
-999
FUNCTIONS
T2996 PULSE: ACCELERATION (M/S**2) AS A FUNCTION OF TIME (S)
42
0 0 0.005 -1.9 0.010 -0.6 0.015 0.5 +
0.020 -0.1 0.025 19.2 0.030 101.4 0.035 109.5 0.040 150.3 +
0.045 144.5 0.050 172.4 0.055 173.2 0.060 185.3 0.065 189.8 +
0.070 175.5 0.075 211 0.080 167.3 0.085 150.6 0.090 139.1 +
0.095 152.1 +
0.100 153 0.105 121.6 0.110 137.1 0.115 109.1 0.120 70.5 +
0.125 26.7 0.130 -9.5 +
0.135 -7.4 0.140 -19.1 0.145 -19.1 0.150 -29.2 0.155 -20.9 +
0.160 -17 0.165 -4.3 0.170 -0.7 0.175 7.4 0.18 17.7 +
0.185 6.5 0.19 6.4 0.195 7.5 0.2 4.7 0.25 6
2
0 -9.8 0.25 -9.8
-999

```

Contact interaction model

In the wheelchair-sled contact, XEL represents the hysteresis elastic limit characteristics. The boundary area (FIN = 0.01 m) was allowed for contact correction. A correction factor (COR) was applied to allow for the initial penetration into the

plane. CHO is selection parameter for elastic contact characteristics. CHO = 1 was selected to use the characteristics of the ellipsoid. FRI is a parameter of contact friction. FRI = 0.7 was used to limit wheelchair move further. DAFR is selection parameter for damping and friction. The damping coefficient equals the product of the function values specified by d_1 and d_2 corresponding to the velocity and amplified elastic force dependent factor respectively.

```

CONTACT INTERACTIONS
PLANE-ELLIPSOID
WHEELCHAIR - SLED CONTACT
SY PL SY EL CHO LO UNL HYS XEL D1 FRI FIN COR DAFR DAMP2(D2)
-1 1 1 1 4 1 0 0 0 0 0.7 0.01 0 0
-1 1 1 2 4 1 0 0 0 0 0.7 0.01 0 0
-1 1 1 3 4 1 0 0 0 0 0.7 0.01 0 0
-1 1 1 4 4 1 0 0 0 0 0.7 0.01 0 0
WHEELCHAIR - OCCUPANT
1 1 2 1 4 2 0 0 0 0 0.7 0.01 0 0
1 1 2 11 4 0 0 0 0 0 0.7 0.01 0 0
1 1 2 14 4 0 0 0 0 0 0.7 0.01 0 0
1 3 2 3 4 0 0 0 0 0 0.3 0.01 0 0
1 3 2 2 4 0 0 0 0 0 0.3 0.01 0 0
1 3 2 1 4 0 0 0 0 0 0.3 0.01 0 0
1 4 2 13 4 0 0 0 0 0 0.3 0.01 0 0
1 4 2 16 4 0 0 0 0 0 0.3 0.01 0 0
-999
FUNCTIONS
2
0 0 0.001 35000
2
0 0 0.001 80000
-999
ELLIPSOID-ELLIPSOID
SY EL SY EL CHO LO UNL H X D1 FRI COR DAFR DAMP2(D2)
2 6 2 7 2 1 0 0 0 0.3 0.01 0 0
2 6 2 8 2 1 0 0 0 0.3 0.01 0 0
2 6 2 9 2 1 0 0 0 0.3 0.01 0 0
2 6 2 10 2 1 0 0 0 0.3 0.01 0 0
2 6 2 11 2 1 0 0 0 0.3 0.01 0 0
2 6 2 12 2 1 0 0 0 0.3 0.01 0 0
2 6 2 13 2 1 0 0 0 0.3 0.01 0 0
2 6 2 14 2 1 0 0 0 0.3 0.01 0 0
2 6 2 15 2 1 0 0 0 0.3 0.01 0 0
2 6 2 16 2 1 0 0 0 0.3 0.01 0 0
-999
FUNCTIONS
3
0 0 0.01 375 0.02 1000
-999
END CONTACT INTERACTIONS

```

Multibody belt force model

The belt model route was to attach a belt segment to the upper torso on his left shoulder, attach the next segment to the lower torso on the right side, to the belt buckle on the right side, lap belt to lower torso on the left side and to the sled

floorboard. COR (=1) was belt correction factor specified to allow for fixing point deformation. If it was reduced to 0, the belt elongation would be reduced and belt load could be higher to increase belt penetration into the dummy and increase the seat loads. ADDLEN (400 mm) was the added belt length allowing for the section across the chest. We attached one point next to the hip, allowing slip to occur between the two segment. If belt tension of two segment was larger than 1 N, slip would occur from lower segment to the higher one. PRET was pre-tension of the belt. The slack (58 mm) was given to simulate the 75 mm³ block attached between chest and belt.

BELTS

```
SY1 BOD1 X1 Y1 Z1 SY2 BOD2 X2 Y2 Z2 LO UNL HYS XEL FRIC PRET ADDLEN COR ID
-1 0 -0.085 0.35 1.185 2 3 0.105 0.09 0.267 1 2 1790000 0.4 0.4 -0.058 0.4 1 diag. top (Bpillar-ut)
2 3 0.105 0.08 0.292 2 1 0.09 -0.164 0.0 1 2 1790000 0.4 0.4 0 0.4 1 diag. bott (ut-ltright)
-999
```

FUNCTIONS

```
4
0 0 0.04 8000 0.18 18000 0.2 20000
```

```
3
0 0 0.1 0 0.23 8000
```

-999

BELTS

```
SY1 BOD1 X1 Y1 Z1 SY2 BOD2 X2 Y2 Z2 LO UNL HYS XEL FRIC PRET ADDLEN COR ID
2 1 0.10 0.155 0 -1 0 -0.085 0.35 0.00 1 2 1790000 0.4 0.4 0 0 1 lappt (lleft-floorpt)
-1 0 -0.085 -0.35 0.00 2 1 0.1 -0.155 0 1 2 1790000 0.4 0.4 0 0 1 lapst (floorst-ltright)
-999
```

FUNCTIONS

```
4
0 0 0.04 8000 0.18 18000 0.2 20000
```

```
3
0 0 0.1 0 0.23 8000
```

-999

- Output Parameters

The components of the linear acceleration were expressed with respect to the inertial co-ordinate system (IWO = 0). Fx, Fy, and Fz were parameters for the correction of the calculated linear acceleration for a prescribed deceleration field. Fx =1 prescribed acceleration field in x direction which was subtracted from the calculated acceleration. A HIC value of less than 1000 was considered acceptable.

LINACC

```
SYS BO X Y Z FX Y Z IWO ID
2 5 0 0 0.063 1 0 0 0 head centre
2 3 0.029 0 0.162 1 0 1 0 chest
```

-999

INJURY PARAMETERS

HIC

```
1 0.036
```

-999

END INJURY PARAMETERS

9.3 Taxi Rearward Facing Frontal Impact Model

A combination of the MADYMO multibody techniques with finite element analysis validated by dynamic sled tests allowed a more detailed description of the contact interactions with the wheelchair-occupant system in a taxi Rearward Facing Frontal (RFF) impact model.

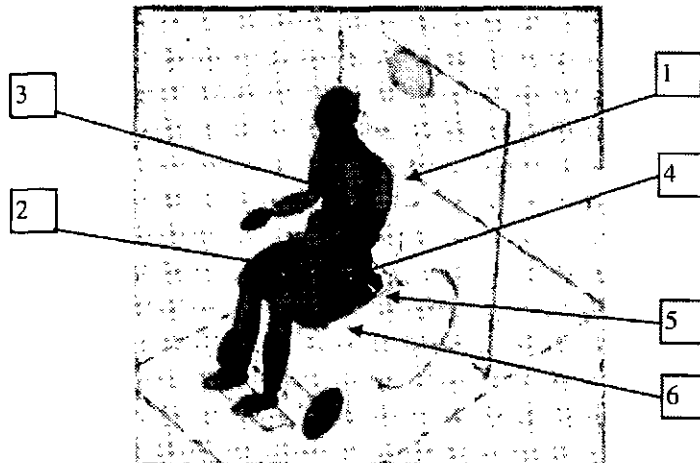


Figure 9.3a Taxi model set-up

9.3.1 Model Set-up

The following six systems were written in a taxi model within MADYMO3D package (Figure 9.3a):

System 1: ISO wheelchair or manual wheelchair;

System 2: Hybrid II dummy;

System 3: sternum;

System 4: belt buckle;

System 5: wheelchair tiedown inertia reel;

System 6: Y shape tiedown knot.

9.3.2 Model descriptions

- *Vehicle (sled) model*

Due to the one dimensional nature of the vehicle motion in the sled tests, the sled mass, moment of inertia and centre of gravity were not defined. The sled was simplified by one plane in the model. Input for the simulation was the same velocity

data to the sled tests, while a various acceleration field was applied to simulate impact.

- The bulkhead and a headrest model

A simplified bulkhead was modelled by one plane. In addition, the headrest was taken into account with one ellipsoid and the contact characteristics were estimated.

- Wheelchair model

The wheelchair was represented in the present model by one system. The mass of the wheelchair was located in the centre of gravity. The total mass of the ISO-SWC was set at 83 kg and the manual wheelchair at 15 kg. The dimensions of the wheelchairs were based on actual measurements, whilst the moment of inertia and centre of gravity were determined using the finite element code, PAFEC. The wheelchair geometry was represented by four planes: one seat plane, one seat front panel and both sides of foot rests. The six ellipsoids represented four wheels of the wheelchair, one chair backrest and one chair seat. In addition, two ellipsoid were defined to represent both sides of handles in a manual wheelchair.

Force-deflection characteristics of the wheels were determined using static compression tests. As no local stiffness data were available for the wheelchair and the taxi's bulkhead, model parameters for these contacts, such as, the chair backrest contact with back support belt, were estimated by the webbing belt deformation during static tension tests. A coulomb friction coefficient of 0.3 was specified for the contacts with the wheelchair.

- Dummy model

A 50th% Hybrid II adult dummy database (MADYMO 5.2) was used in the model while a finite element lap belt was attached to the dummy. In addition, the dummy positions were adjusted to sit in the wheelchair.

- Y shape webbing tiedown model

The wheelchair with a Y shape tiedown restraint system was modelled using a multibody module. This model consisted of two independent systems, one single inertia reel and one knot of a webbing. This model approach allowed the actual Y shape tiedown to be taken into account.

- A back support belt model

The wheelchair back support belt which underwent large deformations was designed using finite element models within MADYMO3D program to allow a more detailed analysis of those parts and a more detailed description of the contact interactions (Figure 9.3b). Ninety-six (96) membrane elements were used in the finite element belt model in order to be able to model contact between the critical dummy parts and the wheelchair.

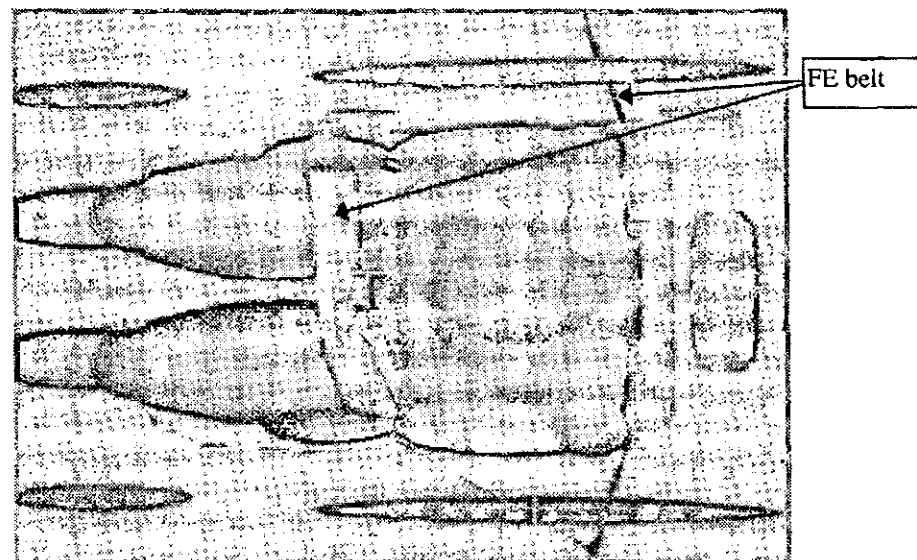


Figure 9.3b A back support FE belt model and lap FE belt

9.3.3 Summary

The RFF impact of the wheelchair-occupant system demonstrated more effective capacities for protecting the occupant than the FFF impact (Gu and Roy, 1995). Analysis of the dynamic sled tests (Appendix 5D) and computer models helped to draw the following summary:

- The simulation produced by the CVS model compared reasonably well to the actual test results from the full scale dynamic sled tests. The close approximation was made even more accurate by adjusting the various stiffness functions, friction penetration factors, and correction factors, although it is difficult to produce a simulation true to life because the exact properties of the various parts could not be taken into account, e.g. the transverse webbing belt buckle deformation.
- Further computer modelling of the rearward facing manual wheelchair-occupant system needs to be conducted in a parameter study. In the previous tests and model, the bulkhead stiffness was assumed rigid. This needs to be modified to the actual taxi structure stiffness. The dynamic variations obtained according to the position of the rear tiedown will be further investigated.

9.4 Modelling Discussions

The problems during modelling of WTORS are explained as follows:

- *Sled floating*

In the initial ATB modelling of WTORS, the rear anchorage position was defined as four duplicated segments. This resulted in rear tiedown acting as a rigid beam, which pushed the wheelchair forward or backward. This problem was solved using two segments instead of four.

- *WTORS submarining*

The problem that could be noted in the previous DYNAMAN model was that the rear wheel seemed to sink into the sled floorboard (Figure 9.4). It was later found that this was due to the improper function block given to the rear wheels. The static compressing of wheels only allowed to interpolate the value of 1,600 N force specified. From video footage review and ATB/DYNAMAN output check, it was found that the force sustained was much higher than this value, but the MADYMO program assumed the same deflection rate. During impact, the rear wheels were subjected to the weight transfer of the wheelchair and dummy. Another observation from the tests was that the tyre section of the wheel was compressed almost to the wheel rim at the point where the rear wheel was in contact with the sled floorboard.

Also the spoke section of the wheel was deflected because the wheel had an elliptical shape at the point of maximum weight transfer, at this point the wheel became solid, no more compression took place. It proved that the wheel compression test was inadequate.

Therefore the functions block was modified to account for the wheel becoming almost solid (50 kN) once the metal rim was reached (55 mm penetration). The roll friction of tyre (Roll FRIC) was adjusted to be 0.5. The wheel loads decreased with the coefficient of friction in the range of 0.8 and 0.4. The value of the wheel floor stiffness was varied until the model predictions showed sufficient agreement with actual experimental results.

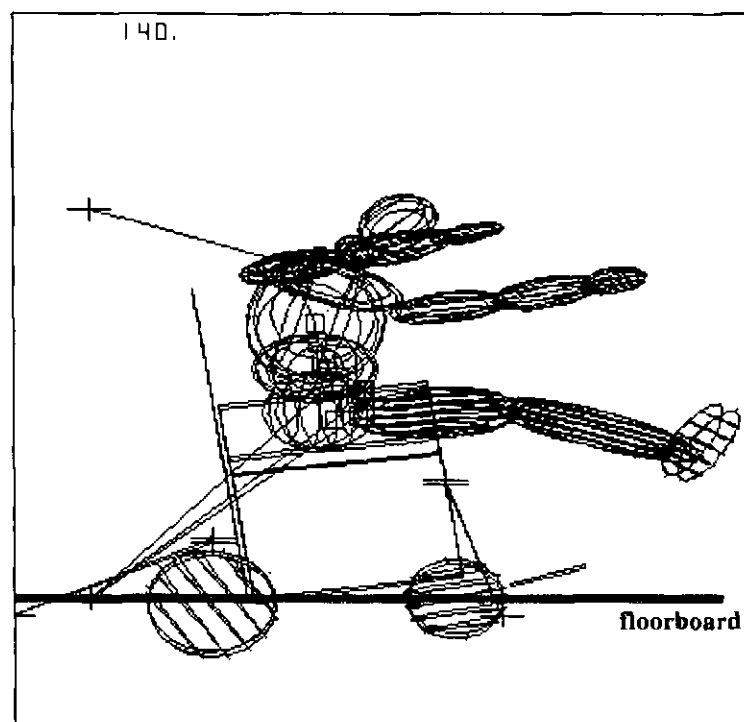


Figure 9.4 Wheelchair submarining

- *Higher wheelchair acceleration*

After examining all the results of wheelchair model, it was found that the value of wheelchair acceleration was higher than the test results. This was because of the lower tiedown static stiffness used in the initial model. The dynamic

characteristics of the webbing tiedown showed that the rear tiedown stiffness has a major effect on wheelchair acceleration.

- *Wheelchair seat penetration*

By examining the frames of high speed video footage, it could be seen that the occupant was drawn into the wheelchair backrest. The upper legs also penetrated into the seat. This could be expected due to the deformation of both these planes and the limbs themselves. The input was also modified to include plane-ellipsoid contacts between the upper legs and the seat plane, lower torso (LT) and the chair backrest, ellipsoid-ellipsoid contacts between dummy's head and the legs, dummy's arms and LT. A correction factor (COR) was given to reduce the penetration into the seat and backrest in the wheelchair. The initial position was also adjusted to keep the system equilibrium.

- *Lap and Diagonal (L/D) belt rupture*

The next problem was found in the L/D belt system when comparing the motion of the dummy in the full scale test with the kinematics obtained in the simulation. In the actual TRL test the dummy's right shoulder is thrown forward, while in the model the dummy's movement was too restrained. This was mainly due to the belt attachment configuration to the body of the dummy. During the frontal impact, the occupant's lap and diagonal belt would slide on chest, the waist and the hip. Because of the limitation of ATB/DYNAMAN programs, the only way to get around this to obtain a reasonable simulation was to design the configuration of a belt, which would be smoothly tangent to the body. The first position of belt had to be changed while the shoulder belt angle varies, such as, the floor mounted configuration. The finite element belt was of benefit to allow the belt to slide on dummy's body.

9.5 Summary

- The initial simulation produced by ATB/DYNAMAN package did not compare reasonably well to the actual test results from the full scale sled tests unless

the certain CVS techniques were involved. It is difficult to produce a simulation true to life because of the limitation of the package. The uncontrollable factors during impact are difficult to model, such as the belt buckle and reel deformations.

- Additional study using more sophisticated program, MADYMO is of benefit in furthering the subject. One of the areas in which an improvement had been achieved was a means of modelling of the contact and friction forces exerted between the ground and the pneumatic tyres. Another area for improvement was the modelling of belt restraint systems by FE belt mesh using MADYMO3D code.
- The study of impact properties has been conducted to get a better correlation between the models and experiments by design and model correlations.

Computer modelling of the crash performance of WTORS will be constructed and validated by the crash tests in the next Chapter.

CHAPTER 10: CVS MODEL VALIDATION AND ANALYSIS

10.1 Model Post-Process

The computer modelling post-process work is an integral process, which combines almost all software applications shown in Figure 10.1a. CVS model validation could be established if the model predictions correlate acceptably with observed facts. More precise defined methods of validation are available in CVS models. The model tuning loop is defined in Figure 10.1b.

Validation processes include four stages: peak value comparison, kinematic comparison, loading trace comparison and interpretation of model results (analysis and assessment). The kinematics of model was compared with the video footage adjusted by dummy lower torso to simulate the trajectory of dummy's head and upper torso. The correlation was made accurately by adjusting the various stiffness functions (CHO contact characteristics), friction penetration factors (FRI) and correction factors (COR). The initial position equilibrium analysis and structure model were also conducted for initial design correlation.

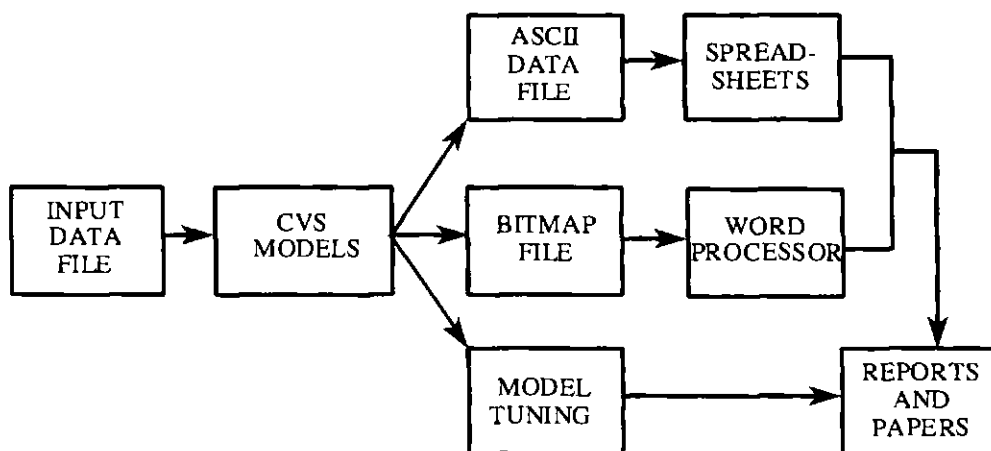


Figure 10.1a CVS model post-process

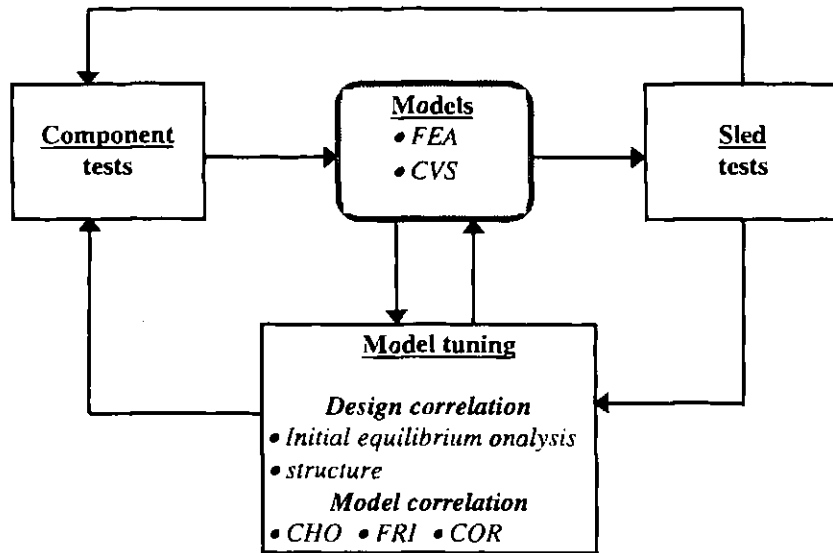


Figure 10.1b Model tuning loop

10.2 TRL Frontal Impact Model Validation

TRL Forward Facing Frontal (FFF) impact model was used to analyse the effect of changing the fixing position of the restraints for both wheelchair and occupant. The rear tiedown angle was varied between 30-degree and 45-degree. From this model, the optimum position was determined, which would cause less injury to the occupant and less damage to the wheelchair.

Experimental results at MURSEL were used to validate the robustness of the model. The TRL model simulation was compared with the full scale sled tests. The head, wheelchair P point and wheel centre movement were then recorded using the DYNAMAN post-processor. The movement of these points relative to the local co-ordinate system of the inertial space was measured. A graphical representation of these results could be seen in the following diagrams in TRL model (Figure 10.2a - 10.2s). The resulting maximum responses were compared to the actual test data (Table 10.2a and 10.2b).

Table 10.2a Comparison of TRL test and CVS results - Level III

Parameters (peak)	Units	TEST RESULTS				CVS RESULTS			
		30-deg	45-deg	30-deg	45-deg	30-deg	45-deg	30-deg	45-deg
Set up conditions		WTRS	WTRS	WTORS	WTORS	WTRS	WTRS	WTORS	WTORS
Test number		T2818	T2819	T2820	T2821				
Sled pulse	g	19.8	20.1	16.1	17.7	11.1	20.1	16.1	17.7
Delta 'V'	km/h	32.7	32.1	31.5	31.4	32.7	32.1	31.5	31.4
OUTPUT:									
w/c FP wheel	kN	6.2	4.7	11.4	11.1	4.7	7.1	11.2	11.4
w/c FS wheel	kN	11.6	11.4	7.7	11.8	11.3	7.2	11.1	11.3
w/c RP wheel	kN	7.1	11.7	7.7	11.1	11.7	14.2	11.2	13.3
w/c RS wheel	kN	11.1	12.4	6.1	11.5	7.1	13.0	11.1	13.3
Single rear wheel	kN	7.1	11.1	6.1	11.2	7.1	13.1	11.4	13.3
Peak Time	ms	120	111	115	110	120	111	115	110
RP tiedown	kN	6.5	7.4	6.5	7.3	6.1	11.1	6.0	6.1
RS tiedown	kN	6.5	6.5	6.5	6.0	6.7	7.1	6.1	6.1
Single rear tiedown	kN	6.5	7.0	6.5	6.5	6.11	11.0	6.1	6.1
Peak Time	ms	111	111	111	110	115	115	115	115
L/D lap load	kN	#	#	6.3	6.1	#	#	4.1	5.2
L/D diagonal load	kN	#	#	11.2	11.1	#	#	11.2	11.6

Table 10.2b The difference between TRL tests and CVS model

Parameters	Units	WTORS (45-degree rear tiedown angle)							
		FP wheel	FS wheel	RP wheel	RS wheel	RP t'down	RS t'down	Lap	Diag.
Test	kN	11.1	11.8	11.1	11.5	7.3	6.0	6.1	11.1
CVS	kN	11.4	11.3	13.3	13.3	6.1	6.1	5.2	11.6
difference %		2.7	4.2	19.8	15.6	16.4	1.7	14.7	4.5

The rear tiedown angle 30-degree WTRS results (Level I) are compiled in Figure 10.2a - Figure 10.2d.

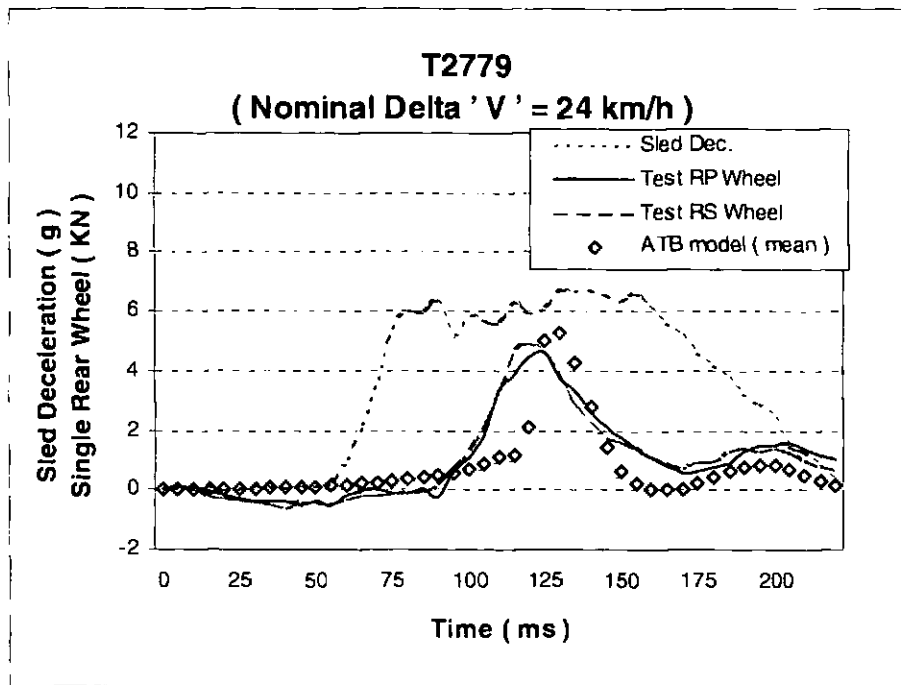


Figure 10.2a Comparison of the single rear wheel loads for TRL tests (T2779)

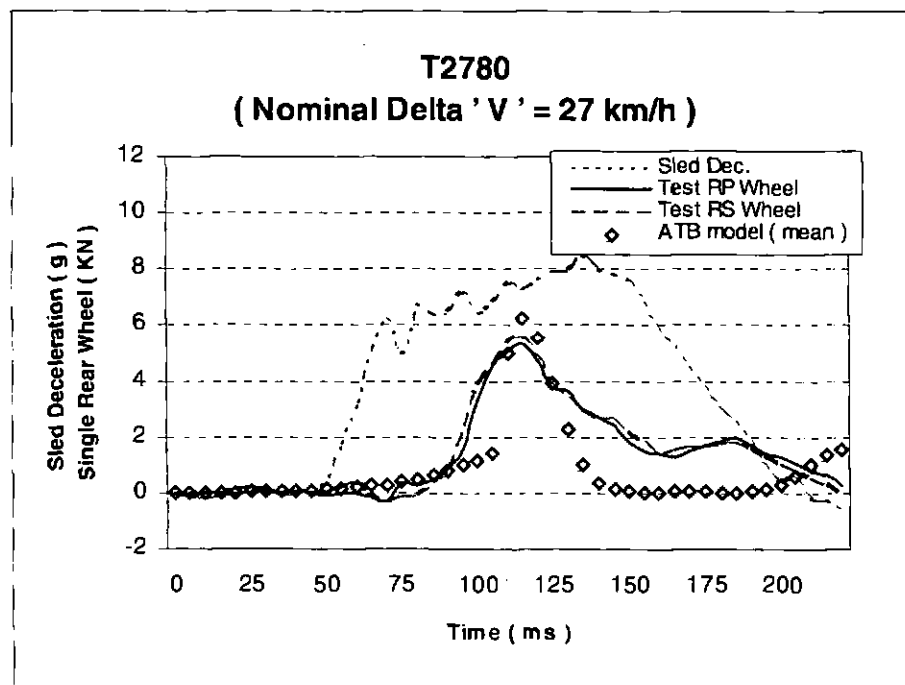


Figure 10.2b Comparison of the single rear wheel loads for TRL tests (T2780)

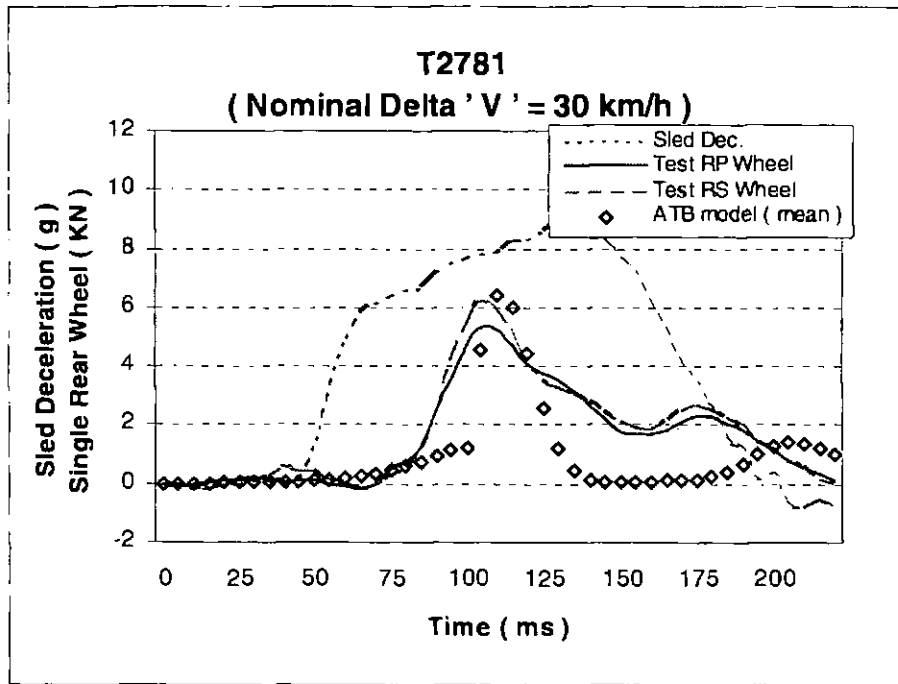


Figure 10.2c Comparison of the single rear wheel loads for TRL tests (T2781)

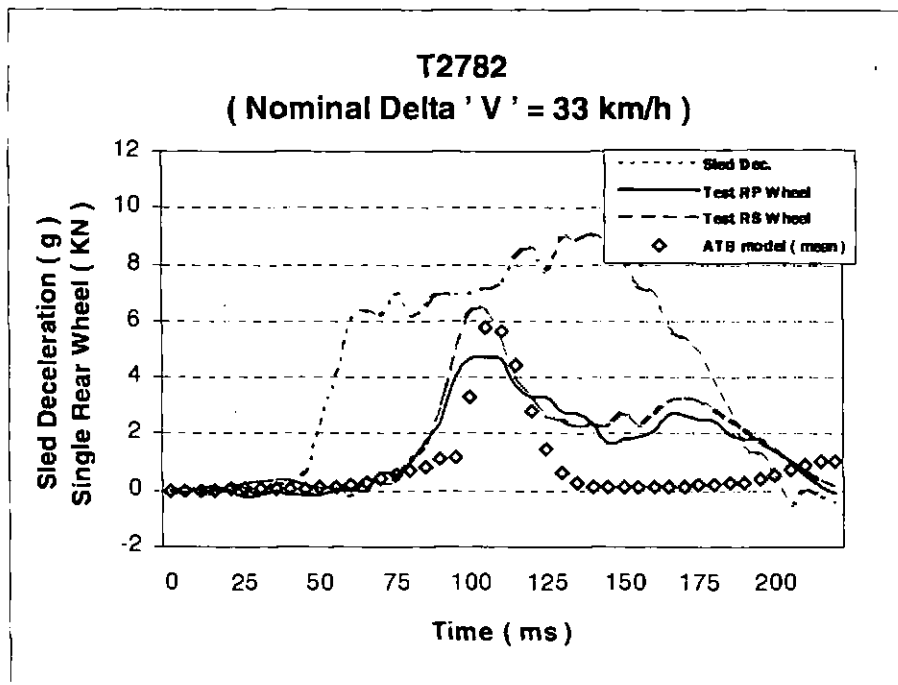


Figure 10.2d Comparison of the single rear wheel loads for TRL tests (T2782)

The rear tiedown angle 30-degree WTRS results (pulse level II) are shown in Figure 10.2e - Figure 10.2h.

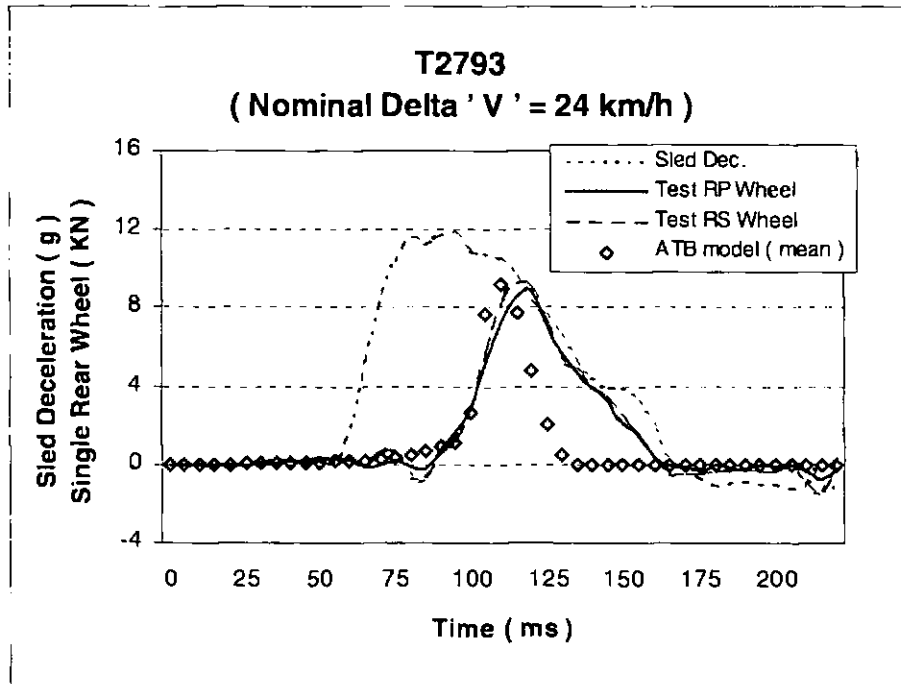


Figure 10.2e Comparison of the single rear wheel loads for TRL tests (T2793)

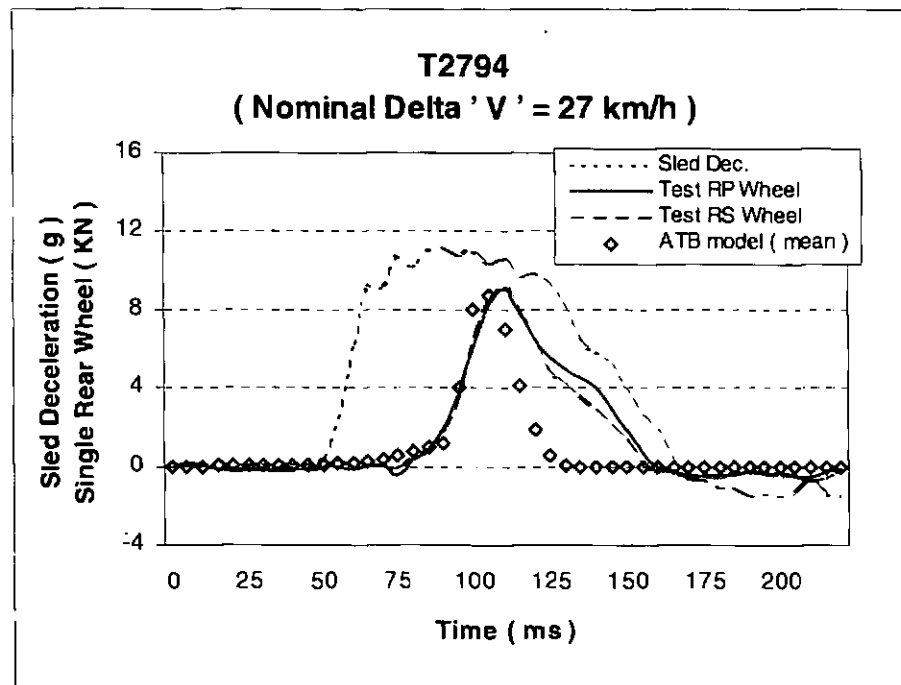


Figure 10.2f Comparison of the single rear wheel loads for TRL tests (T2794)

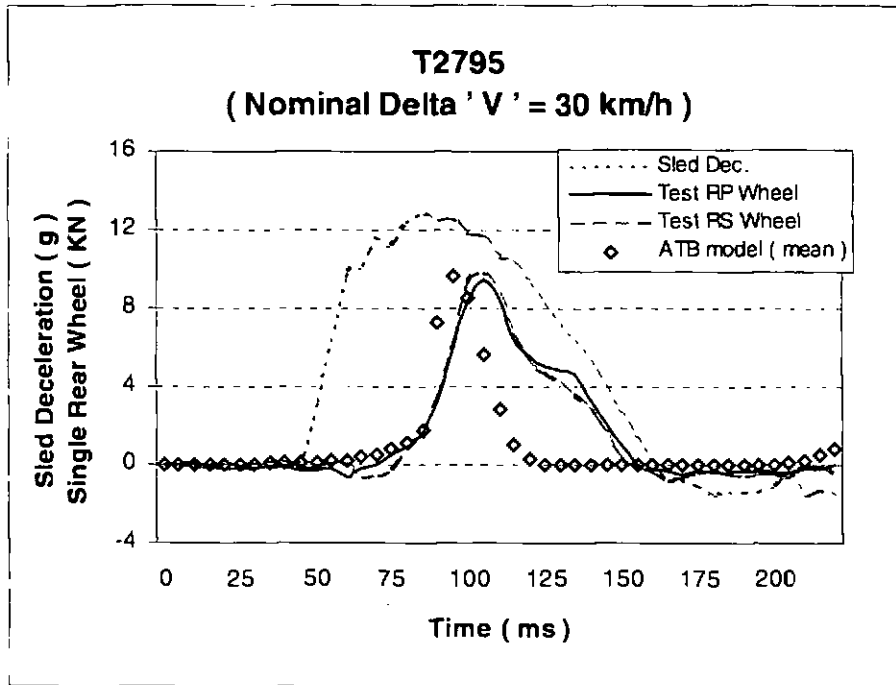


Figure 10.2g Comparison of the single rear wheel loads for TRL tests (T2795)

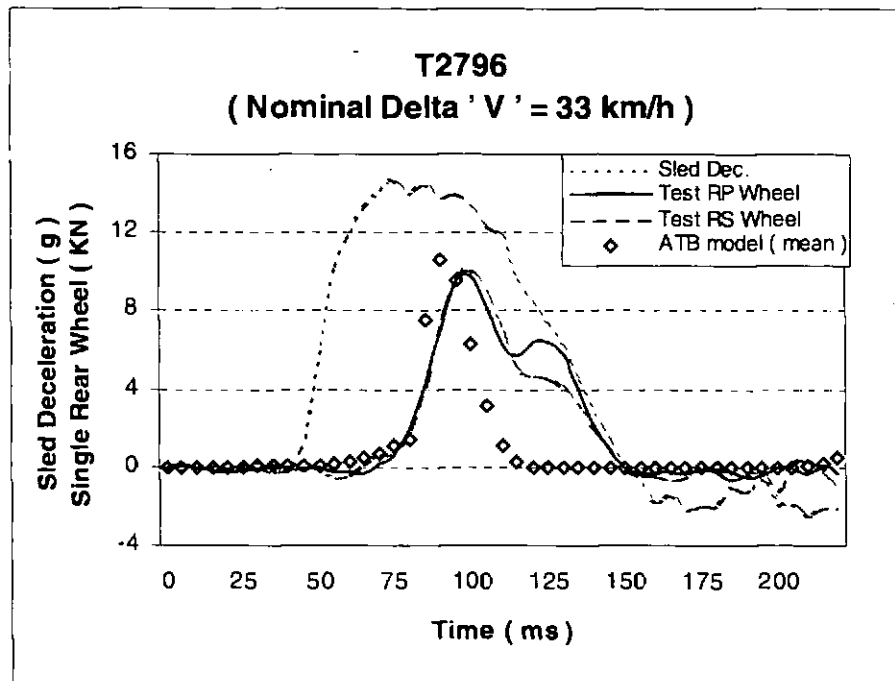


Figure 10.2h Comparison of the single rear wheel loads for TRL tests (T2796)

The rear tiedown angle 45-degree WTRS results (pulse level I) are shown in Figure 10.2i - Figure 10.2l.

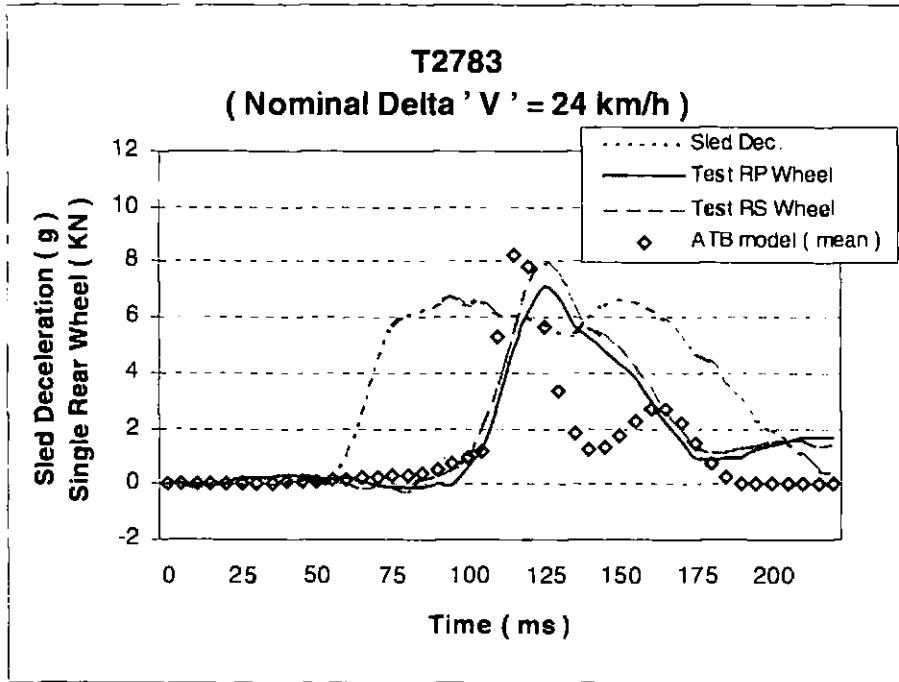


Figure 10.2i Comparison of the single rear wheel loads for TRL tests (T2783)

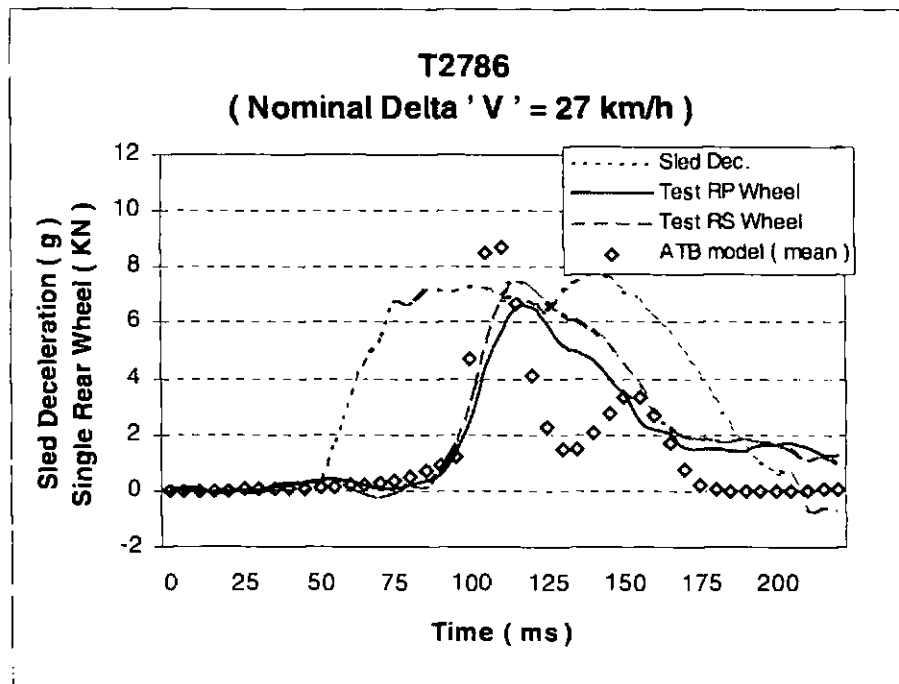


Figure 10.2j Comparison of the single rear wheel loads for TRL tests (T2786)

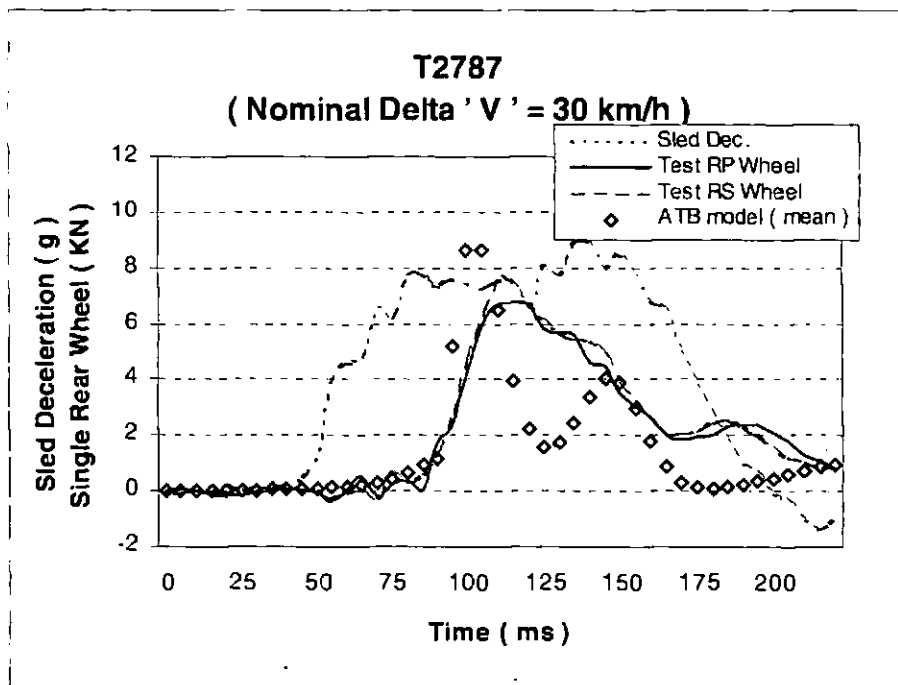


Figure 10.2k Comparison of the single rear wheel loads for TRL tests (T2787)

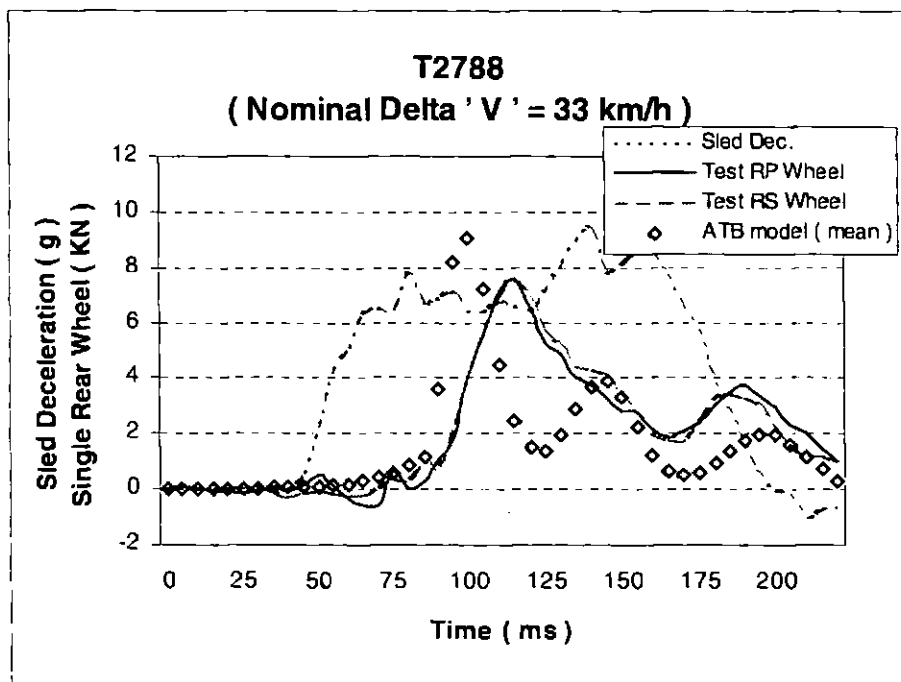


Figure 10.2l Comparison of the single rear wheel loads for TRL tests (T2788)

The rear tiedown angle 45-degree WTRS results (pulse level II) are shown in Figure 10.2m - Figure 10.2p.

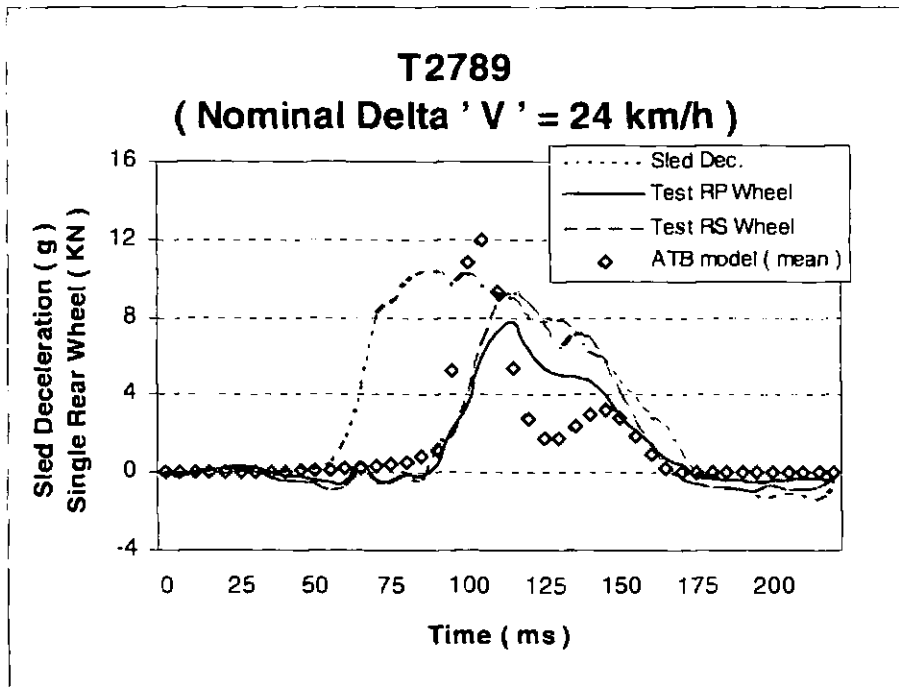


Figure 10.2m Comparison of the single rear wheel loads for TRL tests (T2789)

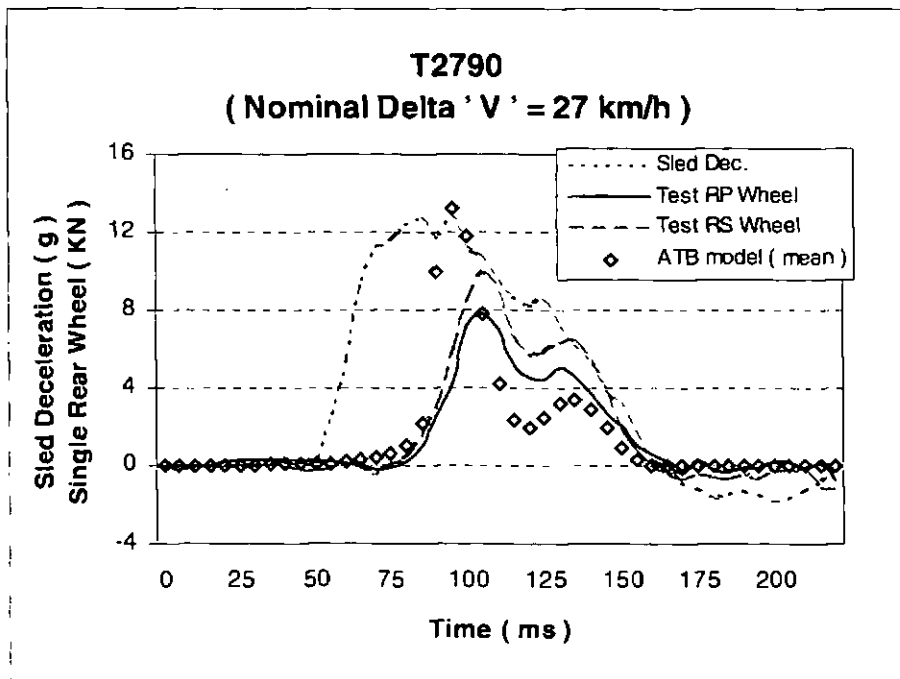


Figure 10.2n Comparison of the single rear wheel loads for TRL tests (T2790)

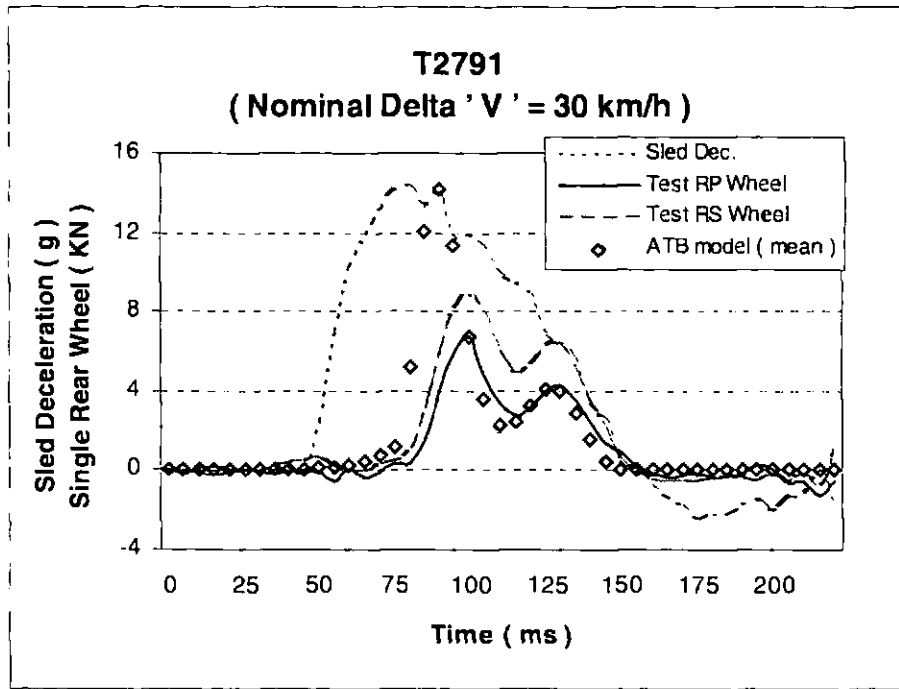


Figure 10.2o Comparison of the single rear wheel loads for TRL tests (T2791)

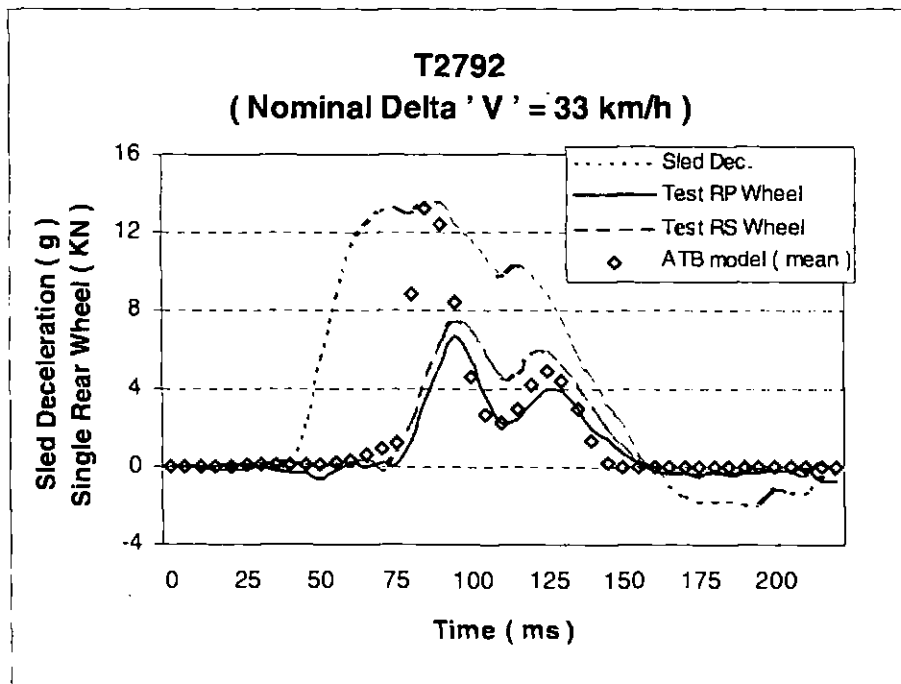


Figure 10.2p Comparison of the single rear wheel loads for TRL tests (T2792)

The rear tiedown angle 30-degree results of WTRS (crash severity of Level III without dummy) are compared with 45 degree shown in Figure 10.2q and Figure 10.2r.

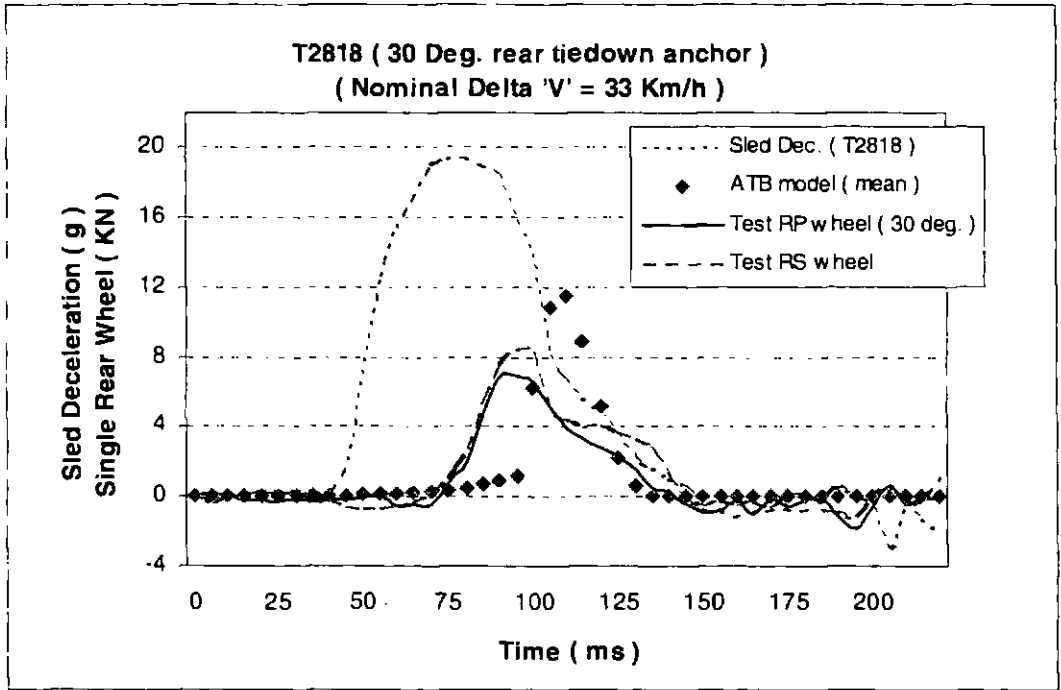


Figure 10.2q Comparison of the single rear wheel loads for TRL tests (T2818)

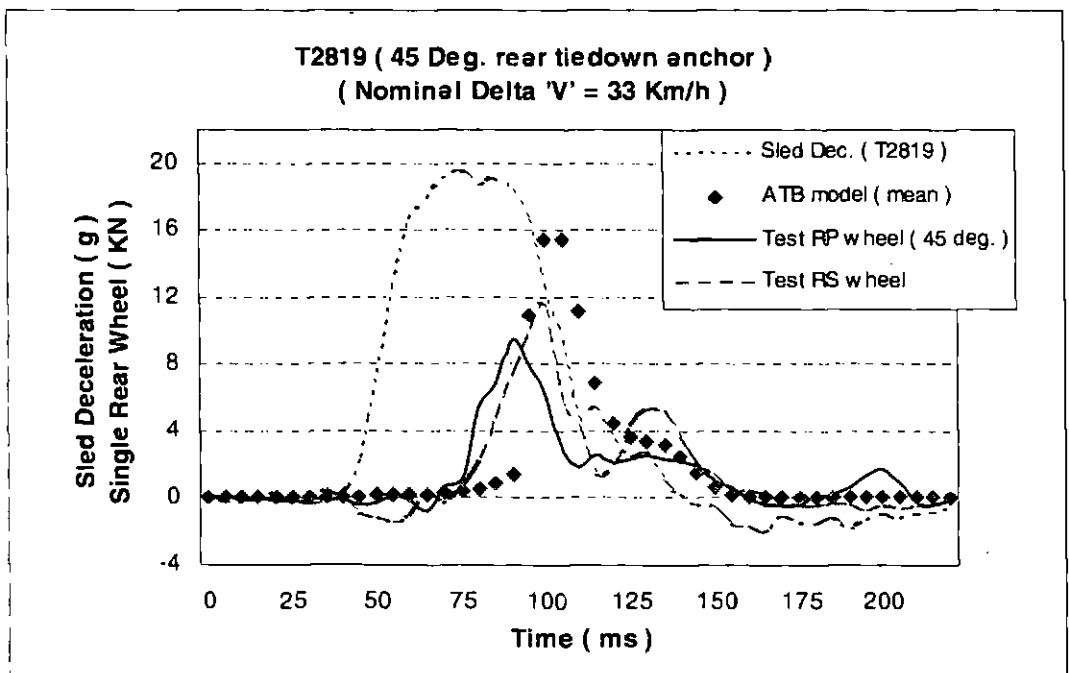


Figure 10.2r Comparison of the single rear wheel loads for TRL tests (T2819)

Two rear tiedown angles results of WTORS (crash severity of Level III with dummy) are shown in Figure 10.2s.

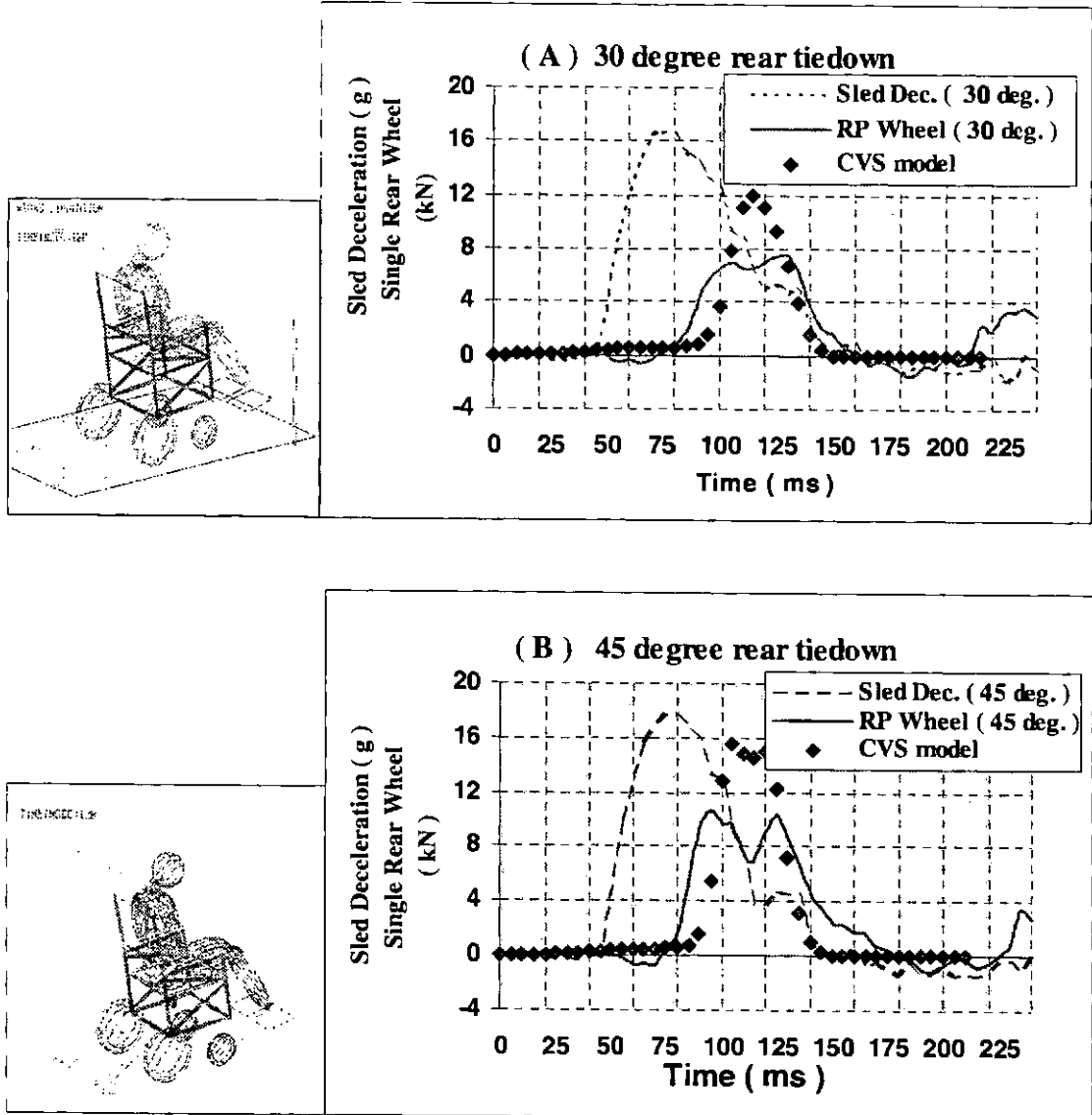


Figure 10.2s Schematic comparison of test and CVS model in WTORS (Level III) (A & B)

Figure 10.2t shows the kinematics of TRL wheelchair with TNO-10 dummy in TRL front impact.

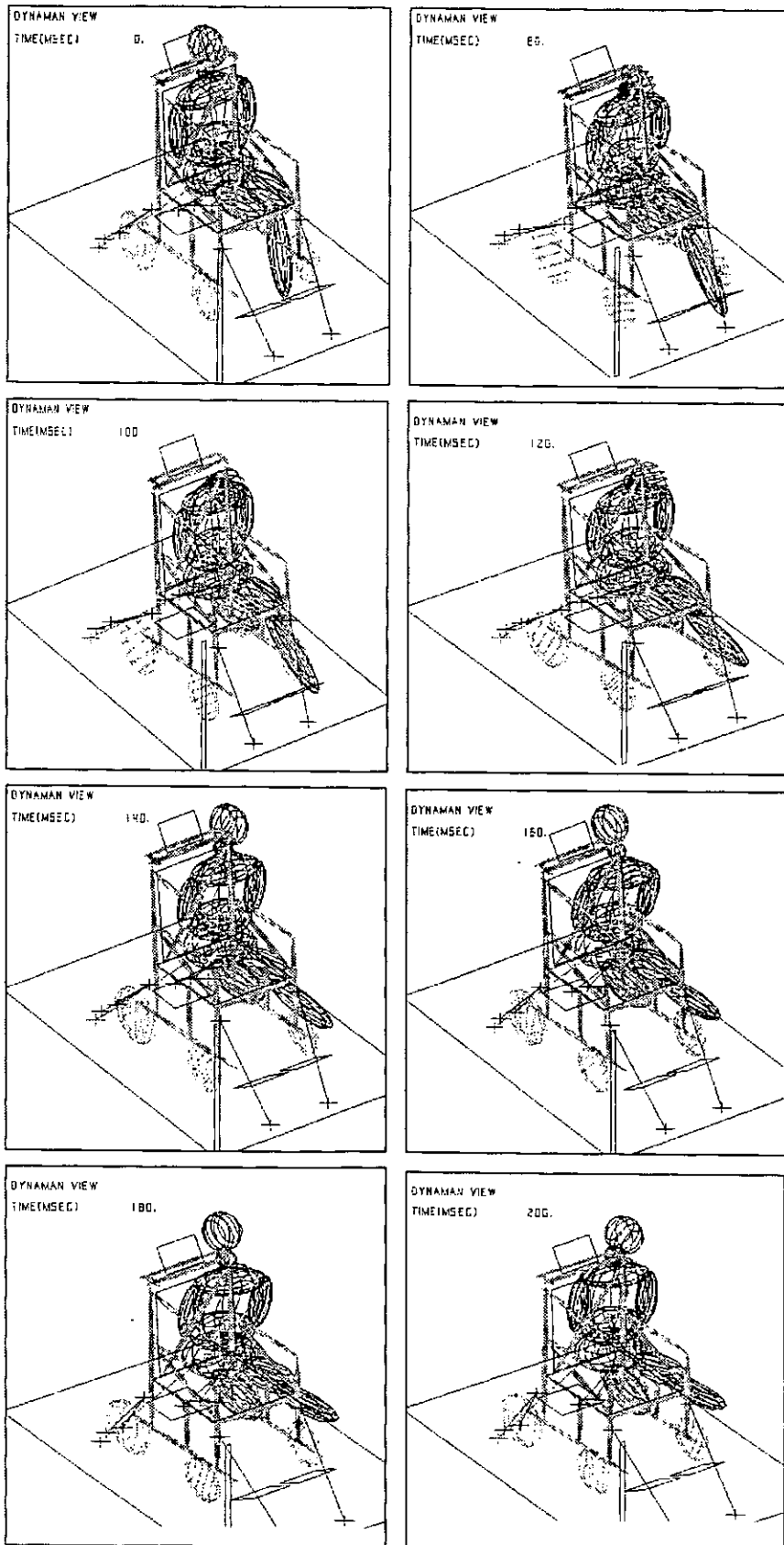


Figure 10.2t Kinematics of TRL wheelchair with TNO-10 dummy

10.3 ISO Frontal Impact Model Validation

The ISO Forward Facing Frontal (FFF) impact models were set-up using both DYNAMAN (CVS1) and MADYMO3D (CVS2). As seen from Table 10.3, most of the peak results obtained were in general agreement with the dynamic test results, except the peak value of the diagonal bottom strap tension (T_2), which was selected at the different time of T_1 . It was expected that the multibody belt model was difficult to simulate the belt buckle deformation at the anchorage of a diagonal bottom strap. The validation was conducted precisely using time-history traces (Figure 10.3a). The simulated diagonal top strap tension in CVS model mirrored the test results.

Table 10.3 Comparison of ISO tests and CVS model results
(Peak values, B pillar, 51 km/h, 21g)

		Test	CVS1	CVS2	diff 1	diff 2
Output	units				%	%
Chest -x	g	38.3	26.3	32.7	31	15
Chest Res.	g	46.6	38.1	53.0	18	14
Diag. top (T_1)	kN	6.9	7.2	7.9	4	14
Diag. bot (T_2)	kN	5.0	5.5*	7.5*	10	50
Lap (T_3)	kN	6.1	7.2	6.3	18	3
Buckle (T_4)	kN	11.1	14.3	13.8	29	24
Seat Sum (C_1)	kN	26.4	26.3	34.7	0	31

* This peak value was selected at the different time of T_1 .

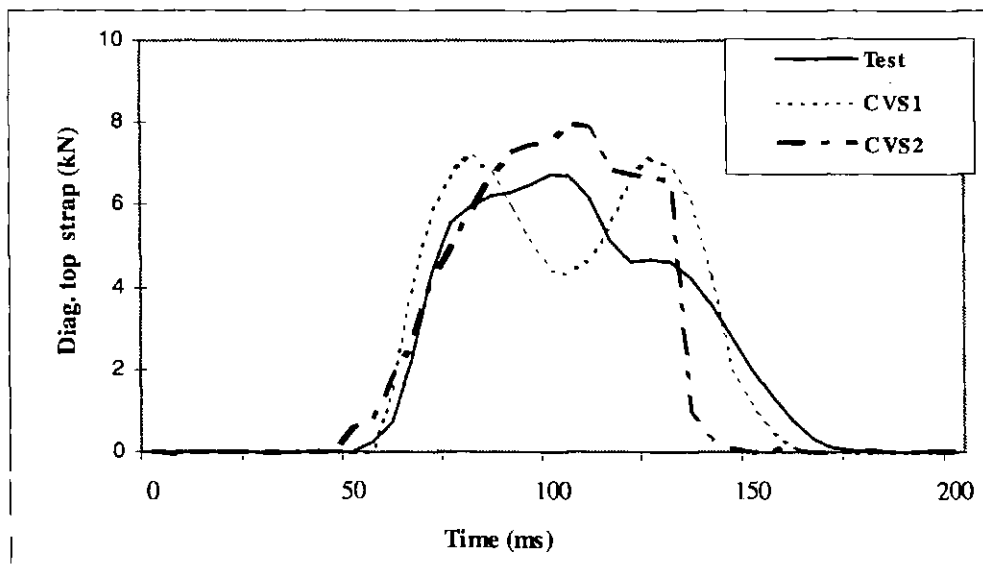


Figure 10.3a Comparison of sled test and CVS models

All peak strap tensions in the CVS models were generally higher than the test results and had a relatively sharper peak response. The contact functions of the wheels had a significant effect on this difference. Furthermore the CVS1 model did not allow for the effect of belt slippage which was evident in the experimental results. The CVS2 model seems more close to the test results than CVS1 model. The kinematics of ISO wheelchair with Hybrid II dummy in ISO frontal impact is shown in Figure 10.3b.

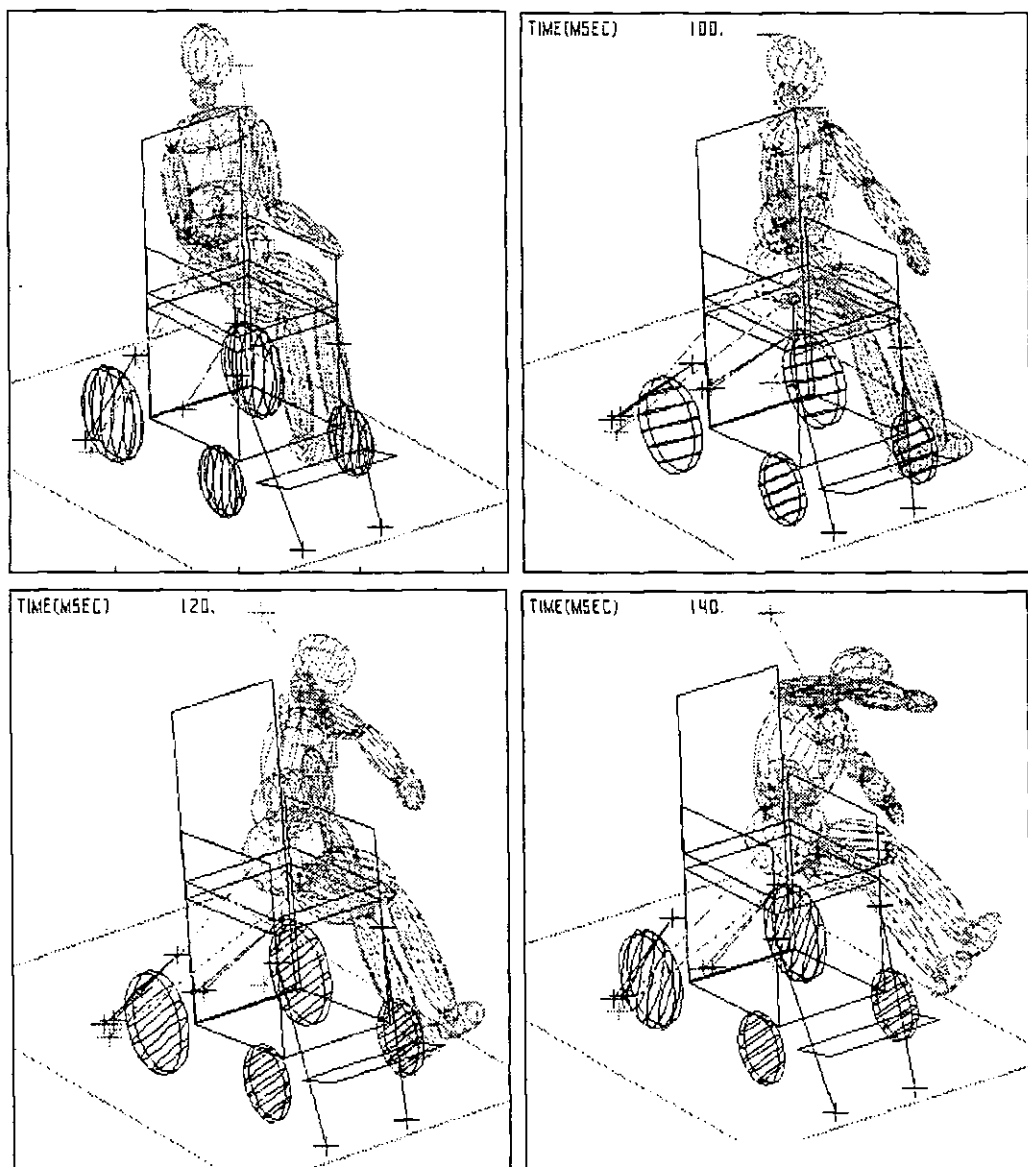


Figure 10.3b Kinematics of ISO wheelchair with Hybrid II dummy

10.4 Rearward Facing Frontal Impact Model Validation

In general, the kinematics of Rearward Facing Frontal (RFF) impact of WTORS (Figure 10.4) appear to be very well in agreement with observations from the high speed video records (Appendix 5D). For instance, the difference in head trajectory between head and headrest, and also, between wheelchair handles and the taxi bulkhead are well illustrated by the model.

Table 10.4a Comparison of taxi tests and CVS results (Series I & II)

Series I & II	Unit	Series I	Model I	Series II	Model II	diff I %	diff II %
Sled pulse	g	21	21	17	17		
	km/h	32	32	32	32		
Acc. chest	g	72.9	58.0	*	43.2	20	*
Acc. head	g	50.6	51.2	50.1	40.9	1	18
Back (Pt.)	kN	3.8	2.6	5.5	4.2	32	24
Back (St.)	kN	3.9	2.8	3.3	3	28	9
Wheel Pt.	kN	13.2	10.8	37.2	37.8	18	2
Wheel St.	kN	13.2	16.6	*	38.6	26	*
Rear T/D	kN	4.3	4.8	5.2	5.6	12	8

Notes: * test data failure

Table 10.4b Comparison of taxi tests and CVS results (Series III & IV)

Series III & IV	Unit	Series III	Model III	Series IV	Model IV	diff III %	diff IV %
Sled pulse	g	19	21	19	21		
	km/h	33	32	33	32		
Acc. chest	g	75.1	60.5	51.6	50.9	19	1
Acc. head	g	75.8	52.0	74.7	50.6	31	32
Back (Pt.)	kN	3.9	3.4	5.2	5.3	13	2
Back (St.)	kN	2.6	1.6	3.3	3.2	38	3
Wheel Pt.	kN	10.7	10.5	10.1	10.5	2	4
Wheel St.	kN	10.9	12.6	10.7	11.1	16	4
Rear T/D	kN	2.1	2.9	1.6	2.1	38	31

Table 10.4a and 10.4b show a comparison between sled test series peak values and the relative models. The discrepancy between the MADYMO model and experiments (Series II) in the back support belt loads (Back Pt and Back St) is up to 24 percent, occurred at different time. The contact-interaction was correlated by dynamic test results.

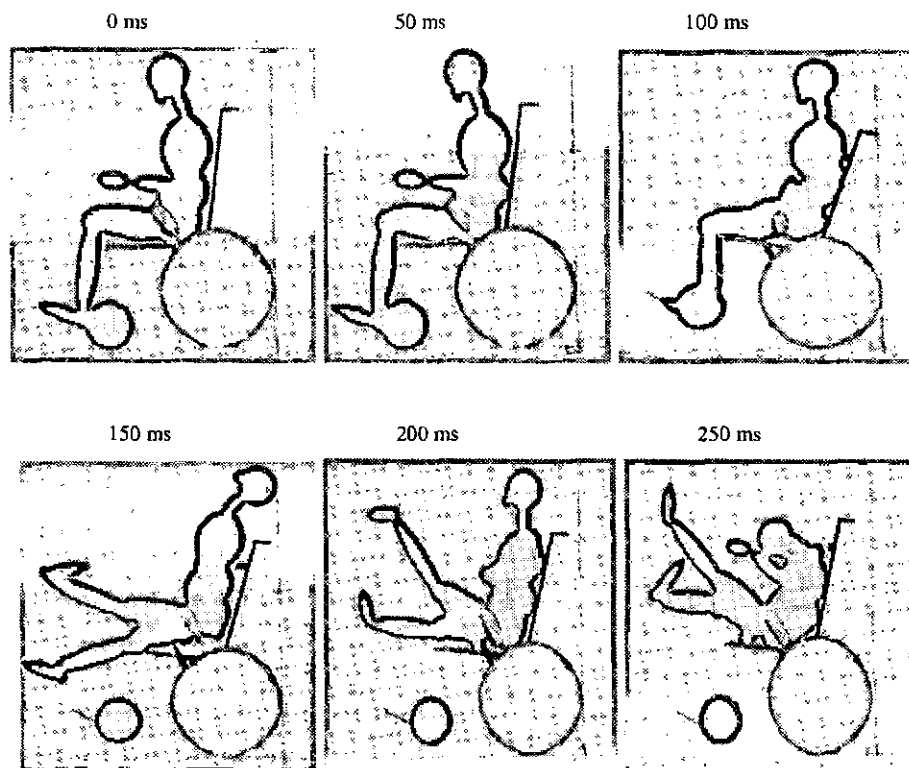


Figure 10.4 Simulated kinematics of a RFF impact of WTORS (Series I)

10.5 Simulation Analysis

10.5.1 FFF impact model analysis

The response parameters of a frontal impact model are a function of many input parameters. These inputs include the dynamic conditions of the crash, the physical properties of the system, and the overall test set-up.

- As expected the overall variability in the model was greater than the experimental results. This is due to the variability of experimental results attributable to uncontrollable errors in test set-up and measurement, such as, the belt buckle and load cell connecting parts deformations, in addition to sled pulse variations. In

computer simulation, these uncontrollable random errors associated with the test set-up are eliminated. It means that outputs are a function of the crash pulse exclusively.

- The ability of this model to predict actual results was good, especially for predicting of loads of WTORS during impact. The relatively large differences between the model predictions and the experimental results were found in the rear wheel loads (less than 38%). The simulation predicted the wheel load going to a peak, particularly in level III (Figure 10.2s). All experimental results have indicated that the pneumatic wheel actually rocked during impact. This will be further investigated using finite element tyre model.
- The differences between the model and the experimental results were primarily due to the structure differences between the multibody-modelled wheels and the actual pneumatic tyres. The ATB/DYNAMAN model was a highly simplified representation of the actual tyres, and the dynamic responses were different.

Once calibrated with dynamic tests, the frontal impact model was used to simulate different restraint configurations to find the optimum positions of restraint anchorage. It will help manufacturers to design the best systems and reduce permanent injury.

10.5.2 RFF impact model analysis

- *Comparison of two configurations in the same manual wheelchair without and with headrest (Series I and III)*

Transducer outputs for two configurations (Series I: without headrest; Series III: with headrest) are shown from Figure 10.5a to Figure 10.5g. The peak values of chest resultant acceleration in two configurations were about same while the values of head resultant acceleration were variable. The total loads acting on the taxi bulkhead were summed from the loads of both sides of the wheels and back support level occurred at the same time. At a ΔV of 32 km/h and sled deceleration of 20g (Level V), the maximum bulkhead load was recorded on impact of 28.5 kN without headrest and 25.4 kN with headrest, a tiedown load on rebound of 4.3 kN without headrest and 2.1 kN with headrest. The relatively large differences between wheelchair with headrest and one without headrest were found in the head resultant acceleration ($> 20g$).

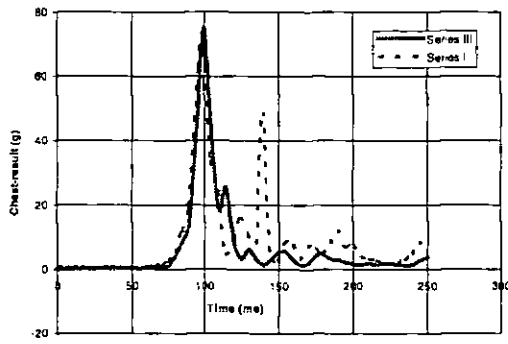


Figure 10.5a Comparison of headrest effect on chest acceleration

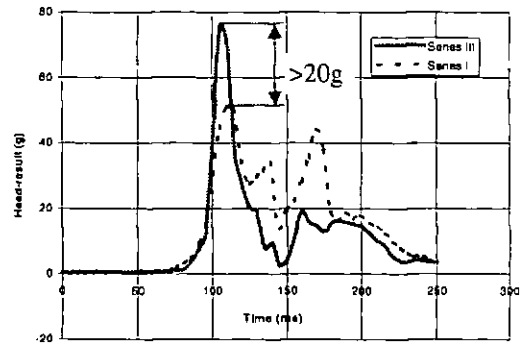


Figure 10.5b Comparison of headrest effect on head acceleration

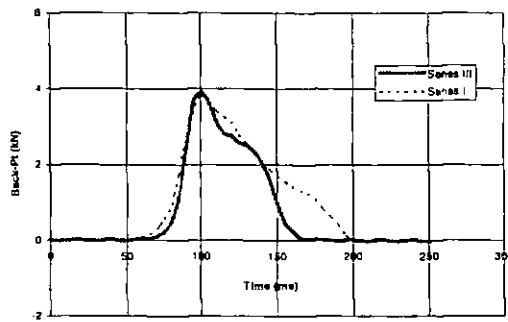


Figure 10.5c Comparison of headrest effect on wheelchair back load (Pt)

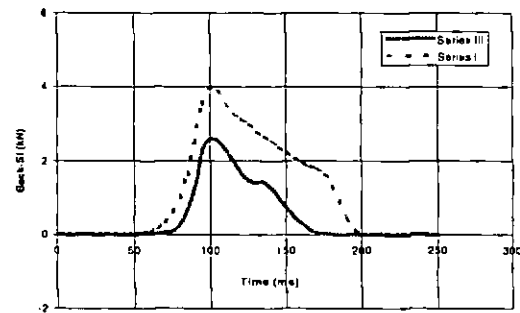


Figure 10.5d Comparison of headrest effect on wheelchair back load (St)

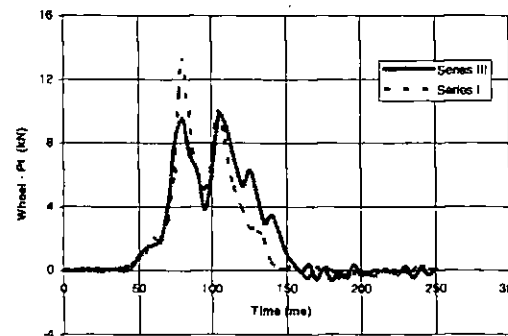


Figure 10.5e Comparison of headrest effect on wheelchair wheel load (Pt)

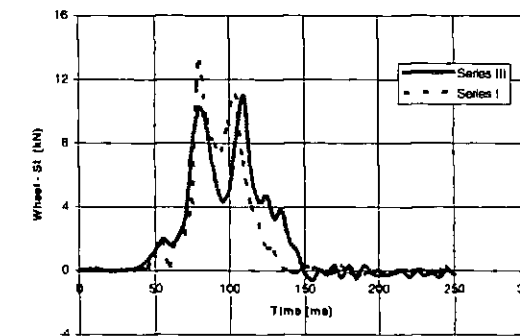


Figure 10.5f Comparison of headrest effect on wheelchair wheel load (St)

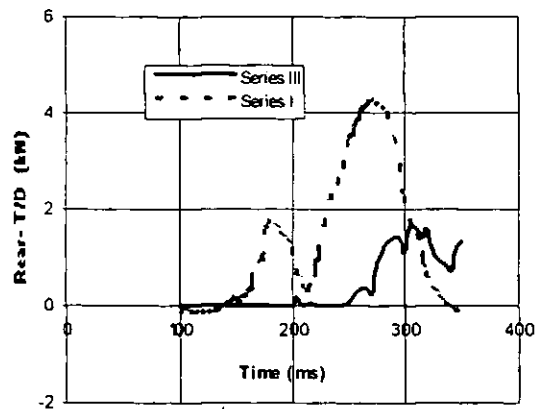


Figure 10.5g Comparison of headrest effect on rear tiedown load

- Comparison of two types of wheelchair: surrogate and manual wheelchair (with headrest) (Series II and III)

Transducer outputs for two different mass of wheelchairs are shown in Figure 10.5h - 10.5n. The ISO-SWC is 83 kg (Series II) and a manual wheelchair is 15 kg (Series III). The peak values of both chest and head resultant acceleration in two types of wheelchair were variable. At a ΔV of 32 km/h and sled deceleration of 17g (crash severity Level IV), the maximum bulkhead load was recorded on impact at 75 kN in the surrogate and 25.4 kN in the manual. The relatively large differences between ISO surrogate wheelchair and manual wheelchair were found in the wheel loads (> 20 kN).

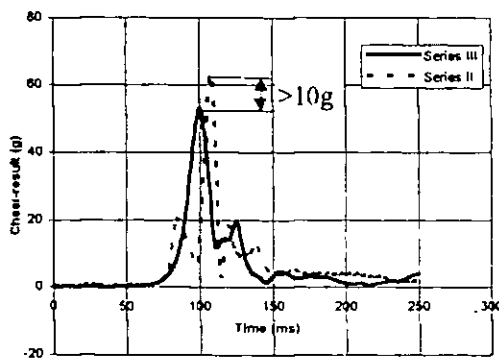


Figure 10.5h Comparison of wheelchair type effect on chest acceleration

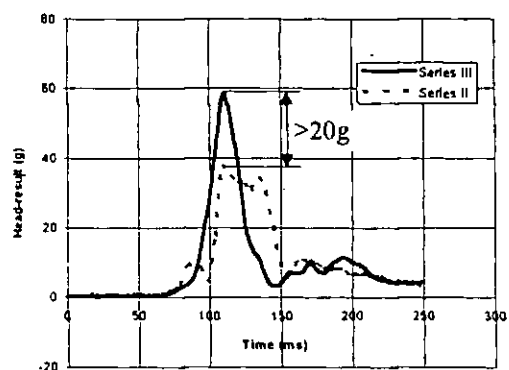


Figure 10.5i Comparison of wheelchair type effect on head acceleration

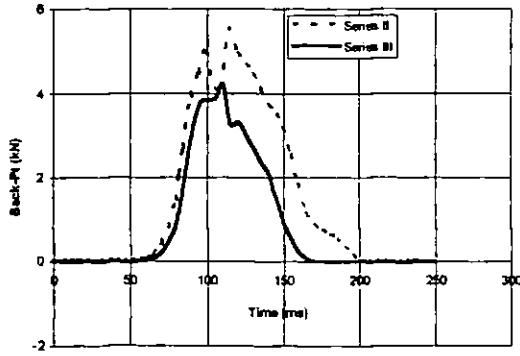


Figure 10.5j Comparison of wheelchair type effect on wheelchair back load (Pt)

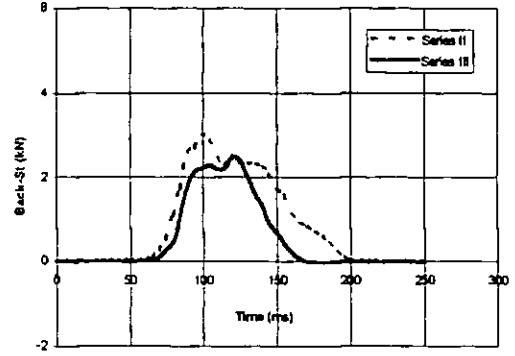


Figure 10.5k Comparison of wheelchair type effect on wheelchair back load (St)

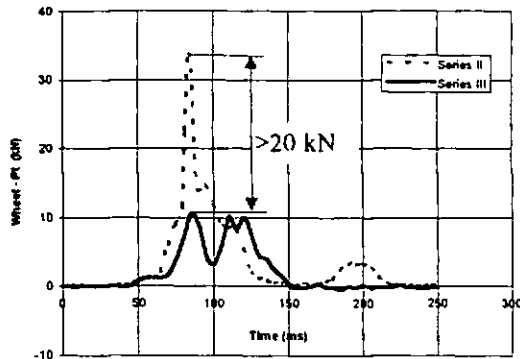


Figure 10.5l Comparison of wheelchair type effect on wheelchair wheel load (Pt)

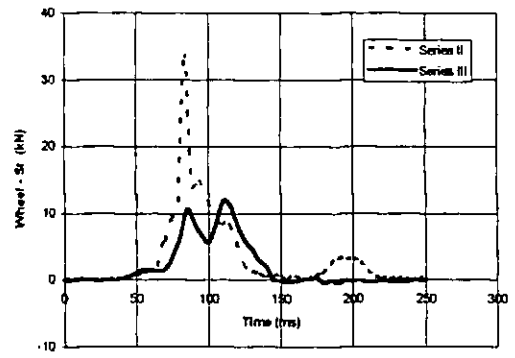


Figure 10.5m Comparison of wheelchair type effect on wheelchair wheel load (St)

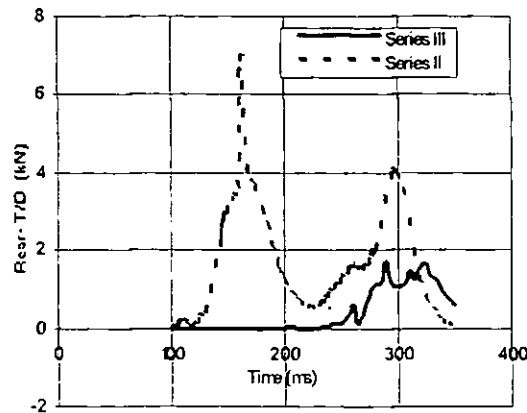


Figure 10.5n Comparison of wheelchair type effect on rear tiedown load

It was observed from the high speed video records that this was due to the rear wheel of the surrogate wheelchair being compressed until the rigid wheel rim contacted the floor load cells during impact. On the other hand, the flexible wheel rim of the manual wheelchair deformed during impact and hence reduced the peak load values.

Test series II revealed modes of hardware failure, such as cutting of a transverse webbing at the areas of high stress concentration. The dummy's movements were more uncoordinated when the ISO wheelchair was used.

- *Comparison of two modes of a manual wheelchairs: with and without handles (with headrest)(Series III and IV)*

In order to avoid the second collision between the wheelchair handles and the taxi bulkhead, the handles were removed in test series IV. This configuration was compared with the standard manual wheelchair (Series III). Transducer outputs for two modes of wheelchairs are shown in Figure 10.5o - 10.5u. The peak values of head resultant acceleration in two configurations were about same while the values of chest resultant acceleration were variable. The relatively large differences between a wheelchair without handles and one with handles were found in the chest resultant acceleration ($> 30g$) at the crash severity Level V.

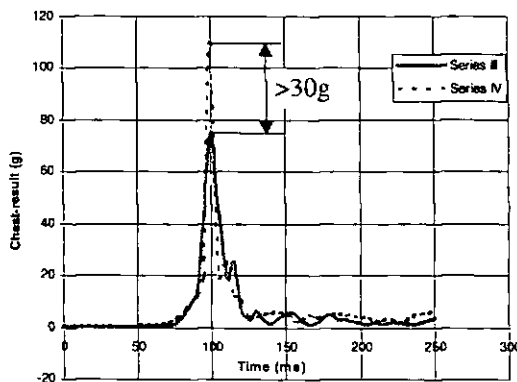


Figure 10.5o Comparison of wheelchair handle effect on chest acceleration

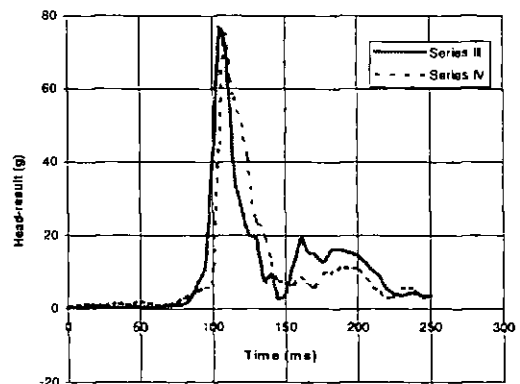


Figure 10.5p Comparison of wheelchair handle effect on head acceleration

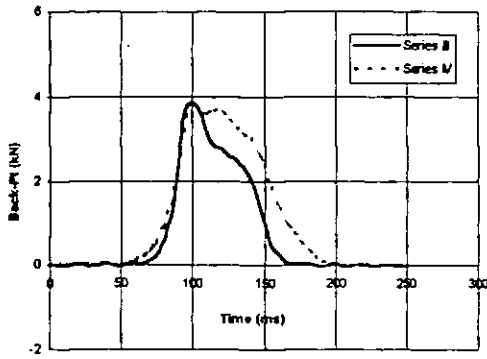


Figure 10.5q Comparison of wheelchair handle effect on wheelchair back load (Pt)

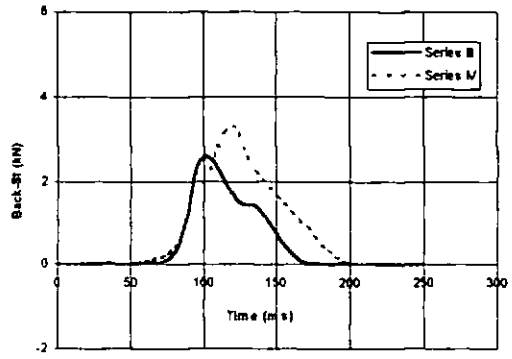


Figure 10.5r Comparison of wheelchair handle effect on wheelchair back load (St)

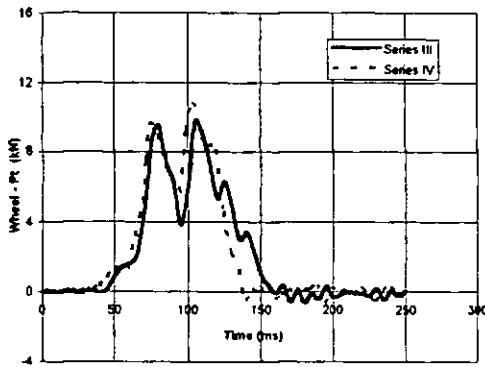


Figure 10.5s Comparison of wheelchair handle effect on wheelchair wheel load (Pt)

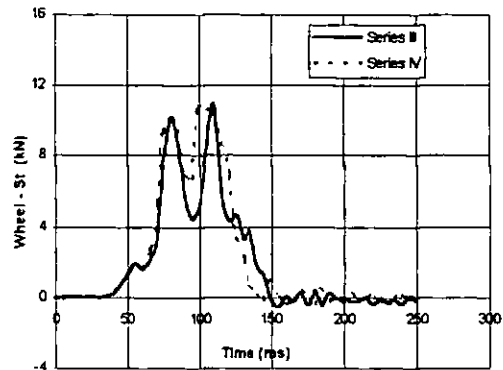


Figure 10.5t Comparison of wheelchair handle effect on wheelchair wheel load (St)

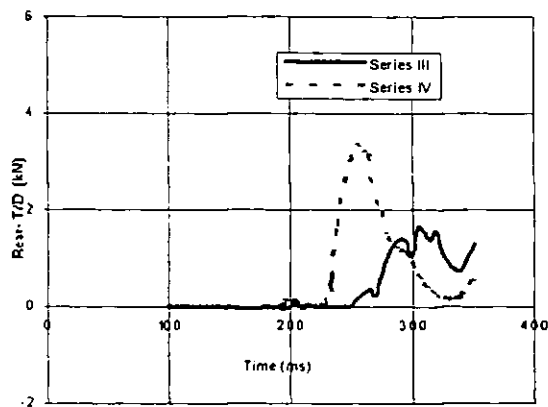


Figure 10.5u Comparison of wheelchair handle effect on rear tiedown load

10.6 Summary

The wheelchair-occupant restraint model was developed by the author and proved to be a good estimator of actual experimental results. The comparison between CVS model and experimental results gives the following summaries.

- The model was utilised to study the relative effects of crash pulse differences on the variability of maximum responses. It was found that crash pulse variations accounted for much of the overall variation in loads and decelerations, while having a negligible influence on maximum excursions.
- In the CVS models, the un-controllable random errors associated with the test set-up were neglected, such as, belt buckle and reel deformations, sled platform stiffness, test apparatus accuracy including instrumentation, etc. The details of tiedown anchorage deformation and testing adjustment i.e. axial bending and belt slippage during impact will be further modelled using finite element models.
- It was unrealistic to think that the DYNAMAN model could be capable of predicting experimental results with a high degree of precision because of its limitation. What the validation study proved, however, was that this model was sufficient for observing gross phenomena and determining approximate loads, deceleration, and excursions, making it useful for a variety of applications. Parameter studies can be conducted by this model to investigate a wide range of cause and effect relationship.
- The validation process is not completed. The objective of TRL model development is not to obtain a very accurate correlation with a real vehicle impact, but rather to be designed as the methodology of a sled simulation of vehicle impact. Now this preliminary step has been successfully accomplished. This study has also proceeded with a systematic investigation by varying the different parameters, which were included in the FFF impact model, taxi RFF impact model. All these models exhibited the structure design objectives, which would offer a better protection to the occupant.
- Further dynamic testing to validate the predictions of the computer model will serve to enhance the model's credibility. Once this is accomplished, computer simulation could become an integral tool in WTORS design and test specification.

CHAPTER 11: GENERAL DISCUSSIONS OF WTORS

This Chapter provides explanations to common dynamic phenomena observed in WTORS impact tests and computer models. The velocity profile and the natural frequency of WTORS were used to explain why the wheelchair and dummy experienced a higher acceleration. The acceleration amplifications could be expressed in terms of a response spectrum to provide a good sense of how varying system parameters affect the amount of wheelchair amplification. What is the effect of variations in the crash pulse within the specified tolerances on the simulation results? The shoulder loads both in the B pillar and floor-mounted configurations were calculated by a beam element analysis method. The shoulder belt load at floor-mounted configuration was found to be higher than that at B pillar configuration. A four-point tiedown restraint system was analysed and used to explain how quasi-static analysis in the past underestimated the peak tiedown loads. Energy principles were applied to show why 30-degree tiedown configuration generates lower tiedown loads than 45-degree configuration? Finally, the rebound of the sled was analysed to investigate the spring deflection and stop distance, and also to explain why the rebound velocity could be neglected in a mass-spring model.

11.1 Investigation of the Amplification Effect

In a crash environment, the wheelchair and its occupant exerted peak acceleration in excess of the peak deceleration of the sled. This phenomenon is called the amplification effect. Both the sled and the wheelchair were initially travelling at v_0 prior to impact. The wheelchair relative to the sled allowed the wheelchair to continue moving forward at v_0 when the sled started slowing down. The chair continued to move at nearly a constant velocity until the restraint system started to take effect, and the chair began to slow down at a high rate. The slope of the chair's velocity curve at this time was higher than at any other point on the sled's velocity profile, thus the chair's peak acceleration was higher than the sled. When the chair reached its maximum forward movement corresponding to the maximum tiedown elongation, the

chair was essentially connected to the sled platform rigidly. From this point on, the chair and the sled decelerated at the same level.

The sled was coming to a stop while the chair and dummy continued translation. The increased acceleration occurred due to the relative movement of the chair and dummy with respect to the sled. Acceleration amplifications led to a more severe crash environment, causing higher head and chest accelerations, resulting in the potential for more serious injury, severe occupant restraint loads, excessive occupant excursions, and a greater chance of impact with interior vehicle structures.

Computer models suggested that the amplification effect was a function of the tiedown compliance (Chapter 6). It was found that the degree of acceleration amplification was determined by the natural frequency of the system given by the wheelchair mass and tiedown stiffness ($\mathbf{a}_m = \mathbf{u}_m \cdot \omega_0^2$, $\omega_0^2 = \mathbf{k}/\mathbf{m}$), in addition to the crash pulse shape and pulse duration. As the compliance of the wheelchair tiedown restraint system increased, the associated amplification increased, resulting in a greater chair acceleration amplification. Theoretically, an infinitely stiff wheelchair restraint system would result in no amplification so that the chair's acceleration would be identical to the sled. For occupant lap belt systems, acceleration amplification of the head and chest is greater to cause jack-knifing. When a shoulder belt is added to restrain the upper torso, the whipping and jack-knifing action of the head and chest relative to the lower torso is reduced, and as a result, the peak acceleration are decreased.

11.2 Beam Element Analysis of Shoulder Loads

The belt loading distribution around the dummy upper torso can be expressed in Figure 11.2a. The axial tensile forces in the shoulder belt are equal if friction was neglected. The shoulder reaction force $S_f = T_1 + T_2$, resolved in the direction of torso centre line. In the frontal impact of WTORS, The dummy upper torso reaction was simulated using three beam elements. The beam element 1 and 2 linked to form new element 3.

In order to compare the crash performance of two shoulder belt anchorage positions (B pillar and floor-mounted configurations), the following parameters were considered:

- ΔV : Sled velocity change;
- t : Time of peak diagonal top strap tension (T_1);
- α : Diagonal top strap angle to the horizontal at the time of t ;
- β : Occupant torso forward angle from vertical at the time of t ;
- γ : Diagonal top strap angle with reference to a vertical plane parallel to the sled fore and aft centre line;
- H_{exc} : Dummy head target maximum excursion;
- T_1 : Diagonal top strap tension;
- T_2 : Diagonal bottom strap tension;
- T_3 : Lap strap tension;
- T_4 : Buckle strap tension;
- C_f : Wheelchair seat sum load;
- $S_f(B)$: Occupant shoulder load function in B pillar configuration;
- $S_f(F)$: Occupant shoulder load function in floor-mounted configuration.

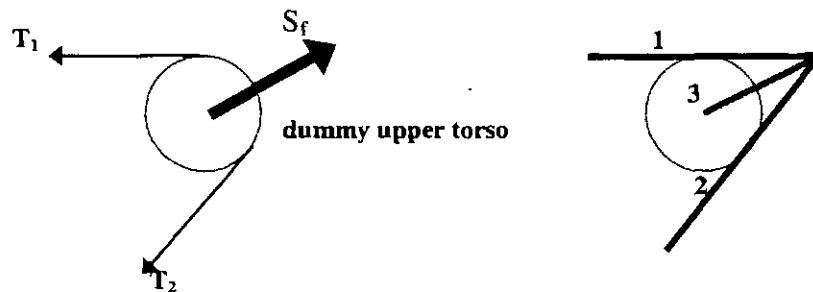


Figure 11.2a Static analysis of shoulder belt loads

The occupant shoulder load functions were computed in the direction of the torso centre line in order to obtain a value of the downward load on the shoulder of the dummy. It should be noted that T_1 did not lie in a vertical plane parallel to the sled centre line, whilst T_2 , T_3 and T_4 did (Figure 11.2b). It is difficult to measure the dummy forward angle (β) as the thorax of the dummy twisted during the impact. Some assumptions were made to simplify the model. The same angle of 44 degrees to the horizontal was assumed for both the diagonal bottom strap and lap belts. The angle γ was

estimated from the EktaPro records and the initial setting of the Hybrid II dummy. The shoulder load functions in two configurations are defined as follows:

$$S_f(B) = T_1 \cos \gamma \sin(\beta - \alpha) + T_2 \sin(44 + \beta) \tag{11.2-1}$$

$$S_f(F) = T_1 \cos \gamma \sin(\beta + \alpha) + T_2 \sin(44 + \beta) \tag{11.2-2}$$

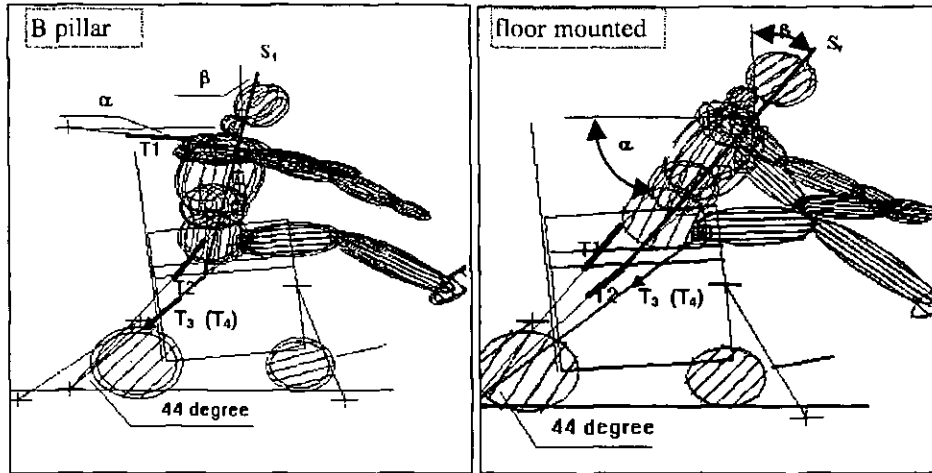


Figure 11.2b Free body diagram for occupant torso

The dummy shoulder loads were estimated and the results are listed in Tables 11.2a and 11.2b.

Table 11.2a Shoulder load calculation at B pillar configuration (at the time of peak T₁ load)

ΔV km/h	t ms	α deg	β deg	γ deg	H_{exc} mm	T_1 kN	T_2 kN	T_3 kN	C_f kN	$S_f(B)$ kN
15	165	5	4	17	168	2.50	1.63	1.40	4.54	1.17
18	145	5	4	10	216	2.99	2.23	1.40	4.72	1.61
20	135	5	10	13	254	3.67	2.87	2.18	5.63	2.63
23	125	5	10	8	256	3.90	2.72	2.30	6.53	2.54
25	125	5	16	8	269	3.92	2.90	2.82	8.46	3.25
27	125	5	16	8	272	4.10	2.77	3.28	9.78	3.17
34	120	5	16	8	296	4.77	2.57	3.56	11.3	3.13
40	115	8	20	6	304	5.41	2.69	3.85	11.8	3.54
45	95	10	22	31	369	5.98	4.57	5.39	12.6	5.24
51	95	10	30	32	384	6.51	4.01	6.24	14.7	5.74

**Table 11.2b Shoulder load calculation at floor-mounted configuration
(at the time of peak T_1 load)**

ΔV	t	α	β	γ	H_{exc}	T_1	T_2	T_3	C_f	$S_r(F)$
km/h	ms	deg	deg	deg	mm	kN	kN	kN	kN	kN
15	210	28	10	<1	272	3.02	0.68	0.68	4.59	2.41
18	200	23	15	<3	312	3.17	0.85	0.79	4.87	2.68
20	190	23	16	<2	360	3.73	1.03	0.93	5.60	3.24
23	175	23	20	<1	360	3.79	1.33	0.87	6.63	3.78
25	155	20	22	<2	368	4.04	1.21	1.76	8.01	3.81
27	155	20	28	4	392	4.18	1.43	1.67	8.77	4.46
34	145	15	35	6	450	5.89	1.68	1.75	9.11	6.14

- ***The diagonal strap belt configurations***

The diagonal strap belt were used either by floor-mounted configuration in one case (denoted subscript 'floor') or by B pillar configuration (denoted subscript 'B'). These are non-linear systems. The kinetic energy theory is not be able to explain the effect of upper diagonal strap configurations on diagonal top strap load (T_1) and to give the following conclusion:

$$(T_1)_{\text{floor}} > (T_1)_B \quad (11.2-3)$$

Comparison of values in Table 11.2a and 11.2b, shows that at the same crash severity of 34 km/h, 13g, the floor-mounted T_1 is 5.89 kN. The diagonal bottom strap load (T_2) is only about one third of T_1 , while B pillar case $T_2 = 1/2 T_1$, the total shoulder belt load is about same in both configurations. The peak value of T_1 for the B pillar anchored system occurred 25 ms before that of floor-mounted system.

- ***Occupant restraint and seat loads as a function of time***

Figure 11.2c shows that in the B pillar configuration the peak values of buckle strap tension (T_4), both diagonal top and bottom tensions (T_1 and T_2) occur around the same time of 120 ms. Fig 11.2d shows that in the floor-mounted configuration, the peak value of T_1 reached at the time of 170 ms. It lagged the peak seat sum (C_f) and T_4 by about 35 ms. This delayed response of T_1 was supported by observations from the EktaPro video record of the greater forward displacement of the dummy torso,

thus causing mass transfer to the front of the chair. The greater value of the front wheel loads for the floor-mounted configuration also support this observation.

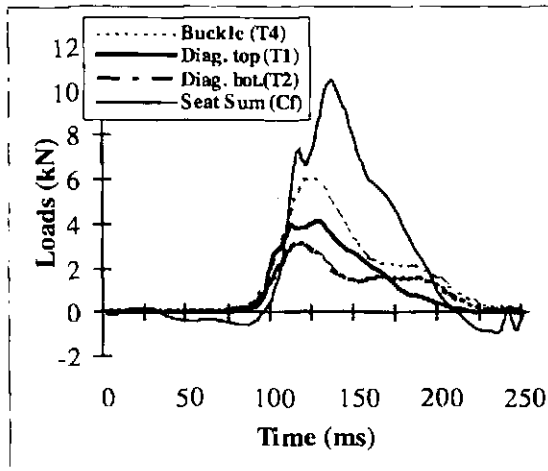


Figure 11.2c Load distribution in B pillar configuration (11g, 27 km/h)

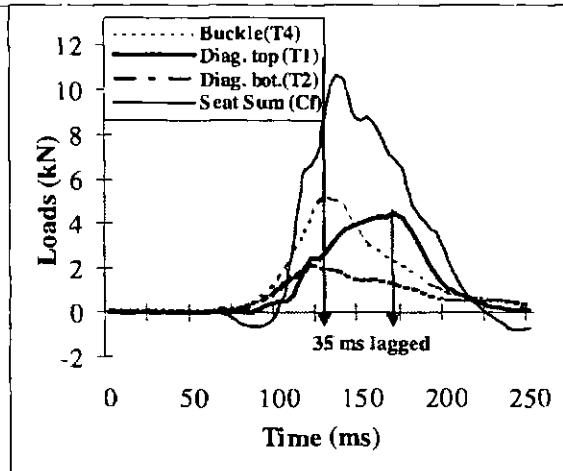


Figure 11.2d Load distribution in floor-mounted configuration (11g, 27 km/h)

- **Occupant restraint and seat loads as a function of sled velocity change**

Fig 11.2e and Fig 11.2f suggest that the peak loads such as overall seat (C_f), diagonal top (T_1), lap belt (T_3), and shoulder loads [$S_r(F)$ and $S_r(B)$] generally increase with the velocity change (ΔV) in two configurations.

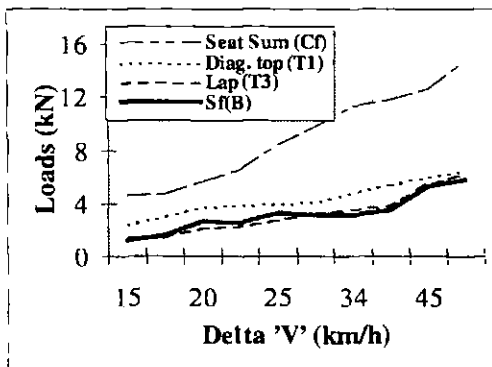


Figure 11.2e Peak parameter variation (B pillar configuration)

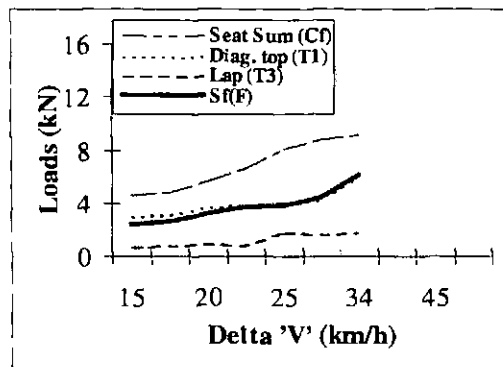


Figure 11.2f Peak parameter variation (floor-mounted configuration)

11.3 Load Characteristics in WTORS

Manufacturers in the past have designed wheelchair structure to withstand loads produced in a 48 km/h-20g frontal impact based on a simple quasi-static calculation (Figure 11.3a). The force balance is written as:

$$T_r \sin\theta_r + mg = N_r + N_f \quad (11.3-1)$$

$$\mu(N_r + N_f) + T_r \cos\theta_r = ma_s \quad (11.3-2)$$

where: ma_s equals the mass of the chair times the peak deceleration of vehicle or sled a_s , N_f and N_r are wheelchair's frontal and rear wheel loads respectively, T_r is the rear tiedown load, θ_r is the horizontal angle of the rear tiedown strap.

This function underestimated the actual loads and oversimplified the force distribution given by the free body diagram as the amplification effect was not accounted for. Obviously, the peak acceleration of the chair is not equal to the peak deceleration of the vehicle.

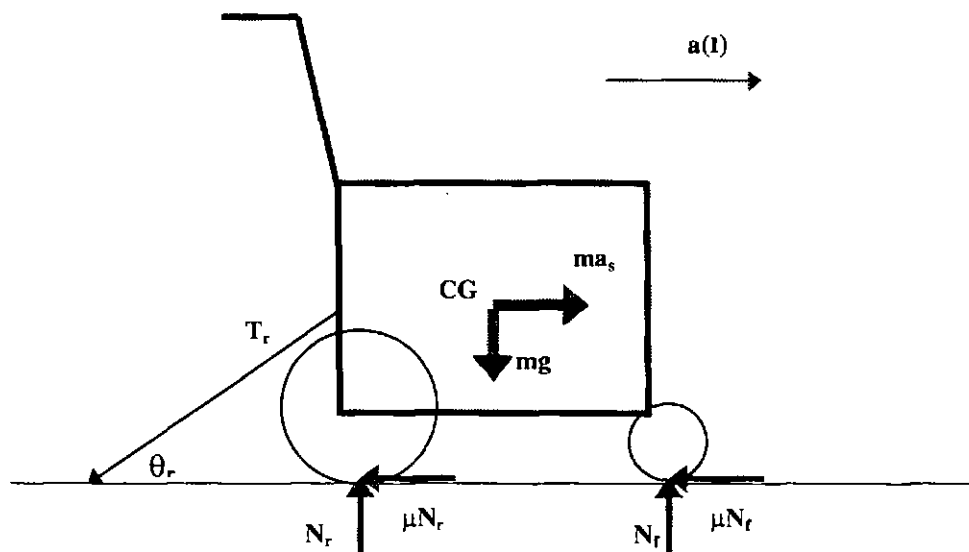


Figure 11.3a Static analysis of wheel loads

A more appropriate force decomposition is shown in Figure 11.3b. It was assumed that the ATD did not transfer any loads to the chair. The effects of the wheelchair amplification, the frontal tiedown loads (T_f) and the dummy's interaction with the chair are now considered. The force balance is resolved vertically and horizontally as follows:

$$T_r \sin\theta_r + T_f \sin\theta_f + (m_c + m_d) g + (T_1 + T_2) \sin\alpha = N_r + N_f \quad (11.3-3)$$

$$T_r \cos\theta_r - T_f \cos\theta_f + (T_1 + T_2) \cos\alpha + \mu(N_r + N_f) = m_c a_c + m_d a_d \quad (11.3-4)$$

where: $m_c a_c$ is the mass of the chair times the peak acceleration of the chair a_c , $m_d a_d$ equals the mass of the dummy times the peak chest acceleration of dummy a_d , T_r and T_f represent the rear and frontal tiedown loads respectively.

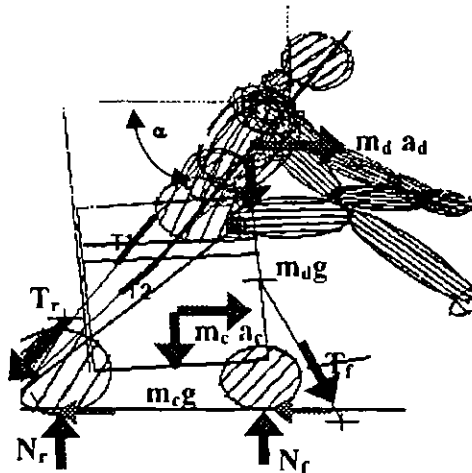


Figure 11.3b Further analysis of wheel loads

If we resolve accelerations at the angle β for the ATD and γ for the wheelchair vertically and horizontally, the equations (11.3-3 and 11.3-4) can be written as follows:

$$\begin{aligned} T_r \sin\theta_r + T_f \sin\theta_f + (m_c + m_d) g + (T_1 + T_2) \sin\alpha \\ = m_c a_c \sin \gamma + m_d a_d \sin \beta + N_r + N_f \end{aligned} \quad (11.3-5)$$

$$\begin{aligned}
 T_r \cos\theta_r - T_f \cos\theta_f + (T_1 + T_2) \cos\alpha + \mu(N_r + N_f) \\
 = m_c a_c \cos\gamma + m_d a_d \cos\beta
 \end{aligned}
 \tag{11.3-6}$$

An examination of the load time histories for the frontal and rear tiedown revealed that the frontal tiedown experienced a small load at the same time when the rear tiedown experienced its maximum load (at approximately 120 ms). The frontal tiedown is loaded because the tiedown attachment points above the chair CG create a moment and allows the chair to pitch. The frontal tiedown load is relatively low because the dummy slides forward on the seat of the chair and its weight is shifted to the front of seat during the FFF impact. Unfortunately, the relative influence of friction between the dummy and the chair could not be determined easily as the dummy was twisted uncertainly under dynamic conditions. The dummy-seat and wheel-floorboard interactions were modelled as the point contact in a multibody model. Further study will be focused on the bearing area contact characteristics using finite element seat and tyre models.

11.4 Energy Analysis of Tiedown Loads

The computer models suggested that the rear tiedown angles were significantly effect on tiedown and wheel loads. One of the most important design criteria for the tiedown systems is the determination of tiedown stiffness characteristics. The tiedown stiffness is related to the resulting amplification effect and it also determines the amount of the tiedown load. For a given mass to restrain, experiments showed that stiffer tiedown, such as, in the 45-degree rear tiedown angle configuration, were exposed to higher loads compared to more compliant tiedown in the 30-degree configuration. The following kinetic energy theory analysis offers the same explanation.

A given wheelchair system is restrained by 45-degree rear tiedown in one case (denoted subscript '45') and by 30-degree rear tiedown (denoted subscript '30'). The kinetic energy of the wheelchair is managed by the wheelchair tiedown system and the wheelchair itself. Writing in the form of an energy balance,

$$\mathbf{K} = \mathbf{K}_{\text{tiedown}} + \mathbf{K}_{\text{chair}} \quad (11.4-1)$$

The kinetic energy associated with the 45-degree is the same as the 30-degree if the identical chairs are travelling at the same velocity v_0 ,

$$\mathbf{K} = \frac{1}{2} m v_0^2 = \mathbf{K}_{45} = \mathbf{K}_{30} \quad (11.4-2)$$

Substituting (11.4-2) into (11.4-1)

$$(\mathbf{K}_{\text{tiedown}} + \mathbf{K}_{\text{chair}})_{45} = (\mathbf{K}_{\text{tiedown}} + \mathbf{K}_{\text{chair}})_{30} \quad (11.4-3)$$

Assuming identical chairs are used, the energy managed by the chair, $\mathbf{K}_{\text{chair}}$ is the same in the 45 and 30 cases, that is, $(\mathbf{K}_{\text{chair}})_{45} = (\mathbf{K}_{\text{chair}})_{30}$, therefore

$$(\mathbf{K}_{\text{tiedown}})_{45} = (\mathbf{K}_{\text{tiedown}})_{30} \quad (11.4-4)$$

The energy transferred to the tiedown is either dissipated through plastic deformation and frictional losses (\mathbf{K}_{diss}), or stored as potential energy (\mathbf{J}) due to elastic deformation of webbing belt:

$$\mathbf{K}_{\text{tiedown}} = \mathbf{K}_{\text{diss}} + \mathbf{J} \quad (11.4-5)$$

The more stiff the tiedown is, the less energy is dissipated and the more load it is subject to. That is,

$$(\mathbf{K}_{\text{diss}})_{45} < (\mathbf{K}_{\text{diss}})_{30} \quad (11.4-6)$$

For linear systems, the potential energy is equal to the square of the elongation of the spring (δ_s) times the spring stiffness (\mathbf{k}). Thus (11.4-4) can be written as:

$$(\mathbf{K}_{\text{diss}} + \frac{1}{2} \mathbf{k} \delta_s^2)_{45} = (\mathbf{K}_{\text{diss}} + \frac{1}{2} \mathbf{k} \delta_s^2)_{30} \quad (11.4-7)$$

The relationship given by (11.4-7) indicates that the potential energy associated with the 45-degree tiedown must be greater than the potential energy of the 30-degree tiedown, that is,

$$(\frac{1}{2} k \delta_s^2)_{45} > (\frac{1}{2} k \delta_s^2)_{30} \quad (11.4-8)$$

Hooke's Law for linear systems is given by $T = k\delta_s$. Substituting this expression into (11.4-8), it is proven that the force experienced by the 45-degree tiedown must be greater than the force experienced by the 30-degree, that is:

$$T_{45} > T_{30} \quad (11.4-9)$$

Depending on the duration of the crash event, the stiffness of tiedown system may lead to excess chair acceleration. This analysis indicates that the load in the tiedown system could be reduced if energy is dissipated by some mechanical geometry.

11.5 Rebound Characteristics in a Sled Simulation

The deformation of the chair backrest on dummy rebound allowed excessive rearward excursions. Although rebound is not addressed in the current standards, it appears that it can be a common mechanism for occupant injury and therefore should be addressed in the future. Figure 11.5a represents a sled mass-spring model. The d_r represents the sled rebound and is the deviation between d_1 and d_2 , that is,

$$d_r = (d_1 - d_2)$$

d_1 - the distance where the olives touch the tapered polyurethane tubes within spring deflection δ before impact;

d_2 - the distance where the olives stop inside the polyurethane tubes by the way of friction within δ after impact;

L - initial position of the sled before triggering;

L_r - final position of the sled after triggering.

S represents stop distance of the sled. It is the deviation between initial position and final position and also in account of the sled rebound, that is,

$$S = (L - L_r) + d_r$$

The points (1), (2), and (3) indicate three positions in the interval of motion. Point (1) is the initial position of the block of WTORS. Point (2) is the position of maximum deflection of the spring within the block at rest. Point (3) is the rest position of the block after rebound. The block mass M represents the total mass of WTORS and sled. The spring stiffness k represents contact stiffness between the polyurethane tube and the olive, which it is used to simulate the sled pulse. The v_1 is the initial velocity of sled. The following three elements are considered here:

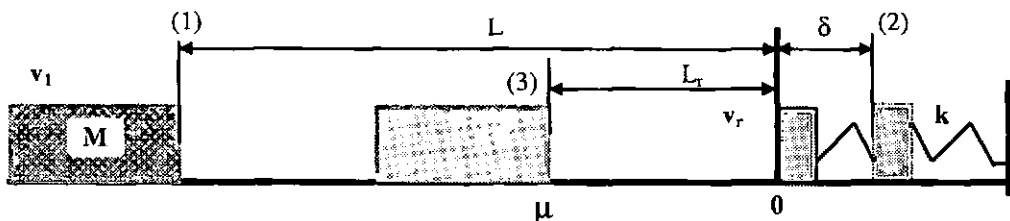


Figure 11.5a A sled mass-spring model

Element 1: the maximum value of the deflection of the spring, δ

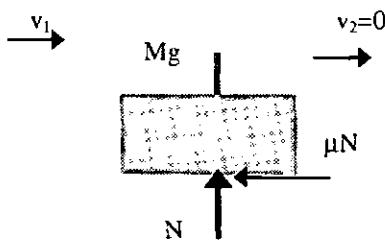


Figure 11.5b Loads from position 1 to 2

The energy terms at positions (1) and (2)

are:

$$K_1 = \frac{1}{2} M(v_1)^2 \quad K_2 = 0 \text{ (as } v_2 = 0 \text{),}$$

$$J_1 = 0, \quad J_2 = \frac{1}{2} k\delta^2$$

As shown in Figure 11.5b, the work

done between (1) and (2) is given by

$$W = -\mu \cdot N \cdot (L + \delta) \quad N = Mg$$

Using the work energy equation:

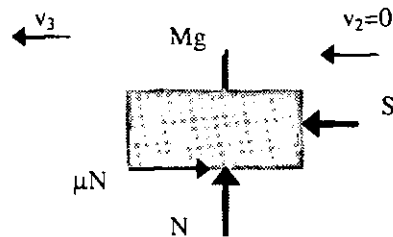
$$W = (K_2 - K_1) + (J_2 - J_1)$$

The positive root is used, and we get

$$\delta = \mu \cdot Mg/k + [(\mu \cdot Mg)^2 - k \cdot L(\mu \cdot M \cdot g) + kM(v_1)^2/2]^{1/2}/k \quad (11.5-1)$$

Formula (11.5-1) indicates that the maximum travel distance of the olive (δ) is the function of the total mass on the sled (M), stiffness of polyurethane tubes (k), the sled starting position (L), the sled initial velocity (v_1) and sled friction (μ). If the values of M , L , v_1 , and μ are constant, δ only depends on k , which could be determined by olive size and the type of tubes and surrounding temperature.

Element 2: the maximum travel of the sled after rebound, L_r



The energy terms at position 2 and 3 are

$$K_2 = 0 \text{ (as } v_2 = 0) \quad K_3 = \frac{1}{2} M(v_3)^2$$

$$J_2 = \frac{1}{2} k \delta^2 \quad J_3 = 0$$

Figure 11.5c Loads from position 2 to 3

As shown in Figure 11.5c, the work done between 2 and 3 is

$$W = -\mu \cdot N \cdot (L_r + \delta)$$

Using the work energy equation,

$$W = (K_3 - K_2) + (J_3 - J_2)$$

$$L_r = [k \cdot \delta^2 - M(v_3)^2]/2\mu Mg - \delta \quad (11.5-2)$$

If $L_\tau > L$ the sled comes to the rest to the left of its initial position.

Element 3: the rebound velocity v_r

Assuming of two masses, m_A is the mass of sled and m_B is the mass of spring. From impact conservation of momentum equation:

$$m_A \cdot (v_A)_1 + m_B \cdot (v_B)_1 = m_A \cdot (v_A)_2 + m_B \cdot (v_B)_2$$

As $(v_A)_2 = (v_B)_2 = v_r$, we get:

$$m_A \cdot (v_A)_1 + m_B \cdot (v_B)_1 = (m_A + m_B) \cdot v_r \quad (v_B)_1 = 0$$

$$v_r = m_A \cdot v_1 / (m_A + m_B) \quad (11.5-3)$$

As the spring mass is much small than the total mass on the sled ($m_B \ll m_A$), the v_r could be considered as equal to the v_1 , that is, the rebound velocity could be neglected.

CHAPTER 12: CONCLUSIONS AND FURTHER WORK

This research has been concerned with the effects to which the occupant of a wheelchair secured by a WTORS is subjected in a frontal impact. Both occupant Forward Facing Frontal (FFF) and Rearward Facing Frontal (RFF) impact configurations have been considered. Three tools have been employed in the research programme as follows:

- Accident investigation
- Experimental crash investigation using MURSEL test rig and sub-system test equipment at Middlesex University
- Mathematical models using PAFEC computerised Finite Element Analysis (FEA) model and two Crash Victim Simulation (CVS) programs: ATB/DYNAMAN and MADYMO3D.

12.1 Research Progresses

Details of research progress are described as follows:

- A review of fatal accident statistics has highlighted the desirability of investigating the impact performance of WTORS.
- It is the first comprehensive study of WTORS dynamic performance, which has confirmed the expected improvements in frontal impact performance, such as wheel loads, occupant shoulder load and bulkhead loads, etc.
- The crash performance of different types of wheelchairs has been summarised. Work has been conducted to investigate some of the parameters affecting injury potential to the occupant spine and shoulder.
- Three comprehensive research projects (TRL, ISO and Taxi) have been undertaken and the results in terms of chair wheel loads, occupant shoulder loads and bulkhead loads have been presented respectively in three international papers [1][2][3] and also contributed to the ISO working group. The paper of FEA model [4] was published in the book, Modern Practice in Stress and Vibration Analysis. The

application of finite element module in MADYMO3D to tyre model was presented in a paper [6].

- Work has commenced on the effect of side impact of Child Restraint System (CRS) by a CVS model using MADYMO3D package. The results have been presented in a paper [5]. This CRS model will be further extended to WTORS.
- The different anchorage configurations (B pillar and floor-mounted) in FFF impact have been firstly presented to make comparisons with the performance of the current systems. Analysis of the results suggested that despite significant improvements in many aspects, attention should be focused on the shoulder loading experienced by occupants in some types of L/D occupant restraint configurations.
- The new concept of taxi RFF impact of WTORS has been presented. The methodology of experimental and computer models have been designed by the author. It comprises the development of an improved wheelchair model to represent a variation of wheelchair structure, an FEA model of seat belt and a modelling of pneumatic wheelchair tyres.
- Experimental work has been carried out using both stiff and relatively flexible production wheelchairs both in FFF and RFF impacts. This work has been validated and supported by FEA model and CVS models.
- TNO-10 dummy database was developed using static test results and Hybrid II dummy database.
- One of the areas in which an improvement was achieved is a means of modelling of the contact and friction forces exerted between the ground and the pneumatic tyres. This has been conducted using non-linear spring tyre model. Another area for improvement was the modelling of belt restraint systems. This has been simulated by Finite Element (FE) belt mesh using MADYMO3D code.
- The velocity profile analysis helped to explain why the wheelchair and dummy experience acceleration amplification relative to the sled. Consideration of forces using the computer model showed why quasi-static analysis is insufficient in WTORS design. Energy principles were used to explain why steeper tiedown systems subject restraints to a more severe crash environment. Empirical observation of

kinematic response of WTORS was employed to explain why shoulder belt load at floor-mounted configuration exerts higher load than that at B pillar configuration.

The above research progresses have been made to help advance the field of WTORS simulation technology, so that one day, the disabled people in the vehicles can be guaranteed the same level of protection to the able-bodied occupant in the event of an accident.

12.2 Experimental Conclusions

A quantitative assessment of the test results was performed using a standard statistical analysis of maximum outputs for a given test series. A time history post-processor plotted outputs at discrete intervals over the course of the entire event. This qualitative assessment provides a better evaluation of repeatability because output parameter responses could agree in different levels and in certain time.

The test programme proved conclusively to replicate test results when using a full chair-dummy system. It should be noted that injury mechanism study has been only conducted in investigation of WTORS restraint injury using ATD resultant acceleration results and visual observations of impact tests. A comparative injury parameter Δa has been proposed and defined as the absolute values of the deviation between the peak resultant acceleration forces applied to the chest and head within 30 ms time period for a given input severity. It has been used to estimate the potential for a particular injury mechanism, and then to evaluate the design of wheelchair and its restraint systems. Further computer models will be used to validate this proposal.

The effect of the following five elements (including sled crash pulse) on the loads in WTORS evaluated both by experimental work and computer models, led to the following conclusions.

12.2.1 Wheelchair structure

- The surrogate wheelchair testing based on the TRL design indicated that the rear axle and front castors in the TRL surrogate wheelchair were insufficiently reinforced.
- Production wheelchairs were crash tested both in FFF and RFF impacts. They validated the surrogate system's ability to simulate the real crash dynamics. The

production wheelchair tests provided insight into possible modes of structural failure of the chair seat and backrest, which may cause injury to the occupant.

- Experimental tests indicated that the tyres in the wheelchairs were shown to have significant effect on WTORS crash performances.
- Analysis suggested that the wheelchair backrest material and structure should be improved to minimise occupant injury when the occupant rebounded during FFF impact. This could be satisfied by using an energy absorbing backrest during an impact. At present, no wheelchair designs satisfy this requirement. The higher hysteresis backrest model was developed to meet this requirement. A quasi-static sub-system test of the wheelchair backrest was conducted during the initial engineering phase.
- ISO test results indicated that the peak value of the total vertical load on the seat (seat sum load) in the ISO surrogate wheelchair (ISO-SWC) was 26.4 kN at crash severity of 51 km/h, 21g. It was expected to be considerably higher than those in the manual wheelchair (M-W/C). This suggested that the seat cushion in the M-W/C absorbed some energy from impact and reduced the peak seat loads.
- At a ΔV of 32 km/h and sled deceleration of 17g (crash severity Level IV) RFF impact, the maximum bulkhead load was recorded on impact as 75 kN in the ISO-SWC and 25.4 kN in the M-W/C. The increase in mass ratio of 4.5 from 15 kg to 83 kg, resulted in about double increase of bulkhead loads. Relatively large differences between ISO-SWC and M-W/C were found in the wheel loads (> 20 kN).
- The relatively large differences between a wheelchair without handles and one with handles were found in the chest resultant acceleration ($> 30g$) at the crash severity Level V of RFF impact.

12.2.2 Wheelchair tiedown systems

- The single rear tiedown load generated in the 45-degree rear tiedown configuration (3.7 kN at crash severity of 32 km/h, 18g) was higher than those in the 30-degree case, the maximum difference being 12 % of the 30-degree values.
- The geometry of restraint systems in TRL tests indicated that a single rear wheel load generated in the 45-degree case (9.5 kN at crash severity of 32 km/h, 18g) was

higher than that in 30-degree case, the maximum difference being 56 % of the 30-degree values.

12.2.3 Occupant

- TRL test results indicated that the single rear wheel load (12.4 kN at crash severity of 32 km/h, 20g) was greater than the frontal one (8.4 kN) in the WTS (without dummy). When the dummy was present (WTORS) the effect of mass transferred from the rear to the front partially reduced the rear wheel loads 23% at the same crash severity.
- Few ATD dummies existing today would give an appropriate response of spinal injury assessment in a crash test. Further Computer Interfaced Dummy (CID) mathematical models need to be developed with the sub-system tests, combined with geometry requirements in order to address different disabled occupant postures. The relative movements between adjacent vertebrae and in the occipital joint should be minimised. The curvature of the spine should change as little as possible during the impact.

12.2.4 Occupant restraint system

ISO test results indicated that the diagonal top strap anchorage configurations had a significant effect on the dummy's shoulder load, the values of the diagonal strap tensions, dummy movement and front wheel loads. All these values were measured at the time of peak T_1 load.

- At all values of sled velocity change the floor-mounted configuration exhibited a peak shoulder load greater than that for the B pillar configured system. At a crash severity of 34 km/h, 13g the value (6.14 kN) was higher by 96 %.

The floor-mounted diagonal top strap load (T_1) is 5.89 kN, the diagonal bottom strap load (T_2) is only about one third of T_1 , while in the B pillar case $T_2 = 1/2 T_1$, the total shoulder belt load ($T_1 + T_2$) is about same value (7.6 kN) both floor-mounted and B pillar configurations.

- At all values of sled velocity change, the floor-mounted configuration exhibited a maximum dummy head target excursion greater than that for the B pillar configured system. At a crash severity of 34 km/h, 13g the value of head excursion

(450 mm) was higher by 52%. This value was not reached by the B pillar system. At a crash severity of 27 km/h, 11g the value of the head excursion (392 mm) was higher by 44%.

The frontal wheel loads exhibited similar variations. The peak value was 4.7 kN (about double the value of B pillar system). It indicated that the mass was transferred to the front of the wheelchair in the floor mounted shoulder belt system as the maximum head target forward excursion was reached.

- In general the total peak load in the wheelchair seat for the floor-mounted configuration was 9.11 kN at a crash severity of 34 km/h, 13g, which was 19% smaller than that in B pillar configuration. The loading phase for the former acted over 25 ms longer period (145 ms) than the latter one.

Taking into account the implications of the above conclusions on the occupant and the wheelchair it is considered that the B pillar anchorage of the occupant diagonal strap is superior to the floor-mounted configuration.

- It is important to ensure there is adequate support for the wheelchair occupant's head and back. This means in practice that the headrest needs to be fixed on the bulkhead reaching at least a height of 1,200 mm from the taxi floorboard. At a ΔV of 32 km/h and sled deceleration of 20g (Level V) RFF impact, the maximum bulkhead load was recorded on impact of 28.5 kN without headrest and 25.4 kN with headrest, a tiedown load on rebound of 4.3 kN without headrest and 2.1 kN with headrest. The chest resultant acceleration (73g) at time (100 ms) is higher than the head value (50g). If the headrest was put on, the peak value of head acceleration was increased to about the same value of chest acceleration (75g), due to higher stiffness material characteristics used in the headrest. The relatively large difference between wheelchair with headrest and one without was found in the head resultant acceleration (> 20g).

- The webbing restraint device used in RFF impact has potential as it is simple, rapid to install and has very few risks of incorrect use. The enormous advantage of a webbing device is that it does not occupy too much space.

12.2.5 Sled crash pulses

- TRL test results indicated that for the crash severity 25 km/h, 7g (Level I) and 25 km/h, 10g (Level II) the front wheel loads (2.6 kN and 5.6 kN) were less than those at the rear ones (9.4 kN and 12.8 kN). However, when sled deceleration increased to Level III (32 km/h, 18g), the test results suggested that dummy mass transferred to the frontal wheelchair, relatively increased the frontal wheel loads 278% to about the same value of rear wheel load (10.8 kN).
- It can be seen from ISO test results that the wheelchair seat loads varied considerably as a function of crash pulse. From the crash severity of 34 km/h, 13g to 51 km/h, 21g the total vertical load on the seat increased 47% to 26.4 kN, and more load occurred in the frontal seat than the rear.

12.3 Mathematical Model Conclusions

The FEA and CVS models provided an efficient tool for the investigation of the impact properties in a WTORS presented in this thesis.

- FEA model conclusions

- The value solutions, such as, CG, MOI and loading positions, can be estimated from this model to investigate different parameter effect on the wheelchair structure.
- The interconnection between the FEA program and CVS multibody system within MADYMO environment was achieved using support and contact conditions.

- CVS model conclusions

The simulation produced by DYNAMAN compared reasonably well to the actual test results from the full-scale sled tests providing some correlation had been conducted. It is difficult to produce a simulation true to life because of the limitation of this software. The wheelchair-occupant model using MADYMO3D program proved to be a good estimator of actual experimental results. The model was utilised to study the relative effects of crash pulse differences on the variability of maximum responses. It was found that crash pulse variations account for much of the overall variation in loads and deceleration, while having only a negligible influence on maximum excursions.

- The CVS modelling of the TRL wheelchair considered eleven (11) anchorage locations for shoulder belt restraint in the FFF impact. The optimum position was shown to be 17-degree above the occupant shoulder level which is lower the current typical B pillar position.
- The CVS models generated higher loads than those generated in the sled tests, except in the case of the resultant chest acceleration although CVS model replicated the bouncing behaviour of the ISO-SWC. It can be expected by rigid multibody model used. The increase of diagonal top strap tension (T_1) is in the order of 14% of the experimental value. The maximum chest x-component acceleration difference between WTORS model and sled experimental results was 31% smaller using DYNAMAN and 15% smaller using MADYMO.
- One effect that has so far been neglected is the belt slippage because of anchorage deformation and TRL surrogate wheelchair axle bending during impact. This effect is a non-linear effect that could not be avoided. It is rather awkward to handle using CVS multibody models and it will be further simulated using explicit finite element models.
- The major limitations of the CVS technique come by the lack of explicit structural models although some finite element modules are available in MADYMO3D. The wheelchair structure presented in CVS model here was effectively modelled as a rigid structure. In reality the production wheelchair was susceptible to both elastic and plastic deformation. The finite element model of the wheelchair and occupant restraint system will be coupled with CVS model in the future.

12.4 Further Work

The computer modelling and validation process are not completed although research projects have been successfully accomplished. The current model is being refined. The objective of WTORS model development is to design the methodology to simulate WTORS impact. The next step of this study is to proceed with a systematic investigation by varying the different parameters, which are included in the model, and then to exhibit the structure design objectives. WTORS researches need to be continued in the following areas:

- ***Children with disabilities***

Currently there are no requirements in UK legislation for the performance of occupant restraints for children with disabilities. What does exist is a Code of Practice: the safety of passengers in wheelchairs on buses (VSE 87/1). It is recognised that some systems for children with disabilities might comply with more stringent requirements.

- ***Computer modelling technique development***

An important future application of CVS technique will be in the development computer modelling of the RFF impact protection as there are specific injury risks associated with this impact crash. Another application of CVS technique will be in the development of different restraint systems, such as head restraint and airbag. The explicit FEA modelling of the wheelchair seat and backrest need to be developed to interconnect with CVS models. Belt slippage will also be modelled using the explicit FEA method. A biomechanical simulation of an occupant will be developed with a segmented spine simulation of human-like motion to ensure that the design characteristics result in benefits to reduce risk of spinal injury.

- ***Optimisation technique development***

The technique of optimising occupant protection will be used in WTORS model. The injury assessment functions will be improved to assess the risk of injury from impacts, especially for spinal injury. Some new injury parameters will be further investigated. The bearing area contact algorithm will be optimised to meet the requirements of occupant safety. This will be conducted by experimental work in association with commercial industry.

- ***Wheelchair occupant injury database and wheelchair crash impact database***

The wheelchair occupant injury database will be created using different sources, such as wheelchair and minibus manufacturers, police accident reports, insurance company reports, hospital injury reports, questionnaire to wheelchair users, crash test data, etc.

The wheelchair crash impact database will be further developed using computer models and industry impact test results.

REFERENCES

Accident Investigation Manual Vol. 1&2 (1986), *Department of Transport*, Marsham Street, London Distributed by ROSPA, Published by Crown.

Adams T.C. (1994), The Application and Safety of Securements and restraints for Wheelchair Seated Travellers on Public Transit Vehicles. *Proc. of International Research Conference on the Biomechanics of Impact (IRCOBI)*, pp193-204.

American Society for Testing and Materials (ASTM, Practice E691-92, 1992), Standard Practice for Conducting an Interlaboratory Study to Determine the Precision of a Test Method. *ASTM Standard, Lancaster, PA.*

ATB Occupant Simulation Input Data Manual V4.2, May 1990.

Australian Standard (AS2942)(1987), Wheelchair Occupant Restraint Assemblies for Motor Vehicles, *Standards Association of Australia, Sydney.*

Backaitis S. and Enserink E. (1977), Repeatability of Setup and Stability of Anthropomorphic Landmarks and Their Influence on Impact Response of Automotive Crash Test Dummies. *International Automotive Engineering Congress and Exposition*, SAE Paper No. 770260.

Bandstra R. et al. (1998), Seat-Belt Injuries in Medical and Statistical Perspectives. *Proc. 16th International Technical Conference on Experimental Safety Vehicles*, Windsor, ESV Paper No. 98-S6-W-25, pp1347-1359.

Beer G. (1985), An Isoparametric Joint/Interface Element for Finite Element Analysis. *International Journal for Numerical Methods in Engineering*, Vol 21, pp585-600.

Bendjellal F. et al (1998), The Combination of a New Air Bag Technology With a Belt Load Limiter. *Proc 16th International Technical Conference on Experimental Safety Vehicles*, Windsor, ESV Paper No. 98-S5-O-14, pp1092-1102.

Benson J., Schneider L.(1984), Improving the Crashworthiness of Restraints for Handicapped Children. *International Automotive Engineering Congress and Exposition*, SAE Paper No. 840528.

Berg F. A. et al (1996), Crash Tests using Passenger Cars Fitted with Airbags and a Simulated Out-Of-Position Passenger. *Proc. of International IRCOBI Conference on The Biomechanics of Impact*, pp291-302.

Bigi D. et al (1998), A Comparison Study of Active Head Restraints for Neck Protection in Rear-End Collisions. *Proc 16th International Technical Conference on Experimental Safety Vehicles*, Windsor, ESV Paper No. 98-S5-O-15, pp1103-1110.

British Standards Institution (BS3254, 1960, revised 1968), Specification for seat belt assemblies for motor vehicles.

Burger H. et al (1998), Development of a New Crash Cushion for the Protection of People in Wheelchairs in a Road Accident. *Proc 16th International Technical Conference on Experimental Safety Vehicles*, Windsor, ESV Paper No. 98-S5-W-25, pp1147-1162.

Canada Transport (1998), Airbag Deactivation, *Road safety and Motor Vehicle Regulation Directorate, Transport Canada*, Cat. No: T46-25/1998E

Canadian Standards Association (Draft. CAN/CSA-Z604, 1992), Mobility Aid Securement and Occupant Restraint (MASOR) Systems for Motor Vehicles.

Carlsson G., et al (1985), Biomechanical Considerations to Improve Head Restraints, *International IRCOBI Conference on The Biomechanics of Impact*, pp277-290.

Chou C.C. and Nyquist G.W. (1974), Analytical Studies of the Head Injury Criterion (HIC). *International Automotive Engineering Congress and Exposition*, SAE Paper No. 740082.

Code of Practice and Special Provisions for the Carriage of Passengers in Wheelchairs on Public Service Vehicles (Publication VSE 518, May 1982), *Department of Transport, Vehicle Standards and Engineering Division*.

Coo de P.J.A. et al (1991), Simulation Model for Vehicle Performance Improvement in Lateral Collisions. *Proc 13th International Technical Conference on Experimental Safety Vehicles*, Section 3, pp663-668.

Cullen E. et al (1996), Head Restraint Positioning and Occupant Safety in Rear Impacts: the Case for Smart Restraints. *Proc. of International IRCOBI Conference on The Biomechanics of Impact*, pp137-152.

David C. V. (1980). Influence of Initial Length of Lap-Shoulder Belt on Occupant Dynamics- A Comparison of Sled Testing and MVMA-2D Modelling. *24th STAPP Car Crash Conference Proceedings*, Paper No. 801309, pp375-415.

Deng Y.C. (1988), Design Considerations for Occupant Protection in Side Impact - A Modelling Approach. *32nd STAPP Car Crash Conference Proceedings*, Paper No. 881713, pp71-80.

Deng Y.C. (1992), Development of a Submarining Model in the CAL3D Program. *36th STAPP Car Crash Conference Proceedings*, Paper No. 922530, pp273-281.

- Deng Y.C., Ng Peter (1993), Simulation of Vehicle Structure and Occupant Response in Side Impact. *37th STAPP Car Crash Conference Proceedings*, Paper No. 933125, pp175-184.
- Dieu F. et al. (1994), Computer Simulation Model for Side Impact Analysis. *Proc 14th International Technical Conference on Experimental Safety Vehicles*, Germany, ESV Paper No. 94-S6-O-10, pp999-1007.
- Digges K. H. (1994). Modelling Wheelchair/Tie Downs with Wheel Stiffness Variations, *Interim Report, University of Pittsburgh*.
- Dorn M., Roy AP, Lowne RW (1991), Parameters affecting the Performance of Framed Child Seats. *Proc 13th International Technical Conference on Experimental Safety Vehicles*, ESV Paper No. S9-W-38, pp1206-1213.
- Dorn M (1992), MADYMO used in an Investigation of the Parameters which affect the Dynamic Performance of Automotive Framed Child Restraints. *3rd International MADYMO Users Meeting*, pp73-84.
- Dorn M (1994), The Optimisation of Framed Child Seats. *Ph.D. Thesis, RSEL, Middlesex University*.
- EASi-MAD V1.64 (1996), User Manual.
- EASi-CRASH MAD V2.1 (1998), User Manual.
- ECE R16 (1994), Uniform Provisions Concerning the Approval of Safety Belts and Restraint Systems for Adult Occupants of Power Driven Vehicles.
- ECE R16 Addendum 15 (1990), Agreement Concerning the Adoption of Uniform Conditions of Approval and Reciprocal Recognition of Approval for Motor Vehicle Equipment and Parts. *done at Geneva on 20 March 1958. E/ECE/324*.
- ECE R44 (1994), Uniform Provisions Concerning the Approval of Restraining Devices for Child Occupants of Power-Driven Vehicles (Child Restraint System)
- Edward D. and Hamson M. (1996), Mathematical Modelling Skills. *Macmillan College Work Out Series, published by Macmillan Press Ltd*.
- Esping B. J. (1985), A CAD Approach to the Minimum Weight Design Problem. *International Journal for Numerical Methods in Engineering*, Vol 21, pp1049-1066.
- Foret-Bruno J.Y., et al (1991), Influence of the Seat and Head Rest Stiffness on the Risk of Cervical Injuries in Rear Impact. *Proc 13th International Technical Conference on Experimental Safety Vehicles*, ESV Paper No. S8-W-18, pp956-967.

- Foster J.K., Kortge J.O. and Wolanin M.J. (1977), Hybrid III - A Biomechanically-Based Crash Test Dummy. *21st STAPP Car Crash Conference Proceedings*, Paper No. 770938, pp973-1013.
- Fountain M. et al (1996), Hybrid Modelling of Crash Dummies for Numerical Simulation. *Proc. of International IRCOBI Conference on The Biomechanics of Impact*, pp401-420.
- Giess M. and Tomas J. (1998), Improving Safety in Frontal Collisions by Changing the Shape of Structural Components. *Proc 16th International Technical Conference on Experimental Safety Vehicles*, Windsor, ESV Paper No. 98-S1-O-07, pp222-228.
- Gilkey J.C. (1983), Compliance Testing to the New dynamic Standard for Child Restraint Systems. *Society of Automotive Engineers, Inc., Warrendale, PA*. SAE Paper No. 831660, pp137-141.
- Grew N. (1985), Applying Computer Techniques in the Design and Development of an Occupant Restraint System. *Proc.10th International Technical Conference on Experimental Safety Vehicles, Section 4*, pp436-447.
- Gregg D.J., Roy P. (1983), Road Safety Development at Middlesex Polytechnic 1964-1983. *Compendium of Technical Papers, 53rd Annual Meeting, Institute of Transportation Engineers (USA)*, pp108-112.
- Gruber K., et al (1991), Computer Simulation of Side Impact Using Different Mobile Barriers. *International Automotive Engineering Congress and Exposition*. SAE Paper No. 910323.
- Gu J., Roy P. (1994), Application of ATB/CVS Program to Wheelchair Tiedown Occupant Restraint System. *Interim Report (MURSEL)*.
- Gu J., Roy P. (1995), Dynamic Impact Testing and ATB/CVS Modelling of WTRS/WTORS. on behalf of *Department of Transport*, Report No. RSEL 14/172/175.
- Gu J., Roy A.P. (1995), Current Research to Evaluate the Performance of Wheelchairs in Frontal Impacts (Evaluation of Floor Reaction Forces). *Proc 23rd Transport Forum, University of Warwick*, PTRC (0 86050 285 6), pp139-154.
- Gu J., Roy A.P. (1996), Optimisation of Wheelchair Tiedown and Occupant Restraint System (Effect of Diagonal Strap Anchorage Configurations on Occupant Restraint System). *Proc. 15th International Technical Conference on the Enhanced Safety of Vehicles (ESV), Melbourne, Australia*. ESV Paper No. 96-S1-W-21, pp242-250.

- Gu J., Roy A.P. (1997), The Crash Performance of a Rear Facing Wheelchair-Occupant System in Frontal Impact. *Proc. 1st European MADYMO Users' Meeting, Heidelberg*.
- Gu J. (1997), Finite Element Analysis of Wheelchair Structure. *Proc. 3rd International Conference on Modern Practice in Stress and Vibration Analysis*, Dublin, Ireland, pp517-522.
- Gu J., Roy A.P. (1998), Computer Simulation of a Procedure to Assess the Crash Performance of a Child Restraint System (CRS) in Side Impact. *Proc. 2nd International MADYMO Users' Meeting, Windsor, Canada*, pp67-76.
- Haland Y., Nilson G. (1991), Seat Belt Pretensioners to Avoid the Risk of Submarining: A Study of Lap-Belt Slippage Factors. *Proc. 13th International Technical Conference on Experimental Safety Vehicles*, ESV Paper No. 91-S9-O-10, pp1060-1068.
- Harrigan T.P. and Harris W.H. (1991), a Three-Dimensional Non-Linear Finite Element Study of the Effect of Cement-Prosthesis Debonding in Cemented Femoral Total Hip Components. *J. Biomechanics Vol. 24, No. 11*, pp1047-1058.
- Hobatho M. C. et al (1991), Development of a Three-Dimensional Finite Element Model of a Human Tibia Using Experimental Model Analysis. *J. Biomechanics Vol. 24, No. 6*, pp371-383.
- Hobbs C.A. et al (1987), Progress Towards Improving Car Occupant Protection in Frontal Impacts. *Proc. 11th International Technical Conference on the Enhanced Safety of Vehicles (ESV)*, pp582-590.
- Hoffmann R. et al (1990), Finite Element Analysis of Occupant Restraint System Interaction with PAM-CRASH. *34th STAPP Car Crash Conference Proceedings*, Paper No. 902325, pp289-300.
- Huelke D. F. and Moore J. L. (1993), Field Investigations of the Performance of Air Bag Deployments in Frontal Collisions. *Accid. Anal. And Prev. Vol.25, No.6*, pp717-730.
- Hultman R.W., Laske T.G., Lim G.G., Chrobak E. I., Vecchio M. T., and Chou C.C. (1991), NHTSA Passenger Car Side Impact Dynamic Test Procedure - Test-to-Test Variability Estimates. *International Automotive Engineering Congress and Exposition*. SAE Paper No. 910603.
- ISO/CD 10542-1: 1994E, 1995E, and 1996, Wheelchairs Tiedown and Occupant Restraint Systems for Motor Vehicles.

ISO/CD 10542-2: 1994E, 1995E, and 1996, Wheelchair Tiedown and Occupant Restraint Systems for Motor Vehicles - Particular Requirements for Strap Systems.

ISO WD 7176/19 (1995), Wheelchair- Wheeled Mobility Devices for Use in Motor Vehicles- Requirements and Test Methods.

Igarashi M. and Nagai K. (1991), Various Aspects on Crashworthiness Calculations, *13rd International Technical Conference on Experimental Safety Vehicles*, ESV Paper No. 91-S1-W-25, pp181-188.

Jawad S. (1998), Compatibility Study in Frontal Collisions - Mass and Stiffness Ratio. *Proc 16th International Technical Conference on Experimental Safety Vehicles*, Windsor, ESV Paper No. 98-S1-O-14, pp269-274.

Kallieris D. et al (1981), Behaviour and Responsc of Wheelchair, Passenger and Restraint Systems Used in Buses During Impact. *25th STAPP Car Crash Conference Proceedings*, Paper No. 811018, pp613-650.

Kendall D. (1991), The Development of a Computer Program to Enhance the Fit of Seat Belts. *Proc. 13th International Technical Conference on Experimental Safety Vehicles*, ESV Paper No. 91-S9-O-25, pp1147-1151.

Khalil T.B. et al (1991), Finite Element Simulation of Airbag Deployment and Interactions with an Occupant Model Using DYNA3D. *Proc. 13th International Technical Conference on Experimental Safety Vehicles*, ESV Paper No. 91-S9-O-18, pp1103-1113.

King A. et al (1996), A Mathematical Model to Determine Design Parameters that Cause Wheelchair Instability. *Proc. of the 12th International Conference on CAD/CAM Robotics and Factories of the Future*, pp763-768.

Klopp G. S. et al (1997), Risk of Ankle Injury for Humans from Longitudinal Impacts to the Foot. *Proc. of International IRCOBI Conference on The Biomechanics of Impact*, pp73-86.

Kooi J., Janssen E.G. (1988), Safety of Wheelchair Occupants in Road Transport. *Journal of Rehabilitation Sciences*, 1:3, pp167-179.

Kroonenberg A. et al (1997), A Human Model for Low-Severity Rear-Impacts. *Proc. of International Research Conference on the Biomechanics of Impact (IRCOBI)*, pp117-132.

Lakshminarayan V. and Lasry D. (1991), Finite Element Simulation of Driver Folded Air Bag Deployment. *35th STAPP Car Crash Conference Proceedings*, Paper No. 912904, pp227-236

Lawson A.R. et al (1998), Finite Element Modelling of Blunt or Non-Contact Head Injuries. *Proc 16th International Technical Conference on Experimental Safety Vehicles*, Windsor, ESV Paper No. 98-S9-P-26, pp2080-2092.

Lowne R. et al (1984), The Effect of the UK Seat Belt Legislation on Restraint Usage by Children. *28th STAPP Car Crash Conference Proceedings*. Paper No. 840526, pp369-380.

Lowne R. Gloyns P F and Roy P (1987), Fatal Injuries to Restrained Children 0-4 years in Great Britain 1972-86. *Proc. 11th International Conference on Safety Vehicles Washington*, pp227-237.

Lovsund P. et al (1988), Neck Injuries in Rear End Collisions among Front and Rear Seat Occupants, *International IRCOBI Conference on the Biomechanics of Impact*. Paper No. 1988-13-0021.

Lundell B. (1984), Dynamic Response of a Belted Dummy - A Computer Analysis of Crash Pulse Variation. *International Automotive Engineering Congress and Exposition*. SAE Paper No. 840401.

Lundell B. et al (1998), The Whips seat- a Car Seat for Improved Protection Against Neck Injuries in Rear End Impacts. *Proc. 16th International Technical Conference on Experimental Safety Vehicles*, ESV Paper No. 98-S7-O-08, pp1586-1596.

Lupker H.A., et al (1991), Advances in the MADYMO Crash Simulations. *International Congress and Exposition*, SAE Paper No. 910879.

Lupker H.A., Helleman H.B., Fraterman E., Wismans J. (1991), The MADYMO Finite Element Airbag Model. *Proc. 13rd International Technical Conference on Experimental Safety Vehicles*, ESV Paper No. 91-S9-O-23, pp1139-1146.

Mackay M. (1994), Engineering in Accident: Vehicle Design and Injuries. *Injury*, Vol.25, pp615-621.

MADYMO V5.11 (1995), User Manual

MADYMOV5.2 (1996), User Manual

MADYMO V5.2.1 (1997), User Manual

MADYMO V5.3 (1998), User Manual

Makino K. et al (1998), A Simulation Study on the Major Factors in Compatibility. *Proc 16th International Technical Conference on Experimental Safety Vehicles*, Windsor, ESV Paper No. 98-S3-O-03, pp662-666.

- Margulies S.S. et al (1992), A Proposed Tolerance Criterion for Diffuse Axonal Injury in Man. *J. Biomechanics Vol. 25, No. 8*, pp917-923.
- Marous J. et al (1998), Development of a Non-fragible Pedestrian Legform Impactor. *Proc 16th International Technical Conference on Experimental Safety Vehicles, Windsor, ESV Paper No. 98-S10-O-06*, pp2168-2176.
- Matsui S. (1976), A Method of Estimating the Crashworthiness of Body Construction. *Proc. 6th International Technical Conference on Experimental Safety Vehicles*, pp302-309.
- Matsumoto H., Sakakida M. and Kurimoto K. (1990), A Parametric Evaluation of Vehicle Crash Performance. *International Automotive Engineering Congress and Exposition, SAE Paper No. 900465*.
- Maupas A., et al. (1996), Safety of Wheelchair Users in Public Transport Buses, *INRETS, National Institute for Transport Research and Safety, LBSU Report No. 9602*.
- McHenry R.R. (1963), Analysis of the Dynamics of Automobile Passenger-Restraint Systems, *7th STAPP Car Crash Conference Proceedings*, pp207-249.
- Melvin J. W. (1978), Protection of Child Occupants in Automobile Crashes, *International Automotive Engineering Congress and Exposition. SAE Paper No. 780904*, pp673-687.
- Melvin J. W. (1979), Human Neck Injury Tolerance. *International Automotive Engineering Congress and Exposition. SAE Paper No. 790136*.
- Mertz H.J. & Patrick L.M. (1967), Investigation of the Kinematics and Kinetics of Whiplash. *11th STAPP Car Crash Conference Proceedings*, Paper No. 670919, pp267-317.
- Midoun D. E. et al (1991), Dummy Models for Crash Simulation in Finite Element Programs. *35th STAPP Car Crash Conference Proceedings*, Paper No. 912912, pp351-368.
- Millbrook report (1999), ISO 7176/19 Wheelchair and Occupant Restraint System. *Millbrook DETR Mavis Mobility Unit*, Report No. 990015.
- Minton R. et al (1998), Lower Back and Neck Strain Injuries: the Relative Roles of Seat Adjustment and Vehicle/Seat Design. *Proc 16th International Technical Conference on Experimental Safety Vehicles, Windsor, ESV Paper No. 98-S6-W-29*, pp1377-1390.
- Mobility Unit, Department of Transport, UK, 1995-96 Overview.

Myers B. S. et al (1997), The Dynamics of Head and Neck Impact and its role in injury prevention and the complex presentation of cervical spine injury. *Proc. of International IRCOBI Conference on The Biomechanics of Impact*, pp15-33.

Myklebust J. et al (1983), Experimental Spinal Trauma Studies in the Human and Monkey Cadaver. *27th STAPP Car Crash Conference Proceedings*, Paper No. 831614, pp149-162.

National Highway Traffic Safety Administration (NHTSA). National Safety Facts 1992. U. S. *Department of Transportation, Washington, D.C.*

Nambu T. et al (1991), Deformation of the Distal Femur: A Contribution Towards the Pathogenesis of Osteochondrosis Dissecans in the Knee Joint. *Journal of Biomechanics, Vol24, No.6*, pp421-433.

Neilson I. D. (1967), Research at the Road Research Laboratory into the Protection of Car Occupant. *10th STAPP Car Crash Conference Proceedings*, Paper No. 670920, pp319 - 336.

Nieboer J. J. et al (1988), Status of the MADYMO 2D Airbag Model. *32nd STAPP Car Crash Conference Proceedings*, Paper No. 881729, pp223-236.

Nieboer J.J., et al. (1991), Computer Simulation of Motorcycle Airbag System. *Proc 13th International Technical Conference on Experimental Safety Vehicles*, ESV Paper No. 91-S3-O-02, pp268-273.

Nitsche S. et al (1996), Validation of a Finite Element Model of the Human Neck. *Proc. of International IRCOBI Conference on The Biomechanics of Impact*, pp107-122.

Oh S. I. (1982), Finite Element Analysis of Metal Forming Processes with Arbitrarily Shaped Dies. *J. Mech. Sci. Vol. 24, No.8*, pp479-493.

Orme D., Barak E., Fisch R.F. (1976), Design, Test and Development of A Wheelchair Restraint System for Use in Buses. *20th STAPP Car Crash Conference Proceedings*, Paper No. 760809, pp271-301.

PAFEC 75 (1978), Data Preparation.

PAFEC 7.4 (1992), User Manual

Paton I. P. et al (1998), Development of a Sled Side Impact Test for Child Restraint System. *Proc 16th International Technical Conference on Experimental Safety Vehicles*, Windsor, ESV Paper No. 98-S10-O-09, pp2179-2184.

- Petty S.P.F. (1985), The Safe Transportation of Wheelchair Occupants in the United Kingdom. *Proc. 10th International Technical Conference on Experimental Safety Vehicles*, Section 4, pp488-491.
- Pezall J. (1991), Wheelchair and Occupant Restraint Systems for Use in Buses. *Proc 13th International Technical Conference on Experimental Safety Vehicles*, ESV Paper No. 91-S3-W-20.
- Petzall J and Olsson A.(1995), Wheelchair Tie-downs and Occupant Restraint Systems for Use in Motor Vehicles. *Proc 7th International Conference on Mobility and Transport for Elderly and Disabled People*, Reading, pp130-137.
- Prasad P. (1985), Comparative Evaluation of the MVMA2D and MADYMO2D Occupant Simulation Models with MADYMO-Test Comparisons. *Proc. 10th International Technical Conference on Experimental Safety Vehicles*, Section 4, pp480-487.
- Red E., Hale K., McDermott M., and Mooring B. (1982), Wheelchair Restraint Systems, Dynamic Test Results and the Development of Standards. *26th STAPP Car Crash Conference Proceedings*, Paper No. 821161, pp269-290.
- Road Accident Great Britain (RAGB): The Casualty Report, *A publish of the goverment statistical service, Department of Transport*.
- Robbins D. H. (1970), Three-Dimensional Simulation of Advanced Automotive Restraint Systems. *International Automotive Safety Conference*, SAE Paper No. 700421.
- Roy A.P., Gregg D.J. (1985), Child Restraint Development and Usage 1962-1985 *Compendium of Technical Papers, 55th Annual meeting Institute of Transportation Engineers (USA)*, pp108-112.
- Roy P. (1990), Evaluation of the Performance of Wheelchair Tiedowns and Occupant Restraints when subjected to Impacts Simulating Large Bus, Transit and Small Van Crash Pulses (Phase 1). *Road Safety Engineering Laboratory*, Middlesex University, London.
- Roy A.P., Roberts AK (1994), The Frontal Impact Performance of a Sample of Current UK Child Restraint Systems When Mounted in Car Body Shells. *Proc. 14th International Technical Conference on the Enhanced Safety of Vehicles*, ESV Paper No. S10-W-12, pp1668-1678.
- Roy A.P., Stait E. (1995), Development of ISO Standards for the Safe Transport of Wheelchair Occupants. *Proc. of 7th International Conference on Mobility and Transport for Elderly and Disabled People*, Reading, pp121-129.

- Ruckert J. and Lasry D.(1992), A Finite Element Model of the EUROSID Dummy. *36th STAPP Car Crash Conference Proceedings*, Paper No. 922528, pp255-260.
- Scavnicky M. J. (1994), Dynamic Wheelchair Testing and the Development of a Compliance Test for Wheelchair Tiedown and Occupant Restraint System. *University of Virginia, Interim Report*.
- Schneider, L.W., McIvin, J.W., and Cooney C. E. (1979), Impact Sled Test Evaluation of Restraint Systems Used in Transportation of Handicapped Children. *International Automotive Engineering Congress and Exposition*, SAE Paper No. 790074.
- Shams T. (1991), Enhanced Airbag Model for the ATB Program. *Proc. 13th International Technical Conference on Experimental Safety Vehicles*, ESV Paper No. S9-O-16, pp1098-1103.
- Shaw G. et al (UVA), Schneider L.W. (UMTRI), Roy A.P. (MURSEL)(1994), Interlaboratory Study of Proposed Compliance Test Protocol for Wheelchair Tiedown and Occupant Restraint Systems. *38th STAPP Car Crash Conference Proceedings*, Paper No. 942229, pp355-370.
- Simpson D. A. et al (1991), Brain Injuries in Car Occupants: a Correlation of Impact Data with Neuropathological Finds. *Proc. of International IRCOBI Conference on The Biomechanics of Impact*, pp89-100.
- Society of Automotive Engineers, Inc. (SAE). Dynamic Test Procedure - Type 1 and Type 2 Seat Belt Assemblies. *SAE Recommended Practice J117 JAN70*. SAE Handbook Vol.4, 33.04, Warrendale, PA, 1987.
- Society of Automotive Engineers, Inc. (SAE). Instrumentation for Impact Tests. *SAE Recommended Practice J211 JUN80*. SAE Handbook Vol.4, 34.156, Warrendale, PA, 1987.
- Society of Automotive Engineers, Inc. (SAE). Wheelchair Tiedowns and Occupant Restraint Systems for Use in Motor Vehicles. *SAE Working Document as of 3/8/94* Warrendale, PA, 1994.
- Song D. et al (1993), Finite element Simulation of the Occupant/Belt Interaction: Chest and Pelvis Deformation, Belt Sliding and Submarining. *37th STAPP Car Crash Conference Proceedings*, Paper No. 933108, pp13-34.
- Song D. et al (1996), Modelling and Analysis of Interactions Between Occupant, Seatback and Headrest in Rear Impact. *Proc. of International IRCOBI Conference on The Biomechanics of Impact*, pp165-185.

Standards Association of Australia (AS 2942, 1987), Wheelchair Occupant Restraint Assemblies for Motor Vehicles. *The Standards Association of Australia, North Sydney, N.S.W.*

Surrogate Wheelchair Preparation, Fabrication and Assembly Manual (1994), *University of Virginia, Transportation Rehabilitation Engineering Centre.*

Trosseille X. et al (1992), Development of a F.E.M. of the Human Head According to Specific Test Protocol. *36th STAPP Car Crash Conference Proceedings*, Paper No. 922527, pp235-254.

Turbell T. and Aldman B. (1983), A Global Approach to Child Restraint Systems. *26th STAPP Car Crash Conference Proceedings*, Paper No. 831605, pp61-67.

Von K.M. et al (1995), Soft Tissue Injury of the Cervical Spine in Rear-End and Frontal Car Collisions. *International IRCOBI Conference on The Biomechanics of Impact*, pp273-282.

VSE 87/1, 1987, Code of Practice - The Safety of Passengers in Wheelchairs on Buses, DTP, London, May 1987.

Walz F.H., Muser M.H. (1995), Biomechanical Aspects of Cervical Spine Injuries. *Transactions Journal of Passenger Cars, Section 6 - Part 1*. SAE Paper No. 950658. pp1257-1263.

Willinger R. et al (1996), Experimental and Theoretical Modelling of Head Impact - Influence of Head Modelling. *Proc. of International IRCOBI Conference on The Biomechanics of Impact*, pp21-34.

Wismans J., et al (1979), Child Restraint Evaluation by Experimental and Mathematical Simulation. *23rd STAPP Car Crash Conference Proceedings*, Paper No. 791017, pp381-416.

Wismans J., Hoen T. and Wittebrood (1985), Status of the MADYMO Crash Victim Simulation Package 1985. *Proc. 10th International Conference on Experimental Safety Vehicles*, Section 4, pp784-794.

Wismans J., Griffioen J. A. (1988), MADYMO Crash Victims Simulations. *AGARD 66th meeting of the structures and material panels*, Specialists meeting on energy absorption of aircraft structures as an aspect of crash worthiness, Luxembourg.

Witteman W. et al (1998), Modelling of a Unique Frontal Car Structure: Comparable Deceleration Curves at Full Overlap, 40 Percent Offset and 30 Degrees Collisions. *Proc. 16th International Technical Conference on Experimental Safety Vehicles*, ESV Paper No. 98-S1-O-04, pp194-212.

Wykes N. J. (1998), Compatibility Requirements for Cars in Frontal and Side Impact. *Proc 16th International Technical Conference on Experimental Safety Vehicles*, ESV Paper No. 98-S3-O-04, pp667-681.

Wynsberghe D.V. et al (1995), *Human Anatomy & Physiology* (3rd Edition). McGraw-Hill, Inc.

Yang K. H. et al (1992), Finite Element Modelling of Hybrid III Head-Neck Complex. *36th STAPP Car Crash Conference Proceedings*, Paper No. 922526, pp219-235.

Yang J.K. et al (1996), Finite Element Model of the Human Lower Extremity Skeleton System in a Lateral Impact. *Proc. of International IRCOBI Conference on The Biomechanics of Impact*, pp377-390.

Appendix 1A: ISO Standards for WTORS

A Committee Draft standard, ISO/CD 10542-1, has been produced by the International Standards Organisation (ISO) for Wheelchairs Tiedown and Occupant Restraint Systems (WTORS). The crash pulse in this standard, based on that of the US Minivan (People Carrier), has a velocity change of 48 km/h and a peak deceleration of 28g. Current thinking of the severity of the crash pulse suggests that a mini bus exhibits a velocity change of 32 km/h and peak deceleration of 20g whilst a large transit bus 32 km/h and 10g respectively. Thus the severity of the crash pulse used in ISO/CD 10542-1 exceeds that of a typical bus crash. It would be expected that any restraint system whose performance is satisfactory in terms of the criteria in ISO/CD 10542-1 would be appropriate for use in buses. The shoulder belt positions on dummy are defined in this standard and shown in Figure 1A .

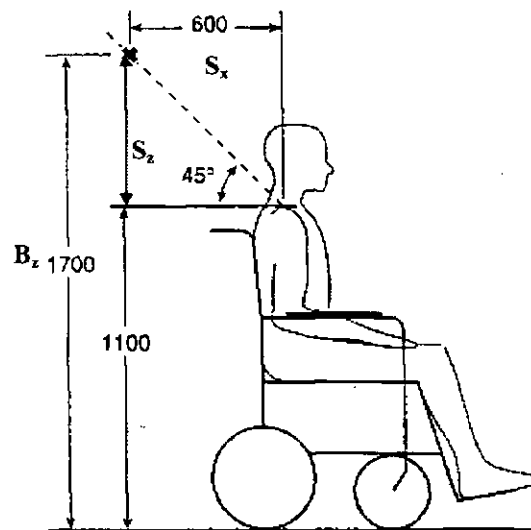


Figure 1A Shoulder belt positions on dummy

This standard, prepared by Technical Committee ISO/TC 173, places particular emphasis on design requirements, test procedures, and performance requirements with regard to the dynamic performance of WTORS in a frontal impact. The performance of WTORS with rearward facing wheelchairs involved in frontal impacts, performance of WTORS in rear, side, and rollover impacts, and performance

of WTORS with wheelchair-seated children will be addressed in other parts of this standard. Transportation related requirements for wheelchairs that remain occupied during motor vehicle transportation are specified in another Working Draft ISO standard (ISO WD 7176/19).

The basic requirements and excursion limits specified in ISO draft standard 10542 are indicated in Table 1A, which forms a checklist written in test reports. These limits are based on a typical safe ride down envelope available in a bus.

Table 1A: WTORS requirements (ISO/CD 10542-1)

Section 6	Requirements	results
6.1	Did the ATD remain in the wheelchair and the wheelchair remain in an upright position on the sled?	y/n
6.2	Did any components with a mass in excess of 100 gm detach?	y/n
6.3	Did any adjustable parts move from their pre-test positions?	y/n
6.4	Was there any leakage from the batteries?	y/n
6.5	Did any load bearing part of the wheelchair fracture completely?	y/n
6.7	Was the ATD released from the occupant restraint and removed from the wheelchair without the use of tools?	y/n
6.8	Was the wheelchair removed from the sled without the use of tools?	y/n
6.9	Was the horizontal movement of the wheelchair (X_{wc}) less than 200 mm? Was the horizontal movement of dummy knee (X_{knee}) less than 375 mm? Was the horizontal movement of dummy head (X_{head}) less than 650 mm?	y/n
6.10	Was the ratio $X_{knee}/X_{wc} > 1.1$?	y/n
remark	If the system met the requirements of 6.1 to 6.10, it could be considered to have exhibited a satisfactory crash performances	
conclusion	The system met (or not met) the requirements of 6.1 to 6.10 .	y/n

Notes:

X_{wc} is the horizontal distance relative to the sled platform between the contrast target placed at or near point P on the surrogate wheelchair at time t_0 , to the point-P target at the time of peak wheelchair excursion.

X_{knee} is the horizontal distance relative to the sled platform between the ATD knee-joint target at time t_0 , to the knee-joint target at the time of peak knee excursion.

X_{head} is the horizontal distance relative to the sled platform between the ATD's head above the nose at time t_0 , to the most forward point on the ATD's head at the time of peak head excursion.

Appendix 1B: Crash Victim Simulation (CVS) Programs

Recently, there has been significant progress in increasing the reliability and accuracy of computer simulation of crashworthiness in various crash modes. These are due to improvement both computer hardware and computational software. Crash Victim Simulation (CVS) can be used to simulate crash situations to a high degree of accuracy and to assess injuries. It can also be used to assess various restraint systems, including seat belts and wheelchair tiedown restraint system. The multibody technique has been used for the simulation of the gross motion of systems of bodies connected by complicated kinematic joints and the finite element techniques for the simulation of structural behaviour.

Articulated Total Body (ATB) was developed by Biomechanics Branch, Biodynamics & Bioengineer Division, Harry G. Armstrong Aerospace Medical Research Laboratory (Ohio, USA). ATB creates compatible binary files, such as, time intervals print file (.006) for results and error messages, picture file (.001), time history file (.008) and restart file (.009). The post-processor, ATBPP, has three basic functions: View, Plot and Tables. ATB is a lumped mass model for simulating three dimensional (3D) motions of connected rigid elements. The model uses a hybrid analytical formulation based on Newton's equations of motion with constants. The various body segments are represented by lumped mass elements connected joints. Each rigid element is assigned the mass and inertia properties of the equivalent body segment. The DYNAMAN package (Version 3.0) is a menu version of the ATB (DYNAMAN User's Manual, 1991), developed by General Engineering and Systems Analysis Company (GESAC, USA). DYNAMAN has four modules: Input (DYNIPP), Simulation (DYNASIM), Output (DYNOPP), and Generator of body data (BODGEN). DYNAMAN use vector exponential variable time step integrator. Screen resolution was set in EGA lower resolution (640x200) or EGA high resolution (640x350) or VGA (640x480).

In 1993 the first commercially available version of MADYMO was released from TNO, the Netherlands (Lupker et al, 1991). The most recent MADYMO version,

v5.3, was released in 1998. MADYMO crash simulation package has proved to be a very valuable tool in the development of the new occupant restraint system, in comparison with expensive and time consuming sled testing.

Computer simulation is a valuable tool for providing insight into the effects of crash pulses variations on output parameters. The results of the simple spring model were only considered as reference because they are based on simplifications of a very complicated system and environment. Based on the knowledge of the theory of mechanical vibration and energy principles (Appendix 6), the spring model was developed using dynamic program, such as FEA approach, ATB/DYNAMAN models and MADYMO models. The modelling flow diagram using CVS programs was designed in Figure 1B.1. Figure 1B.2 introduces three CVS programs to be used in test design and in the dynamic analysis of the wheelchair occupant system. The accurate representation of this system requires component testing, model validation and user experience. The structure of the DYNAMAN input file is designed in Figure 1B.3. The segment structure of the program is displayed in Figure 1B.4.

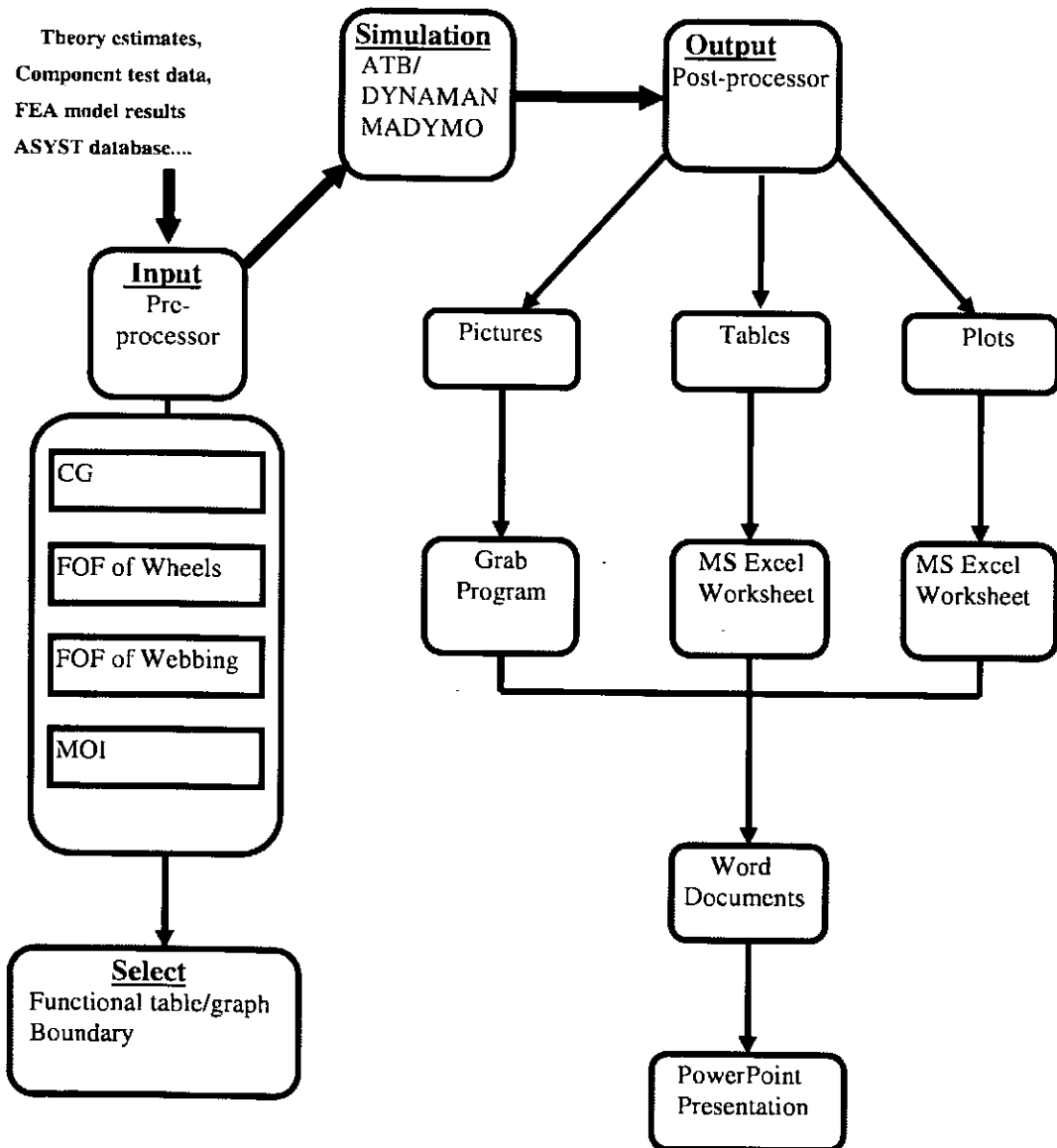


Figure 1B.1 CVS modelling flow diagram

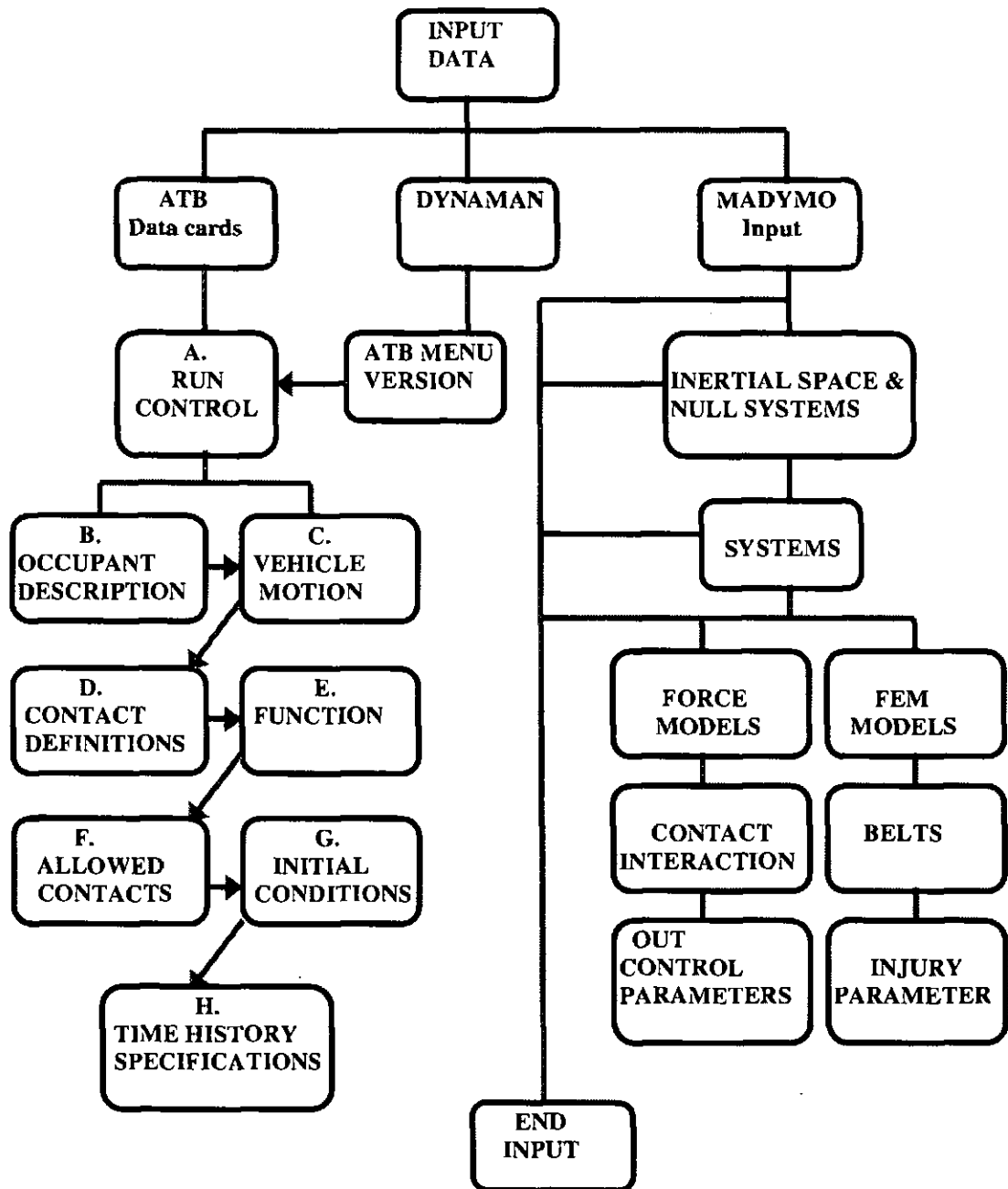


Figure 1B.2 Structure of CVS models input file: Overview

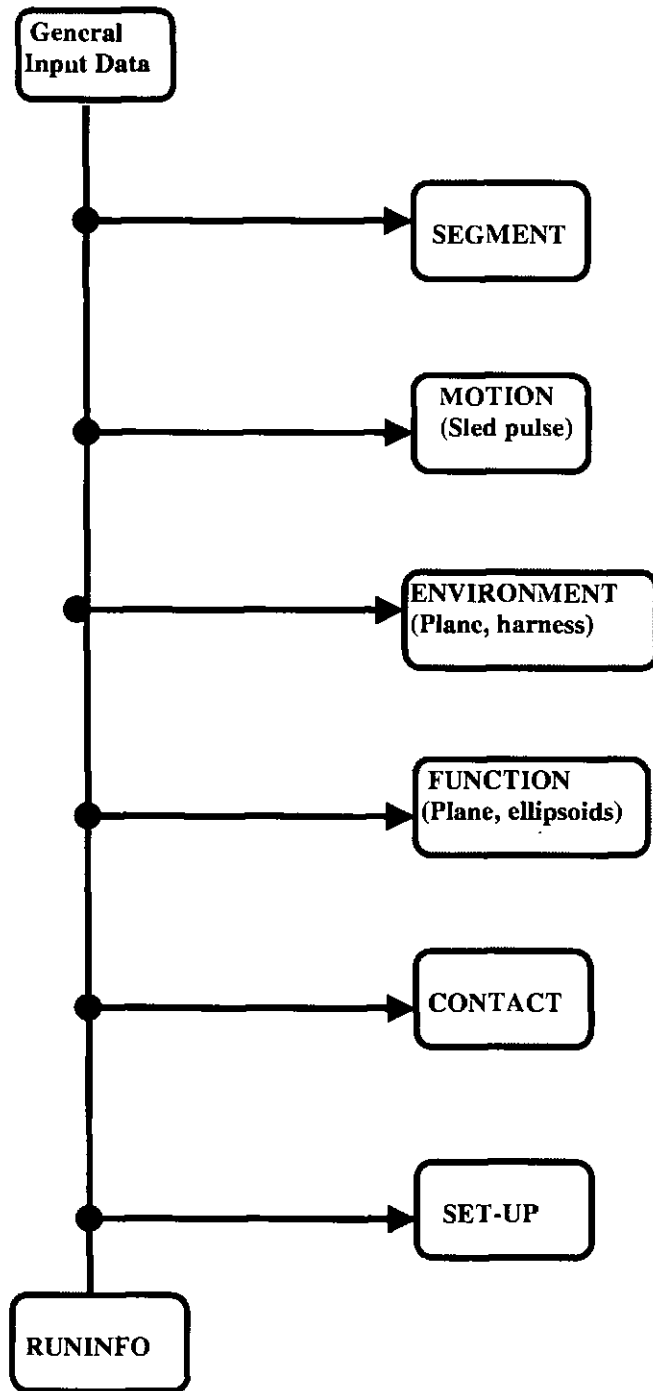


Figure 1B.3 Structure of DYNAMAN input file: Overview

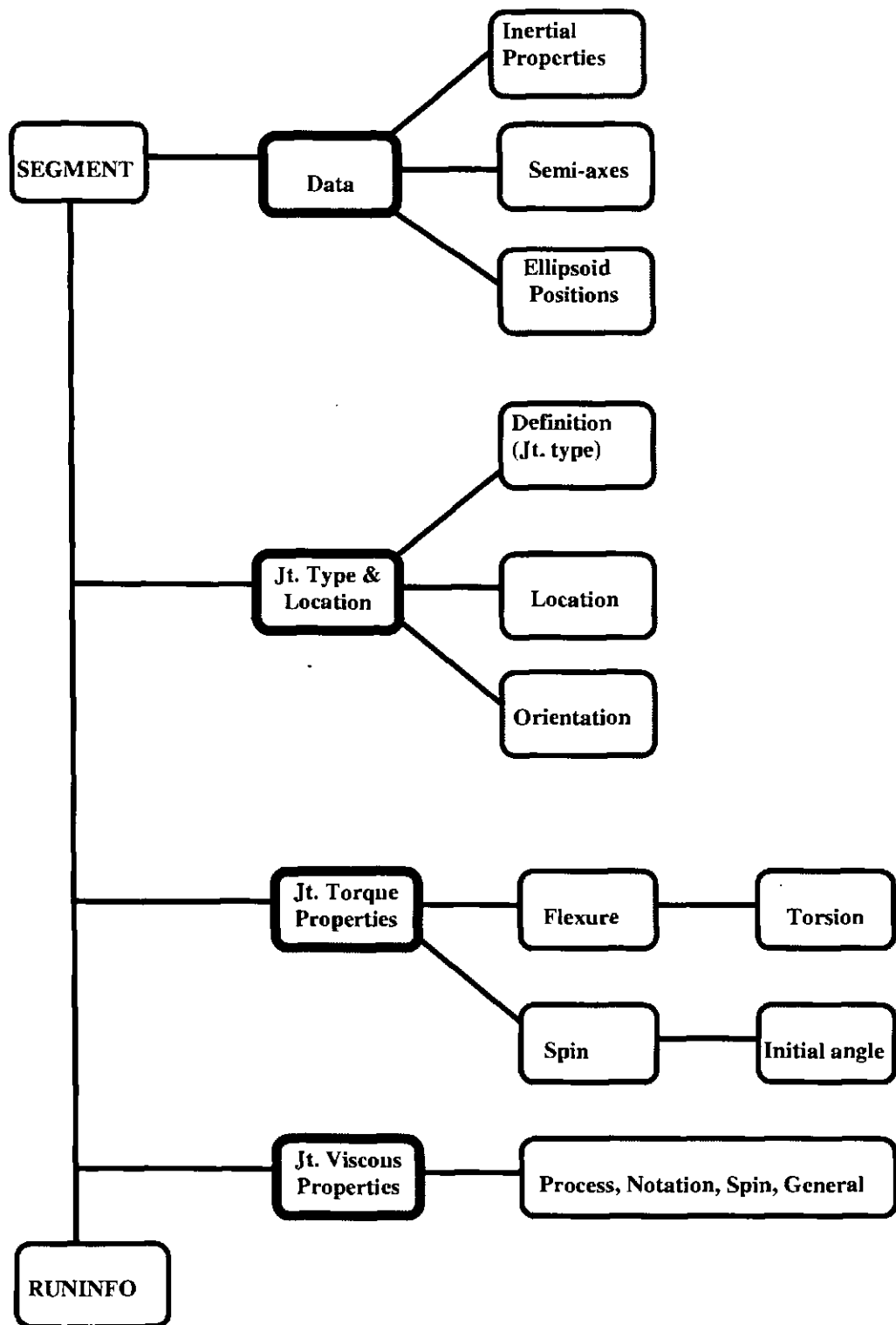


Figure 1B.4 Structure of DYNAMAN input file: Segment

Appendix 2: Modification of ISO Surrogate Wheelchair (SWC)

This Appendix provides design, dimensions, material, and performance specifications for the ISO Surrogate Wheelchair (SWC). These specifications provide a repeatable and reusable device that represents a typical adult sized power wheelchair. Details for the design, fabrication, and maintenance of a suitable surrogate wheelchair are available in Surrogate Wheelchair Manual (1994).

A2.1 ISO Surrogate Wheelchair Requirements

The surrogate wheelchair should meet the following requirements:

- a. be of rigid durable construction, so that there is no permanent deformation of the frame, seat surface, or seat back in a 48 km/h, 20g frontal impact test with a 76.3 kg ATD positioned and restrained in the SWC,
- b. have a total mass of 85 ± 1 kg,
- c. comply with the dimensions shown in the drawings (DRG No. ISO-01, 02, 03)
- d. allow for adjustment to accommodate components and end fittings of different types of tiedown systems,
- e. provide two front securement points and two rear securement points for four-point strap-type tiedowns,
- f. provide pelvic restraint anchor points on both sides of the surrogate wheelchair,
- g. have a centre of gravity located 142 ± 25 mm forward of the rear axle and 287 ± 25 mm above the ground plane for the range of frame-to-floor clearance adjustments allowed,
- h. have a rigid, flat seat surface with dimensions that is oriented at an angle of 4 ± 1.5 degrees to the horizontal (front end up) when the SWC tires are inflated as specified in (m) and (n) below and are resting on a flat horizontal surface,

-
- l. have a rigid oriented at 8 ± 1.5 degrees to the vertical when the inflated tires of the SWC are inflated as specified in (m) and (n) below and are resting on a flat horizontal surface,
 - j. have a 20 to 30 mm thick firm rubber pad fixed to the front surface of the rigid seat back,
 - k. have a detachable but rigid mounting plate for placement of a side-view target at the location of reference point P outboard of tiedown and restraint system components on either side of the SWC,
 - l. have pneumatic front tyres that, when inflated to 760 ± 15 kPa with the unoccupied surrogate wheelchair resting on a flat horizontal surface, have a diameter of 230 ± 10 mm, a width of 75 ± 5 mm, and a sidewall height of 54 ± 5 mm,
 - m. have pneumatic rear tyres that, when inflated to 415 ± 15 kPa with the unoccupied surrogate wheelchair resting on a flat horizontal surface, have a diameter of 325 ± 10 mm, a width of 100 ± 5 mm, and a sidewall height of 70 ± 5 mm.

A2.2 Modification of ISO Surrogate Wheelchair

The earlier version of ISO surrogate wheelchair (referred to as ISO-before) seems not suitable to general requirements of European wheelchair occupants as it is too big, which it is 50 mm higher than the conventional power wheelchairs in UK. It is desirable to modify the ISO-before (DRG No. ISO-01, ISO-02, ISO-03). The modified wheelchair (ISO-after) is shown in DRG No. ISO-04 and ISO-05. This modified SWC was considered to be more representative of power wheelchairs than the ISO-before model, which was under consideration. This Appendix describes modifications to the ISO-before model so that it conforms to the dimensions in the standard. The geometry modification of ISO-SWC are summarised as follows:

- The wheel base was shortened
- The centre of gravity was lowered

- The securement points were lowered and moved closer together on the same level
- The seat length was shortened
- The seat was lowered
- The armrests and footrests were modified similar to the ISO-before seat

A2.3 Moment of Inertia (MOI) Calculations for the Modified Wheelchair

The time required for the system to reach a given speed of rotation is proportional to the mass Δm and to the distance r . The product $r^2 \Delta m$ provides a measurement to the inertial of the system (resistance). This product is called the moment of inertia of the mass Δm with respect to the axis (I).

$$I = \int r^2 dm \quad (\text{A2-1})$$

All moment of inertia are relevant to the centre of its mass. The CG position of the wheelchair was found from a suspension lifting method. It was also calculated and validated using weight measurement method. An ISO surrogate wheelchair consists of the following three basic elements:

1) Tubes (Hollow cylinder): SAE 1010, ϕ 22 mm, thickness $t = 2.8$ mm (0.109"), tube length L , tube volume:

$$V = \pi (R^2 - r^2) L = \pi t (2R - t) L$$

The weight of tube:

$$W = \rho V$$

The mass of tubes:

$$m = W/g$$

put the mass values into the following formula and get I_x , I_y , and I_z (see DRG. No. ISO-01 and ISO-02).

$$I_x = 1/2 m (R^2 - r^2) \quad I_x = I_{x'} + my'^2 \quad (\text{A2-2})$$

$$I_{y'} = 1/12 m[3(R^2 - r^2) + L] \quad I_y = I_{y'} + mx'^2 \quad (\text{A2-3})$$

$$I_{z'} = 1/12 m[3(R^2 - r^2) + L] \quad I_z = I_{z'} + m(x'^2 + y'^2) \quad (\text{A2-4})$$

2) Prism: SAE 1020, 22 x 22 mm, length L

put the mass values into the following formula:

$$I_x = 1/5 m b^2 \quad (\text{A2-5})$$

$$I_y = 1/12 m (L^2 + b^2) \quad (\text{A2-6})$$

$$I_z = 1/12 m (L^2 + b^2) \quad (\text{A2-7})$$

3) Rod: SAE 1020, ϕ 22 mm

Rod volume:

$$V = \pi R^2 L$$

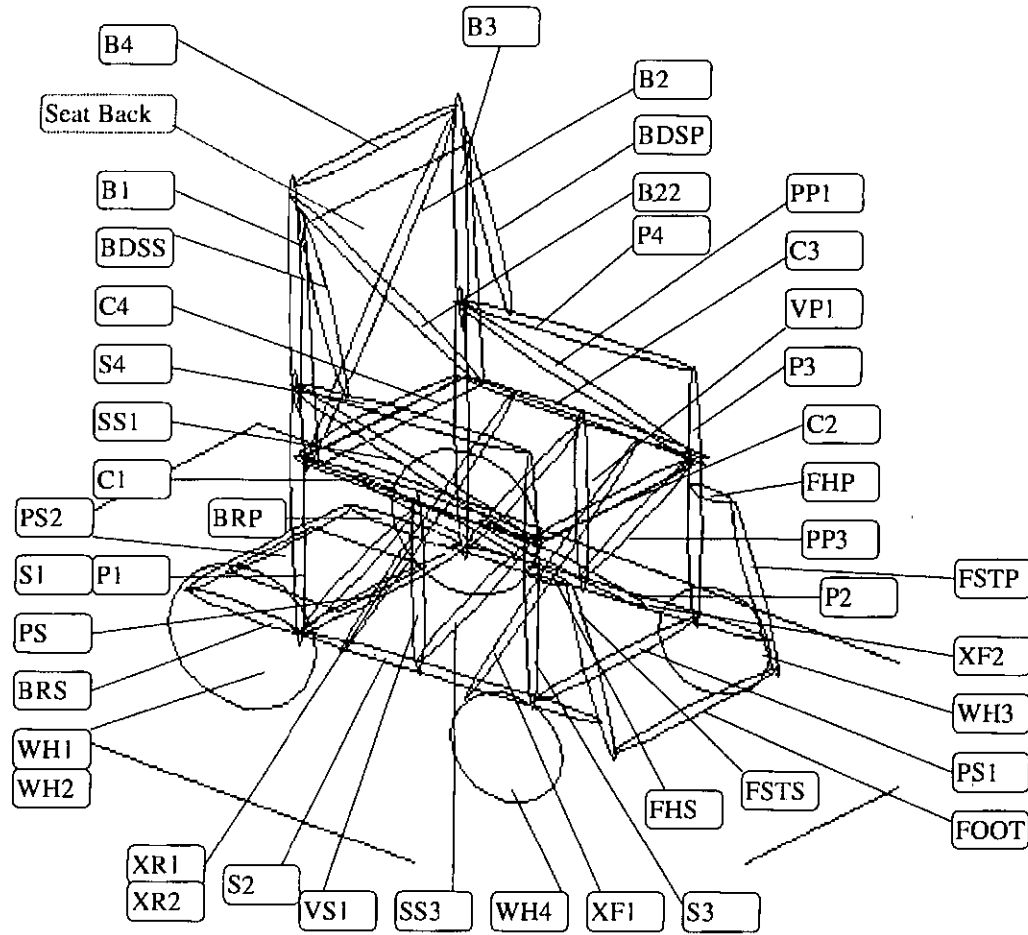
The mass of tubes:


$$m = W/g$$

put the mass values into the following formula:

$$I_x = 1/2 m r^2 \quad (\text{A2-8})$$

$$I_y = I_z = 1/12 m (3r^2 + L^2) \quad (\text{A2-9})$$




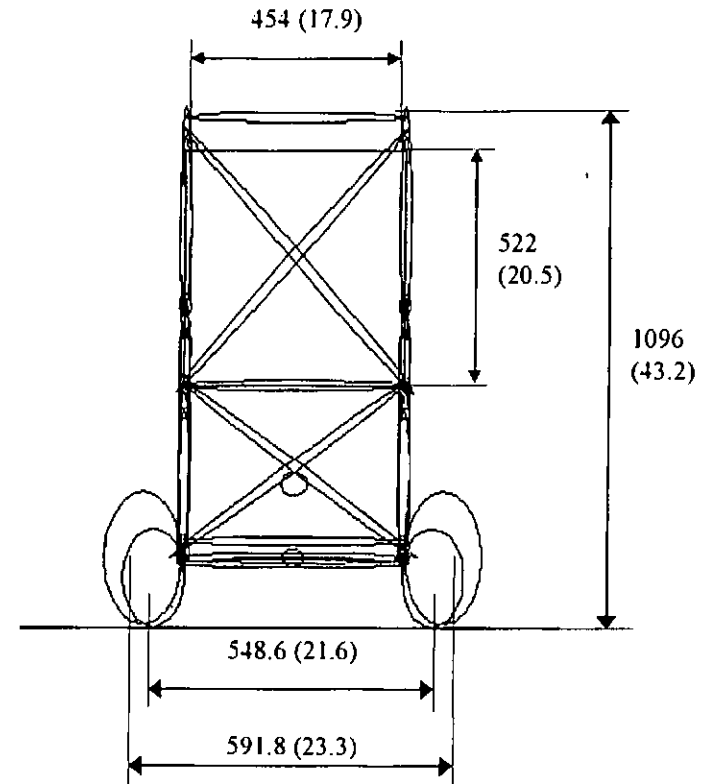
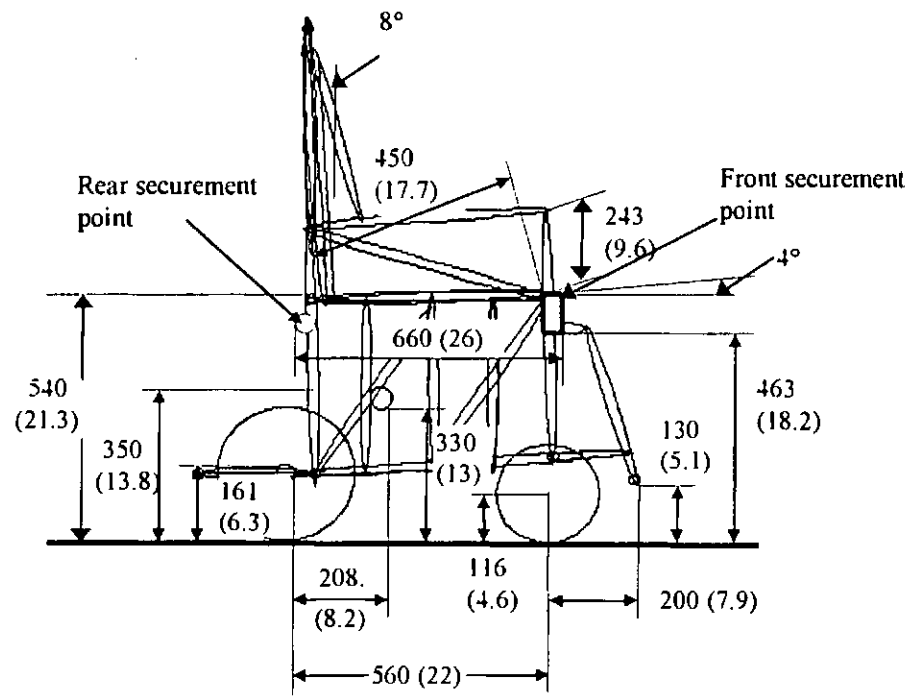
 MIDDLESEX UNIVERSITY	DRAWINGN BY Jun Gu	SIGN:	TITLE: ISO SWC (before modification: ISO-before)	DRG. NO. ISO - 01			
	MATERIAL DATA: 10/08/96	DIMENSIONS IN: mm (in) TOLERANCES: ± 5 mm			ISSUE DRG. NO.	DATE	CHANGE


Appendix 2

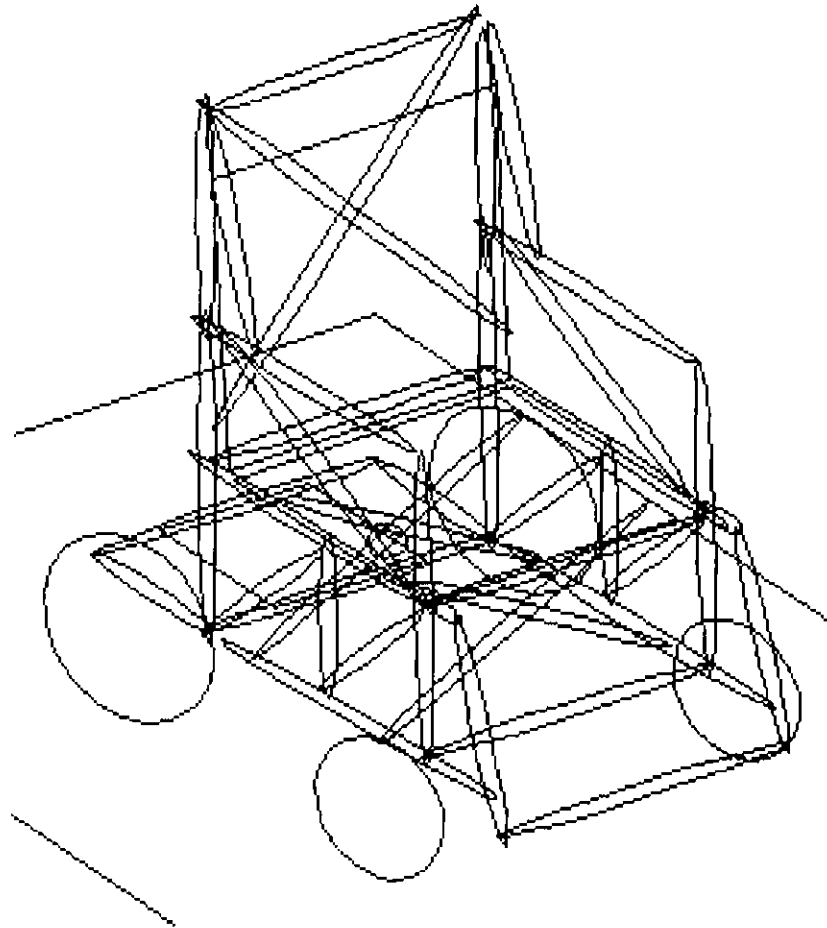
C1	SET HO SU (S)	279	11	11	1	91	279	597	VS1	SID VR SU (S)	11	11	152	1	144	79	85
C2	FR SET TU	11	218	11	1	24	520	544	VP1	SID VR SU (P0)	11	11	152	1	144	79	85
C3	SET HO SU (P)	279	11	11	1	91	279	597	SS3	SID DI SU (F)	11	11	191	1	74	417	491
C4	RR SET TU	11	218	11	1	24	6	32	PP3	SID DI SU (R)	11	11	191	1	74	417	491
B1	BAK TU (S)	11	11	229	1	938	853	85	BDSS	BAK DIAG SU (S)	11	11	203	1	68	79	147
B2	BAK LO TU	11	381	11	1	215	15	229	BDSP	BAK DIAG SU (P)	11	11	203	1	68	79	147
B22	BAK LO TU	11	381	11	1	215	15	229	FHS	FOOT SUP (S)	46	11	11	0	15	126	268
B3	BAK TU (P)	11	11	229	1	938	853	85	FSTS	FOOT SUP (S)	11	11	191	1	62	679	741
B4	BAK UP TU	11	218	11	1	24	6	32	FHP	FOOT SUP (P)	46	11	11	0	15	126	268
P2	BOT FR RD (P)	318	11	11	2	265	1241	1505	FSTP	FOOR SUT ()	11	11	191	1	62	679	741
P3	FR ARM TU (V)	11	11	292	1	326	232	153	FOOT	FOOR SUT ()	11	229	11	1	26	1117	1144
P4	FR ARM TU (H)	254	11	11	1	85	232	509	XF1	LO X FRAME (F)	11	254	11	1	85	435	520
PS	BAT FR SU	11	227	11	2	11348	18	11366	XF2	LO X FRAME (F)	11	254	11	1	88	435	520
PS1	FOOT RST	11	227	11	1	26	541	567	XR1	LO X FRAME (R)	11	254	11	1	88	47	132
PS2	BAT RR SU	11	227	11	2	11348	168	11516	XR2	LO X FRAME (R)	11	254	11	1	88	47	132
BRS	BAT SU RD (S)	127	11	11	1	94	44	138	PP2	SID DI SU (P)	0	0	0	1	74	115	188
BRP	BAT SU RD (P)	127	11	11	1	94	44	138	WH1	REAR WH (P)	152	76	152	0	15	147	15
S1	BAK TUBE (S)	11	11	310	1	379	276	171	WH2	REAR WH (S)	152	76	152	3	15	147	15
S2	BOT FR RD (S)	318	11	11	2	265	1241	1505	WH3	FRONT WH (P)	113	61	113	2	3	59	3
S3	FR ARM TU (V)-S	11	11	292	1	326	232	153	WH4	FRONT WH (S)	113	61	113	2	3	59	3
S4	FR ARM TU (H)-S	254	11	11	1	85	235	509									
P1	BAK TUBE (P)	11	11	310	1	379	276	171									
SS1	ARM DI SU (S)	11	11	254	1	97	303	403									
SS2	SID DI SU	11	11	216	1	74	115	188									
PP1	ARM DI SU (P)	11	11	254	1	97	303	403									
		X	Y	Z		lxx	lyy	lzz			X	Y	Z		lxx	lyy	lzz

SEG.	DESCRIPTION	SEMI	AXIS	DIM.	Wt.	MOI	SEG.	DESCRIPTION	SEMI	AXIS	DIM.	Wt.	MOI
------	-------------	------	------	------	-----	-----	------	-------------	------	------	------	-----	-----

 MIDDLESEX UNIVERSITY	DRAWINGN BY	SIGN:	TITLE:	DRG. NO.			
	Jun Gu	MOI unit: kg mm ²	ISO SWC (before modification: ISO-before)	ISO - 02			
	MATERIAL	DIMENSIONS IN: mm			ISSUE	DATE	CHANGE
RSEL	DATA: 10/08/96	TOLERANCES: ± 5 mm			DRG. NO.		
MME							




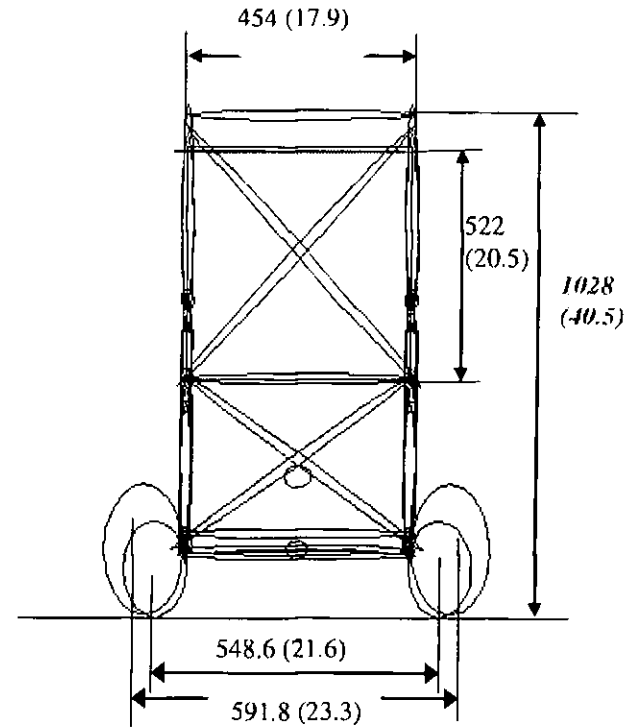
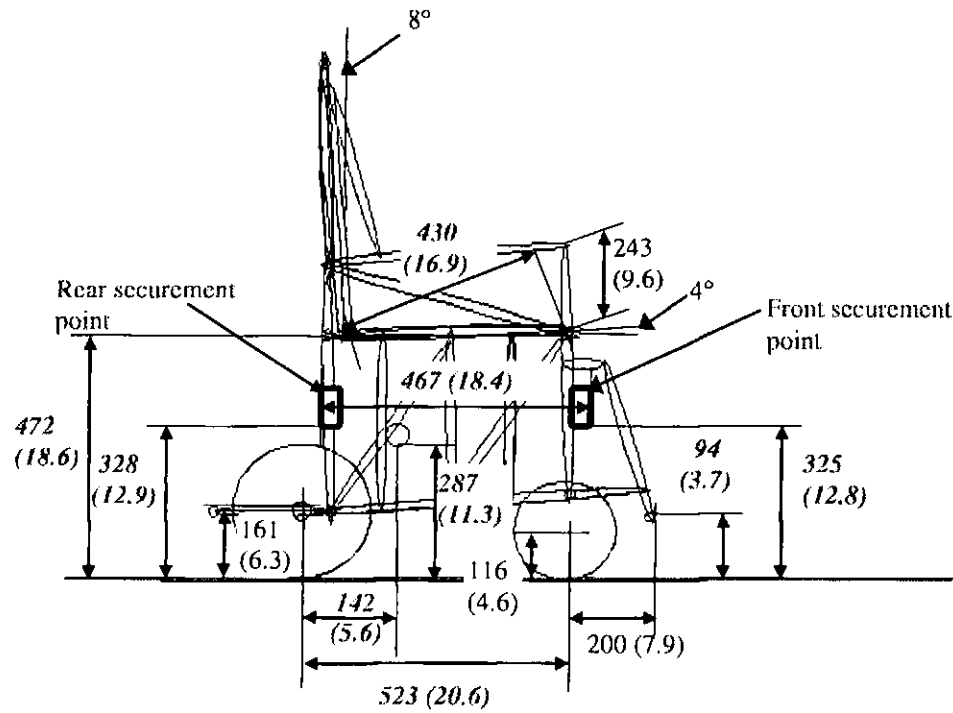
 MIDDLESEX UNIVERSITY RSEL MME	DRAWING BY	SIGN:	TITLE: ISO Surrogate Wheelchair (before modification)	DRG. NO.			
	Jun Gu			ISO - 03			
	MATERIAL	DIMENSIONS IN: mm (in)			ISSUE	DATE	CHANGE
DATA: 10/08/96	TOLERANCES: ± 5 mm			DRG. NO.			



BATTERY CONFIGURATION, STANDARD


1. Wheelchair mass measured: 90 kg (198 lb)
2. Principal Moment (lb in²) and X-Y-Z direction about centroid:
 $I_{xx} = 8.2E6 \text{ kg mm}^2 (28.3E3 \text{ lb in}^2)$
 $I_{yy} = 11.7E6 \text{ kg mm}^2 (39.8E3 \text{ lb in}^2)$
 $I_{zz} = 9.5E6 \text{ kg mm}^2 (32.3E3 \text{ lb in}^2)$
3. Battery box is supported with two bars attached to the axle block
4. Battery weighs: 4.16 kg (9.16 lb)

 MIDDLESEX UNIVERSITY	DRAWING BY	SIGN:	TITLE: ISO SWC (after modification: ISO-after)	DRG. NO.			
	Jun Gu MATERIAL DATA: 10/08/96			DIMENSIONS IN: mm (in) TOLERANCES: ± 5 mm	ISO - 04 ISSUE DRG. NO.	DATE	CHANGE



Notes:

1. CG location relative to the rear wheel axle, tolerance is ± 25 mm
2. Italic dimensions are those after modification

 RSEL MME	DRAWINGN BY	SIGN:	TITLE: ISO SWC (after modification: ISO-after)	DRG. NO.			
	MATERIAL	DIMENSIONS IN: mm (in)		ISO - 05	ISSUE	DATE	CHANGE
	DATA: 10/08/96	TOLERANCES: ± 5 mm		DRG. NO.			

Appendix 3: Load Cell Theory and Design

A3.1 Wheel Load Plate

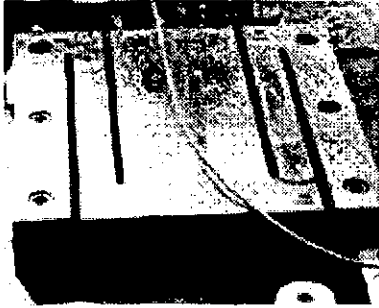


Figure 3A.1 wheel load plate

During a Forward Facing Frontal (FFF) impact, the restrained wheelchair moves forward, and may even twist. The movement of the chair requires load cells to have a relatively large surface area over which vertical loads can be measured accurately and are able to withstand the inertial loads of the crash environment. Unfortunately, typical load cells require the force points of application to remain constant and uniaxial, making them insufficient for recording wheel contact loads during a wheelchair crash.

The initial design at the University of Strathclyde, UK was to measure vertical loads under hospital bed castors. Prior research at University of Virginia (UVA) was to record the vertical load under the wheelchair wheels (Figure 3A.1).

A3.2 Wheel Load Plate Design

According to the UVA prior design, the load plate was made at MURSEL. A 254 x 254 mm (10" x 10") plate of medium carbon steel (instead of aluminium 7075) was milled according to the specifications of Figure 3A.2. Two cantilever sections, each 70 mm (2.75") width, are separated by a 254 x 114 mm (10" x 4.5") loading surface. The load plate was instrumented with KYOWA strain gauges (R1, R3 on top and R2, R4 on bottom) arranged in a 4-arm Wheatstone Bridge Circuit. When the plate is loaded, the bending of the cantilever sections and the resulting strain causes unbalance in the bridge circuit. The location of strain gauges and the corresponding design of the Wheatstone Bridge Circuit ensure that only strains associated with the vertical loads produce a non-zero output milli-voltage (mV). The load plate was calibrated in standard materials testing machine to derive sensitivity relating the output (mV) to the load.

Where: M_{max} is the maximum moment associated with the maximum load,

$$M_{max} = V_{max} L$$

V_{max} is the maximum vertical load;

L is the maximum moment arm 165 mm (6.5");

$y = b/2$ is the distance from the neutral axis where maximum strain occurs; b is the beam (plate) thickness 25.4 mm (1");

$I = w b^3/12$ is the bending moment of inertia;

w is the width of the beam section 70 mm (2.75").

substituting the above terms into (A3.2), the V_{max} is:

$$V_{max} = \frac{b^2 w \sigma_{max}}{6 L} \quad (A3.3)$$

Substituting the numerical values into (A3.3) and noting $\sigma_{max} = \sigma_y$, we obtain $V_{max} = 24.7$ kN. If vertical loads exceed above 24.7 kN the load plate will be yielded. This design is a method of measuring vertical wheel loads only. The wheel load plate cells need to be modified through geometry (b , w , L) and mechanical design (σ_{max}) so that it could sustain over 40 kN vertical loads, which could happen in the rearward facing frontal impact of ISO surrogate wheelchair.

The load plate was calibrated using a general compression testing machine. The sensitivities were verified by recording the output voltages using the MURSEL data acquisition system during the calibration procedure. In this procedure, the plates were loaded in compression from 0 to 22.25 kN in a stepwise fashion, and the load at each increment was recorded. Each plateau in the output voltage time history was averaged. This average output voltage corresponded to the recorded load at the given plateau.

A3.3 Tensile Load Cell ('dogbone')

In order to measure the end loads at the anchorage of a belt, a tensile load cell in the form of 'dog bone' was designed in MURSEL. The 'dogbone' is characterised in two ends bigger than the middle part. While it is loaded (pulled or compressed), the

middle part is initially deformed. The deformation could be measured in strain gauges bonded in the surface of the middle part.

The transducer is manufactured from a fully heat treated aluminium alloy (HP15 WP). The plan of the transducer is in the form of 'dogbone' (12.5 mm thickness) and is shown in Figure 3A.3. On both parallel sections, 90 degree strain gauges roscettes are bonded. The gauges are connected in a full bridge circuit (R1, R3 in the top, and R2, R4 in the bottom).

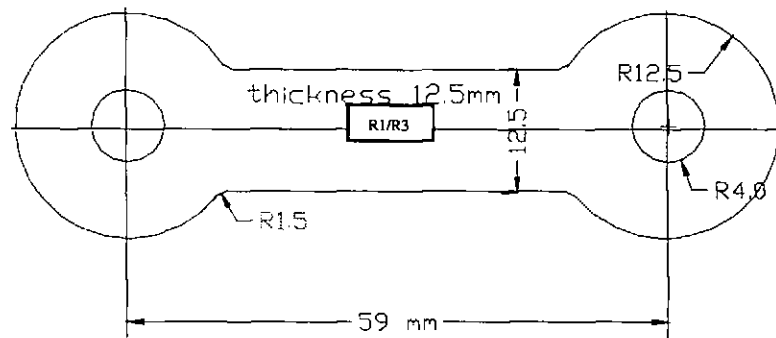


Figure 3A.3 A 'dogbone' dimensions and gauge placement

It was noted from the test results that 'dogbone' was working well to provide results within 10% of those obtained from the Denton load cell. In this research programme, the 'dogbone' load cell was used to measure wheelchair tiedown end loads. The lap and diagonal belt loads were measured using standard Denton load cells.

Appendix 4: Running MADYMO and EASi-MAD

MADYMO stands for MATHematical DYNAMIC MOdel, which has been developed by Crash-Safety Research Centre of TNO Road-Vehicles Research Institute, the Netherlands for the simulation of occupant response in vehicle impact. EASi-MAD is a pre- and post-processor for MADYMO, developed by EASi Engineering, USA.

MADYMO V5.1.1 (1995) was initially installed on SUN station, Crunch1 (UNIX system V release 4.0) in Middlesex University. The post-processors MAPPT could not run on SUN workstation properly as the configuration failed in the University. The following administrative work and technical support were conducted by author before running MADYMO and EASi-MAD.

A4.1 Administrative Work

MADYMO V5.2 (1996) was installed on a Silicon Graphics workstation (SGI), quark, based on Bounds Green Campus. MADYMO V5.2.1 (1997) and V5.3 (1998) were installed in SGI, iris, based on MURSEL, Hendon Campus. The machine was firstly networked through the path (/etc/config) and host address resolver configuration file. The interpreter for the postscript languages, Ghostscript 3.33 was downloaded via Internet to convert RGB image to PS file so that colour image could be printed out. The swapping area was defined for installation. The dials & buttons was connected to get dialbox on MAPPK. The x resources were also specified for MAPPT. The user interface of MAPPT was implemented using x liberia. The x server resource database utility (xrdb) was used to add the specifications: InstallDir/etc/mappt/config/platform/Xdefaults.

The SGI iris (R4000 series, sgi53 platform) uses the IRIX5.3 UNIX operating system and FORTRAN 77 compiler (Table 4A.1).

Table 4A.1 Summary of SGI station

MIPS R4600	Operating system	Platform
Memory (RAM): 32 Mb; Graphic: Indy 9-bit Processor: 132 MHz 24 bit z buffer for hardware shading	Implementation: IRIX (1991) Release: 5.3 Provider: Silicon Graphics Inc.	Designation: IP22 System Identifier (printhead): 1762245998 Platform (local Host name, sys_id): Iris Local Host Internet id (hostid): 9e5e59ca

A4.2 Setting Environment on Iris for MADYMO and EASi-MAD

MADYMO and EASi-MAD programs were installed in the super user, root. The environment variable MDHOME has to be defined. In order to make this environment setting permanently, the following commands were written to `$(HOME)/.cshrc` to run MADYMO3D. The listing of `.cshrc` file is as follows:

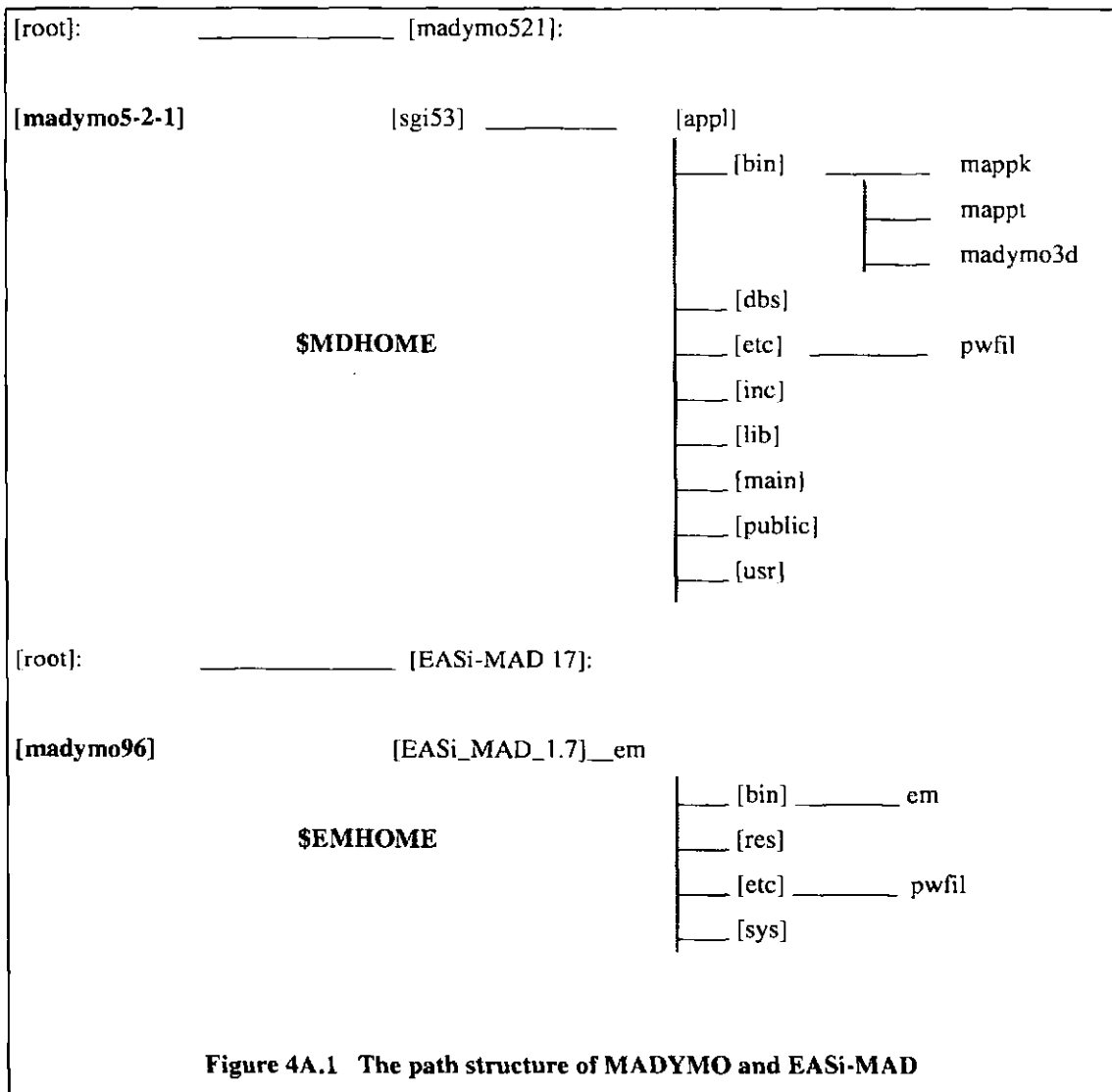
```
*****.cshrc# root's csh settings## "$Revision: 1.12
# source /setup_madymosource /setenv_easi
# source /setenv_madymo96source /setenv_madymo521
setenv DISPLAY iris:0alias madymo521 /madymo5-2-1/madymo_521/madymo521*****
setenv_easisetenv EMHOME /madymo96/EASi-MAD17/EASi-MAD_1.7
set path = ( $path SEMHOME/bin )*****
setenv_madymo521setenv MDHOME /madymo5-2-1/madymo_521/sgi53
set path = ( $path $MDHOME/bin )*****
```

The environment DISPLAY should be set to iris before post-processor programs, MAPPK and MAPPT can be run. Two environment setting files have to be created: `setenv_madymo521` and `setenv_easi`.

The program MADYMO and EASi-MAD were downloaded to the relative directories, `madymo5-2-1` and `madymo96` respectively by the tape archiver (tar). The path structures listed in Figure 4A.1.

The hostid 6909BD6E can be found in the program printhead in `$(MDHOME)/bin` directory. The password file called `pwfil` in the directory `$(MDHOME)/etc` must be initialised before it could be run. The MADYMO password string was issued by TNO and edited in the following file `pwfil`:

```
5.2:6909BD6E:971031:FCFC7:CKZQARHB4MY74:MIDDLESEX SGI IRIS:
```



A4.3 Running MADYMO and EASi-MAD on Iris

The input file for MADYMO, called DAT file, can be created using either standard text editor or EASi-MAD program. The simulation command, mady521, is used to run the DAT file. A system LOG file is created when the batch job is run. This file contains the commands which have been executed and any system error messages. Once the simulation completed, a report file (REP) will be created. This file contains an annotated listing of the input file and any error or warning messages that have occurred. All other output files are optional and are specified in the input listing.

The actual CPU time depends on simulation time required for the models. The elapsed time to complete the simulation varied depending on the simulation size.

A4.4 Post-processor Output from MADYMO

MADYMO3D program itself only outputs numerical and text files. A post-processor, MAPPK, yields graphical outputs which provide a visual representation of the simulation. The configuration file was written to define different colours of ellipsoids and planes to visual properly. The KIN3 file is one of the optional files that must be specified in the MADYMO input data. MAPPK can also hardcopy images into RGB file from the graph display. Once the pictures were displayed in a hardcopy menu, the picture could be directed to a postscript file or to postscript printer HP DeskJet 1600 CM. The command, 'rgbtops', can be used to convert hardcopy files (RGB) to postscript format (PS), which it is black and white version. The interpolator program XV was used to transfer a RGB image to a postscript file (PS) on Crunch1 by colour-map editing.

In order to create time-history plot a separate post-processing system, MAPPT, was required. The output files from MADYMO are ordinary ASCII text, which are organised in a row format rather than a column format. which makes it difficult to use in a spreadsheet or similar software package. It is necessary to use a software programme to re-arrange the MADYMO data files into a different format. This can be achieved in two ways, either by use of a PC based package called ASYST or by use of MAPPT. The latter one (MAPPT) was more convenient to use. Once the file was converted to a more accessible format, it could be read by any spreadsheet package. The data was then presented and analysed at will. The executive command to run MAPPT program is *Smappt -graph LINACC*.

The processes of running MADYMO are summarised in Figure 4A.2. In addition to the MAPPT and MAPPK programs, six other software were implemented to present the results. The kinematic pictures were taken from the monitor screen using a camera mounted on a tripod for a steady images. A 100 mm lens was considered to minimise screen curvature. A slow shutter speed (1/30 sec or less) was set to eliminate screen blanking. A small aperture (f1/16) was also set to ensure the picture in focus. The images

were scanned and captured using Paintshop-Pro program, which it can be used to edit the image with colour professional. The edited images were pasted into Word documents.

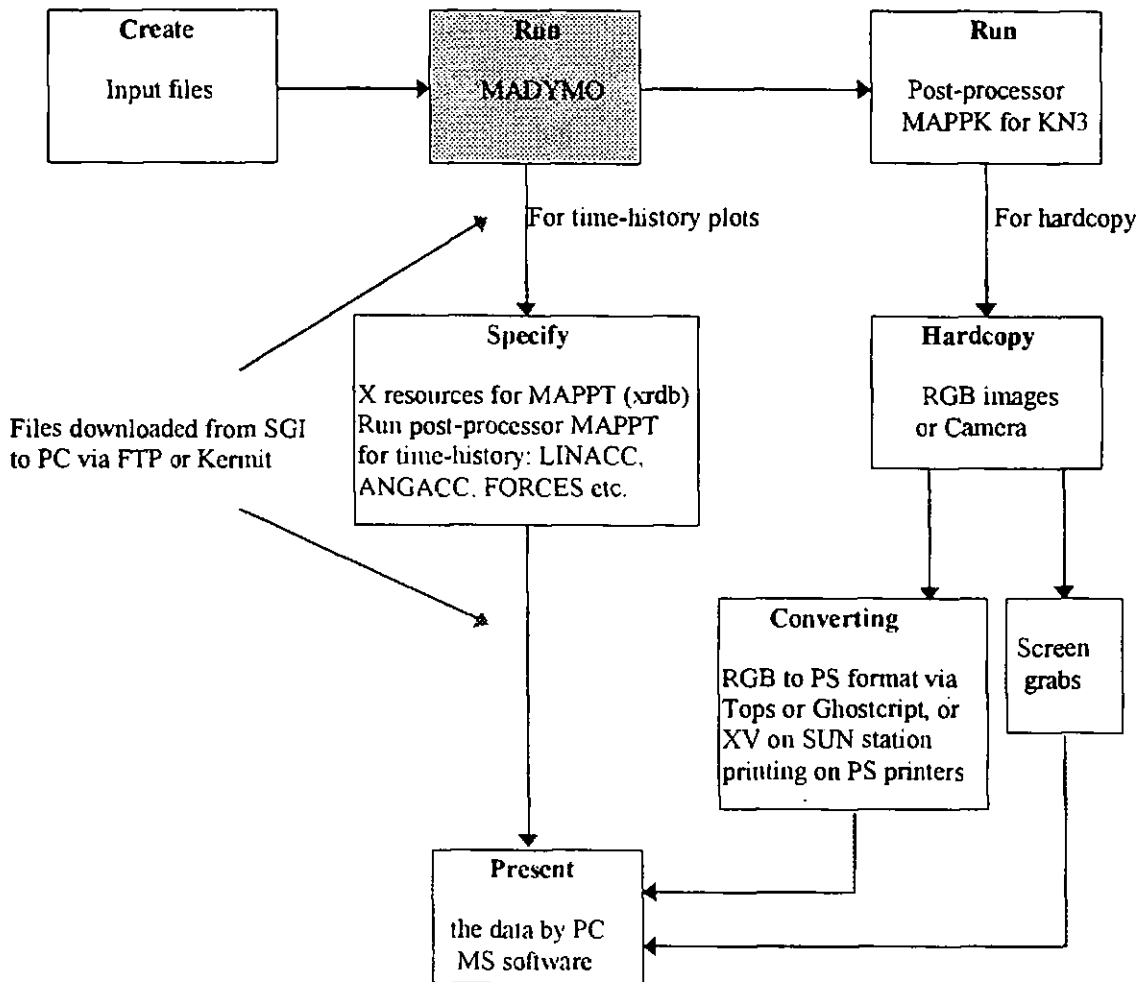


Figure 4A.2 The processes of running MADYMO

In order to present the data using PC document files, the files on SGI workstation were downloaded to PC using two ways, either by FTP or by Kermit (Table 4A.2).

Table 4A.2 Transferring files via FTP or Kermit

Transfer crunch1 files to VAX	Transfer VAX files to PC via Kermit
crunch1>ftp alpha1	vaxa>kermit
ftp>put [files]	mc-kermit>send [files] [alt k]/
ftp>quit	ms-kermit>record [files]
crunch1>telnet vaxa	ms-kermit

Appendix 5A: Interpretation of Industry Test Results

Test Series: Depending on test requirements

Set up: Production wheelchairs, surrogate or commercial restraint systems, TNO-10 or Hybrid II and child dummy, sled pulse within ISO/CD 10542-1, Forward Facing Frontal (FFF) impact.

- Goals:**
- To test the performance of different types of production wheelchairs on the behalf of industrial clients
 - To test production wheelchairs under the identical crash conditions, which were used to test the surrogate system
 - To produce a reference level against the surrogate results

Table 5A.1 A sample of test report for clients

TEST No:	CLIENT:		
DATE:			
TIME(GMT):		RUN No:	
TEST OBJECTIVE:			
<u>TEST PULSE:</u>	ISO Draft Standard 10542		
<u>WHEELCHAIR:</u>	Manufacturer:		
	Model:		
	Sample/tests:	1/1	
	Configuration:		
<u>WHEELCHAIR TIEDOWN:</u>	Manufacturer:		
	Description:		
	Model:		
	Sample/tests:	1/1	
	Configuration:		
<u>OCCUPANT RESTRAINT:</u>	Manufacturer:		
	Description:		
	Model:		
	Sample/tests:	1/1	
	Anchorage:		
<u>DUMMY:</u>	TNO 10/HYBRID II/TNO3-4	75 kg/15 kg	
<u>TRANSDUCERS:</u>	Sled Accelerometer	Endevco uniaxial 7232C/CE38	
<u>PHOTOGRAPHY:</u>	Video	Ektapro 1000 High Speed Video	
	Camera/Analyser	Stills	Pentax SFX
<u>TEST DATA:</u>	SLED	Velocity change (km/h)(ΔV):	
		Stop distance (mm)(S):	
		peak deceleration (g):	
		mean deceleration(g) ($\Delta V^2/2gS$):	
	DUMMY	excursion(mm)	Head:
			Knee:
<u>RESULTS</u>	Wheelchair	Max. forward movement (mm):	
	There are (or not) load carrying parts became fractured or separated during the impact. Both head and knee excursions were within (or not within) the limits prescribed in ISO draft standard 10542		
<u>CONCLUSION</u>	Satisfactory (or Not satisfactory) performance		

MURSEL carries out work on the behalf of industrial clients on wheelchair restraint systems in facing forward and rearward impact to simulate real life vehicle situations using a high speed impact rig. The result is observed in detail by high speed cameras, which can later be used to observe the impact in slow motion frame by frame. The data are recorded on a computer and graphs of the impact are analysed. It is comparable with the surrogate system under the identical conditions. All tests should meet the standard requirements of ISO/CD 10542-1 or ISO WD7176/19. The test report is presented after testing and a sample of test report is shown in Table 5A.1. The typical test results of Buddy wheelchairs are listed in Table 5A.2.

Table 5A.2 Buddy wheelchair test results

Test/ run no.	w/c type & supplier	Set-up	Impact direction	ΔV km/h	Mean Sled g	Peak Sled g	Stop distance mm	Results
3192 /RRS01	Buddy Buggy (25.3 kg, rear wheel ϕ 192, wheelbase 550) Radcliffe Rehabilitation Services	ISO WD7176/19 <u>W/C tiedown:</u> UNWIN slotted floor rail <u>Dummy restraint:</u> UNWIN double inertia reel rail <u>Dummy:</u> TNO 3-4 (15kg)	FFF	51.2	20.8	24.7	484	X_{wc} 139 mm X_{knee} 253 mm X_{head} 416 mm Passed

The typical test results of Sunrise wheelchairs are selected in Table 5A.3. It was found from the video footage that at the point (86 ms) all the loads (dummy and chair) were being taken by the lap and diagonal occupant belt. Hence the dummy is being forced back into the chair resulting in the chair backrest failure.

The test measurements and test results of Cirrus wheelchairs are listed in Table 5A.4 and UNWIN restraint system are listed in Table 5A.5. The test results of manual wheelchairs are listed in Table 5A.6. The test results of Invarcare and SCN wheelchairs are listed in Table 5A.7 and Table 5A.8 respectively.

In the above tables, the wheelbase is defined as the distance between the backward axle of the front wheel and the rear wheel axle. 'x' is measured relative to the rear tyre axle, 'y' measured relative to the sled fore and aft centre line and 'z' measured relative to the sled floorboard. The angle of shoulder belt is projected side view to horizontal, measured above the shoulder. The head excursion is the total forward change in position of the front nose of the head measured at the initial position prior to impact and at the time of maximum forward leading edge of the head

level. The P point is a “reference point that lies at the cross-sectional centre of a 100-mm diameter cylinder positioned with the longitudinal axis perpendicular to the wheelchair reference plane such that the curved surface of the cylinder contacts with the backrest and the upper surface of the seat” (ISO/CD 10542-1, 1996).

Table 5A.3 Sunrise wheelchair test results

Test/ run No.	w/c type & supplier	Set-up	Impact direction	Delta 'V'	Mean Sled	Peak Sled	Stop distance	Results
				km/h	g	g	mm	
3028/ SRM4	Power Tec F50 (57 kg) Sunrise Medical Ltd.	ISO/CD 10542-2 W/C tiedown: UNWIN front - lengthened standard strap rear - standard two ring on track clip Dummy restraint: Double inertia reel Dummy: TNO-10	forward facing	50.5	23.7	25.9	422	X_{wc} 296 mm X_{knee} 214 mm portside tyre punctured backrest deformed rearward 25° failed
3029/ SRM5	Spirit with SAE bracket	ISO/CD 10542-2 W/C tiedown: UNWIN - Rearlok Dummy restraint: automatic double inertia reel Dummy: TNO-10	forward facing	50.1	20.4	23.3	485	X_{wc} 48 mm X_{knee} 177 mm front seat support frame deformed; backrest deformed battery box was released from tray failed
3030/ SRM6	Power Tec F40	ISO/CD 10542-2 W/C tiedown: UNWIN belt front - standard strap rear - standard webbing with karabiners Dummy restraint: Double inertia reel Dummy: TNO-10	forward facing	51.1	21.7	26.3	450	X_{wc} N/A X_{knee} N/A Starboard armrest rotated outwards; rear frame rivets in the upper and lower rails failed. failed
3187/ SRM7	New sprit MT-1 (13.3 kg, wheelbase 470)	ISO/CD 10542-2 W/C tiedown: UNWIN front - heavy duty belt rear - two rings on track clip + karabiners Dummy restraint: Double inertial reel 3pt Dummy: TNO-10	forward facing	50.5	20.9	24	469	X_{wc} 48.8 mm X_{knee} 125.5 mm X_{head} 578.5 mm rear portside wheel punctured, rear wheel axle bend failed
3188/ SRM8	New sprit MR-3 (11 kg, big wheel, wheelbase 400)	ISO/CD 10542-2 W/C tiedown: UNWIN front - heavy duty belt rear - two rings on track clip + karabiners Dummy restraint: Double inertial reel 3 pt Dummy: TNO-10	forward facing	49.6	19.4	22	490	X_{wc} 97.7 mm X_{knee} 83.8 mm X_{head} 495.6 mm rear axle little bent, shld belt come off failed
3189/ SRM9	Sun RF2 (64.8 kg, no tube, wheelbase 530)	ISO/CD 10542-2 W/C tiedown: UNWIN front - heavy duty belt rear - two rings on track clip + karabiners Dummy restraint: Double inertial reel 3 pt Dummy: TNO-10	forward facing	48	18.3	21	484	X_{wc} 49.9 mm X_{knee} 135.7 mm X_{head} 535.5 mm battery come out, backrest deformed failed

Table 5A.4 Sled tests for Cirrus wheelchairs (12/02/97)

Handicare W/c	units	Cirrus Classic (wide) c-15699 wide +D ring attachment + neck rest	Cirrus Classic (wide) c- 15692 wide + Head rest	Cirrus Classic (wide) c- 15691 wide + head rest
Test/run No:		T3316/Sim1	T3317/Sim2	T3318/Sim3
Wheelchair mass	kg	37	37	37
Rear wheel pressure	kPa	276	276	276
Wheelbase	mm	480	480	480
backrest angle to vertical	deg	30	15	15
Seat pan angle to horizontal	deg	15	15	15
Seat surface height (St.)	mm	560	560	560
Rear wheel target:				
x: relative to target on sled	mm	670	740	760
z:	mm	610	610	610
P point target:				
x: relative to target on sled	mm	650	650	650
z:	mm	587	590	590
Wheelchair Tiedown		Q'straint (Q5001-T 116139B)	UNWIN restraint: 4-pt webbing and double inertial reel (3 pt)	Q'straint (Q5001-113935)- 4- eye bolts
Front tiedown:				
x: on floor/on chair	mm	710/510	730/400	810/410
y: on floor/on chair	mm	280	165	280/200
z:	mm	250	290	290
θ_r (40 - 60 deg)	deg	46	36	35
Rear tiedown length:				
x: on floor/on chair	mm	400/80	470/50	420/60
y: on floor/on chair	mm	170/190	170/160	170
z:	mm	330	310	310
θ_r (30 -50 deg)	deg	50	35	35
Occupant Restraint				
R pillar:		no slack,	UNWIN	no slack,
Angle of shld belt:	deg	30	15	15
behind ATD shoulder (S_x)	mm	280	400	420
above ATD shoulder (S_y)	mm	180	180	180
x:	mm	470	370	500
y:	mm	310	310	310
z:	mm	1200	1200	1200
Angle of pelvic belt to horizontal (lap belt)	deg	50	43	45
ATD Positioning				
Head front nose:		TNO-10	TNO-10	TNO-10
x: relative to target on sled	mm	650	645	650
z:	mm	1090	1090	1090
Knee target:				
x: relative to target on sled	mm	100	250	230
z	mm	650	650	650
TEST RESULTS				
Delta 'V'	km/h	48.9	48.9	49.2
peak g	g	24	23	24
stop distance	mm	431	484	472
Excursion (from video)		1 pixel (pxl) = 7.14 mm	1 pxl = 7.40 mm	1 pxl = 7.55 mm
X_{wc} (< 200)	mm	63	45	66
X_{knee} (< 375)	mm	243	235	185
X_{head} (< 650)	mm	322	319	333
visual observations		Neck rest (350 g) out dummy back 20 deg more	Front middle tube bent,	Front middle tube bent;

Table 5A.5 Sled tests for UNWIN restraint system (18/02/97)

TEST SET-UP	units	T3320/UN56	T3321/UN57	T3322/UN58
Wheelchair model		Rossci Bonnyman/Travel (black)	Sunrise Medical/ Spirit (green)	ISO surrogate (modified)
Mass	kg	24 (no armrest)	38 with armrest	85
Rear wheel pressure	kPa	276	276	414
Wheelbase	mm	445	485	530
Backrest angle to vertical	deg	10	10	10
Seat pan angle to horizontal	deg	10	10	0
Seat surface height (St. cross)	mm	450	460	470
Rear wheel target:				
x: relative to target on sled (datum)	mm	780	775	1200
z:	mm	140	150	155
P point target:				
x: relative to target on sled	mm	no armrest	670	850
z:	mm		505	525
Wheelchair Tiedown		UNWIN double lock clamp	UNWIN double lock clamp	Easilok II NUB1477
Clamps or Easilok		Q/ATF/DL/310/R	Q/ATF/DL/310/R	
x: on floor/on chair	mm	178/182	225/227	380/80
y: on floor/on chair	mm	165/230	165/225	165
z:	mm	230	240	200
Occupant Restraint		UNWIN 2-inertia reel	UNWIN 2-inertia reel	Static L/D
Under B pillar Ring:		3-pt QIR/3H/ATF/WH	3-pt QIR/3H/ATF/WH	
Angle of shld belt: top/bottom	deg	0/50	-13/56	5/55
behind ATD shoulder:	mm	200	180	slack 75 block.
above ATD shoulder:	mm	0	0	
B pillar				
x:	mm	325	330	480
y:	mm	300	300	180
z:	mm	1200	1200	1150
Lap belt:		slotted floor rail	slotted floor rail	slotted floor rail
Angle of pelvic belt to horizontal	deg	45	45	45
ATD Positioning		TNO-10	TNO-10	TNO-10
Head front. nose:				
x: relative to target on sled (H _n)	mm	650	650	650
z:	mm	1102	1205	1165
Knee target:				
x: relative to target on sled (K _n)	mm	270	217	380
z:	mm	575	605	575
Hip target:				
x: relative to target on sled (K _h)	mm	668	-	790
z:	mm	510	-	570
TEST RESULTS				
Delta 'V'	km/h	49.9	49.4	48.3
peak g	g	24	23	23
stop distance	mm	478	502	511
Excursion (measured from video)		l pxl = 7.69 mm	l pxl = 7.55 mm	
X _{we} (< 200)	mm	138.4	105.7	-
X _{knee} (< 375)	mm	306.7	416.9	-
X _{head} (< 650)	mm	380.8	383.4	-
visual observations		clamp hook (75 g) fly out; both tubes bent at clamp position; Front wheel axle deformed	both tubes bent at clamp position; cushion pushed down	rear tiedown broken lap belt broken failed

Table 5A.6 Sled tests for manual wheelchairs (12/03/97)

Manual Wheelchairs	units	Rampley 9L, BH53349	Bencraft 8L- 25370	Rempley 9L mkII- hugel back fixed arms	Bencraft 4L- JMKII
Test/run No.		T3349/TRL602	T3350/TRL603	T3351/TRL604	T3352/TRL605
Wheelchair mass	kg	15.7	18.2	15.7	15.7
Rear wheel pressure	kPa	276	262	262	262
Wheelbase	mm	405	423	400	350
Backrest angle to vertical	deg	10	10	10	10
Seat pan angle to horizontal	deg	10	10	10	10
Seat surface height (St)	mm	440	440	440	440
Rear wheel target:					
x: relative to target on sled (datum)	mm	720	745	722	715
z:	mm	155	288	150	150
P point target:					
x: relative to target on sled (P ₁)	mm	650	652	660	625
z:	mm	480	480	480	480
Wheelchair Tiedown					
		UNWIN track	UNWIN track	UNWIN track	
Front tiedown:					
x: on floor/on chair	mm	800/465	810/470	CLAMP	QL/ATF/DL/R
y: on floor/on chair	mm	330/450	330/440		400
z:	mm	265	265		240
θ_r (40 - 60 deg)	deg	40	42		
Rear tiedown length:					
x: on floor/on chair	mm	380/50	450/50	N/A	N/A
y: on floor/on chair	mm	330/450	330/460	clamp	clamp
z:	mm	240	330		
θ_r (30 -50 deg)	deg	32	32		
Occupant Restraint					
		double inertia reel	UNWIN	UNWIN	UNWIN
B pillar:					
Angle of shld belt: behind ATD shoulder:	deg	O ring 20	O ring 20	O ring 20	O ring 20
above ATD shoulder:	mm	230	230	230	230
x:	mm	20	20	20	20
y:	mm	270	350	270	380
z:	mm	330	330	330	330
	mm	1200	1200	1200	1200
Lap belt:					
		adult 4 pt harness	adult 4 pt harness	adult 4 pt harness	adult 4 pt harness
Angle of pelvic belt to horizontal	deg	50	40	50	50
Head front nose:					
		HYBRID II	HYBRID II	TNO-10	TNO-10
x: relative to target on sled (H _x)	mm	650	650	650	650
z:	mm	1110	1115	1150	1135
Knee target:					
x: relative to target on sled (K _x)	mm	240	250	260	190
z:	mm	605	610	555	555
Delta 'V'	km/h	49.1	49.8	49.1	49.5
peak g	g	20	20	20	20
stop distance	mm	471	514	474	495
Excursion (measured from video)					
X _{wc} (< 200)	mm	104.4	131.1		
X _{knee} (< 375)	mm	252.9	267.9		
X _{head} (< 650)	mm	423.2	387.8		
visual observations					
		dummy left arm broken; rear axle bending; seat down 70 mm; w/c back (pt) bend;	dummy left arm broken; rear axle bending; seat down 70 mm; w/c back (pt) bend; rear tiedown (pt) slipped 30 mm; panel >100g	w/c collapsed castor (st) broken down; castor tube cracked; seat bar broken; failed	w/c collapsed castor (st) broken down; castor tube cracked; seat bar broken;

Table 5A.7 Invacare wheelchair test results (05/97)

Invacare w/c	units	manual	manual	manual	power	power	power
Test No.		T3416	T3417	T3418	T3419	T3420	T3421
Wheelchair model		Action 2000	C54	Zipper	Phoenix	Storm XL	Comet
Mass	kg	20	20	13.2	50	106	50
Rear wheel pressure	kPa	447	447	no	276	no	276
Wheelbase	mm	370	410	450	450	455	415
Backrest angle to vertical	deg	8	8	8	8	8	8
Seat pan angle to horizontal	deg	8	8	8	8	8	8
Seat surface height (st. cross)-before	mm	415	470	455	465	480	420
after (Ave)		400	465	438	370	405	380
Rear wheel target:							
x: relative to target on sled (datum)	mm	780	772	866	880	860	935
z:	mm	300	305	155	145	165	150
P point target:							
x: relative to target on sled (P _i)	mm	780	743	754	763		837
z:	mm	-	510	490	505		475
Wheelchair Tiedown (4 pt QB20/2/CU1 heavy)							
Clamps or rear webbing length	mm	clamp	457	422	461	520	416
x: on floor/on chair	mm	120/110	345	250	255/80	470/115	250/80
y: on floor/on chair	mm	330/430	330/440	330/430	330/450	330/460	330/300
z:	mm	220	300	340	430	380	380
θ_r	deg	-	40	47	47	43	47
Front tiedown (2 double lock clamps Q- /ATF/DL/245/R)							
x			810/450	750/550	800/510	730/540	740/450
y			330/380	330/440	330/480	330/460	330/300
z			250	260	270	330	290
θ_r	deg		37	47	37	45	37
Occupant Restraint (3 pt double inertia QIP/34/WH)							
B pillar - x:	mm	350	350	260	250	280	200
B pillar - z:	mm	1210	1210	1210	1210	1210	1210
Lap belt - x	mm	367	350	240	250	250	250
Angle of pelvic belt to horizontal	deg	45	45	60	45	45	45
ATD Positioning							
		TNO-10	TNO-10	TNO-10	TNO-10	TNO-10	P10
Head front nose:							
x: relative to target on sled (H _x)	mm	650	650	794	670	585	903
z:	mm	1072	1150	1140	1130	1175	1040
Knee target:							
x: relative to target on sled (K _x)	mm	347	310	350	341	264	543
z	mm	560	595	570	610		618
Delta 'V'	km/h	51.2	49.7	50	49.2	48.2	50.2
peak g	g	25.3	22.7	25.3	24.1	25.0	23.1
stop distance	mm	492	510	519	495	-	502
Excursion (measured from video)							
X _{wc} (< 200)	mm						210
X _{knee} (< 375)	mm						372
X _{head} (< 650)	mm						319
visual observations		rear wheel punctured elamp collapsed	backrest collapsed	rear wheel punctured armrest broken	both wheel collapsed	come apart failed	rear wheel collapsed

Table 5A.8 SCN wheelchair test results (13/05/97)

SCN w/c	units	power	power	power	manual	manual	manual
Test/run No.		T3430/S1	T3431/S2	T3432/S3	T3433/S4	T3435/S5	T3436/S6
Wheelchair model		TORNADO	CORBIE	POPULAR	COMFORT	Al light 60333	Al light 60333
Mass	kg	68	80	52	40	15.8	20.5
Rear wheel pressure	kPa	276	207	276	345	447	447
Wheelbase	mm	470	460	470	410	420	410
Backrest angle to vertical	deg	5	5	5	5	8	5
Seat pan angle to horizontal	deg	15	15	15	15	15	10
Seat surface height (st)- before/after :	mm	530	560/550	470/460	525/520	50 mm cushion	470 440/425
Rear wheel target:							
x: relative to target on sled (datum)	mm	885	896	895	770	798	744
z:	mm	150	170	155	300	300	300
P point target :					FI		
x: relative to target on sled (P _x)	mm	814	694	755	610	798	700
z:	mm	570	605	505	610	555	510
Wheelchair tiedown:							
Rear webbing length	mm	442	539	445	467	517	492
x: on floor/on chair	mm	405/40	405/80	415/40	460/120	410/20	390/0
y: on floor/on chair	mm	330/420	330/330	330/380	330/380	330/420	330/40
z:	mm	250	430	240	320	340	300
θ _r	deg	33	36	32	45	38	40
Front tiedown							
x: on floor/on chair	mm	750/530	810/500	790/540	790/500	800/440	620/40
y: on floor/on chair	mm	330/440	330/420	330/450	330/550	330/440	330/40
z:	mm	250	270	270	270	270	250
θ _r	deg	46	36	43	42	36	42
B pillar							
x:	mm	260	290	240	370	430	390
z:	mm	1210	1210	1210	1210	1210	1210
Lap belt:							through back
x	mm	260	290	240	260	315	390
Angle of pelvic belt to horizontal	deg	60	60	60	60	55	46
ATD Positioning		TNO-10	TNO-10	TNO-10	TNO-10	H-II	H-II
Head Frt. nose:							
x: relative to target on sled (H _x)	mm	734	764	708	565	777	597
z:	mm	1240	1250	1160	1220	1230	1105
Knee target:							
x: relative to target on sled (K _x)	mm	353	286	344	210	354	178
z	mm	570	640	595	660	585	585
Delta 'V'	km/h	48.4	48.6	49.7	48.7	50.5	50.4
peak g	g	23.3	23.8	23.8	24	26.7	26.3
stop distance	mm	464	475	482	474	441	455
Excursion (measured from video)							
X _{wc} (< 200)	mm				110		87.6
X _{knee} (< 375)	mm				365		259.6
X _{head} (< 650)	mm				483		344
visual observations		lap broken battery off failed	stake buckle failed cushion down	St. armrest out pt back lie down passed	passed	dummy out lapbelt failed	pt leg off; dummy out failed

Appendix 5B: Interpretation of TRL Test Results

Test Series: Phase I, Phase II and Phase III

Set up: TRL surrogate wheelchair; 4-point surrogate webbing tiedowns, TNO-10 dummy, three sled pulse levels (Level I, Level II and Level III), Forward Facing Frontal (FFF) impact

Goals:

- To assess rigidity and durability of TRL surrogate wheelchair and occupant restraint loads by varying the rear tiedown angles
- To establish test procedures and CVS model

In the following tables and figures, FP represents front portside, FS is front starboard, RP is rear portside and RS is rear starboard.

Table 5B.1 Load differences between Level I and II (mean peak values) - Phase II

Set up	Units	WTORS (TRL W/C + TNO-10 dummy)					
		Level I			Level II		
Pulse levels		30-deg	45-deg	diff %	30-deg	45-deg	diff %
Rear tiedown angles		30-deg	45-deg	diff %	30-deg	45-deg	diff %
INPUT:							
Sled pulse	g	7.82	7.0	11.4	10.2	10.7	4.6
ΔV	km/h	25.7	25.7	0.1	25.6	25.6	0.2
OUTPUT:							
w/c FP wheel load	kN	2.97	2.86	3.8	6.75	5.94	12
w/c FS wheel load	kN	1.68	2.17	29.2	5.06	5.20	2.5
Single front floor loads	kN	2.30	2.51	16.5	5.91	5.57	7.3
w/c RP wheel load	kN	7.18	10.80	50.4	9.78	13.90	42.2
w/c RS wheel load	kN	5.31	7.96	50	8.17	11.83	44.8
Single rear wheel load	kN	6.25	9.40	50.2	8.97	12.87	43.5
RP tiedown	kN	2.80	3.54	25	4.50	5.57	23.7
RS tiedown	kN	2.74	2.77	1.1	4.10	4.71	14.6
single rear tiedown load	kN	2.78	3.15	13.1	4.30	5.14	19.2
L/D lap load	kN	2.65	3.28	23.4	4.10	5.16	25.8
L/D diagonal load	kN	3.88	3.92	0.8	5.80	6.25	7.9

**Table 5B.2 Load differences between WTS and WTORS
(mean peak values) - Phase III**

Parameters (peak)	Units	TEST RESULTS (Level III)					
		30-deg	45-deg	diff %	30-deg	45-deg	diff %
Set up conditions		WTS	WTS		WTORS	WTORS	
INPUT:							
Sled pulse	g	19.8	20.1	1.5	16.9	17.7	4.7
ΔV	km/h	32.7	32.8	0.3	31.5	31.4	0.3
OUTPUT:							
w/c FP wheel	kN	6.2	4.7	24.2	9.5	10.9	14.7
w/c FS wheel	kN	8.6	8.4	2.3	7.6	9.8	28.9
w/c RP wheel	kN	7.1	9.7	36.6	7.7	10.8	40.3
w/c RS wheel	kN	8.9	12.4	39.3	6.1	9.5	55.7
Single rear wheel	kN	8	11.1	38.8	6.9	10.2	47.8
Peak Time	ms	(120ms)	(110ms)		(105ms)	(100ms)	
RP tiedown	kN	6.5	7.4	13.8	6.6	7.4	12.1
RS tiedown	kN	6.5	6.6	1.5	6.5	6.0	7.7
Single rear tiedown	kN	6.5	7	7.7	6.5	6.5	3.1
Peak Time	ms	(110ms)	(110ms)		(110ms)	(100ms)	
L/D lap load	kN	#	#	#	6.3	6.9	9.5
L/D diagonal load	kN	#	#	#	9.1	9.1	1.1

Table 5B.3 Load differences among Level I, II and III

Parameters	Units	WTORS (45 degree rear tiedown angle)				
		Level I	Level II	Level III	I&II diff %	I&III diff %
Set up conditions						
Sled Pulses	g	7	10.7	17.7	52.9	152.9
Rear Wheel Loads	kN	9.4	12.8	10.2	36.2	8.5
Front Wheel Loads	kN	2.6	5.6	10.4	115.4	300

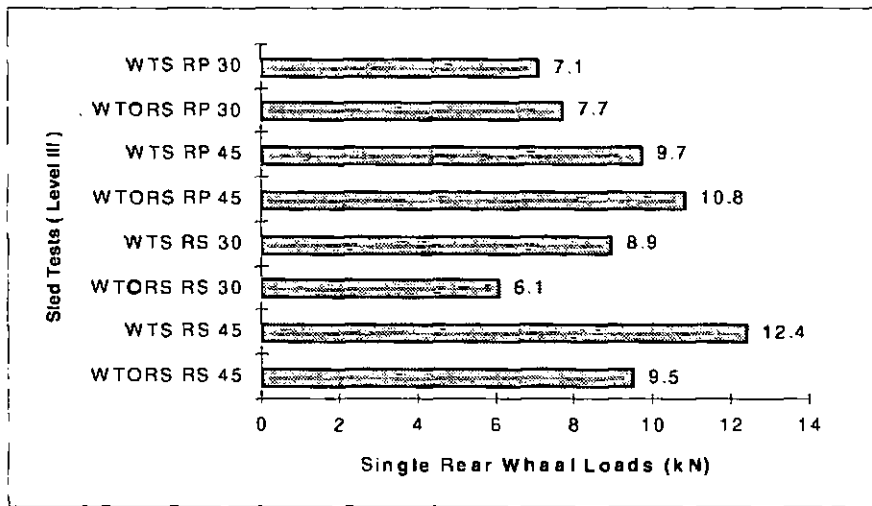


Figure 5B.1 Comparison of rear wheel loads in WTS/WTORS (Level III)

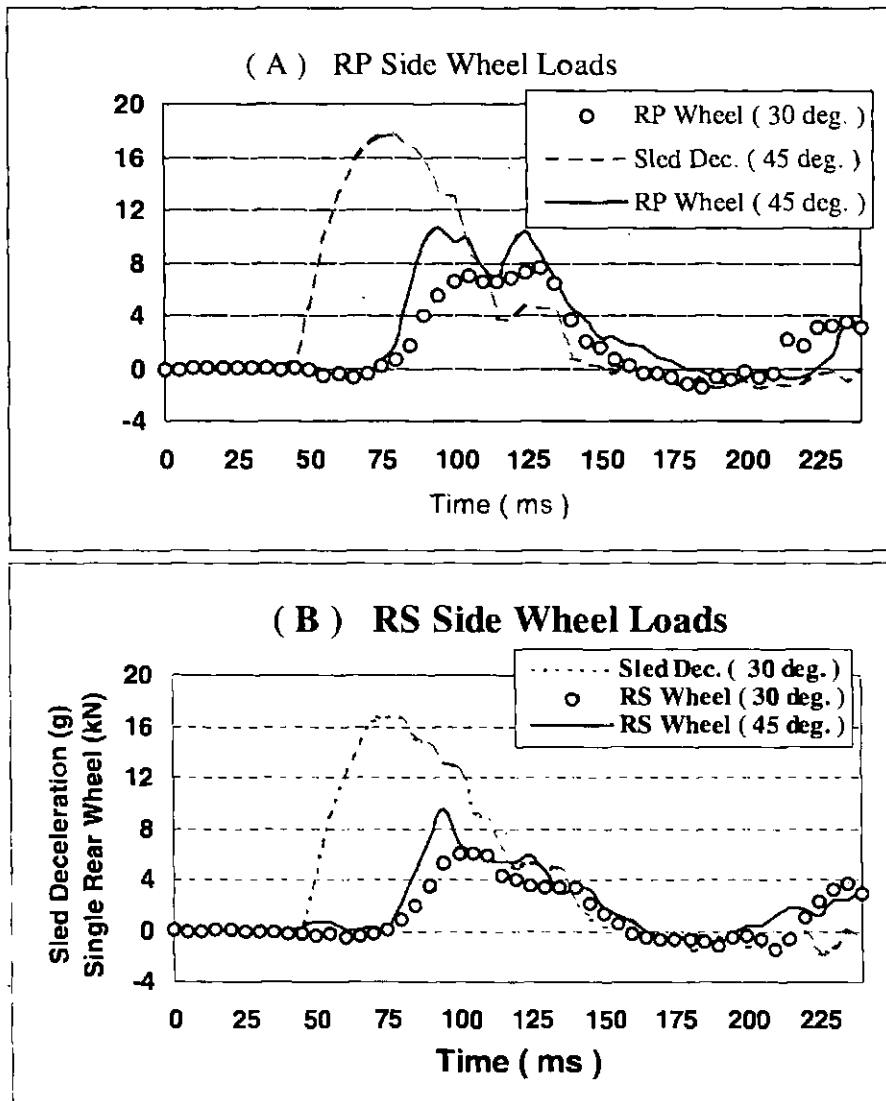


Figure 5B.2 Dynamic testing of rear wheel loads in WTORS (Level III)

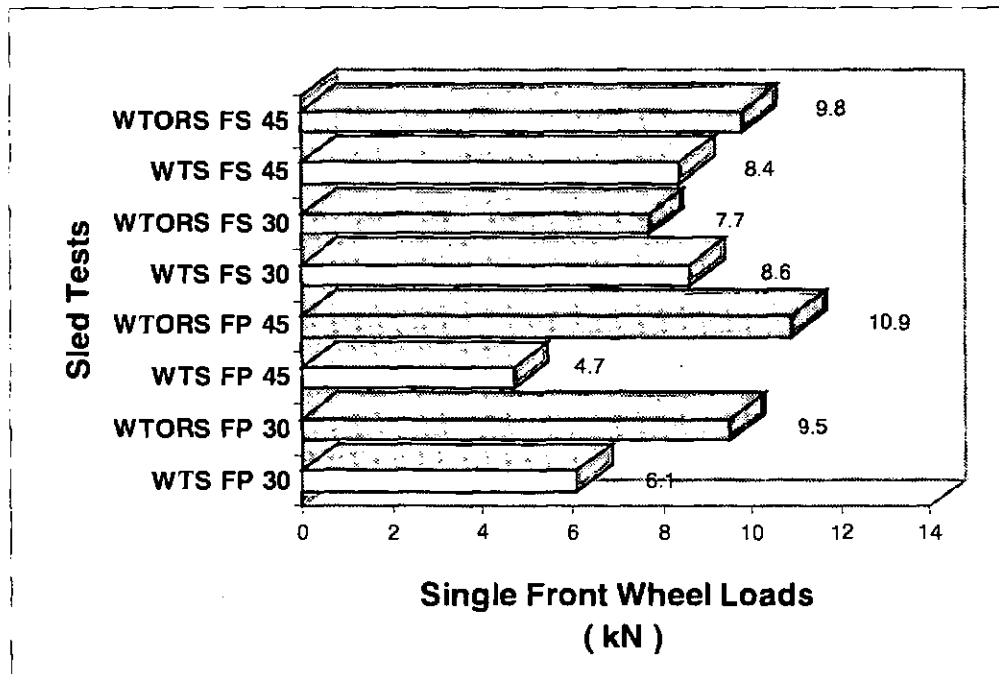


Figure 5B.3 Comparison of frontal wheel loads in WTS/WTORS (Level III)

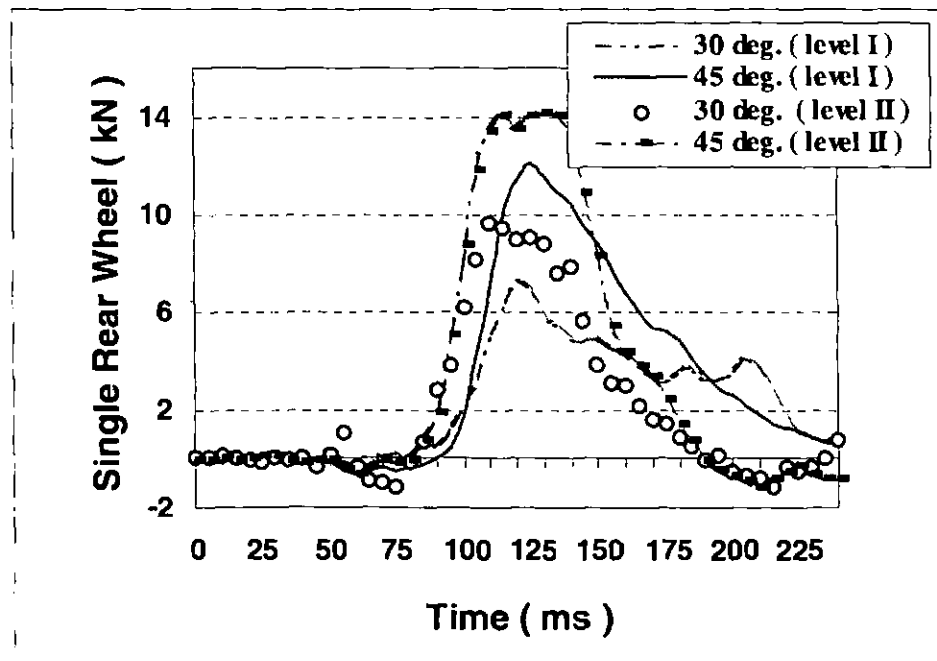


Figure 5B.4 Wheel load variation in WTORS as a function of crash pulses (Level I & II)

Appendix 5C: Interpretation of ISO Test Results

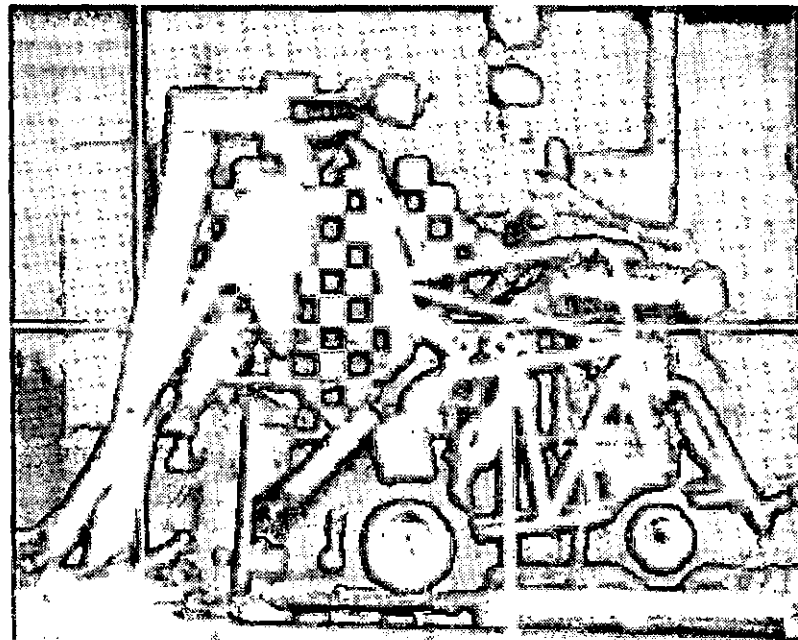
Test Series: Series I, II, and III

Set up: The pre-designed ISO Surrogate Wheelchair (SWC), TNO-10, Hybrid II dummy and surrogate tiedown restraint systems were used. It was varied by shoulder belt anchorage positions to investigate the effect on shoulder belt load on dummy responses.

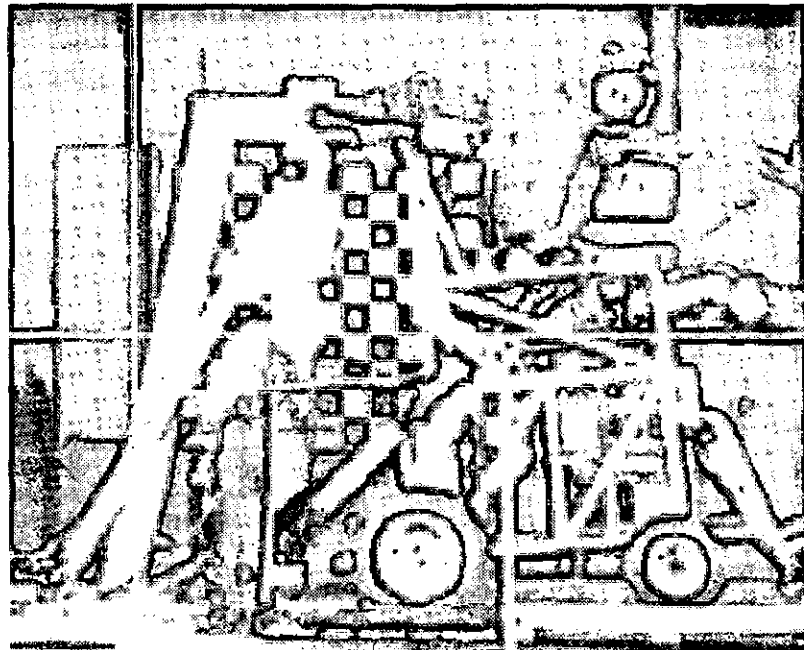
Goals:

- To determine the crashworthiness of ISO surrogate wheelchair in Forward Facing Frontal (FFF) impact.
- To develop regulations for FFF impact of wheelchair occupants

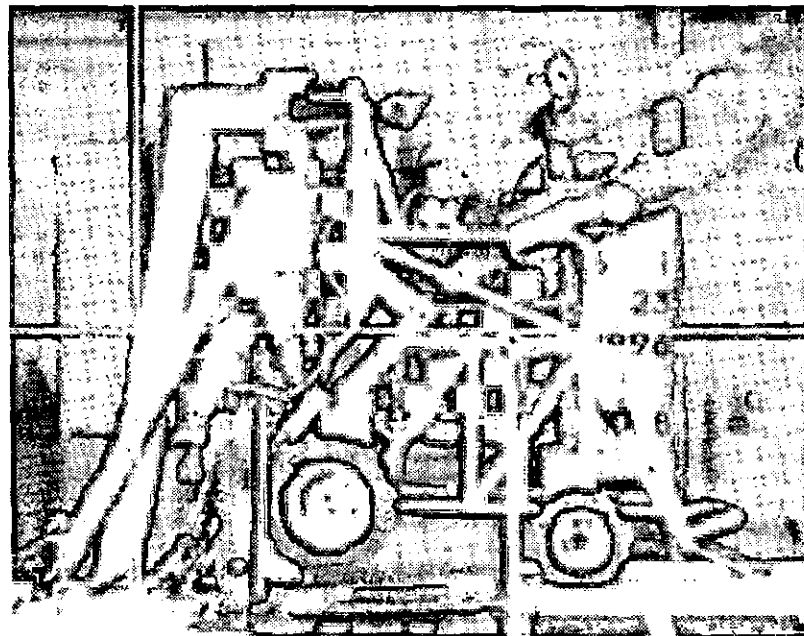
In ISO crash test, the sequence of motion was divided into the following three phases:



Phase 1 - The dummy slid across the seat plate essentially in the horizontal plane whilst the effect of the rear tiedowns was to compress the rear tyres and rotate the rear seat pancake load cells downwards. This was verified by the increasing of the loads monitored by the rear pancake load cells. The wheelchair front wheels lifted off the sled floorboard.



Phase 2 - The dummy continued to slide horizontally and loaded the occupant restraint straps whilst the wheelchair rear tyres recovered and the front wheels moved down onto the sled and compressed.



Phase 3 - The dummy reached its furthest forward movement, the tensions in the occupant restraint straps reached their maximum values, and weight transferred from the dummy to the front pancake load cells and the front wheels. Finally the cantilever load cells under the front wheels exhibited an increased value. And then the front tyres started to recover and rebound commenced.

A test protocol for WTORS testing was developed based on the results of twenty-five (25) sled tests. Tables 5C.1 and Table 5C.2 are summary for the ISO test results. The peak values are given for each parameter. The difference (diff %) indicates the deviation from B pillar to floor configuration expressed as a percentage. The values of front and rear seat are the total seat loads of two load cells on each side. The wheel sum is a total of the four appropriate wheel load plate transducers. The dynamic testing of Level III (B pillar configuration) concentrated on the investigation of the seat load distribution (Table 5C.3).

Table 5C.1 ISO test results (Level 1: 6 g, 15 km/h)

Configurations		B pillar	Floor	diff %
Parameters	units			
Chest Res.	g	12.23	11.40	6.8
T ₁	kN	2.50	3.10	24.0
T ₂	kN	1.70	1.40	17.6
T ₃	kN	1.86	1.32	29.0
Front seat	kN	4.04	3.20	20.8
Rear seat	kN	4.31	3.60	16.5
FP wheel	kN	1.70	4.90	188.2
FS wheel	kN	1.80	3.90	116.7
RP wheel	kN	11.40	10.80	5.3
RS wheel	kN	11.50	10.70	6.9
Wheel Sum	kN	26.40	30.30	14.8

Table 5C.2 ISO test results (Level II: 11 g, 27 km/h)

Configurations		B pillar	Floor	diff %
Parameter	units			
Chest Res.	g	21.40	19.00	11.2
T ₁	kN	4.10	4.50	9.7
T ₂	kN	3.00	2.10	30.0
T ₃	kN	3.38	3.27	3.3
Front seat	kN	6.01	5.80	3.5
Rear seat	kN	6.47	6.20	4.2
FP wheel	kN	2.30	4.70	104.4
FS wheel	kN	0.90	3.50	288.9
RP wheel	kN	23.30	22.70	2.6
RS wheel	kN	19.90	20.60	3.5
Wheel Sum	kN	46.40	51.50	11.0

Table 5C.3 ISO test results (Level III: 13 - 21 g, 34 - 51 km/h)

Delta ' V'	km/h	34	40	45	51
Sled pulse	g	13	16	17	21
OUTPUT:					
Chest Res.	g	49.10	34.00	39.94	46.6
T ₁	kN	4.77	5.41	5.98	6.5
T ₂	kN	3.78	4.38	4.65	5.0
T ₃	kN	4.10	4.90	5.20	6.1
FP seat	kN	4.80	5.10	6.50	7.7
FS seat	kN	5.90	5.80	6.60	8.3
RP seat	kN	3.90	4.40	5.40	5.9
RS seat	kN	3.40	4.40	4.10	4.5
Seat Sum	kN	18.00	19.70	22.60	26.4

Appendix 5D: Interpretation of Taxi Test Results

Test Series: Series I, II, III, IV, and V

Set up: The modified ISO Surrogate Wheelchair (SWC) and production wheelchairs, Hybrid II dummy and surrogate rear restraint systems were used. The structures of the wheelchair and headrest have been varied to investigate the effect on taxi bulkhead loads and dummy responses.

Goals:

- To determine the crashworthiness of wheelchair systems in the Rearward Facing Frontal Impact (RFF)
- To develop regulations for the carriage of rearward facing wheelchair occupants by taxi and contribute to the ISO standards.

Series I: Standard Manual Wheelchairs (without headrest)

Visual observation of the wheelchair and dummy movements at the moment of impact are reproduced in the following four phases at the crash severity Level V. Failure of the backrest and cushions in the wheelchair occurred on the starboard side. Slight deformation of the rear wheels of the wheelchair was also observed. The results from representative tests are shown in Table 5D.1.

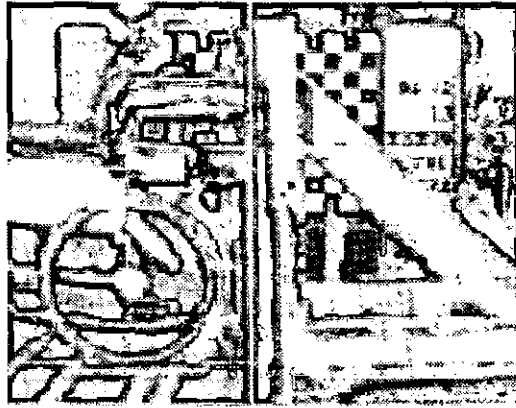
In the Table 5D.1:

Acc. head: peak resultant head acceleration filtered according to ISO standards

time: moment of impact at which maximum acceleration occurs

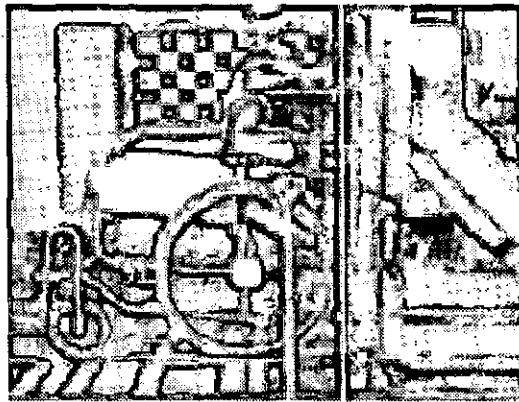
Bulkhead: the total loads acting on the taxi bulkhead. It is summed from both sides of the rear wheel loads and back support restraint loads, occurred at the same time.

Δa : the absolute values of the deviation between the peak resultant acceleration forces applied to the chest and head within 30 ms time period for a given input severity, $\Delta a = |a_{rc} - a_{rh}|$.



t=0 ms, starting of impact

Phase I: The clearance between the wheelchair handles and the vertical bulkhead was set at 300 mm. The backrest of the wheelchair was set against the transverse webbing belt and the rear wheels against the vertical load plates.



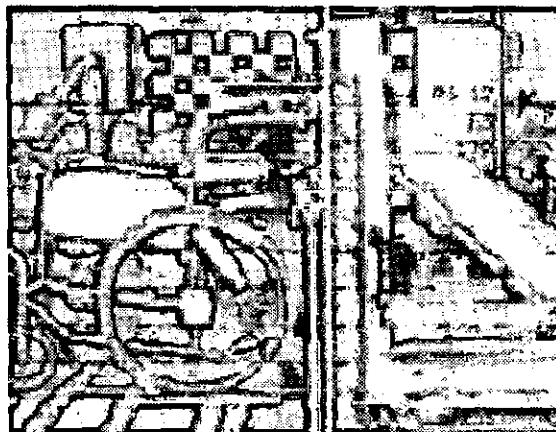
t=58 ms, rear wheel maximum deformed

Phase II: The wheelchair is found to tip upwards around the axle of the large wheels, causing the castors to rise approximately 53 mm off the floorboard. The castors turn approximately 20 degree from the portside (Pt.) to starboard (St.) after impact.



t= 96 ms, maximum excursions of head and knee

Phase III: Tipping of the wheelchair upwards causes the knees to rise. The thighs lift off the seat of the wheelchair and the feet lift off the footrests. The arms rise up from the armrests. The head and chest of the dummy are thrown forwards causing the wheelchair to rotate around the axis of the large wheels. The dummy's trajectory is up towards the wheelchair backrest, until it is in contact along the entire spinal column. The back of dummy and wheelchair are together pushed against the transverse-webbing belt. The webbing flexes by 50 mm at the horizontal level. Because the headrest was not put on the frame, the back of the dummy's head made a slight contact with the frame, causing the second peak value.



t=532 ms, head maximum movement. (rebound)

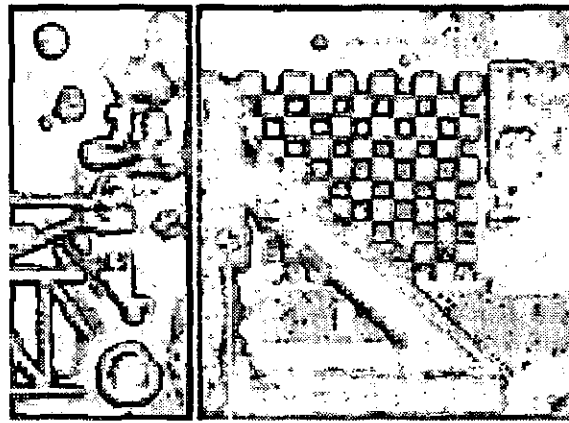
Phase IV (rebound phase): the legs and arms move rearwards, as the wheelchair rebounds.

Table 5D.1 Taxi test results (peak) - Series I

Series I	Unit	Level I	Level II	Level V
Sled pulse	g	11	13	21
ΔV	km/h	25	30	32
Acc. chest	g	32.3	55.5	72.9
time	ms	120	110	100
Acc. head	g	28.5	55.8	50.6
time	ms	130	130	115
Δa	g	3.8	0.3	22.3
Back (Pt.)	kN	3.2	3.5	3.8
time	ms	125	110	100
Back (St.)	kN	2.7	3.6	3.9
time	ms	125	120	100
Wheel Pt.	kN	7.7	8.2	13.2
time	ms	130	105	80
Wheel St.	kN	8.7	9.7	13.2
time	ms	125	105	80
Rear T/D	kN	1.5	3.7	5.3
time	ms	300	280	275
Bulkhead	kN	21.2	23.9	28.5
time	ms	130	105	105
Excursion:				
Wheelchair	mm.	11.9	36.9	61.5
Head	mm	196.5	190.5	281.8

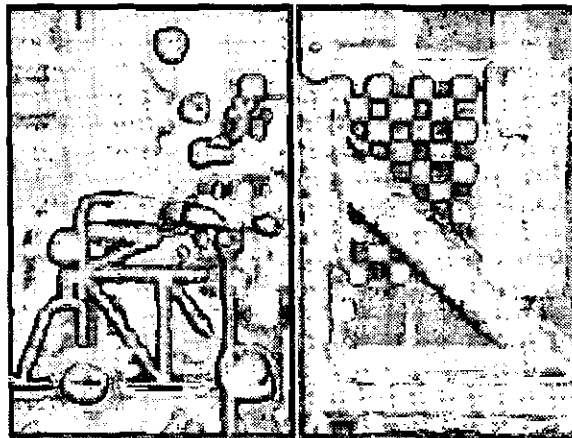
Series II: Modified ISO Surrogate Wheelchair (with headrest)

The performance of the wheelchair-occupant system is described in the following four phases (Level III: 32 km/h, 15g). Results from representative tests are shown in Table 5D.2.



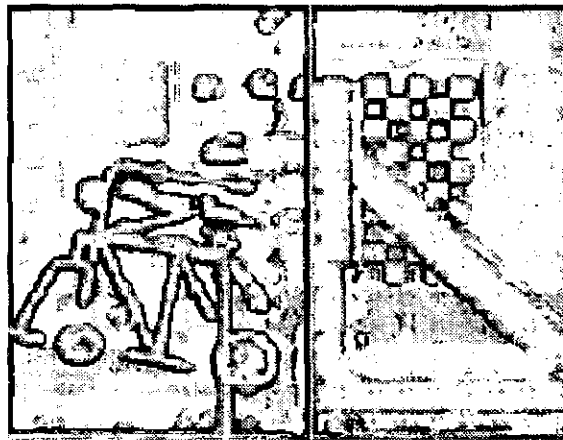
t=0 ms, starting of impact

Phase I: The clearance between the wheelchair handles and the vertical bulkhead was set at 280 mm. The backrest of the wheelchair was set against the transverse webbing belt and the rear wheels against the vertical load plates.



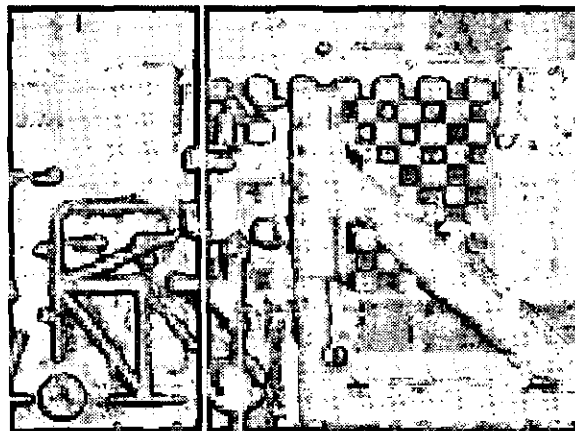
t= 55 ms, rear wheel maximum deformed

Phase II: forward rotation of the wheelchair occurs around the axis of the large wheels. The castors of the wheelchair rise 100 mm off the floor. The rigid wheel rims contact the load plate as a result of tyre compression during the impact.



t = 102 ms, head and knee maximum excursions

Phase III: the head hits the headrest causing it bend slightly. This mechanism seems to prevent the wheelchair from tipping over completely and thus stops the dummy from falling out forwards. The lower limbs of dummy and the front of the wheelchair continue to rise. The angle of the inclination of the wheelchair reaches 30 degree with respect to the horizontal. The feet lift off the footrests.



t = 552 ms, head maximum movement. (rebound)

Phase IV (rebound phase): the head slides off the headrest. The dummy slides to the front of the wheelchair.

Table 5D.2 Taxi test results (peak) - Series II

Series II	Unit	Level I	Level II	Level III	Level IV
Sled pulse	g	11	13	15	17
ΔV	km/h	32	32	32	32
Acc. chest	g	51.8	75.2	61.0	96
time	ms	120	120	110	110
Acc. head	g	51.2	57.6	37.3	50.1
time	ms	150	130	110	120
Δa	g	0.6	17.6	23.7	45.9
Back (Pt.)	kN	5.7	5.5	5.5	5.5
time	ms	120	125	115	105
Back (St.)	kN	2.8	3.1	3.0	3.3
time	ms	125	125	100	105
Wheel Pt.	kN	19.1	25.5	-	37.2
time	ms	100	90	-	90
Wheel St.	kN	17.1	25.7	33.7	-
time	ms	100	90	85	-
Rear T/D	kN	3.7	3.3	7.0	5.2
time	ms	190	170	165	170
Bulkhead	kN	51.1	55.3	58.1	59.9
time	ms	105	90	85	90
Excursion:					
Chair	mm	63.8	53.8	53.6	79.8
Knee	mm	162.5	152.8	170.8	189.9
Head	mm	355.1	328.1	299.1	367.5

Table 5D.3 Taxi test results (peak) - Series III

Series III	Unit	Level II	Level III	Level IV	Level V
Sled pulse	g	13	15	17	19
ΔV	km/h	33	33	33	33
Acc. chest	g	55.6	55.6	52.9	75.1
time	ms	105	95	100	100
Acc. head	g	58.1	59.7	58.9	75.8
time	ms	115	105	110	105
Δa	g	2.5	4.1	6	0.7
Back (Pt.)	kN	3.6	3.5	5.2	3.9
time	ms	105	105	110	100
Back (St.)	kN	2.2	2.5	2.2	2.6
time	ms	105	100	100	100
Wheel Pt.	kN	9.7	10.2	10.2	9.7
time	ms	85	115	110	105
Wheel St.	kN	7.7	10.8	11.9	10.9
time	ms	85	120	110	110
Rear T/D	kN	3.5	1.7	1.7	2.1
time	ms	265	185	190	265
Bulkhead	kN	23.5	25.6	28.5	25.5
time	ms	105	115	110	110

Series III: Standard Manual Wheelchair (with headrest)

Results from representative tests are shown in Table 5D.3.

Series IV and Series V: Modified Manual Wheelchair (with headrest)

In the test series IV, a modified manual wheelchair (without handles) was employed to further investigate the Δa , as a comparison with the results of series III. Data from representative tests of series IV are shown in Table 5D.4. The results from the test series V to investigate the ΔV effect on WTORS performance are shown in Table 5D.5.

Table 5D.4 Taxi test results (peak) - Series IV

Series IV	Unit	Level II	Level III	Level IV	Level V
Sled pulse	g	13	15	17	19
ΔV	km/h	33	33	33	33
Acc. chest	g	122.9*	127.5*	55.5	51.6
time	ms	110	115	105	105
Acc. head	g	56.7	79.3	65.7	75.7
time	ms	130	125	120	115
Δa	g	*	*	10.2	24.1
Back (Pt.)	kN	3.7	5.3	5.6	5.2
time	ms	110	105	110	120
Back (St.)	kN	2.7	3.6	3.5	3.3
time	ms	130	110	110	115
Wheel Pt.	kN	9.9	9.5	9.5	10.1
time	ms	115	80	105	115
Wheel St.	kN	9.5	8.7	10.3	10.7
time	ms	110	80	105	80
Rear T/D	kN	2.7	1.6	2.1	1.6
time	ms	165	220	265	170
Bulkhead	kN	25.7	19.2	27.9	25.2
time	ms	115	80	105	115

Notes: * test data failure

Table 5D.5 Taxi test results (peak) - Series V

Series V	Unit	Test 1	Test 2	Test 3	Test 4
Sled pulse ΔV	g	13	16	19	22
	km/h	21	25	29	33
Acc. chest time	g	53.0	38.5	85.5	77.9
	ms	135	120	105	95
Acc. head time	g	31.5	50.6	59.3	68.5
	ms	155	130	115	110
Back (Pt.) time	kN	3.9	5.1	3.7	3.9
	ms	150	120	120	100
Back (St.) time	kN	2.5	3.1	3.2	3.2
	ms	135	130	120	105
Wheel Pt. time	kN	3.9	8.8	9.2	11.7
	ms	130	120	85	100
Wheel St. time	kN	8.2	9.3	9.7	9.8
	ms	130	120	105	100
Rear T/D time	kN	2.3	2.9	3.5	3.7
	ms	175	165	150	150
Bulkhead time	kN	18.1	25.2	25.9	27.5
	ms	135	120	105	105
Excursion					
Chair	mm	21.0	-	21.1	15.9
Head	mm	238.3	-	268.9	275.5

Appendix 6: Dynamic Vibration Theory and Applications

A6.1 Vibration Systems

Most vibrations in mechanical impact structures are undesirable because the increased stresses and energy losses will accompany them. They should be eliminated or reduced as much as possible by appropriate design. A wheelchair occupant restraint system can be designed as a mechanical vibration system, which is displaced from a position of stable equilibrium during impact.

The analysis of vibration has become increasingly important in recent years due to the current trend toward higher speed impact and lighter structures. If the motion is maintained only by the restoring forces such as elastic forces or gravitational forces, the vibration is said to be a free vibration. When a periodic force is applied to the system, the resulting motion is described as a forced vibration. If the effects of friction could be neglected, the vibrations are said to be undamped. However, all vibrations are actually damped to some degree.

A6.2 Work-Energy Methods

Further to discussion of a spring-damper system, the fundamental definition of the work done change (dW) when a force (F) acts through a displacement change (du) is:

$$dW = -F \cdot du \quad F = k \cdot u \quad (A6.1)$$

$$W = \int_{u_1}^{u_2} (-ku) \cdot du = \frac{1}{2} \cdot m \cdot (u_1)^2 - \frac{1}{2} \cdot m \cdot (u_2)^2 \quad (A6.2)$$

where k is the spring constant, with the units of force per unit length.

The work of the elastic force depends only upon the initial and final deflections of the spring, $u = u_1$, $u = u_2$ (Figure 6A.1).

The potential energy (J), kinetic energy (K) and conservation of energy (W) are discussed as follows. The symbol J is used to represent the potential energy of a mass element. The change of the potential energy, ΔJ , is defined to be

$$\Delta J = J_2 - J_1 \quad (\text{A6.3})$$

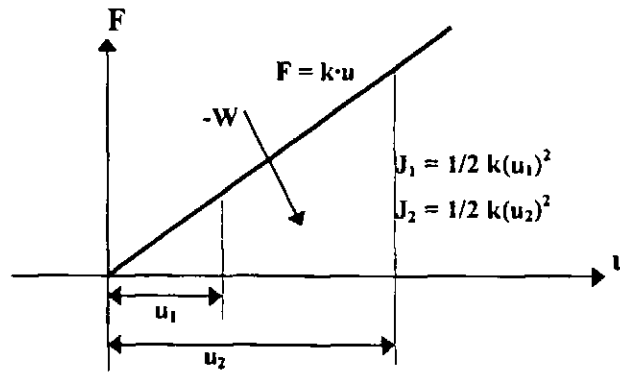


Figure 6A.1 The potential energy, J

where the subscripts 1 and 2 represent the initial and final endpoints of the interval of motion of interest respectively. One of the potential energy, the energy stored in a spring because of the deflection of this element, is defined in WTORS model. The following equation illustrates this effect. The change in the potential energy as the spring is stretched from 1 to 2 is

$$\Delta J = \frac{1}{2} \cdot k(u_2)^2 - \frac{1}{2} \cdot k(u_1)^2 \quad (\text{A6.4})$$

From Newton's second law in the tangential direction,

$$F = m \cdot (dv/dt) = mv (dv/du) \quad (\text{A6.5})$$

where v is the scalar magnitude of the velocity of the particle. The symbol K is used to designate the kinetic energy of the particle.

$$K = \int_{1 \rightarrow 2} F \cdot du = \frac{1}{2} \cdot m \cdot (v_2)^2 - \frac{1}{2} \cdot m \cdot (v_1)^2 \quad (\text{A6.6})$$

The work of the force is independent of the path followed and is equal to the sum of the changes in the potential energy and the kinetic energy. The force that satisfies this is said to be a conservative force.

We write

$$W = \Delta K + \Delta J = (K_2 - K_1) + (J_2 - J_1) = 0 \quad (\text{A6.7})$$

that is,

$$K_2 + J_2 = K_1 + J_1 \quad (\text{A6.8})$$

It indicates that when a system of particles moves under the action of conservative forces, the sum of the kinetic energy and of the potential energy of the system remains constant. The sum $K + J$ is called the total mechanical energy of the system and is denoted by E_M . In the example of sled impact, if the impact is perfectly plastic, $E_M = 0$, the sled and tube block move together after the impact.

A6.3 Wheelchair Impact Application

In effect the motion of wheelchair can be described as a damped forced vibration, where the tiedown restraint force occurs over a period of time and the system settles down into a steady state after an initial transient period, providing that the force is periodic.

During an impact the first period of a forced vibration is transient. The velocity and the acceleration could be obtained by differentiating the displacement equation once to attain velocity (v) and differentiating the velocity again to obtain acceleration. Even with no applied damping in the real world there will always be some friction and air resistance. The transient solution will die out.

The sled and TRL wheelchair impact results are interpreted in Figure 6A.2. The sled starts to decelerate approximately 35 ms before wheelchair evidence of the visco-elastic effects of the belt tiedown, which rear wheels of the wheelchair start to compress the load plates (about 75 ms). It can also be noticed that there is a pronounced second smaller peak for the wheelchair, this is the rebound value and can be attributed to the visco-elastic properties of the tiedown.

Theoretically the maximum load on the tiedown belts could occur at the same time as the peak acceleration of the wheelchair because it is at this point that the wheelchair can not move any forward.

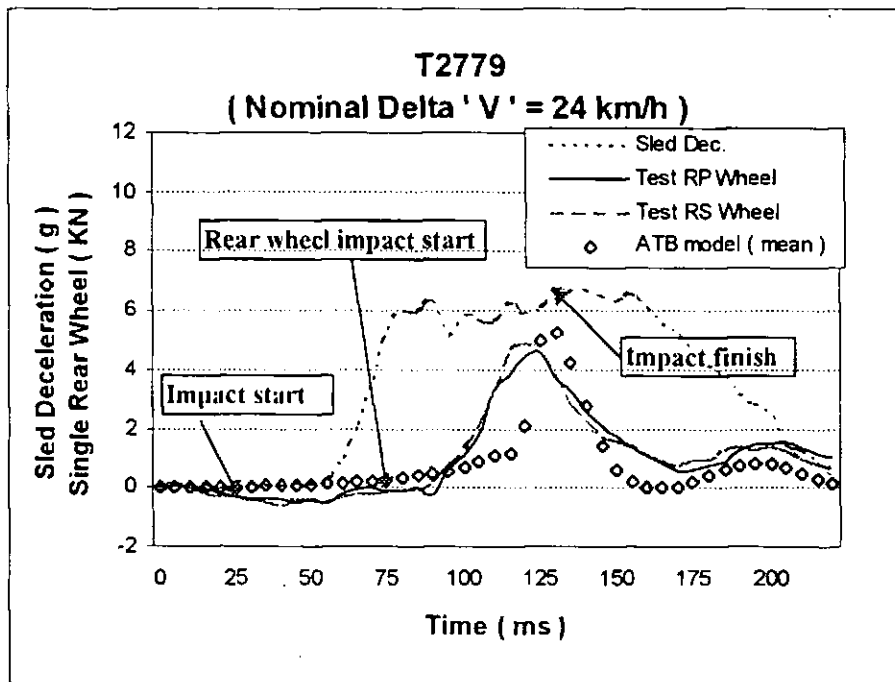


Figure 6A.2 Sled and TRL wheelchair impact

Appendix 7A: Running PAFEC and FEA Model Input Data

A7.1 Running PAFEC and Associated Programs

PAFEC program was developed by PAFEC Ltd, UK and run on the ALPHA system in Middlesex University. The OUT file contains all run results (10 phases) and error messages. Phase 1 in PAFEC model includes all about loads, material, PAFBLOCK, IN and OUT DRAW. Phase 6 tell you about mass and inertia, loads and moments. Phase 7 is about displacement for loadcases and displacement at nodes. Phase 9 is about principal stresses.

The PIGS postprocessor program runs both on a VAX station and a networked PC. In a networked PC, TCP on Telnet (Nevell TCP/IP Transport V4.2) was loaded and Exceed w4.1 was run. As the upper memory block (UMB) code space could not be allocated, RAM was relocated.

Data modules are stored on the backing store file (BS files) which could be retrieved by post-processor program, PIGS. The LOADCASE function key (FA) in PIGS was implemented to get the different loading results. The view angles (VS5) was selected x, y, z as 15,-15,1.5 to get 3D clear view. The analysis module (AN) was used to translate the model results. The post-process procedure was listed as follows:

AN3 → AN10 → FA1

In PIGS, the images were transferred into BS format file. The screen capture and Paintshop-Pro or Paintbrush programs were also used to transfer BS format into bitmap (BMP) files, which were pasted into document files.

A7.2 The Complete FEA Model Input Data

PAFBLOCK was used to generate elements with no more than one mid-side node. The complete finite element analysis of manual wheelchair model file is listed as follows:

** PAFBLOCK WHEELCHAIR FRAME STRUCTURE NON-LINEAR ANALYSIS-MODES DHSS 8L WHEELCHAIR: BRAZING VARIOUS PRE-SHAPED TUBULAR PARTS TO FORM A RIGID FRAMES (BS5568:1978)- - WRITTEN BY JUN GU. in 1996 **

CONTROL

SKIP.COLLAPSE

CONCATENATE.OUTPUT

FULL.CONTROL

PHASE=1,2,4,6,7,9

STOP

CONTROLEND

NODES

NODE.NUM X Y Z

1 0 0 0

2 3 0 0

3 .52 .095 0

4 .52 .16 0

5 .52 -.0045 0

6 .46328 .14672 0

7 .04172 .14672 0

8 .03 .27 0

9 0 .24 0

10 .03 3 0

11 .475 3 0

12 .03 .345 0

13 -.04355 .629 0

14 -.2 .652 0

15 0 .158 0

NODE=1-15 =16-30

16 0 0 .455

17 3 0 .455

18 .52 .095 .455

19 .52 .16 .455

20 .52 -.0045 .455

21 .46328 .14672 .455

22 .04172 .14672 .455

23 .03 .27 .455

24 0 .24 .455

25 .03 3 .455

26 .475 3 .455

27 .03 .345 .455

28 -.04355 .629 .455

29 -.2 .652 .455

30 0 .158 .455

NODE=31-35 CROSS

31 .224 0 0

32 .224 0 .455

33 .224 .15 .2275

34 .224 3 .435

35 .224 3 0.02

NODE=11(36, 38), 10 (37, 39)

36 .475 3 .02

37 .03 3 .02

38 .475 3 .435

39 .03 3 .435

40 -.12 0

41 -.12 0 .455

REAR WHEEL CENTRE

42 0 .158 -.05

43 0 .158 .505

44 .07 .135

45 .435 .135

46 .475 .175

47 .03 .175

48 .07 .135 .455

49 .435 .135 .455

50.475.175.455
51.03.175.455
52.475.3.02
53.03.3.02
54.475.3.435
55.03.3.435
56.435.175.0
57.07.175.0
58.435.175.455
59.07.175.455
60.-.10716.552.0
61.-.10716.552.455
62.-.009.571.0
63.-.10716.652.0
64.-.009.571.455
65.-.10716.652.455
66.225.158-.05
67.159.317-.05
68.0.383-.05
69.-.159.317-.05
70.-.225.158-.05
71.-.159-.001-.05
72.0-.067-.05
73.159-.001-.05
74.225.158.505
75.159.317.505
76.0.383.505
77.-.159.317.505
78.-.225.158.505
79.-.159-.001.505
80.0-.067.505
81.159-.001.505
82.52-.0045-.01
83.52-.0045.465
84.5825-.0045-.01
85.564.0395-.01
86.52.058-.01
87.476.0395-.01
88.4575-.0045-.01
89.476-.04869-.01
90.52-.067-.01
91.564-.04869-.01
92.5825-.0045.465
93.564.0392.465
94.52.058.465
95.476.0395.465
96.4576-.0045.465
97.476-.04869.465
98.52-.067.465
99.564-.04869.465
PAFBLOCK
TYPE=6
BLOCK ELEMENT TYPE PROPERTIES N1 TOPOLOGY
1 34000 1 1 1 31
2 34000 1 1 2 3
3 34000 3 1 3 6
4 34000 3 1 3 4
5 34000 3 1 4 5
6 34000 2 1 44 45
7 34000 2 1 46 11
8 34000 1 1 52 35
9 34000 2 1 12 10
10 34000 2 1 10 8
11 34000 2 1 8 9

12 34000 2 1 8 47
13 34000 2 1 15 1
FRONT ELEMENT FINE DEFINED
14 34000 2 3 12 62
15 34000 2 1 63 14
16 34000 2 1 9 15
17 34000 1 1 16 32
18 34000 1 1 17 18
19 34000 3 1 18 21
20 34000 3 1 18 19
21 34000 3 1 19 20
22 34000 2 1 48 49
23 34000 2 1 50 26
24 34000 1 1 34 54
25 34000 2 1 27 25
26 34000 2 1 25 23
27 34000 2 1 23 24
28 34000 2 1 23 51
FRONT ELEMENT FINE DEFINED
29 34000 2 3 30 16
30 34000 2 1 27 64
31 34000 2 1 65 29
32 34000 2 1 24 30
33 34000 1 1 31 2
34 34000 1 1 32 17
35 34000 1 1 35 53
36 34000 1 1 34 55
37 34000 4 1 31 33
38 34000 4 1 33 34
39 34000 4 1 33 35
40 34000 4 1 32 33
41 34000 1 1 1 40
42 34000 1 1 16 41
43 34100 5 1 15 42
44 34100 5 1 30 43
45 34100 1 1 11 36
46 34100 1 1 10 37
47 34100 1 1 26 38
48 34100 1 1 25 39
49 34300 6 1 45 6
50 34300 6 1 6 46
51 34300 7 1 44 7
52 34300 7 1 7 47
53 34300 8 1 49 21
54 34300 8 1 21 50
55 34300 9 1 48 22
56 34300 9 1 22 51
57 34300 10 1 62 13
58 34300 10 1 3 63
59 34300 11 1 64 28
60 34300 11 1 28 65
61 34300 12 1 66 67
62 34300 12 1 67 68
63 34300 12 1 68 69
64 34300 12 1 69 70
65 34300 12 1 70 71
66 34300 12 1 71 72
67 34300 12 1 72 73
68 34300 12 1 73 66
69 34300 13 1 74 75
70 34300 13 1 75 76
71 34300 13 1 76 77
72 34300 13 1 77 78
73 34300 13 1 78 79

74 34300 13 1 79 80
75 34300 13 1 80 81
76 34300 13 1 81 74
77 34300 14 1 84 85
78 34300 14 1 85 86
79 34300 14 1 86 87
80 34300 14 1 87 88
81 34300 14 1 88 89
82 34300 14 1 89 90
83 34300 14 1 90 91
84 34300 14 1 91 84
85 34300 15 1 92 93
86 34300 15 1 93 94
87 34300 15 1 94 95
88 34300 15 1 95 96
89 34300 15 1 96 97
90 34300 15 1 97 98
91 34300 15 1 98 99
92 34300 15 1 99 92
93 34000 5 1 5 82
94 34000 5 1 20 83
95 34000 5 1 82 84
96 34000 5 1 82 85
97 34000 5 1 82 86
98 34000 5 1 82 87
99 34000 5 1 82 88
100 34000 5 1 82 89
101 34000 5 1 82 90
102 34000 5 1 82 91
103 34000 5 1 83 92
104 34000 5 1 83 93
105 34000 5 1 83 94
106 34000 5 1 83 95
107 34000 5 1 83 96
108 34000 5 1 83 97
109 34000 5 1 83 98
110 34000 5 1 83 99
111 34000 5 1 42 66
112 34000 5 1 42 68
113 34000 5 1 42 70
114 34000 5 1 42 72
115 34000 5 1 43 74
116 34000 5 1 43 76
117 34000 5 1 43 78
118 34000 5 1 43 80
MESH
REFE SPAC.LIST
1 1
3 5
BEAMS
SECTION.NUM IYY IZZ AXIS.NUM BETA TORSIONAL.CONSTANT AREA NODE.NUM
1 .31E-8 .31E-8 0 90 .62E-8 .797E-4 0
2 .445E-8 .445E-8 0 90 .89E-8 .81E-4 0
3 1.69E-8 1.69E-8 0 90 3.38E-8 2.99E-4 0
4 1.25E-8 1.25E-8 0 90 3.38E-8 1.68E-4 0
5 .11E-8 .11E-8 0 90 .22E-8 .98E-4 0
6 .445E-8 .445E-8 0 0 .89E-8 .81E-4 56
7 .445E-8 .445E-8 0 0 .89E-8 .81E-4 57
8 .445E-8 .445E-8 0 0 .89E-8 .81E-4 58
9 .445E-8 .445E-8 0 0 .89E-8 .81E-4 59
10 .445E-8 .445E-8 0 0 .89E-8 .81E-4 60
11 .445E-8 .445E-8 0 0 .89E-8 .81E-4 61
12 .445E-8 .445E-8 0 0 .89E-8 .81E-4 62
13 .445E-8 .445E-8 0 0 .89E-8 .81E-4 63

```

14 .31E-8 .31E-8 0 0 .62E-8 .797E-4 82
15 .31E-8 .31E-8 0 0 .62E-8 .797E-4 83
AXES
AXISNO RELAXISNO TYPE NODE.NO ANGI ANG2 ANG3
TYPE=1 CARTESIAN AXIS SET USED IN THE SAME X DIRECTIONS; 2=CYLIND POLAR
16 1 1 31 0 -90 -45
17 1 1 32 0 -90 45
RESTRAINTS
NODE.NUM DIRECTION
15 23
30 23
42 23
43 23
5 23
20 23
82 23
83 23
MEMBER LOADS
ELEMENT.NUM LOAD.CASE TYPE DISTANCE DIRECTION ONE
CASE=1 UNIFORME DISTRIBUTION, IGNORE CROSS-BRACED SEAT SUPPORT MEMBER
8 1 1 0 2 -1200
35 1 1 0 2 -1900
24 1 1 0 2 -1200
36 1 1 0 2 -1900
CASE=2 THE WORSE CASE IN THE FRONT
8 2 0 0 2 -500
24 2 0 0 2 -500
CASE3 TO DETERMINE THE JOINTS WITH THE HIGHEST BENDING MOMENT SO THAT THESE
JOINTS ON THE REAL W/C COULD HAVE STRAIN GAUGE APPLIED TO THEM
NODE=FRONT 3,6,8 REAR BOTTOM 1,15
15 3 0 0 1 1200
31 3 0 0 1 1200
25 3 0 0 1 2400
9 3 0 0 1 2400
HINGES AND SLIDES
N1 N2 DIRECTION
36 52 123
37 53 123
38 54 123
39 55 123
GRAPH
FRAME=1
TOLERANCE=.1
GRAPH TYPE LIST
1 1 1-99
2 2 1-99
3 20 1-99
IN.DRAW
TYPE,NUM INFORMATION,NUM ORIENTATION
TYPE=3 SOLID BOUDARY, BROKEN INTERIOR
INF=1 NODE CIRCLES, 3=ELEMENT NUMS 5=RESTRAINT 9=ELEMENT MATERIAL PROPERTY
3 1359 4
OUT.DRAW
PLOT,TYPE CASE,NUM ORIENTATION
TYPE 1=DISPLACED SHAPE, 4=X,Y,Z COMPONENTS OF DISPLACEMENT AT ALL NODE
ORIENTATION=4 4 DIFFERENT VIEWS
143010 1 4
143010 2 4
143010 3 4
END.OF.DATA

```

Appendix 7B: Contact Characteristics in CVS Models

The input data for CVS model requires force functions for all of the contact interactions. In addition the joint in a system must have a stiffness function defined for all degrees of freedom of that joint. These functions could be estimated based on good knowledge of the subject. Some of the functions were measured experimentally in a quasi-static method. It has certain errors because the real crash is a dynamic situation. For accurate results some of the functions were obtained by finite element model calculations adjusted by functions from the published papers (Deng, et al, 1993). Since no structural separation was observed in WTORS sled test, the spring was assigned a higher stiffness.

The joint stiffness for the dummy system was included in the Hybrid II database as supplied by TNO with the MADYMO3D package. The force functions required to construct the model are as follows:

- *Adult seat belt stiffness*
- *Wheelchair tiedown stiffness*
- *Contact between dummy and wheelchair seat*
- *Wheelchair tyre stiffness*

7B.1 Adult seat belt and wheelchair tiedown stiffness

In order to measure adult seat belt (Figure 7B.1) and wheelchair tiedown webbing stiffness (Figure 7B.2), a standard Avery tensile test machine was used. Measurements of the elongation of a sample of 300 mm length webbing belt were taken at given load intervals and thus the force-extension functions were found. The static test results were adjusted by sled testing of WTORS, using physical measurement of webbing extension after impact and comparing with the certain video footage investigation. The CVS model input was also improved by individual model set-up. MADYMO models require the relative elongation of the function to be in terms of extension to the original length. The CVS model input force functions for the L/D seat belt are shown in Figure 7B.3 and 7B.4. As 4-belt rear tiedown configuration geometry

were designed in MADYMO model, the stiffness characteristics of each belt was considered about half values of the tiedown stiffness in the DYNAMAN models (Figure 7B.5 and 7B.6). The conventional belt model and a finite element belt model have been physically compared (Chapter 8).

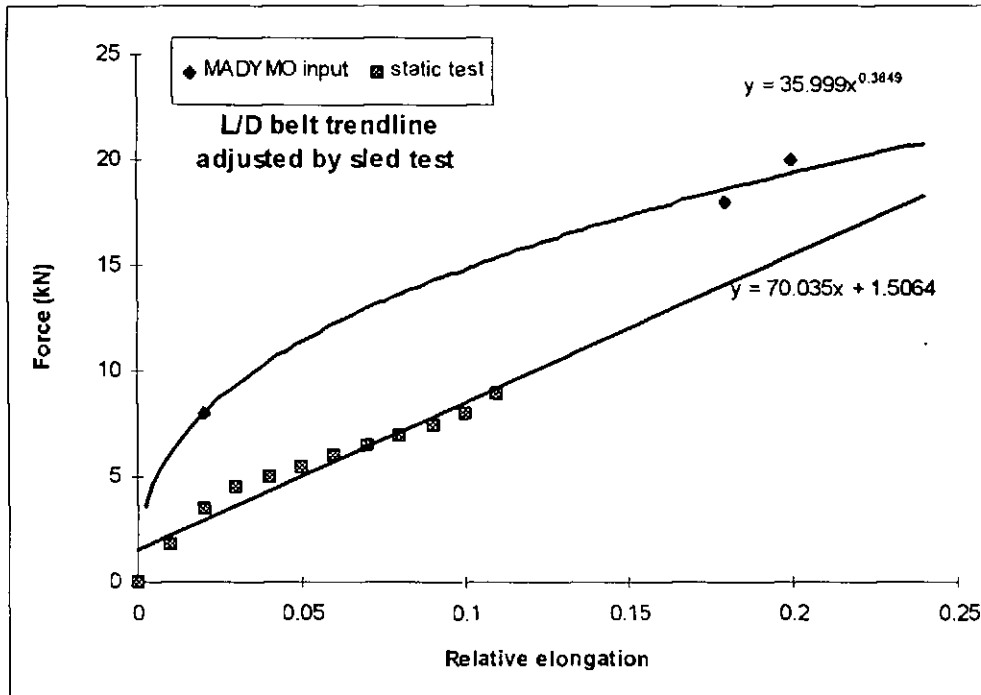


Figure 7B.1 L/D seat belt characteristics

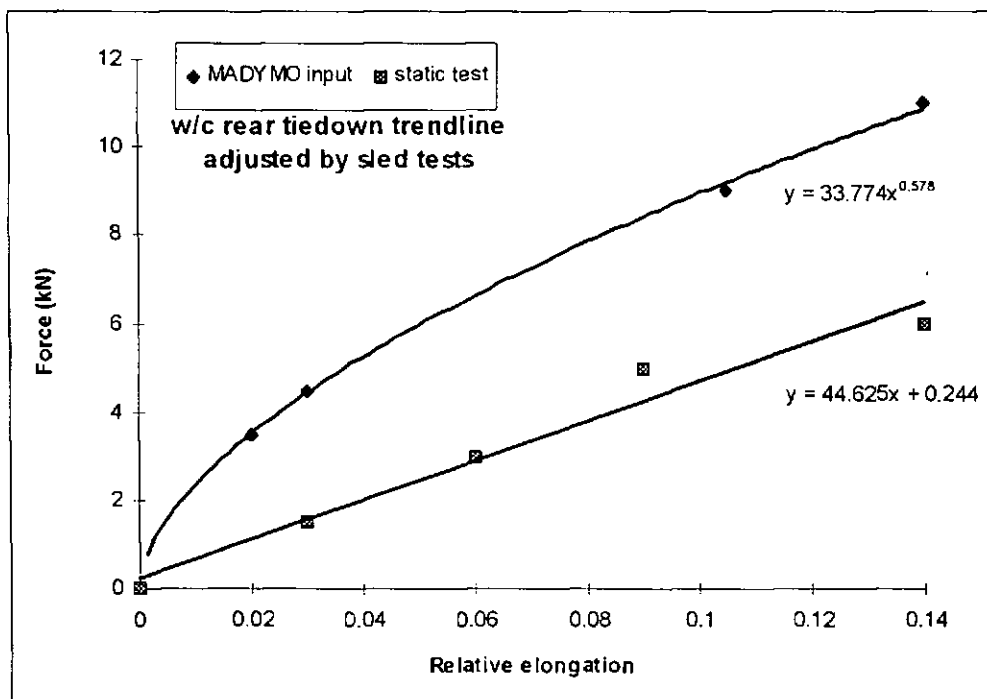


Figure 7B.2 Wheelchair tiedown characteristics

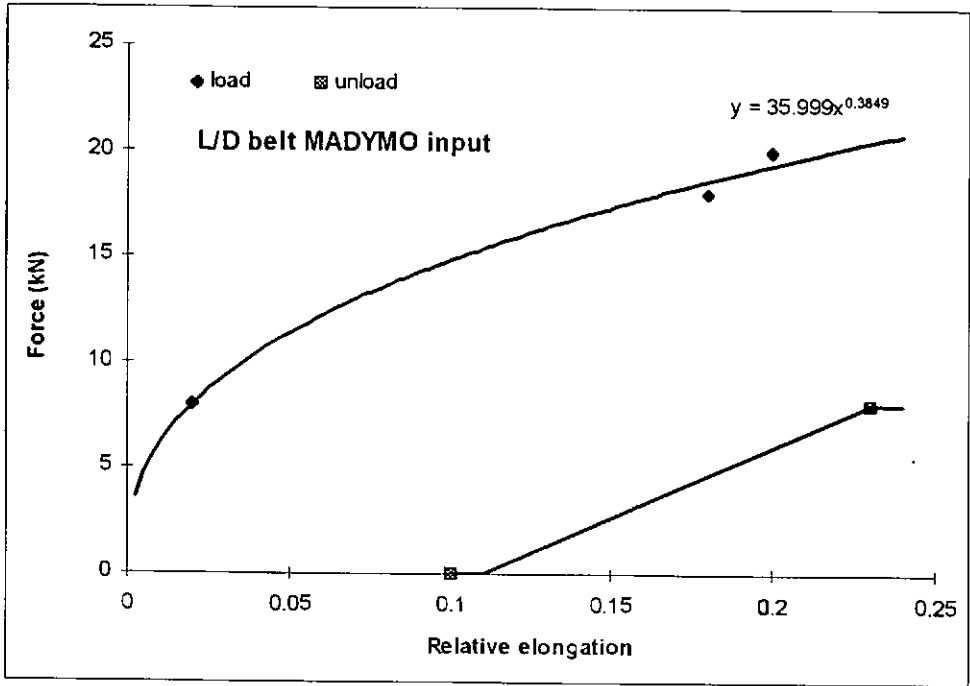


Figure 7B.3 L/D seat belt MADYMO input

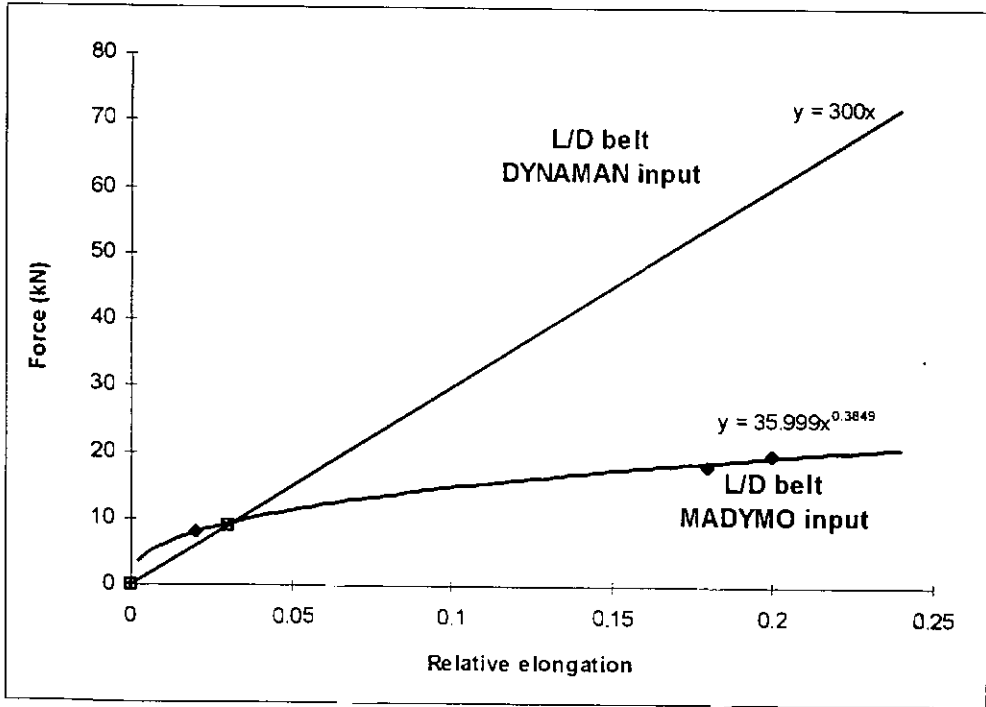


Figure 7B.4 L/D seat belt DYNAMAN input

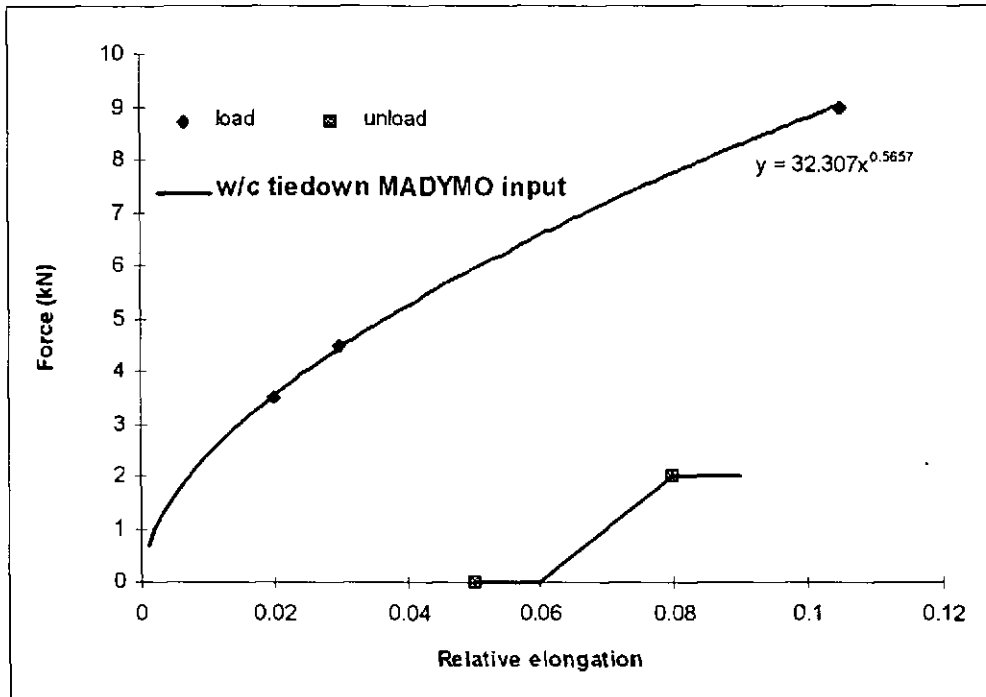


Figure 7B.5 Wheelchair tiedown MADYMO input

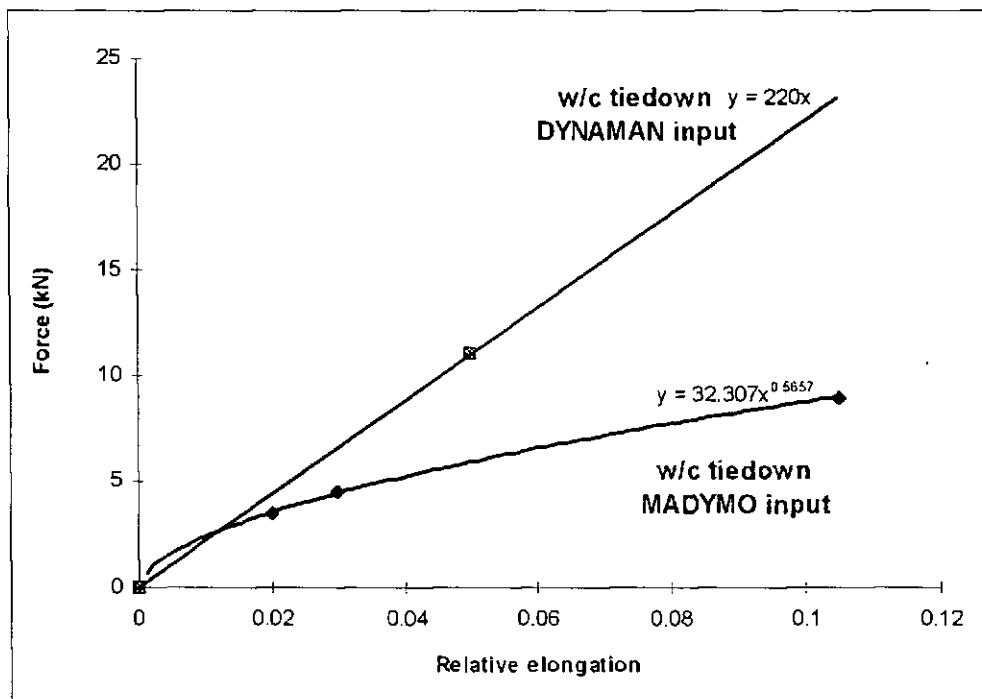


Figure 7B.6 Wheelchair tiedown DYNAMAN input

7B.2 Contact between the dummy and wheelchair seat

Contact occurs at the bearing area between the dummy at the lower torso/upper leg and wheelchair seat interface. In order to gain a reasonably accurate measurement of the contact function at this area it is necessary to load (quasi-static) either the wheelchair or the dummy. In the taxi model, the manual wheelchair was loaded by the actual dummy using an object of similar bearing area to the dummy. The test methodology was to load an area of the chair seat, where the dummy was thought likely to contact, with static load provided in the form of an increasing number of finite weights. The deflection of the seat was measured using a dial gauge placed at under the seat at the centre of the load. In the ISO model, the surrogate wheelchair seat contact was estimated to be stiffer. The results of this estimation were correlated by seat gauge plates (pancake type load cells) in dynamic modelling of ISO model (Chapter 9).

7B.3 Wheelchair tyre stiffness

In order to ensure a suitable crashworthiness for WTORS, the proposed ISO standard (ISO/CD 10542-1:1995E) specifies that the ISO surrogate wheelchairs 'have pneumatic front tires that, when inflated to 759 kN/m^2 (7.59 bar), have a diameter of 230 +/-10 mm, a width of 75 +/- 5 mm, and a sidewall height of 54 +/- 5 mm, have pneumatic rear tires that, when inflated to 414 kN/m^2 (414 kPa), have a diameter of 325 +/- 10 mm, a width of 100 +/- 10 mm, and sidewall height of 70 +/- 5 mm, include hard rubber stops located inboard of each rear wheel to limit rear tire compression to 45 +/- 5 mm during the frontal impact test'.

Before performing the following static test the wheels were inflated to the specified pressure using a foot pump, rear tyre 410 kN/m^2 , a sidewall height measured 65 mm, frontal tyre 720 kN/m^2 , a sidewall height measured 50 mm. The force function was initially estimated by experiment in a quasi-static method and then modified using dynamic sled tests and CVS models. The apparatus used in this programme was:

1) Avery compressive test machine (Model 7108 DCN, Max. 60 kN)

Range: 0 - 2400 N in 10 N divisions

2) A dial test indicator (DTI)

Range: 0 - 30 mm, 1 revolution = 0.2 mm with 0.002 mm divisions

3) A magnetic stand (MERCER Series 590)

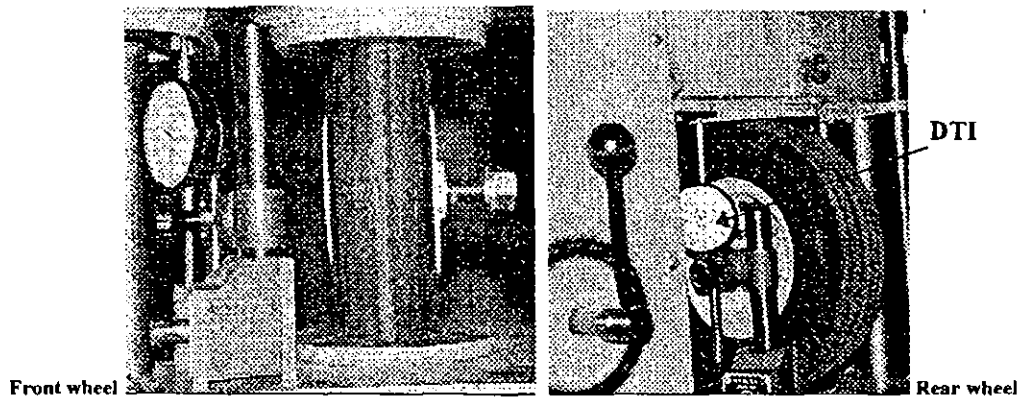


Figure 7B.7 Static testing of wheelchair tyres

After checking that all the apparatus was functionally correctly, the compressive machine was set to a given range. The DTI was mounted on the magnetic stand. The wheel was placed between the compression plates of the test machine. The upper plate lowered down to touch the wheel's upper surface (Figure 7B.7). The DTI was set to zero. The wheel was then loaded in increment of 40 N. The rear wheel of ISO Surrogate Wheelchair (ISO-SWC) was compressed in two steps. The first step was up to 1000 N and the second was up to 1760 N (Table 7B).

The static test was carried out both the front and rear wheels of the ISO surrogate wheelchair. The rear wheel stiffness was found to be 52 kN/m from Figure 7B.8. This is the result under the condition of two-point contact. In the real contact with sled floorboard, only one point contact was found during impact. Thus approximately double value of rear wheel stiffness (90 kN/m) was initially used to produce the function block for the rear wheel model, and then tuned by dynamic tests by adding the deflection/force data: 55 mm/50 kN to account for the wheel rim contacted to the floorboard. The frontal tyre of the wheelchair was compressed in an Avery compressive test machine up to 1600 N. The front wheel stiffness was assumed about 25% higher than the rear one as the diameter of the front tyre is about three-fourth of the rear one in ISO wheelchair. It should be noted that this is only point contact and the bearing area contact condition should be used in contact algorithm in MADYMO3D or simulated using finite element model.

Table 7B Wheel compressive test results

TRL rear wheels			ISO wheels (1st step)		ISO wheels (2nd step)		
	Load	Unload	ISO/RW	ISO/FW		ISO/RW	ISO/FW
Force	Deflection	Deflection	Deflection	Deflection	Force	Deflection	Deflection
(N)	(mm)	(mm)	(mm)	(mm)	(N)	(mm)	(mm)
0	0	0	0	0	1040	24.23	20.39
40	3.62	3.66	4.03	1.87	1080	25.25	20.9
80	7.56	6.01	4.75	3.06	1120	26.1	21.62
120	9.39	8.2	6	4.15	1160	27.18	22.13
160	10.95	10.08	7.18	5.29	1200	28.49	22.75
200	12.25	11.68	8.15	6.04	1240	29.03	23.34
240	13.55	13.53	8.99	7.02	1280	29.66	23.85
280	14.86	15.04	9.59	8.01	1320	30.32	24.5
320	16.23	16.39	10.31	8.85	1360	31.06	25.21
360	17.43	17.83	10.93	9.78	1400	31.66	25.55
400	18.65	19.32	12.63	10.49	1440	32.45	25.98
440	19.83	20.51	12.73	11.22	1480	33.22	26.62
480	20.94	21.74	12.88	11.74	1520	33.96	26.85
520	22.12	23.04	13.03	12.44	1560	34.78	26.85
560	23.27	24.23	13.69	12.98	1600	35.58	26.85
600	24.36	25.36	14.31	13.62	1640	36.4	
640	25.58	26.42	15.08	14.3	1680	37.26	
680	26.52	27.61	15.88	14.88	1720	38.3	
720	27.73	28.59	16.68	15.46	1760	39.05	
760	28.88	29.96	17.37	16.09			
800	30.14	30.58	18.18	16.67			
840	31.5	31.55	19.06	17.2			
880	32.67	32.54	20.02	17.81			
920	33.79	33.52	20.64	18.45			
960	35.01	34.41	21.82	18.95			
1000	36.22	36.22	23.98	19.76			

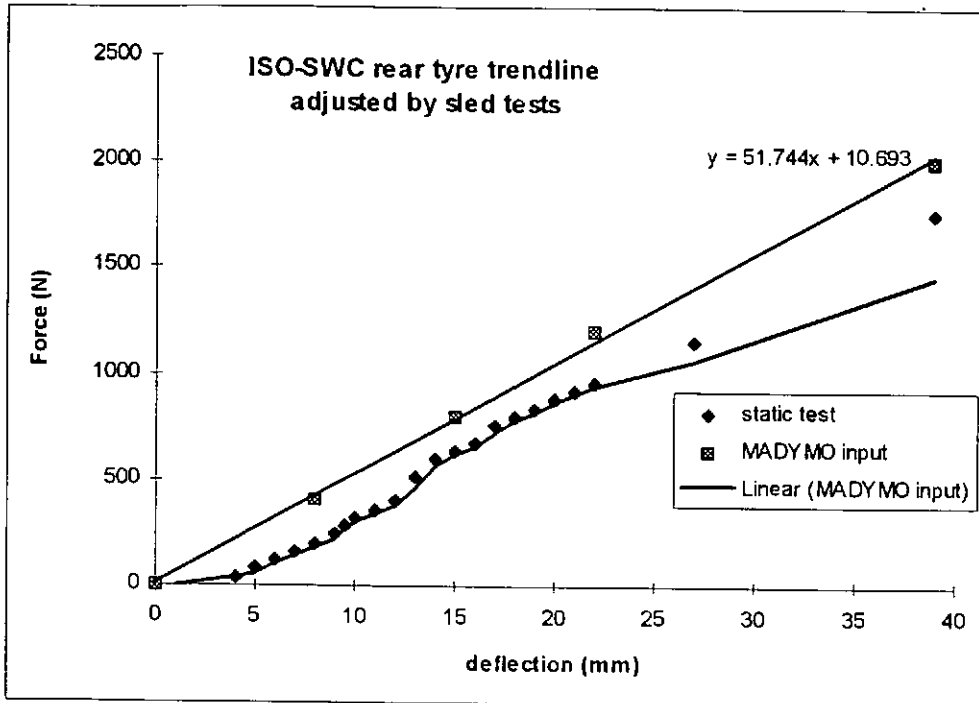


Figure 7B.8 Wheelchair stiffness in ISO surrogate wheelchair

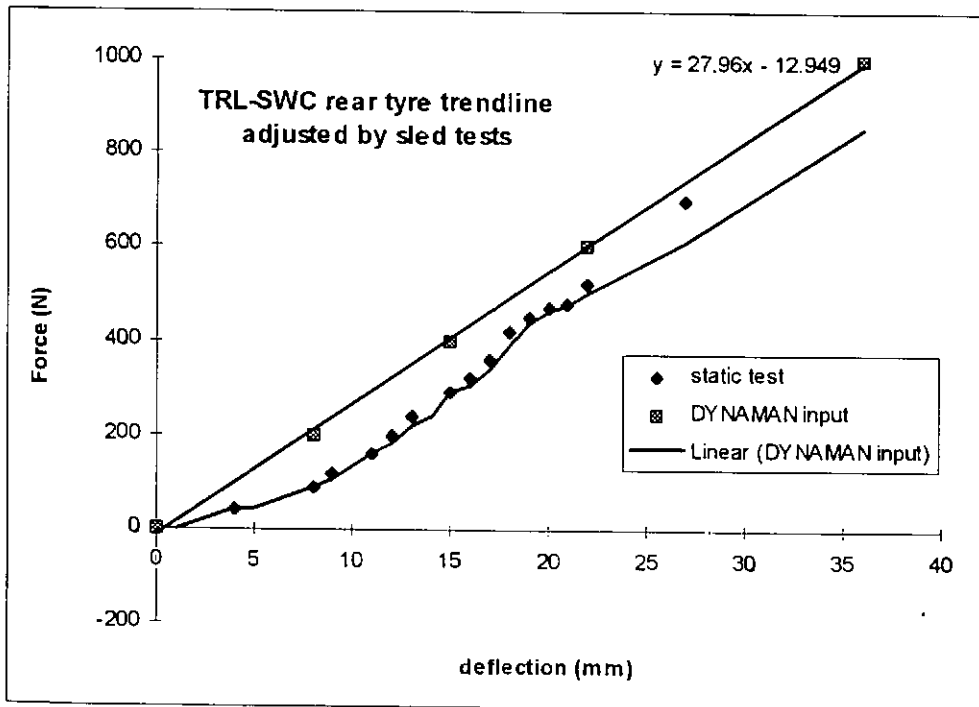


Figure 7B.9 Wheelchair stiffness in TRL surrogate wheelchair

The TRL prototype surrogate wheelchair (TRL-SWC) was manufactured by Transport Research Laboratory (TRL), UK. The TRL wheelchair rear wheels were also compressed in the same way and the results are shown in Figure 7B.9 and Table 7B. Concerning of the dynamic impact facts, the DYNAMAN tyre contact function was adjusted by adding three sets of deflection/force data: 45 mm/10 kN, 50 mm/15 kN and 55 mm/27 kN.

It was found from sled test results that the value of rear wheel stiffness had a significant effect on the floor reaction force. Therefore a correlation of stiffness between static and the dynamic loading is necessary to improve the CVS models. In addition to the wheel stiffness the damping coefficient was also specified in CVS models.

WH1 5.0000.05000.50000.050006.30001.00006.3000.00000.00000.00000 0
 WH2 5.0000.05000.50000.050006.30001.00006.3000.00000.00000.00000 0
 WH3 2.0000.01000.20000.010003.7400.400003.7400.00000.00000.00000 0
 WH4 2.0000.01000.20000.010003.7400.400003.7400.00000.00000.00000 0
 ANC1 5.E-0510E-0610E-0610E-065.E-055.E-055.E-05.00000.00000.00000 0
 ANC2 5.E-0510E-0610E-0610E-065.E-055.E-055.E-05.00000.00000.00000 0
 ANC3 5.E-0510E-0610E-0610E-065.E-055.E-055.E-05.00000.00000.00000 0
 ANC4 5.E-0510E-0610E-0610E-065.E-055.E-055.E-05.00000.00000.00000 0
 P 1 -4-2.150.00000-1.660-.3500.000002.5600 0.00000.00000 B.3
 .00000.00000.00000.00000.00000.00000.00000.00000.00000 3 2 1 3 2 1
 W 2 -4-.3500.00000-2.560-.8900.000005.8500 0.00000.00000
 .00000.00000.00000.00000.00000.00000.00000.00000.00000 3 2 1 3 2 1
 CU 3 -4.00000.00000-.1000.00000.00000.10000 0.00000.00000
 .00000.00000.00000.00000.00000.00000.00000.00000.00000 3 2 1 3 2 1
 NP 4 0.00000.00000-5.760.00000.000002.7600 0.00000.00000
 .00000-10.000000.00000.00000.00000.00000.00000.00000.00000 3 2 1 3 2 1
 HP 5 0.00000.00000-1.340-.5500.000003.5000 0.00000.00000
 .00000.00000.00000.00000.00000.00000.00000.00000.00000 3 2 1 3 2 1
 RH 1 1-.11003.15001.2400.00000.00000-9.960 0.00000.00000
 .00000090.000.00000.00000.00000.00000.00000.00000.00000 3 2 1 3 2 1
 LH 1 1-.1100-3.1501.2400.00000.00000-9.960 0.00000.00000
 .00000090.000.00000.00000.00000.00000.00000.00000.00000 3 2 1 3 2 1
 MK 8 1.000003.15006.5600-.2000.00000-6.740 0.00000.00000
 .00000.00000.00000.0000055.000.00000.00000.00000.00000 3 2 1 3 2 1
 RS 4 -41.00007.3800-2.660.00000.00000-5.430 0.00000.00000
 .00000090.000.00000.00000.00000.00000.00000.00000.00000 3 2 1 3 2 1
 LS 4 -41.0000-7.380-2.660.00000.00000-5.430 0.00000.00000
 .00000090.000.00000.00000.00000.00000.00000.00000.00000 3 2 1 3 2 1
 NN1 0 0.00000.00000.00000.00000.00000.00000 0.00000.00000
 .00000.00000.00000.00000.00000.00000.00000.00000.00000 3 2 1 3 2 1
 C1S1 12 -41.50009.0000-12.95.00000.00000.00000 0.00000.00000
 .00000.00000.00000.00000.00000.00000.00000.00000.00000 3 2 1 3 2 1
 C2S3 12 -417.50009.0000-13.95.00000.00000.00000 0.00000.00000
 .00000.00000.00000.00000.00000.00000.00000.00000.00000 3 2 1 3 2 1
 c3p1 12 -41.5000-9.000-12.95.00000.00000.00000 0.00000.00000
 .00000.00000.00000.00000.00000.00000.00000.00000.00000 3 2 1 3 2 1
 B1B4 12 -4-1.6509.0000-32.00.00000.00000.00000 0.00000.00000
 .00000.00000.00000.00000.00000.00000.00000.00000.00000 3 2 1 3 2 1
 B2S4 12 -4.39009.0000-20.00.00000.00000.00000 0.00000.00000
 .00000.00000.00000.00000.00000.00000.00000.00000.00000 3 2 1 3 2 1
 B3P4 12 -4.39000-9.000-20.00.00000.00000.00000 0.00000.00000
 .00000.00000.00000.00000.00000.00000.00000.00000.00000 3 2 1 3 2 1
 B4B3 12 -4-1.650-9.000-32.00.00000.00000.00000 0.00000.00000
 .00000.00000.00000.00000.00000.00000.00000.00000.00000 3 2 1 3 2 1
 psp1 12 -42.0000-9.000-3.500.00000.00000.00000 0.00000.00000
 .00000.00000.00000.00000.00000.00000.00000.00000.00000 3 2 1 3 2 1
 P12 12 -42.0000-9.000-3.500.00000.00000.00000 0.00000.00000
 .00000.00000.00000.00000.00000.00000.00000.00000.00000 3 2 1 3 2 1
 P23 12 -418.000-9.000-4.500.00000.00000.00000 0.00000.00000
 .00000.00000.00000.00000.00000.00000.00000.00000.00000 3 2 1 3 2 1
 P34 12 -416.000-9.000-20.50.00000.00000.00000 0.00000.00000
 .00000.00000.00000.00000.00000.00000.00000.00000.00000 3 2 1 3 2 1
 P2PS 12 -42.0000-9.000-3.500.00000.00000.00000 0.00000.00000
 .00000-10.00.00000.00000.00000.00000.00000.00000.00000 3 2 1 3 2 1
 PS1S 12 -418.0009.0000-4.500.00000.00000.00000 0.00000.00000
 .00000.00000.00000.00000.00000.00000.00000.00000.00000 3 2 1 3 2 1
 PSS2 12 -42.00009.0000-3.500.00000.00000.00000 0.00000.00000
 .00000.00000.00000.00000.00000.00000.00000.00000.00000 3 2 1 3 2 1
 S12 12 -4.570009.0000-3.500.00000.00000.00000 0.00000.00000
 .00000090.000.00000.00000.00000.00000.00000.00000.00000 3 2 1 3 2 1
 S23 12 -418.0009.0000-4.500.00000.00000.00000 0.00000.00000
 .00000.00000.00000.0000055.000.00000.00000.00000.00000 3 2 1 3 2 1
 S34 12 -416.0009.0000-20.50.00000.00000.00000 0.00000.00000
 90.000.00000.0000090.000.00000.00000.00000.00000.00000 3 2 1 3 2 1

0.000000	22.440000	-1.770000			
69.000000	-22.440000	-1.770000			
3 FOOTREST-S	0 0		D.2		
26.000000	9.000000	0.4375690			
26.000000	1.000000	0.4375690			
33.000000	9.000000	-1.053431			
4 FOOTREST-P	0 0		D.2		
26.000000	-9.000000	0.4375690			
26.000000	-1.000000	0.4375690			
33.000000	-9.000000	-1.053431			
5 SEAT CUSHION-W	0 0		D.2		
1.500000	-9.000000	-12.950000			
1.500000	9.000000	-12.950000			
17.500000	-9.000000	-13.920000			
6 SEAT BACK 1-W	0 0		D.2		
0.39000000	-9.000000	-20.000000			
-1.657000	-9.000000	-32.000000			
0.39000000	9.000000	-20.000000			
7 ARM REST - S	0 0		D.2		
0.56990000	8.000000	-19.150000			
16.000000	8.000000	-20.800000			
0.56990000	10.000000	-19.150000			
8 ARM REST - P	0 0		D.2		
0.56990000	-8.000000	-19.150000			
16.000000	-8.000000	-20.800000			
0.56990000	-10.000000	-19.150000			
0 0 0 0 0 0 0 0 0 0 0 0 0 0 0 0 0 0					
0 0 0 0 0 0 0 0 0 0 0 0 0 0 0 0 0 0					
0 0 0 0 0 0					
1 SEAT CUSH FDF (O)	1 1		E.1		
0.000000	-3.000000	0.000000	0.000000	0.000000	
7					
0.000000	0.000000	0.50000000	100.0000	0.75000000	400.0000
1.000000	1000.0000	1.50000000	3000.0000	2.00000000	6000.0000
3.000000	15000.00				
2 SEAT BACK FDF (O)	1 1		E.1		
0.000000	-4.000000	0.000000	0.000000	0.000000	
6					
0.000000	0.000000	1.000000	500.0000	1.500000	1000.0000
2.000000	2000.0000	3.00000000	5000.0000	4.00000000	10000.00
3 FLOORBOARD FDF (O)	1 1		E.1		
0.000000	-8.000000	0.000000	0.000000	1.000000	
6					
0.000000	0.000000	1.000000	860.0000	2.000000	1690.0000
3.000000	2270.0000	4.00000000	2380.0000	8.00000000	2380.0000
4 SEAT PAN FDF (O)	1 1		E.1		
0.000000	-1.000000	0.000000	0.000000	1.000000	
3					
0.000000	0.000000	0.20000000	2000.0000	1.00000000	20000.00
5 SHLD BELT FDF	3 1		E.1		
0.000000	-0.12000000	0.000000	0.000000	0.000000	
2					
0.000000	0.000000	0.12000000	2500.0000		
6 LAP BELT FDF	3 1		E.1		
0.000000	-0.12000000	0.000000	0.000000	0.000000	
2					
0.000000	0.000000	0.12000000	3500.0000		
7 TIRE FDF (REAR)	1 1		E.1		
0.000000	-2.160000	0.000000	0.000000	1.000000	
9					
0.000000	0.000000	0.30000000	45.000000	0.59000000	90.000000
0.89000000	135.0000	1.19000000	180.0000	1.48000000	225.0000
1.78000000	2250.0000	1.97000000	3375.0000	2.16000000	6075.0000
8 CHEST FDF	1 1		E.1		

0.000000	-1.500000	0.000000	0.000000	0.000000	
6					
0.000000	0.000000	0.2500000	50.00000	0.5000000	200.0000
1.000000	3000.000	1.200000	7000.000	1.500000	15000.00
9 Spring Func	5 1			E.1	
-4.000000	-2.000000	0.000000	0.000000	0.000000	
7					
-4.000000	-4000.000	-2.000000	-200.0000	-1.000000	0.000000
0.000000	0.000000	1.000000	0.000000	1.500000	5000.000
2.000000	10000.00				
10 BELLY FDF	1 1			E.1	
0.000000	-1.000000	0.000000	0.000000	0.000000	
3					
0.000000	0.000000	0.2500000	5000.000	1.000000	15000.00
11 SEAT CUSHION R	1 3			E.1	
0.000000	0.000000	0.1000000	0.000000	0.000000	
12 SEAT BACK R (O)	1 3			E.1	
0.000000	0.000000	0.1000000	0.000000	0.000000	
13 FLOORBOARD R (O)	1 3			E.1	
0.000000	0.000000	0.1000000	0.000000	0.000000	
14 CHEST R	1 3			E.1	
0.000000	0.000000	0.7000000	0.000000	0.000000	
15 BELT R (MGA)	3 3			E.1	
0.000000	0.000000	0.1000000	0.000000	0.000000	
16 TIEDOWN F (REAR)	3 1			E.1	
0.000000	-0.2000000	0.000000	0.000000	0.000000	
2					
0.000000	0.000000	0.2000000	2600.000		
17 TIEDOWN F (FRONT)	3 0			E.1	
0.000000	-0.2000000	0.000000	0.000000	0.000000	
2					
0.000000	0.000000	0.2000000	2000.000		
18 CHEST G	1 4			E.1	
0.000000	0.000000	0.5000000	0.000000	0.000000	
19 TIRE FDF (FRONT)	1 1			E.1	
0.000000	-2.160000	0.000000	0.000000	1.000000	
9					
0.000000	0.000000	0.3000000	45.00000	0.5900000	90.00000
0.8900000	135.0000	1.190000	180.0000	1.480000	225.0000
1.780000	2250.000	1.970000	3375.000	2.160000	6075.000
21 SEAT CUSH G (O)	1 4			E.1	
0.000000	0.000000	0.5000000	0.000000	0.000000	
22 SEAT BACK G (K)	1 4			E.1	
0.000000	0.000000	0.5000000	0.000000	0.000000	
23 FLOORBOARD G (O)	1 4			E.1	
0.000000	0.000000	0.8800000	0.000000	0.000000	
24 BELT G (MGA)	3 4			E.1	
0.000000	0.000000	0.3000000	0.000000	0.000000	
25 BAR R	2 3			E.1	
0.000000	0.000000	0.7000000	0.000000	0.000000	
30 TIRE ROLL FRIC	1 5			E.1	
0.000000	0.000000	0.5000000	0.000000	1.000000	
31 SEAT CUSH CF (O)	1 5			E.1	
0.000000	0.000000	0.3000000	0.000000	0.5000000	
32 BELT FRIC B	3 5			E.1	
0.000000	0.000000	0.2500000	0.000000	0.000000	
33 BELT FRIC C	3 5			E.1	
0.000000	0.000000	0.8000000	0.000000	0.1000000	
34 BELT FRIC D	3 5			E.1	
0.000000	0.000000	10.00000	0.000000	0.1000000	
35 MID CF (K)	1 5			E.1	
0.000000	0.000000	1.000000	0.000000	1.000000	
36 BELT CF (K)	3 5			E.1	
0.000000	0.000000	0.8000000	0.000000	0.000000	

37	TIRE R (O)	1 3		E.1	
	0.000000	0.000000	0.100000	0.000000	0.000000
38	TIRE G (O)	1 4		E.1	
	0.000000	0.000000	0.300000	0.000000	0.000000
39	TIEDOWN R (O)	3 3		E.1	
	0.000000	0.000000	0.100000	0.000000	0.000000
40	TIEDOWN G (O)	3 4		E.1	
	0.000000	0.000000	0.300000	0.000000	0.000000
999					
41	RIGHT SHOULDER JOINT	6 0		E.7	
	0.000000	0.000000	0.000000	0.000000	0.000000
	-4 8				
	151.0000	0.000000	87900.00	0.000000	
	75.00000	0.000000	13700.00	0.000000	
	0.000000	0.000000	-312.0000	11800.00	
	66.00000	0.000000	7780.000	3010000.	
	68.00000	0.000000	22200.00	376000.0	
	89.00000	0.000000	22000.00	0.000000	
	111.0000	0.000000	2470.000	17600.00	
	153.0000	0.000000	13000.00	0.000000	
42	LEFT SHOULDER JOINT	6 0		E.7	
	0.000000	0.000000	0.000000	0.000000	0.000000
	-4 8				
	151.0000	0.000000	87900.00	0.000000	
	153.0000	0.000000	13000.00	0.000000	
	111.0000	0.000000	2470.000	17600.00	
	89.00000	0.000000	22000.00	0.000000	
	68.00000	0.000000	22200.00	376000.0	
	66.00000	0.000000	7780.000	3010000.	
	0.000000	0.000000	-312.0000	11800.00	
	75.00000	0.000000	13700.00	0.000000	
43	SITTING RIGHT HIP	6 0		E.7	
	0.000000	0.000000	0.000000	0.000000	0.000000
	19 4				
	0.000000	7.000000	22.00000	52.00000	112.0000
	472.0001	952.0002	1910.000	3830.000	7670.000
	30700.00	61400.00	123000.0	246000.0	492000.0
	1970000.				983000.0
	0.000000	17.00000	51.00000	119.0000	255.0000
	1070.000	2160.000	4340.000	8690.002	17400.00
	69700.00	139000.0	279000.0	557000.0	1110000.
	4460000.				2230000.
	0.000000	8.000000	17.00000	28.00000	50.00000
	182.0000	358.0000	710.0000	1410.000	2820.000
	11300.00	22500.00	45100.01	90100.02	180000.0
	721000.0				360000.0
	0.000000	7.000000	13.00000	18.00000	23.00000
	53.00000	93.00000	173.0000	333.0000	653.0000
	2570.000	5130.000	10300.00	20500.00	41000.00
	164000.0				81899.98
44	SITTING LEFT HIP	6 0		E.7	
	0.000000	0.000000	0.000000	0.000000	0.000000
	19 4				
	0.000000	7.000000	22.00000	52.00000	112.0000
	472.0001	952.0002	1910.000	3830.000	7670.000
	30700.00	61400.00	123000.0	246000.0	492000.0
	1970000.				983000.0
	0.000000	7.000000	13.00000	18.00000	23.00000
	53.00000	93.00000	173.0000	333.0000	653.0000
	2570.000	5130.000	10300.00	20500.00	41000.00
	164000.0				81899.98
	0.000000	8.000000	17.00000	28.00000	50.00000
	182.0000	358.0000	710.0000	1410.000	2820.000
	11300.00	22500.00	45100.01	90100.02	180000.0
	721000.0				360000.0


```

0 0 0 0 0 0 0 0 0 0 0 0 0 0 0 0
0 0 0 0 0
0 0 0 0 0 0 0 0 0 0 0 0 0 0 0 0 0 F.5
0 0 0 0 0 0 0 0 0 0 0 0 0 0 0 0 0
0 0 0 0 0
2 6 F.8.A
9 9 F.8.B
5 0 15 24 0 0.500000 0 0 0
43 0 1 1 0 0 0 0 0 19.909178 -8.808765 -49.473431
0.000000 0.000000 0.000000 0.000000 0.000000 -1.000000
4 4 0 0 8 0 14 18 34 2.818949 -2.422708 -0.832097
0.000000 0.000000 0.000000 0.000000 0.000000 0.000000
4 4 0 0 8 0 14 18 34 3.981118 -0.826067 2.232970
0.000000 0.000000 0.000000 0.000000 0.000000 0.000000
3 3 0 0 8 0 14 18 34 4.369034 0.610670 -0.390206
0.000000 0.000000 0.000000 0.000000 0.000000 0.000000
3 3 0 0 8 0 14 18 34 4.322883 1.409031 0.944090
0.000000 0.000000 0.000000 0.000000 0.000000 0.000000
3 3 0 0 8 0 14 18 34 4.236056 3.005575 3.389913
0.000000 0.000000 0.000000 0.000000 0.000000 0.000000
3 3 0 0 8 0 14 18 34 3.005862 4.123076 5.471999
0.000000 0.000000 0.000000 0.000000 0.000000 0.000000
3 3 0 0 8 0 14 18 34 1.178110 4.921412 7.257435
0.000000 0.000000 0.000000 0.000000 0.000000 0.000000
43 0 1 1 0 0 0 0 0 16.500000 12.500000 0.000000
0.000000 0.000000 0.000000 0.000000 0.000000 -1.000000
6 0 15 24 0 0.000000 0 0 0
43 0 1 1 0 0 0 0 0 16.500000 -12.500000 0.000000
0.000000 0.000000 0.000000 0.000000 0.000000 -1.000000
1 1 0 0 10 0 14 18 32 2.117691 -5.879315 0.459376
0.000000 0.000000 0.000000 0.000000 0.000000 0.000000
1 1 0 0 10 0 14 18 33 3.587214 -4.761753 -0.853525
0.000000 0.000000 0.000000 0.000000 0.000000 0.000000
1 1 0 0 10 0 14 18 33 4.708301 -2.901662 -1.685729
0.000000 0.000000 0.000000 0.000000 0.000000 0.000000
1 1 0 0 10 0 14 18 33 4.793403 -0.027878 -1.204061
0.000000 0.000000 0.000000 0.000000 0.000000 0.000000
1 1 0 0 10 0 14 18 33 4.708301 2.526587 -1.685729
0.000000 0.000000 0.000000 0.000000 0.000000 0.000000
1 1 0 0 10 0 14 18 33 3.372296 4.657859 -0.907104
0.000000 0.000000 0.000000 0.000000 0.000000 0.000000
1 1 0 0 10 0 14 18 32 2.117886 6.254417 0.459429
0.000000 0.000000 0.000000 0.000000 0.000000 0.000000
43 0 1 1 0 0 0 0 0 16.500000 12.500000 0.000000
0.000000 0.000000 0.000000 0.000000 0.000000 -1.000000
2 2 2 2 2 2 F.8.B
16 0 39 40 0 0.000000 0 0 0
43 0 1 1 0 0 0 0 0 16.770000 -8.000000 0.000000
0.000000 0.000000 0.000000 0.000000 0.000000 -1.000000
39 39 1 1 0 0 0 0 0 0.900000 0.000000 -0.900000
0.000000 0.000000 0.000000 0.000000 0.000000 -1.000000
16 0 39 40 0 0.000000 0 0 0
43 0 1 1 0 0 0 0 0 16.770000 -8.000000 0.000000
0.000000 0.000000 0.000000 0.000000 0.000000 -1.000000
39 39 1 1 0 0 0 0 0 0.900000 0.000000 -0.900000
0.000000 0.000000 0.000000 0.000000 0.000000 -1.000000
16 0 39 40 0 0.000000 0 0 0
43 0 1 1 0 0 0 0 0 16.770000 8.000000 0.000000
0.000000 0.000000 0.000000 0.000000 0.000000 -1.000000
40 40 1 1 0 0 0 0 0 0.900000 0.000000 -0.900000
0.000000 0.000000 0.000000 0.000000 0.000000 -1.000000
16 0 39 40 0 0.000000 0 0 0
43 0 1 1 0 0 0 0 0 16.770000 8.000000 0.000000
0.000000 0.000000 0.000000 0.000000 0.000000 -1.000000

```


0	H.4
0	H.5
0	H.6
0	H.7
0	H.8
0	H.9
0	H.10
0 0	H.11

Appendix 9B ISO Frontal Impact Model Data File

The following code is an example of MADYMO3D program which was used to obtain the full scale WTORS model (ISO wheelchair + Hybrid II dummy).

```

RUN 1
WTORS SLED TEST
WRITTEN BY JUN GU MAR 4 1996
*****
* GENERAL INITIAL INFORMATION *
*****
TO          TE
0.0000 0.2300
4th order runge-kutta with fixed time step
INT          TS(s) TOL
0 5.0E-4 0.005 0.002
RAMP1(rad/s) RAMP2 RAC01 RAC02(m/s)
0.0000 0.5000 0.0100 0.1000
*****
* DEFINE A SLED AS THE INETIAL SPACE - 1 *
*****
INERTIAL SPACE
x-forward y-starboard z-down
RSEL HENDON SLED
PLANES
assume sled as a solid rigid entity
BODY X1 Y1          Z1          X2 Y2          Z2          X3 Y3          Z3 LO UNL HYS ID
0 -1.0 -.5700 0.000 1.00 -.5700 0.0000 1.0 0.570 0.000 0 0 0 0 SLED
.999
END INERTIAL SPACE
*****
* DEFINE THE WHEELCHAIR AS SYSTEM 1 *
*****
SYSTEM 1
ISO SURROGATE CHAIR
CONFIGURATION
1
.999
GEOMETRY
RIX Y Z CGX Y Z          ID
0 0 0 0.218 0 0.363 WH.CH.RE
.999
INERTIA
MASS IXX IYY          IZZ
90 8.24 11.66 9.47
.999
ELLIPSOIDS
semi-axes (m)  centre of gravity
BODY A B C MX MY          MZ DEG LO UNLO HYS ID
1 0.161 0.05 0.161 0 -0.295 0.161 2 1 0 0 REAR.LH.WHEEL
1 0.161 0.05 0.161 0 0.295 0.161 2 1 0 0 REAR.RH.WHEEL
1 0.12 0.035 0.12 0.38 -0.275 0.12 2 0 0 0 FRONT.LH.WHEEL
1 0.12 0.035 0.12 0.38 0.275 0.12 2 0 0 0 FRONT.RH.WHEEL
.999
FUNCTIONS
8
0 0 0.008 400 0.015 800 0.022 1200 0.039 2000 +
0.045 2400 0.05 2600 0.055 50000
.999
PLANES
BODY X1 Y1          Z1          X2 Y2          Z2          X3 Y3          Z3 LO UNL HYS ID
1 0.064 -0.22 0.581 0.559 -0.22 0.602 0.559 0.22 0.602 1 0 0 PANCAKE
1 0.064 -0.22 0.521 0.559 -0.22 0.542 0.559 0.22 0.542 1 0 0 SEATPL
1 0.064 -0.22 1.07 0.102 -0.22 0.533 0.102 0.22 0.533 1 0 0 UPBACK
1 0.685 -0.22 0.16 0.838 -0.22 0.216 0.838 0.22 0.216 0 0 0 FOOTUP
.999
FUNCTIONS
2
0 0 0.001 50000
.999
*****
* INITIAL POSITION AND VELOCITY OF W/C *
*****
INITIAL CONDITIONS
X Y          Z          VX VY VZ CHO
0 0 -0.008 0 0 0 0
END SYSTEM 1
*****
* DEFINE THE DUMMY AS SYSTEM 2 *
*****
SYSTEM 2
PART 572
CONFIGURATION

```

```

5 4 3 2 1
7 6 3 2 1
9 8 3 2 1
11 10 1
13 12 1
-999
GEOMETRY
RUX      Y      Z      CGX  Y  Z      ID
0.000 0.000 0.000 0.026 0.000 -0.079 LOWER TORSO
0.000 0.000 0.000 0.033 0.000 0.072 SPINE
0.000 0.000 0.132 0.029 0.000 0.162 UPPER TORSO
0.065 0.000 0.318 0.000 0.000 0.063 NECK
0.000 0.000 0.124 0.006 0.000 0.028 HEAD
0.030 0.189 0.260 0.000 0.000 -0.122 UPPER ARM LEFT
0.000 0.000 -0.261 0.000 0.000 -0.167 LOWER ARM LEFT
0.030 -0.189 0.260 0.000 0.000 -0.122 UPPER ARM RIGHT
0.000 0.000 -0.261 0.000 0.000 -0.167 LOWER ARM RIGHT
0.042 0.087 -0.072 0.000 0.006 -0.207 UPPER LEG LEFT
0.000 0.008 -0.405 0.016 0.000 -0.272 LOWER LEG LEFT
0.042 -0.087 -0.072 0.000 -0.006 -0.207 UPPER LEG RIGHT
0.000 -0.008 -0.405 0.016 0.000 -0.272 LOWER LEG RIGHT
-999
INERTIA
MASS  IXX  IYY  IZZ
11.76 0.1297 0.0817 0.1393
2.69 0.0140 0.0159 0.0186
17.36 0.2352 0.1896 0.1508
0.88 0.01 0.01 0.01
4.42 0.0248 0.0307 0.0184
2.22 0.0161 0.0156 0.01
2.15 0.0311 0.0301 0.01
2.22 0.0161 0.0156 0.01
2.15 0.0311 0.0301 0.01
9.68 0.1300 0.1387 0.0170
4.42 0.1315 0.1271 0.01
9.68 0.1300 0.1387 0.0170
4.42 0.1315 0.1271 0.01
-999
ORIENTATIONS
BODY ICH IOR PAR1 PAR2
5 0 1 2 -0.733
-999
CARDAN JOINTS
EL LO UNL HYS XEL L U H X  L U H X  PHI THETA PSI  PHI THETA PSI
10 1 0 0 0 2 0 0 0 3 0 0 0 6.00 6.00 5.00 39. 39. 12.
12 1 0 0 0 4 0 0 0 3 0 0 0 6.00 6.00 5.00 39. 39. 12.
11 5 0 0 0 6 0 0 0 6 0 0 0 5.00 7.50 4.00 12.
13 5 0 0 0 6 0 0 0 6 0 0 0 5.00 7.50 4.00 12.
6 7 0 0 0 6 0 0 0 8 0 0 0 2.00 4.00 4.00 12. 0. 12.
8 7 0 0 0 6 0 0 0 9 0 0 0 2.00 4.00 4.00 12. 0. 12.
7 10 0 0 0 6 0 0 0 11 0 0 0 2.00 4.00 2.00 4. 0. 4.
9 10 0 0 0 6 0 0 0 11 0 0 0 2.00 4.00 2.00 4. 0. 4.
-999
ORIENTATIONS
BODY ICH IOR PAR
10 1 1 3 1.5708
10 10 1 3 1.5708
12 1 1 3 1.5708
12 12 1 3 1.5708
11 10 1 3 1.5708
11 11 1 3 1.5708
13 12 1 3 1.5708
13 13 1 3 1.5708
6 3 1 1 1.5708 2 1.5708
6 6 1 1 1.5708 2 1.5708
8 3 1 1 1.5708 2 1.5708
8 8 1 1 1.5708 2 1.5708
7 6 1 2 -1.5708 1 -1.5708
7 7 1 2 -1.5708 1 -1.5708
9 8 1 2 -1.5708 1 -1.5708
9 9 1 2 -1.5708 1 -1.5708
-999
FUNCTIONS
5
-3.280 -540. -2.280 -40. -1.570 0. +
0.000 0. 1.000 500.
5
-1.880 -568. -0.880 -68. 0.000 0. +
0.175 14. 1.175 514.
4
-2.000 -500. -1.000 0. 1.000 0. +
2.000 500.
5
-1.175 -514. -0.175 -14. 0.000 0. +
0.880 68. 1.880 568.
4
-1.000 -500. 0.000 0. 2.300 0. +
3.300 500.
2
-1.000 -500. 1.000 500.
4
-4.120 -500. -3.120 0. 1.260 0. +
2.260 500.
3
0.000 0. 2.500 0. 3.500 500.

```

```

3
-3.500 -500. -2.500 0. 0.000 0.
4
-1.880 -500. -0.88 0. 0.880 0. +
1.880 500.
6
-3.300 -600. -2.300 -100. -2.000 -35. +
-1.000 -10. 0.000 0. 1.000 500.
-999
FLEXION-TORSION
ELASTIC(Rx) (torsion) DAMPING FRICTION
EL LO UNL HYS XEL L U H X (Nm/grad) (Nm)
2 1 0 0. 0. 2 0 0. 0. 3.00
3 1 0 0. 0. 2 0 0. 0. 3.00
4 3 0 0. 0. 4 0 0. 0. 1.00
5 3 0 0. 0. 4 0 0. 0. 1.00
-999
ORIENTATIONS
BODY ICH IOR PAR
4 3 1 2. 0.35
-999
FUNCTIONS
2
0.000 0. 1.000 317.
4
-1.000 -126. -0.175 -40. 0.175 40. +
1.000 126.
2
0.000 0. 1.000 154.
4
-1.000 -103. -0.175 -28. 0.175 28. +
1.000 103.
-999
ELLIPSOIDS
BODY A B C MX MY MZ DEG LO UNLO HYS ID
1 0.115 0.165 0.115 0.045 0.000 -0.045 2. 0 0 0. LOWER TORSO
2 0.110 0.150 0.110 0.024 0.000 0.066 2. 0 0 0. SPINE
3 0.120 0.155 0.175 0.024 0.000 0.163 2. 0 0 0. UPPER TORSO
3 0.050 0.210 0.050 0.030 0.000 0.260 2. 0 0 0. SHOULDERS L&R
4 0.040 0.040 0.065 0.000 0.000 0.062 2. 0 0 0. NECK
5 0.090 0.078 0.115 0.0225 0.000 0.025 2. 0 0 0. HEAD
6 0.047 0.042 0.141 0.000 0.000 -0.1305 2. 0 0 0. UPPER ARM LEFT
7 0.040 0.040 0.235 0.000 0.000 -0.185 2. 0 0 0. LOWER ARM LEFT
8 0.047 0.042 0.141 0.000 0.000 -0.1305 2. 0 0 0. UPPER ARM RIGHT
9 0.040 0.040 0.235 0.000 0.000 -0.185 2. 0 0 0. LOWER ARM RIGHT
10 0.080 0.085 0.2775 0.000 0.000 -0.1925 2. 0 0 0. UPPER LEG LEFT
11 0.060 0.047 0.270 0.000 0.000 -0.180 2. 0 0 0. LOWER LEG LEFT
11 0.130 0.045 0.040 0.100 0.000 -0.455 2. 0 0 0. FOOT LEFT
12 0.080 0.085 0.2775 0.000 0.000 -0.1925 2. 0 0 0. UPPER LEG RIGHT
13 0.060 0.047 0.270 0.000 0.000 -0.180 2. 0 0 0. LOWER LEG RIGHT
13 0.130 0.045 0.040 0.100 0.000 -0.455 2. 0 0 0. FOOT RIGHT
-999
INITIAL CONDITIONS
X Y Z VX VY VZ CHD
0.24 0.0 0.71
ORIENTATIONS
BODY ICH IOR PAR
1 -1 1 2. -0.5236
2 -1 1 2. -0.3236
3 -1 1 2. -0.2236
4 -1 1 2. 0.35
5 -1 1 2. 0.35
6 -1 1 2. -0.3926
7 -1 1 2. -1.57
8 -1 1 2. -0.3926
9 -1 1 2. -1.57
10 -1 1 2. -1.6708
11 -1 1 2. 0.0873
12 -1 1 2. -1.6708
13 -1 1 2. 0.0873
-999
END SYSTEM 2
*****
* FORCE MODELS - FIELDS - BELTS *
*****
FORCE MODELS
ACCELERATION FIELDS
SYS BODY FLNCX Y Z
0 0 1 0 2
-999
FUNCTIONS
42
0 0 0.005 -1.9 0.010 -0.6 0.015 0.5 +
0.020 -0.1 0.025 19.2 0.030 101.4 0.035 109.5 0.040 150.3 +
0.045 144.5 0.050 172.4 0.055 173.2 0.060 185.3 0.065 189.8 +
0.070 175.5 0.075 211 0.080 167.3 0.085 150.6 0.090 138.1 +
0.095 152.1 +
0.100 153 0.105 121.6 0.110 137.1 0.115 109.1 0.120 70.5 +
0.125 26.7 0.130 -8.5 +
0.135 -7.4 0.140 -18.1 0.145 -18.1 0.150 -29.2 0.155 -20.9 +
0.160 -17 0.165 -4.3 0.170 -0.7 0.175 7.4 0.18 17.7 +
0.185 6.5 0.19 6.4 0.195 7.5 0.2 4.7 0.25 6
2
0 -9.8 0.25 -9.8
-999

```

```

*****
*INITIAL CONTACTS BETWEEN DUMMY-W/C*
*****
CONTACT INTERACTIONS
PLANE-ELLIPSOID
WHEELCHAIR - SLED CONTACT
SY PL SY EL CHO LO UNL HYS XEL D1 FR1 FIN COR DAFR DAMP2(D2)
-1 1 1 4 1 0 0 0 0 0.7 0.01 0 0
-1 1 1 2 4 1 0 0 0 0 0.7 0.01 0 0
-1 1 1 3 4 1 0 0 0 0 0.7 0.01 0 0
-1 1 1 4 4 1 0 0 0 0 0.7 0.01 0 0
WHEELCHAIR - OCCUPANT
1 1 2 1 4 2 0 0 0 0 0.7 0.01 0 0
1 1 2 11 4 0 0 0 0 0 0.7 0.01 0 0
1 1 2 14 4 0 0 0 0 0 0.7 0.01 0 0
1 3 2 3 4 0 0 0 0 0 0.3 0.01 0 0
1 3 2 2 4 0 0 0 0 0 0.3 0.01 0 0
1 3 2 1 4 0 0 0 0 0 0.3 0.01 0 0
1 4 2 13 4 0 0 0 0 0 0.3 0.01 0 0
1 4 2 16 4 0 0 0 0 0 0.3 0.01 0 0
-999
FUNCTIONS
2
0 0 0.001 35000
2
0 0 0.001 80000
-999
ELLIPSOID-ELLIPSOID
SY EL SY EL CHO LO UNL H X D1 FR1 COR DAFR DAMP2(D2)
2 6 2 7 2 1 0 0 0 0.3 0.01 0 0
2 6 2 8 2 1 0 0 0 0.3 0.01 0 0
2 6 2 9 2 1 0 0 0 0.3 0.01 0 0
2 6 2 10 2 1 0 0 0 0.3 0.01 0 0
2 6 2 11 2 1 0 0 0 0.3 0.01 0 0
2 6 2 12 2 1 0 0 0 0.3 0.01 0 0
2 6 2 13 2 1 0 0 0 0.3 0.01 0 0
2 6 2 14 2 1 0 0 0 0.3 0.01 0 0
2 6 2 15 2 1 0 0 0 0.3 0.01 0 0
2 6 2 16 2 1 0 0 0 0.3 0.01 0 0
-999
FUNCTIONS
3
0 0 0.01 375 0.02 1000
-999
END CONTACT INTERACTIONS
*****
* BELT CONTACTS BETWEEN OCCUPANT-SLED *
*****
BELTS
SY1 BOD1 X1 Y1 Z1 SY2 BOD2 X2 Y2 Z2 LO UNL HYS XEL FRIC PRET ADDLEN COR ID
-1 0 -0.085 0.35 1.185 2 3 0.105 0.09 0.267 1 2 1790000 0.4 0.4 -0.058 0.4 1 diag. top (Bpillar-w)
2 3 0.105 0.08 0.292 2 1 0.09 -0.164 0.0 1 2 1790000 0.4 0.4 0 0.4 1 diag. bott (ul-tright)
-999
FUNCTIONS
4
0 0 0.04 8000 0.18 18000 0.2 20000
3
0 0 0.1 0 0.23 8000
-999
BELTS
SY1 BOD1 X1 Y1 Z1 SY2 BOD2 X2 Y2 Z2 LO UNL HYS XEL FRIC PRET ADDLEN COR ID
2 1 0.10 0.155 0 -1 0 -0.085 0.35 0.00 1 2 1790000 0.4 0.4 0 0 1 lappt (hicfr-floorpt)
-1 0 -0.085 -0.35 0.00 2 1 0.1 -0.155 0 1 2 1790000 0.4 0.4 0 0 1 lapst (floorst-tright)
-999
FUNCTIONS
4
0 0 0.04 8000 0.18 18000 0.2 20000
3
0 0 0.1 0 0.23 8000
-999
BELTS
-1 0 -0.33 0.25 0.0 1 1 -0.022 0.22 0.38 1 2 1300000 0.04 +
0.4 0 0 1 OUT REAR RP1
1 1 -0.022 0.22 0.38 -1 0 -0.33 0.165 0.0 1 2 1300000 0.04 +
0.4 0 0 1 INN REAR RP2
-999
FUNCTIONS
4
0 0 0.02 3500 0.03 4500 0.105 9000
3
0 0 0.05 0 0.08 2000
-999
BELTS
-1 0 -0.33 -0.25 0.00 1 1 -0.022 -0.22 0.38 1 2 1300000 0.04 +
0.4 0 0 1 OUT REAR RS1
1 1 -0.022 -0.22 0.38 -1 0 -0.33 -0.165 0 1 2 1300000 0.04 +
0.4 0 0 1 OUT REAR RS2
-999
FUNCTIONS
4
0 0 0.02 3500 0.03 4500 0.105 9000
3
0 0 0.05 0 0.08 2000
-999

```



```
BELTS
-1 0 0.902 0.165 0.00 1 1 0.62 0.22 0.47 1 2 1300000 0.04 +
0.4 0 0 1 FRT FS TIEDOWN
-999
FUNCTIONS
4
0 0 0.02 3500 0.03 4500 0.105 9000
3
0 0 0.05 0 0.08 2000
-999
BELTS
-1 0 0.902 -0.165 0.00 1 1 0.62 -0.22 0.47 1 2 1300000 0.04 +
0.4 0 0 1 FRT FS TIEDOWN
-999
FUNCTIONS
4
0 0 0.02 3500 0.03 4500 0.105 9000
3
0 0 0.05 0 0.08 2000
-999
END FORCE MODELS
*****
"      OUTPUT FILES      "
*****
OUTPUT CONTROL PARAMETERS
IOUT IKIN TSKIN IPTKIN TSOUT
0 0 0.005 3 0.005
LINDIS
SYS1 BO1 X1 Y1 Z1 S2 B2 ID
2 5 0 0 0.063 -1 0 head centre
1 1 0.401 -0.22 0.466 -1 0 xpoint
1 1 0 -0.275 0.16 -1 0 rear wL centre
-999
LINACC
SYS BO X Y Z FX Y Z TWO ID
2 5 0 0 0.063 1 0 0 0 head centre
2 3 0.029 0 0.162 1 0 1 0 chest
-999
FORCES
BELT LOADS
4 1
4 2
PANCAKE-LT
1 5
-999
INJURY PARAMETERS
HIC
1 0.036
-999
END INJURY PARAMETERS
END OUTPUT CONTROL
END INPUT DATA
```

LIST OF PUBLICATIONS

- [1] CURRENT RESEARCH TO EVALUATE THE PERFORMANCE OF WHEELCHAIRS IN FRONTAL IMPACTS
(Evaluation of Floor Reaction Forces)
Gu J., Roy A.P. (1995). *Proc. of 23rd Transport Forum, University of Warwick, PTRC (0 86050 285 6)*, pp139-154.
- [2] OPTIMISATION OF THE WHEELCHAIR TIEDOWN AND OCCUPANT RESTRAINT SYSTEM
(Effect of Diagonal Strap Anchorage Configurations on Occupant Restraint System)
Gu J., Roy A.P. (1996). *Proc. of 15th International Technical Conference on the Enhanced Safety of Vehicles (ESV), Melbourne Australia, Paper No. 96-S1-W-21*, pp242-250.
- [3] THE CRASH PERFORMANCE OF A REAR FACING WHEELCHAIR OCCUPANT SYSTEM IN FRONTAL IMPACT
Gu J., Roy A.P. (1997). *Proc. of 1st European MADYMO Users' Conference, Heidelberg*.
- [4] FINITE ELEMENT ANALYSIS OF WHEELCHAIR STRUCTURE
Gu J. (1997). *Proc. of 3rd International Conference on Modern Practice in Stress and Vibration Analysis, Dublin/Ireland*, pp517 - 522.
- [5] COMPUTER SIMULATION OF A PROCEDURE TO ASSESS THE CRASH PERFORMANCE OF A CHILD RESTRAINT SYSTEM [CRS] IN SIDE IMPACT
Gu J., Roy P. (1998). *Proc. of 7th International MADYMO Users' Conference, Windsor, Canada*, pp67-76
- [6] STRUCTURAL MODELLING OF WHEELCHAIR TYRE USING MADYMO
Gu J., Roy P. (1999). *Proc. of 2nd European MADYMO Users' Conference, Germany*.